Non-collinear magnetism in Density-Functional Theories

Im Fachbereich Physik
der Freien Universität Berlin
eingereichte

Dissertation

zur Erlangung des akademischen Grades

doctor rerum naturalium

Florian Gregor Eich

Institut für Theoretische Physik
Freie Universität Berlin

2012

Diese Arbeit entstand im Zeitraum von Januar 2008 bis August 2012 in der Forschungsgruppe von Prof. E.K.U. Gross am Institut für Theoretische Physik der Freien Universität Berlin und am Max-Planck-Institut für Mikrostrukturphysik in Halle.

Datum der Abgabe: 31.10.2012

Erstgutachter: Prof. Dr. E.K.U. Gross
Zweitgutachter: Prof. Dr. J. Bosse

Datum der Disputation: 19.12.2012

Abstract

Density-Functional Theory (DFT) is presently the most widely used approach to determine the electronic structure of atoms, molecules and solids. Its applicability depends crucially on physically sound and numerically accessible approximations to the exchange-correlation-energy functional. Despite the fact that the original Hohenberg-Kohn theorem was generalized to explicitly include the spin degrees of freedom by von Barth and Hedin more than 30 years ago, recent applications are mostly based on approximations to the exchange-correlation energy devised to describe collinear spin magnetizations. In this thesis we present a novel functional for Spin-Density-Functional Theory (SDFT) that is explicitly constructed for non-collinear spin magnetizations, i.e. , it appreciates the possibility for the spin magnetization to change its orientation and not only its magnitude. The functional is constructed in close analogy to the well-known Local-Spin-Density Approximation (LSDA) which uses the uniform electron gas with a constant spin magnetization as reference system. We define a semi-local approximation for the exchange-correlation energy by generalizing the reference system to the uniform electron gas in the spin-spiral-wave (SSW) state. The SSW state, discovered by Overhauser, is investigated using various many-body techniques in order to obtain the required reference data. We demonstrate that it is possible to extend the idea of the LSDA by the inclusion of a Spin-Gradient Extension (SGE), derived from the aforementioned SSW state. By construction the SGE yields exchange-correlation-magnetic fields that are non-collinear w.r.t. the spin magnetization. This indicates that the new functional will improve the description of spin dynamics, by means of Time-Dependent Spin-Density-Functional Theory (TD-SDFT), because it takes into account that the Kohn-Sham spin-current density does not reproduce the physical spin-current density. This is of importance for the ab-initio description of spintronics, i.e. , the manipulation and control of the spin degrees of freedom from first principles, which in recent years emerged as an important field of research due to its potential application for data storage and information processing.

Contents

Notation and conventions

Throughout the thesis we will use Hartree atomic units (a.u.), i.e. , $\hbar = m_e = e = 1$. We will employ the formalism of second quantization to represent operators acting in Fock space. The field operators are denoted by $\hat{\phi}_\uparrow(\boldsymbol{r})$ and $\hat{\phi}_\downarrow(\boldsymbol{r})$. They satisfy the fundamental anti-commutation relation

$$\left\{\hat{\phi}_\sigma(\boldsymbol{r})\,, \hat{\phi}^\dagger_{\sigma'}(\boldsymbol{r}')\right\} = \delta_{\sigma\sigma'}\delta(\boldsymbol{r}-\boldsymbol{r}')\,.$$

Since the thesis is focused on non-collinear magnetism we will collect the spin-up and the spin-down field operators in the two-component Pauli field

$$\hat{\Phi}(\boldsymbol{r}) = \begin{pmatrix}\hat{\phi}_\uparrow(\boldsymbol{r})\\ \hat{\phi}_\downarrow(\boldsymbol{r})\end{pmatrix} \quad , \quad \hat{\Phi}^\dagger(\boldsymbol{r}) = \begin{pmatrix}\hat{\phi}^\dagger_\uparrow(\boldsymbol{r}) & \hat{\phi}^\dagger_\downarrow(\boldsymbol{r})\end{pmatrix}.$$

Products in the internal space of the Pauli field follow the rule of matrix multiplication, i.e. , $\hat{\Phi}^\dagger\hat{\Phi}$ represents a scalar-valued field and $\hat{\Phi}\hat{\Phi}^\dagger$ represents a 2×2-matrix-valued field. This leads to the somewhat unconventional definition of the operator representing the one-particle-reduced density matrix

$$\hat{\gamma}(\boldsymbol{r};\boldsymbol{r}') = -:\hat{\Phi}(\boldsymbol{r})\,\hat{\Phi}^\dagger(\boldsymbol{r}'):,$$

employing the normal ordering operator $::$. Normal ordering is always taken w.r.t. the true vacuum $|\Omega\rangle$ and not the Fermi sea. Single-particle orbitals will be denoted by $\Phi_j(\boldsymbol{r})$, where the meaning of the index j will be defined in the context. Note the missing $\hat{}$ compared to the fundamental Pauli fields $\hat{\Phi}(\boldsymbol{r})$. The Kohn-Sham orbitals will have their own symbol $\Phi^s_j(\boldsymbol{r})$, due to their central role in Density-Functional Theories. Spin-spiral-wave states have their own symbol $\xi_{\boldsymbol{k}b=\mp}(\boldsymbol{r})$, because they are a central object in this thesis. Vectors in physical space are denoted by bold symbols, e.g. $\boldsymbol{v}$, and second-rank tensors by underlined bold symbols, e.g. $\underline{\boldsymbol{T}}$. Inner products of vectors in physical space ($\mathbb{R}^3$) are indicated by $\cdot$, while external products of vectors in physical space are denoted by $\otimes$. Traces over Fock space are indicated by $\mathrm{Tr}\{\ldots\}$ and traces over the internal (spin) space by $\mathrm{tr}\{\ldots\}$. The symmetric definition of the Fourier

transformation is used, i.e. ,

$$f(\boldsymbol{k}) = \frac{1}{\sqrt{2\pi}^3} \int \mathrm{d}^3 r \; e^{\imath \boldsymbol{k}\cdot\boldsymbol{r}} f(\boldsymbol{r}) \,,$$
$$f(\boldsymbol{r}) = \frac{1}{\sqrt{2\pi}^3} \int \mathrm{d}^3 k \; e^{-\imath \boldsymbol{k}\cdot\boldsymbol{r}} f(\boldsymbol{k}) \,.$$

This leads to the convention that a Dirac delta function evaluated at zero contributes $(2\pi)^{-3}$ irrespective of whether its argument is in momentum or position space. Moreover this implies that the volume of an extended system is set to one. The vector $\boldsymbol{\sigma}$ denotes the vector of Pauli matrices. They obey

$$\left[\sigma^\kappa, \sigma^\lambda\right] = \imath 2 \epsilon_{\kappa\lambda\mu} \sigma^\mu,$$
$$\sigma^\kappa \sigma^\lambda = \delta_{\kappa\lambda} + \imath \epsilon_{\kappa\lambda\mu} \sigma^\mu,$$

with $\epsilon_{\kappa\lambda\mu}$ being the totally anti-symmetric Levi-Civita tensor. Sometimes we add the 2×2-unit matrix σ^0 to the set of Pauli matrices. We employ a definition of the spin magnetization that excludes the factor μ_B compared to the physical definition of the spin magnetization. This means that the factor μ_B is inserted as coupling constant between an external magnetic field and the spin magnetization. In contrast to the definition of the density we retain the $-$ sign, due to the negative electronic charge, in the definition of the spin magnetization in order to emphasize that the magnetic moment due to the electronic spin aligns with an external magnetic field. The fundamental single-particle Hamiltonian of this thesis is the Pauli Hamiltonian, obtained by means of the Foldy-Wouthuysen transformation [FW50], i.e. , the weakly-relativistic limit, applied to the Dirac equation. Throughout this thesis we will neglect spin-orbit coupling terms, because they correspond to a higher order relativistic correction ($\frac{1}{c^2}$). Furthermore we will neglect the coupling of the vector potential to the current. This is justified *a posteriori* by the fact that we are using the external magnetic field as a tool to motivate the inclusion of the spin magnetization as a fundamental variable in Spin-Density-Functional Theory. After the inclusion of the spin magnetization as fundamental variable we are considering only systems with a vanishing external magnetic field. Any aberration on the aforementioned conventions will be mentioned explicitly.

Chapter 1

Introduction and guide through the thesis

The advent of quantum theory is one of the most celebrated discoveries in natural science. Since the fundamental equation was laid out by Schrödinger in 1926 [Sch26], numerous phenomena, related to the microscopic structure of matter, could be explained and quantified. Soon it became clear, however, that the solution of the Schrödinger equation for interacting particles is out of reach, except for systems with a only a few degrees of freedom. Even the enormous technological advances in electronics, which themselves were made possible due to the understanding of microscopic physics, did not, and probably will not, enable us to solve the interacting many-body problem exactly.

In their seminal work Hohenberg and Kohn [HK64] proved that it is possible, in principle, to reformulate quantum theory in terms of the electronic density, which only depends on one coordinate in contrast to the wave function which depends on N coordinates if the system is composed of N electrons. In chapter 2 we introduce the fundamental idea and basic principles of Density-Functional Theories. Practical implementations of Density-Functional Theories rely on the idea, due to Kohn and Sham [KS65], to connect a system of interacting electrons to a system of non-interacting electrons. This non-interacting system, dubbed the Kohn-Sham system, incorporates the complications arising due to the interaction of the electrons in an averaged way discussed in chapter 3.

The virtue of Density-Functional Theories is that this mapping of an interacting system onto a non-interacting system can in principle be done exactly. In practice this mapping has to be approximated in form of the so-called exchange-correlation-energy functional. The main routes for the construction of density functionals are described in chapter 4. Since the uniform electron gas is the paradigm for interacting electrons and hence plays an important role in the construction of functionals we review its basic properties in chapter 5.

As suggested by the title, this thesis is focused on the treatment of non-collinear magnetism in Density-Functional Theories. In classical electrodynamics magnetism occurs due to the presence of moving charges, i.e. , charge currents. The experiment conducted by Stern and Gerlach in 1922 [GS22], however, gave the first indication that the electron possesses an intrinsic magnetic moment. They found that a beam of neutral silver atoms is split into two beams by the application of an inhomogeneous magnetic field. This was rather puzzling since if the recently by Bohr proposed quantization of the angular momentum was taken seriously, it seemed strange that the beam was split into two beams that are both deflected by the same amount in opposite directions. From Bohr's quantization of the angular momentum one expects that there should be also one part of the beam that remains unaltered by the inhomogeneous magnetic field. Pauli solved this mystery in 1927 by proposing a modified version of the Schrödinger equation [Pau27] in which he introduced a two component wave function, the so-called Pauli spinor. The two-componentness of the wave function reflects the fact that an electron possesses an intrinsic magnetic moment. In 1928 Dirac proposed his equation unifying special relativity and quantum mechanics [Dir28], from which the Pauli equation emerges in the weakly-relativistic limit and hence explains the appearance of the internal structure of the electron as a necessity following from the compliance of quantum theory with special relativity.

The intrinsic magnetic moment is always present in contrast to the orbital-magnetic moment which is only present if the electron is in a quantum mechanical state that carries a current. This permanent magnetic moment is a rather strange property of the electrons for it does not have a classical analogy. Its strangeness may be exemplified by considering a superposition of a quantum mechanical state representing an intrinsic magnetic moment that points upwards (spin-up) and a quantum mechanical state representing an intrinsic magnetic moment that points downwards (spin-down). One might naively expects that the resulting state has no magnetic moment, but in reality the superposition represents a quantum mechanical state that has a magnetic moment orthogonal to the up-down direction. Considering also the spatial degree of freedom of the electron the situation is even more complicated, because now the meaning of the up-down direction may change in space. A spatially varying intrinsic magnetic moment is the key characteristic of non-collinear magnetism.

In spite of the fact that the interaction between electrons is a charge-charge interaction, i.e., it formally does not involve the intrinsic magnetic moment, it is due to the Pauli-exclusion principle that the intrinsic magnetic moment plays a crucial role in the description of interacting electrons. This was spectacularly demonstrated by Overhauser [Ove62] in his seminal work on the instability of the uniform electron gas w.r.t. the formation of a spin-spiral wave, which represents an explicit example of non-collinear magnetism resulting from interactions between

the electrons. The spin-spiral wave state is the central theme of this thesis. It is quantitatively analyzed employing Hartree-Fock theory and Reduced-Density-Matrix-Functional Theory in chapter 6.

In 1972 von Barth and Hedin [vBH72] extended the charge-only Density-Functional Theory to explicitly include the intrinsic magnetic moment. The inclusion of the spin magnetization as fundamental variable in Spin-Density-Functional Theory not only facilitates the description of systems exposed to an external magnetic field but also enables us to explicitly investigate the influence of interaction on the magnetic structure. Hence in chapter 7 we employ Spin-Density-Functional Theory in order to complement our studies of the spin-spiral-wave state of the uniform electron gas.

In chapter 8 we address the problem of constructing viable approximations to the exchange-correlation-energy functional of Spin-Density-Functional Theory. Most functionals for the description of non-collinear magnetism used presently are ad hoc generalizations of functionals constructed for collinear systems. We demonstrate that it is possible to generalize the well-known Local-Spin-Density Approximation by considering the aforementioned spin-spiral-wave state of the uniform electron gas as reference system. The main result of this thesis is the Spin-Spiral-Wave functional, which may also be viewed as a Spin-Gradient Extension to the Local-Spin-Density Approximation. While by construction it yields exchange-correlation-magnetic fields that are non-collinear w.r.t. the spin magnetization it retains the formal and numerical simplicity of local approximations in Density-Functional Theories.

Chapter 2

Introduction to Density-Functional Theories

Density-Functional Theories (DFTs) aim at the efficient description of many-particle systems. The key idea is to replace the wave function as fundamental variable by one-particle densities, e.g. the charge density. Hohenberg-Kohn-like theorems guarantee that a description in terms of these densities is possible by establishing a one-to-one correspondence between the densities and their corresponding conjugated potentials. Even in the absence of a Hohenberg-Kohn-like theorem it is still possible to obtain a variational scheme for the determination of the ground-state energy and densities through the so-called constrained-search formalism. Aim of this chapter is to clarify the aforementioned features of, and present an introduction to Density-Functional Theories. A thorough introduction to DFTs may be found in [DG90].

2.1 The Hohenberg-Kohn theorem

We consider a many-body Hamiltonian of the form

$$\hat{\mathcal{H}} = \hat{\mathcal{T}} + \hat{\mathcal{V}} + \hat{\mathcal{W}}, \tag{2.1}$$

where $\hat{\mathcal{T}}$ is the kinetic energy and $\hat{\mathcal{V}}$ the external potential. They are referred to as single-particle contributions to the Hamiltonian. $\hat{\mathcal{W}}$ is the contribution due to interactions between the particles. Usually $\hat{\mathcal{W}}$ indicates a two-particle interaction, e.g. the Coulomb repulsion of two charged particles. Here we shall only consider particle-number conserving Hamiltonians, i.e. ,

$$\left[\hat{\mathcal{H}}, \hat{\mathcal{N}}\right] = 0, \tag{2.2}$$

with $\hat{\mathcal{N}}$ being the particle-number operator. Hence we can always choose to diagonalize the Hamiltonian and the particle-number operator simultaneously, leading to the spectral representations

$$\hat{\mathcal{H}} = \sum_{N=0}^{\infty} \sum_{\alpha} |N, \alpha\rangle \, \mathcal{E}_{\alpha}^{N} \, \langle N, \alpha| \,, \tag{2.3}$$

$$\hat{\mathcal{H}} \, |N, \alpha\rangle = \mathcal{E}_{\alpha}^{N} \, |N, \alpha\rangle \,, \tag{2.4}$$

$$\hat{\mathcal{N}} = \sum_{N=0}^{\infty} \sum_{\alpha} |N, \alpha\rangle \, N \, \langle N, \alpha| = \sum_{N=0}^{\infty} N \mathbb{1}_{N}, \tag{2.5}$$

$$\hat{\mathcal{N}} \, |N, \alpha\rangle = N \, |N, \alpha\rangle \,, \tag{2.6}$$

where the quantum numbers N, α label the common eigenstates of the Hamiltonian and the particle-number operator. The quantum number α, labeling the energy levels for a fixed number of particles N, might be discrete, continuous or partially discrete and partially continuous. In practice the determination of the full spectrum for a given number of particles is hardly possible. In fact even the computation of the few lowest-energy eigenstates of an interacting system is not tractable, given the currently available computing facilities, except for systems with a very small number of particles.

One way to approach the problem of calculating properties of an interacting system is to reformulate the theory in terms of more tractable quantities than the state vector or wave function. In their seminal work Hohenberg and Kohn [HK64] suggested the use of the particle density, i.e. , the probability density of finding a particle at a given position, as fundamental variable. The Hohenberg-Kohn theorem in its original version applies to non-degenerate ground states with a fixed number of particles N. It states that the ground-state density

$$n_0(\boldsymbol{r}) = \langle N, 0| \, \hat{\Phi}^{\dagger}(\boldsymbol{r}) \, \hat{\Phi}(\boldsymbol{r}) \, |N, 0\rangle \,, \int \mathrm{d}^3 r \; n_0(\boldsymbol{r}) = N, \tag{2.7}$$

is in one-to-one correspondence with the external potential $\hat{\mathcal{V}}$. This is a very powerful statement in that it allows to view all observables of the quantum system governed by the Hamiltonian $\hat{\mathcal{H}}$, given in Eq. (2.1), as functionals of the ground-state density. This follows from the fact that the external potential is a functional of the ground-state density and therefore, since the kinetic energy and the interaction $\hat{\mathcal{W}}$ are kept fixed, the Hamiltonian is fully determined by its ground-state density. By solving for the eigenstates of the Hamiltonian, we can obtain any observable of the system. In practice, however, the external potential, determined by the position of the nuclei in a molecule or solid, is given and not the ground-state density. It is possible to use the Rayleigh-Ritz variational principle in connection with the Hohenberg-Kohn

theorem in order to determine the ground-state energy and its corresponding density n_0,

$$\mathcal{E}_0 = \inf_{n_0} \langle \Psi\left[n_0\right] | \hat{\mathcal{H}} | \Psi\left[n_0\right] \rangle , \tag{2.8}$$

where the Hamiltonian $\hat{\mathcal{H}}$ is given and $|\Psi\left[n_0\right]\rangle$ is the ground state as a functional of the ground-state density as implied by the Hohenberg-Kohn theorem. This construction is a reformulation of the Rayleigh-Ritz variational principle in terms of ground-state densities instead of N-particle states. The basic idea of DFTs is to take the variation of the energy functional over more manageable quantities, i.e. , the set of ground-state densities. Ground-state densities depend only on one spatial argument whereas the N-particle states depend on N spatial arguments, as can be inferred from writing down the Rayleigh-Ritz variational principle in terms of the position representation of the state, i.e. , the wave function,

$$\begin{aligned} \mathcal{E}_0 = \inf_{\Psi_0} \iint \mathrm{d}^3 r_1 \mathrm{d}^3 r_2 \ \ldots \int \mathrm{d}^3 r_N \\ \times \Psi_0^\dagger(\boldsymbol{r}_1, \boldsymbol{r}_2, \ldots, \boldsymbol{r}_N)\, \hat{\mathcal{H}}(\boldsymbol{r}_1, \boldsymbol{r}_2, \ldots, \boldsymbol{r}_N)\, \Psi_0(\boldsymbol{r}_1, \boldsymbol{r}_2, \ldots, \boldsymbol{r}_N) , \end{aligned} \tag{2.9}$$

$$\hat{\mathcal{H}}(\boldsymbol{r}_1, \boldsymbol{r}_2, \ldots) = \sum_i \left(\tfrac{1}{2} \overleftarrow{\nabla}_i \cdot \overrightarrow{\nabla}_i + V(r_i) \right) + \tfrac{1}{2} \sum_{i,j}^{N} \frac{1}{|\boldsymbol{r}_i - \boldsymbol{r}_j|}. \tag{2.10}$$

For systems with more than 10 particles it is simply impossible to even store a single wave function $\Psi_0(\boldsymbol{r}_1, \boldsymbol{r}_2, \ldots)$. Reformulating the Rayleigh-Ritz variational principle in terms of the fundamental densities comes at the price that the functional dependence on the fundamental variables is not known and therefore has to be approximated in practice. A caveat of the Hohenberg-Kohn theorem is that it establishes a one-to-one correspondence between ground-state densities and an equivalence class of potentials. External potentials are considered equivalent if they differ only by a constant.

2.2 External potentials and the chemical potential

In the following we will discuss the role of a constant variation of the external potential in Hamiltonian Eq. (2.1) in greater detail in order to prepare a different route to obtain the energy as a functional of the density. Let us first consider the ground-state energy as a function of the number of particles

$$\mathcal{E}_0^N = \mathcal{E}(N) \ : \ \mathbb{N} \to \mathbb{R}. \tag{2.11}$$

We assume that this function is convex, i.e. , we have

$$\mathcal{E}(N+1) - \mathcal{E}(N) \geq \mathcal{E}(N) - \mathcal{E}(N-1) , \tag{2.12}$$

which is known as Lieb's conjecture [Lie83]. This is certainly true for a non-interacting fermionic system, because adding particles to the systems requires the occupation of energetically higher single-particle orbitals. Note that it is not assumed that the occupied single-particle orbitals have positive energy, i.e. , the ground-state energy is not a monotonically increasing function w.r.t. the number of particles. The only way to obtain an equality in Eq. (2.12) would be to have degeneracies, or equivalently symmetries, in the systems, because only then two successive additions of particles would change the energy twice by the same amount. In writing down Eq. (2.12) we implicitly relate the ground-state energies at different particle numbers by keeping the external potential fixed for all N. This means that the constant of the external potential appearing in Hamiltonian (2.1) is the same for all N. This can be achieved by setting for finite systems the smallest asymptote of the potential and for periodic systems the average potential to zero. In order to extend definition Eq. (2.11) to non-integer number of particles we borrow the concept of the statistical operator $\hat{\mathcal{D}}$ from statistical quantum mechanics. This concept was born out of the necessity to describe the statistical uncertainty - as opposed to the fundamental Heisenberg uncertainty - present in experiments. On a theoretical level this uncertainty can be taken into account by representing the quantum mechanical system by the aforementioned statistical operator instead of representing it by a state vector $|\Psi\rangle$. The statistical operator itself is defined as a weighted sum over projections on state vectors, i.e. ,

$$\hat{\mathcal{D}} = \sum_i w_i \left|\Psi_i\right\rangle \left\langle\Psi_i\right| \quad , \quad \sum_i w_i = 1. \tag{2.13}$$

Expectation values of a generic operator $\hat{\mathcal{O}}$ are calculated by tracing over $\hat{\mathcal{D}}\hat{\mathcal{O}}$, e.g.

$$\mathcal{E} = \mathrm{Tr}\Big\{\hat{\mathcal{D}}\hat{\mathcal{H}}\Big\} = \sum_i w_i \left\langle\Psi_i\right| \hat{\mathcal{H}} \left|\Psi_i\right\rangle , \tag{2.14}$$

$$N = \mathrm{Tr}\Big\{\hat{\mathcal{D}}\hat{\mathcal{N}}\Big\} = \sum_i w_i \left\langle\Psi_i\right| \hat{\mathcal{N}} \left|\Psi_i\right\rangle . \tag{2.15}$$

Therefore the expectation values of operators for a system described by $\hat{\mathcal{D}}$ are given as weighted averages over the expectation values of the operators w.r.t. the states comprising $\hat{\mathcal{D}}$. Using the statistical operator $\hat{\mathcal{D}}$ we can define a generalized Rayleigh-Ritz variational principle in order to define the minimal energy corresponding to an arbitrary non-integer number of particles $\mathcal{N}$,

$$\mathcal{E}(\mathcal{N}) = \inf_{\hat{\mathcal{D}}_\mathcal{N}} \mathrm{Tr}\Big\{\hat{\mathcal{D}}_\mathcal{N}\hat{\mathcal{H}}\Big\} , \tag{2.16}$$

where the infimum runs over all statistical operators $\hat{\mathcal{D}}_\mathcal{N}$ having $\mathcal{N}$ particles. From Lieb's conjecture (cf. (2.12)) it is evident that only the two ground states with integer particle number just below and above $\mathcal{N}$ can enter in the minimizing statistical operator $\hat{\mathcal{D}}^0_\mathcal{N}$. Appreciating the

linear dependence on the weights $\{w_i\}$ it is straight forward to define a ground-state ensemble representing a system with non-integer number of particles, i.e. ,

$$\hat{\mathcal{D}}^0_{\mathcal{N}=N+\delta} = (1-\delta)\,|N,0\rangle\,\langle N,0| + \delta\,|N+1,0\rangle\,\langle N+1,0| \quad , \quad \delta \in [0,1] \tag{2.17}$$

$$n_0(\boldsymbol{r}) = \mathrm{Tr}\Big\{\hat{\mathcal{D}}^0_{\mathcal{N}=N+\delta}\hat{\Phi}^\dagger(\boldsymbol{r})\,\hat{\Phi}(\boldsymbol{r})\Big\} \quad , \quad \int \mathrm{d}^3r\; n_0\left(\boldsymbol{r}\right) = N+\delta = \mathcal{N}, \tag{2.18}$$

$$\mathcal{E}(\mathcal{N}=N+\delta) = \mathrm{Tr}\Big\{\hat{\mathcal{D}}^0_{\mathcal{N}=N+\delta}\hat{\mathcal{H}}\Big\} = (1-\delta)\,\mathcal{E}(N) + \delta\mathcal{E}(N+1)\,. \tag{2.19}$$

We can investigate the ground-state energy as a function of $\mathcal{N}$ further by looking at its Legendre transformation

$$\mathrm{LT}\{\mathcal{E}\}(\mu) = -\inf_{\mathcal{N}}\{\mathcal{E}(\mathcal{N}) - \mu\mathcal{N}\} = -\mathcal{E}(\mu)\,. \tag{2.20}$$

The Legendre transform $-\mathcal{E}(\mu)$ contains the same information as the original function $\mathcal{E}(\mathcal{N})$, but now this information is encoded in a function of μ, the conjugated variable to the number of particles $\mathcal{N}$. Explicitly it returns for a given μ the ground-state energy $\mathcal{E}(N) - \mu N$ with N being integer. In fact for a range $\mu \in [\mu_-, \mu_+]$ the same N is picked, as can be deduced from the piecewise linear behavior of the function $\mathcal{E}(N) - \mu N$ (cf. Fig. 2.1). This is a consequence of the fact that the Legendre transformation maps points to lines and vice versa. Rewriting the term added to the ground-state energy in Eq. (2.20)

$$-\mu\mathcal{N} = -\int \mathrm{d}^3r\; \mu n_0(\boldsymbol{r})\,, \tag{2.21}$$

and comparing it to

$$\mathrm{Tr}\Big\{\hat{\mathcal{D}}_{\mathcal{N}}\hat{\mathcal{V}}\Big\} = \int \mathrm{d}^3r\; V(\boldsymbol{r})\, n_0(\boldsymbol{r})\,, \tag{2.22}$$

it seems that we re-introduced a constant to the potential. It is important to realize that this constant is not the arbitrary constant of the Hohenberg-Kohn theorem, but it is only arbitrary within an interval $[\mu_-, \mu_+]$ for a given number of particles N. The range of the interval $[\mu_-, \mu_+]$ depends crucially on the ground-state energies at different particle numbers for the system under investigation and therefore on the external potential $\hat{\mathcal{V}}$ itself. The physical interpretation of μ is evident: it is the chemical potential, i.e. , the potential between the system and a reservoir of particles. The ambiguity of the chemical potential stems from the fact that the ground-state energy of the system with N particles may differ from the ground-state energy of the system with $N+1$ particles by a finite amount. This energy difference has to be overcome by changing the chemical potential in order to provide the necessary energy to add a particle to the system.

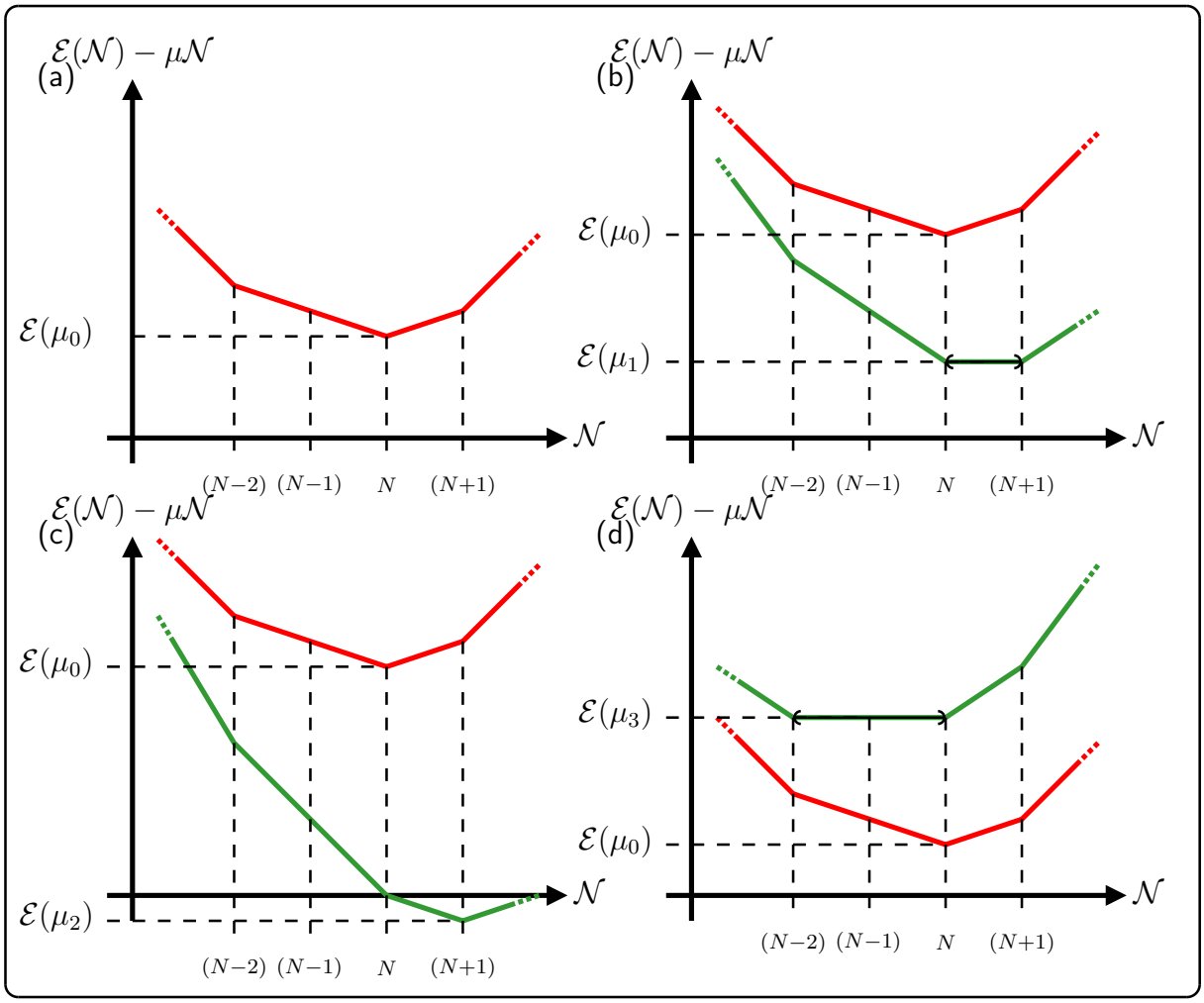

Figure 2.1: The panels (a)-(d) show $\mathcal{E}(\mathcal{N}) - \mu\mathcal{N}$ as a function of the particle number $\mathcal{N}$ for various μ. The values of $\mathcal{E}(\mu) = \inf_{\mathcal{N}} \{\mathcal{E}(\mathcal{N}) - \mu\mathcal{N}\}$ are indicated by the horizontal dashed lines.

Panel (a): $\mathcal{E}(\mathcal{N}) - \mu_0\mathcal{N}$ is minimal for $\mathcal{N} = N$.

Panel (b): $\mu_1 = A_N$, i.e. , the electron affinity of the N-particle system. For this specific value μ_1 the function $\mathcal{E}(\mathcal{N}) - \mu_1\mathcal{N}$ is minimal for $\mathcal{N} \in [N, N+1]$. The minimal value is $\mathcal{E}(\mu_1)$.

Panel (c): $\mu_2 > A_N$ and less than the electron affinity of the $(N+1)$-particle system A_{N+1}. $\mathcal{E}(\mathcal{N}) - \mu_2\mathcal{N}$ is minimal for $\mathcal{N} = (N+1)$ as long as $\mu \in [A_N, A_{N+1}]$. Comparison to the situation in panel (b) exemplifies the duality of points and lines by means of the Legendre transformation (cf. Eq. (2.20)).

Panel (d): $\mu_3 = I_N$, i.e. , the ionization potential of the N-particle system. Here we sketch a situation in which the second ionization potential I_{N-1} is equal to I_N. This occurs for example if the two highest occupied orbitals of a non-interacting system are degenerate. Accordingly $\mathcal{E}(\mathcal{N}) - \mu_3\mathcal{N}$ is minimal for $\mathcal{N} \in [N-2, N]$.

2.3 The Levy-Lieb constrained-search formalism

In Eq. (2.8) we defined the ground-state energy as the infimum of an energy functional $E_{\mathrm{HK}}[n_0]$ over all ground-state densities n_0. The energy functional can be split into two contributions,

$$\begin{aligned} E_{\mathrm{HK}}[n_0] &= \langle \Psi\,[n_0]|\,\hat{\mathcal{H}}\,|\Psi\,[n_0]\rangle && (2.23)\\ &= \langle \Psi\,[n_0]|\,\hat{\mathcal{T}}+\hat{\mathcal{W}}\,|\Psi\,[n_0]\rangle + \langle \Psi\,[n_0]|\,\hat{\mathcal{V}}\,|\Psi\,[n_0]\rangle \\ &= F_{\mathrm{HK}}[n_0] + \int \mathrm{d}^3r\; V(\boldsymbol{r})\, n_0(\boldsymbol{r})\,, && (2.24) \end{aligned}$$

i.e. , a contribution linear in n_0 and V and the remainder $F_{\mathrm{HK}}[n_0]$. $F_{\mathrm{HK}}[n_0]$ is called the universal functional, because it does not depend on the external potential and therefore does not depend on the system under investigation.

Alternatively the ground-state energy can be obtained by minimizing the expectation value of the Hamiltonian $\hat{\mathcal{H}}$ over all statistical operators $\hat{\mathcal{D}}$,

$$\mathcal{E}_0 = \inf_{\hat{\mathcal{D}}} \mathrm{Tr}\Big\{\hat{\mathcal{D}}\left(\hat{\mathcal{H}}-\mu\hat{\mathcal{N}}\right)\Big\}\,. \tag{2.25}$$

Note that we introduced the chemical potential in order to take the infimum over all statistical operators in contrast to Eq. (2.16). This is only compatible with Eq. (2.16) if Lieb's conjecture is true. A neat idea to derive the energy as a functional of the density was independently proposed by Levy [Lev82] and Lieb [Lie83]. They suggested the so-called constrained-search formalism. It is implemented by splitting the minimization process into two parts: in a first step the minimization is carried out over all statistical operators yielding a prescribed density $n(\boldsymbol{r})$, and then, in a second step, the minimum over all densities is found,

$$\begin{aligned} \mathcal{E}_0 &= \inf_n \left\{ \inf_{\hat{\mathcal{D}}\to n} \mathrm{Tr}\Big\{\hat{\mathcal{D}}\left(\hat{\mathcal{H}}-\mu\hat{\mathcal{N}}\right)\Big\}\right\} && (2.26)\\ &= \inf_n \left\{ \inf_{\hat{\mathcal{D}}\to n} \mathrm{Tr}\Big\{\hat{\mathcal{D}}\left(\hat{\mathcal{T}}+\hat{\mathcal{W}}\right)\Big\} + \int \mathrm{d}^3r\;\left(V(\boldsymbol{r})-\mu\right) n(\boldsymbol{r})\right\} \\ &= \inf_n \left\{ F_{\mathrm{L}}[n] + \int \mathrm{d}^3r\;\left(V(\boldsymbol{r})-\mu\right) n(\boldsymbol{r})\right\}. && (2.27) \end{aligned}$$

Accordingly we have an alternative definition of the energy as a functional of the density (cf. Eq. (2.24))

$$E_{\mathrm{L}}[n] = F_{\mathrm{L}}[n] + \int \mathrm{d}^3r\;\left(V(\boldsymbol{r})-\mu\right) n(\boldsymbol{r})\,. \tag{2.28}$$

The main difference between Eq. (2.24) and Eq. (2.28) is the domain of the functional. The Levy-Lieb energy functional is defined over all densities n stemming from a statistical operator

$\hat{\mathcal{D}}$, whereas the Hohenberg-Kohn energy functional is defined over all ground-state densities n_0. Densities obtained from $\hat{\mathcal{D}}$ via

$$n(\boldsymbol{r}) = \mathrm{Tr}\Big\{\hat{\mathcal{D}}\hat{\Phi}^\dagger(\boldsymbol{r})\,\hat{\Phi}(\boldsymbol{r})\Big\}\,, \tag{2.29}$$

are called ensemble N-representable. Since the set of ensemble N-representable densities encompasses the set of ground-state densities, the Levy-Lieb functional is defined over a broader set of densities. Note that, in the constrained-search formalism, no reference to the Hohenberg-Kohn theorem is made and therefore the Levy-Lieb functional does not rely on the Hohenberg-Kohn theorem. Minimizing both functionals yields the same ground-state energy. In the following we will denote the universal functional by $F[n]$, but the distinction between the Hohenberg-Kohn universal functional and the Levy-Lieb universal functional will be recalled if necessary.

2.4 The universal functional and conjugated variables

In the previous section we introduced the energy functional

$$E[n] = F[n] + \int \mathrm{d}^3r\ \left(V(\boldsymbol{r}) - \mu\right) n(\boldsymbol{r})\,. \tag{2.30}$$

When minimized over all densities n for a fixed potential V we obtain the ground-state energy of the system characterized by the external potential V. Hence we can view the ground-state energy $\mathcal{E}_0$ as a functional of the external potential, i.e. ,

$$\mathcal{E}_0[V] = \inf_n \Big\{ F[n] + \int \mathrm{d}^3r\ \left(V(\boldsymbol{r}) - \mu\right) n(\boldsymbol{r}) \Big\}\,. \tag{2.31}$$

Comparing Eq. (2.31) to the definition of the Legendre transformation (cf. Eq. (2.20)) we can identify $\mathcal{E}_0[V]$ as the (negative) Legendre transform of the universal functional. Since the Legendre transformation is its own inverse, much like the Fourier transformation, the universal functional is the Legendre transform of $-\mathcal{E}_0[V]$. The duality relation

$$-\mathcal{E}_0[V] \quad \overset{\text{Legendre transformation}}{\Longleftrightarrow} \quad F[n]\,, \tag{2.32}$$

proposes the notion of n and V being conjugated variables. Using the concept of conjugated variables we can motivate the extension of the charge-density-only DFT proposed by Hohenberg and Kohn to include more densities as fundamental variables. If the Hamiltonian $\hat{\mathcal{H}}$ includes additional external potentials, e.g. a magnetic field, vector potential, etc. , we include the densities that couple linearly to the additional potentials, e.g. the spin magnetization, the charge-current density, etc. , as fundamental variables. The physical motivation to introduce

more fundamental variables even if there are no additional external potentials is closely related to spontaneous symmetry breaking. If the symmetry breaking is accompanied by the appearance of a characteristic order parameter, the inclusion of the order parameter as a fundamental variable facilitates the construction of approximations to the universal functional considerably. As an example we consider magnetic systems. They are characterized by a a non-vanishing spin-magnetization

$$\boldsymbol{m}(\boldsymbol{r}) = -\operatorname{Tr}\Big\{\hat{\mathcal{D}}\hat{\Phi}^{\dagger}(\boldsymbol{r})\,\boldsymbol{\sigma}\hat{\Phi}(\boldsymbol{r})\Big\}\,. \tag{2.33}$$

Taking into account that the spin-magnetization directly couples to an external magnetic field, we now consider Hamiltonians of the form

$$\hat{\mathcal{H}} = \hat{\mathcal{T}} + \hat{\mathcal{V}} + \hat{\mathcal{B}} + \hat{\mathcal{W}}, \tag{2.34}$$

where $\hat{\mathcal{B}}$ is the contribution to the Hamiltonian due to the presence of an external magnetic field $\boldsymbol{B}$. Employing the constrained-search formalism we can define the ground-state energy as a functional of the external potentials

$$\mathcal{E}_0[V,\boldsymbol{B}] = \inf_{n,\boldsymbol{m}}\left\{F[n,\boldsymbol{m}] + \int \mathrm{d}^3r\ \left(V(\boldsymbol{r})-\mu\right)n(\boldsymbol{r}) - \int \mathrm{d}^3r\ \mu_{\mathrm{B}}\boldsymbol{B}(\boldsymbol{r})\cdot\boldsymbol{m}(\boldsymbol{r})\right\}, \tag{2.35}$$

$$F[n,\boldsymbol{m}] = \inf_{\hat{\mathcal{D}}\to\{n,\boldsymbol{m}\}} \operatorname{Tr}\Big\{\hat{\mathcal{D}}\left(\hat{\mathcal{T}}+\hat{\mathcal{W}}\right)\Big\}, \tag{2.36}$$

where we implicitly defined a new universal functional in terms of the fundamental variables $\{n,\boldsymbol{m}\}$. The DFT including besides the charge density n also the spin magnetization $\boldsymbol{m}$ was first proposed by von Barth and Hedin [vBH72]. In contrast to the construction via the constrained-search formalism, given in Eq. (2.35), Barth and Hedin followed the original approach of Hohenberg and Kohn and proved the Hohenberg-Kohn theorem for Spin-Density-Functional Theory (SDFT).

This illustrates the general scheme for the construction of various DFTs. First a new density, helping to characterize the system, is added as fundamental variable. Then, the potential conjugated to the new density is added to the Hamiltonian even if this additional potential is set to zero later on. Next a new universal functional is defined via the constrained-search formalism. Finally we minimize

$$\begin{aligned} E[n,\boldsymbol{m},\ldots] = F[n,\boldsymbol{m},\ldots] &+ \int \mathrm{d}^3r\ \left(V(\boldsymbol{r})-\mu\right)n(\boldsymbol{r}) \\ &- \int \mathrm{d}^3r\ \mu_{\mathrm{B}}\boldsymbol{B}(\boldsymbol{r})\cdot\boldsymbol{m}(\boldsymbol{r}) + \int \mathrm{d}^3r\ \ldots, \end{aligned} \tag{2.37}$$

in order to obtain the ground-state energy and densities $\{n_0,\boldsymbol{m}_0,\ldots\}$ corresponding to the system characterized by the external potentials $\{V,\boldsymbol{B},\ldots\}$. As already mention in the discussion of the constrained-search formalism, no reference to any Hohenberg-Kohn-like theorem

has been made. This means that the determination of the ground-state energy by minimizing $E[n,\ldots]$ does not rely on establishing a one-to-one correspondence between densities and the conjugated external potentials. However, once we are interested in observables other then the ground-state energy, such a one-to-one correspondence has to be proved in order to justify the calculation of the observables in terms of the densities.

2.5 Reduced-Density-Matrix-Functional Theory

Reduced-Density-Matrix-Functional Theory (RDMFT) might be viewed as the most general static DFT. As discussed, new DFTs can be devised by including more densities as fundamental variables. A natural way to extend the original charge-density DFT is suggested by the equation of motion (EOM) for the density, i.e. , the continuity equation. It relates changes in the density to the divergence of the charge-current density

$$\boldsymbol{j}(\boldsymbol{r}) = \tfrac{1}{2i}\,\mathrm{Tr}\Big\{\hat{\mathcal{D}}\left(\hat{\Phi}^\dagger(\boldsymbol{r})\left(\nabla\hat{\Phi}(\boldsymbol{r})\right) - \left(\nabla\hat{\Phi}^\dagger(\boldsymbol{r})\right)\hat{\Phi}(\boldsymbol{r})\right)\Big\} \tag{2.38}$$

$$= \lim_{\boldsymbol{r}'\to\boldsymbol{r}} \tfrac{1}{2i}\left(\nabla - \nabla'\right)\mathrm{Tr}\Big\{\hat{\mathcal{D}}\hat{\Phi}^\dagger(\boldsymbol{r}')\,\hat{\Phi}(\boldsymbol{r})\Big\}. \tag{2.39}$$

The EOM for the current, i.e. , the momentum-balance equation, relates the changes in the current to the divergence of a stress tensor

$$\underline{\boldsymbol{T}}(\boldsymbol{r}) = \tfrac{1}{4}\,\mathrm{Tr}\Big\{\hat{\mathcal{D}}\left(\nabla\hat{\Phi}^\dagger(\boldsymbol{r})\right)\otimes_{sym}\left(\nabla\hat{\Phi}(\boldsymbol{r})\right)\Big\} \tag{2.40}$$

$$= \lim_{\boldsymbol{r}'\to\boldsymbol{r}} \tfrac{1}{4}\left(\nabla\otimes\nabla' + \nabla'\otimes\nabla\right)\mathrm{Tr}\Big\{\hat{\mathcal{D}}\hat{\Phi}^\dagger(\boldsymbol{r}')\,\hat{\Phi}(\boldsymbol{r})\Big\}, \tag{2.41}$$

plus terms depending on two-particle densities if a two-particle interaction is present in the Hamiltonian. The trace of the stress tensor, obtained by replacing the tensor product $\otimes$ by the inner product $\cdot$, is the well-known kinetic-energy density

$$T(\boldsymbol{r}) = \tfrac{1}{2}\,\mathrm{Tr}\Big\{\hat{\mathcal{D}}\left(\nabla\hat{\Phi}^\dagger(\boldsymbol{r})\right)\cdot\left(\nabla\hat{\Phi}(\boldsymbol{r})\right)\Big\}, \tag{2.42}$$

$$= \lim_{\boldsymbol{r}'\to\boldsymbol{r}} \tfrac{1}{2}\left(\nabla\cdot\nabla'\right)\mathrm{Tr}\Big\{\hat{\mathcal{D}}\hat{\Phi}^\dagger(\boldsymbol{r}')\,\hat{\Phi}(\boldsymbol{r})\Big\}. \tag{2.43}$$

The scheme proposed by the hierarchy of the EOMs would be to devise a corresponding hierarchy of DFTs. As suggested by Eqs. (2.39), (2.41), (2.43), this hierarchy of DFTs would include more and more higher order gradients of the object

$$\gamma(\boldsymbol{r};\boldsymbol{r}') = -\,\mathrm{Tr}\Big\{\hat{\mathcal{D}}:\hat{\Phi}(\boldsymbol{r})\,\hat{\Phi}^\dagger(\boldsymbol{r}'):\Big\}, \tag{2.44}$$

the so-called one-particle-reduced density matrix (1RDM). The limiting case of including gradients up to infinite order would then correspond to choosing the 1RDM itself as fundamental

variable. The 1RDM may be considered the non-local generalization of the usual density. In Eq. (2.44) we employ the normal ordering operator : : in order to carry over the internal structure - representing the spin degrees of freedom - of the fundamental Pauli fields $\hat{\Phi}$ to the definition of the 1RDM. Note that the product $\hat{\Phi}^\dagger(\boldsymbol{r}')\,\hat{\Phi}(\boldsymbol{r})$ is a scalar field operator whereas the product

$$\hat{\Phi}(\boldsymbol{r})\,\hat{\Phi}^\dagger(\boldsymbol{r}') = \begin{pmatrix}\hat{\phi}_\uparrow(\boldsymbol{r})\\ \hat{\phi}_\downarrow(\boldsymbol{r})\end{pmatrix}\begin{pmatrix}\hat{\phi}^\dagger_\uparrow(\boldsymbol{r}') & \hat{\phi}^\dagger_\downarrow(\boldsymbol{r}')\end{pmatrix} = \begin{pmatrix}\hat{\phi}_\uparrow(\boldsymbol{r})\,\hat{\phi}^\dagger_\uparrow(\boldsymbol{r}') & \hat{\phi}_\downarrow(\boldsymbol{r})\,\hat{\phi}^\dagger_\uparrow(\boldsymbol{r}')\\ \hat{\phi}_\uparrow(\boldsymbol{r})\,\hat{\phi}^\dagger_\downarrow(\boldsymbol{r}') & \hat{\phi}_\downarrow(\boldsymbol{r})\,\hat{\phi}^\dagger_\downarrow(\boldsymbol{r}')\end{pmatrix},$$

is a 2×2-valued field operator. The normal-ordering operator forces the fundamental field operators $\hat{\phi}(\boldsymbol{r})$,$\hat{\phi}^\dagger(\boldsymbol{r}')$ to switch places.

In his seminal paper [Gil75] Gilbert derived the Hohenberg-Kohn theorem for the 1RDM. The Gilbert theorem states that the 1RDM is in one-to-one correspondence with the ground-state wave function. In contrast to the Hohenberg-Kohn theorem the Gilbert theorem does not establish a one-to-one correspondence between the the 1RDM and its conjugated *non-local* potential. As a consequence only ground-state expectation values can be written as functionals of the ground-state 1RDM $\gamma_0(\boldsymbol{r};\boldsymbol{r}')$. Excited state properties, such as transition matrix elements, are in principle out of reach. The construction of an energy functional is most efficiently done by employing the constrained-search formalism,

$$E[\gamma] = W[\gamma] + \iint \mathrm{d}^3r\mathrm{d}^3r'\; H_0(\boldsymbol{r}';\boldsymbol{r})\,\gamma(\boldsymbol{r};\boldsymbol{r}')\,, \tag{2.45}$$

$$W[\gamma] = \inf_{\hat{\mathcal{D}}\to\gamma} \mathrm{Tr}\Big\{\hat{\mathcal{D}}\hat{\mathcal{W}}\Big\}\,, \tag{2.46}$$

$$\begin{aligned}\iint \mathrm{d}^3r\mathrm{d}^3r'\; H_0(\boldsymbol{r}';\boldsymbol{r})\,\gamma(\boldsymbol{r};\boldsymbol{r}') = \int \mathrm{d}^3r\,\Big(&\,\mathrm{tr}\Big\{\lim_{\boldsymbol{r}'\to\boldsymbol{r}}\nabla'\cdot\nabla\gamma(\boldsymbol{r};\boldsymbol{r}')\Big\}\\ &+\tfrac{1}{c}\boldsymbol{A}(\boldsymbol{r})\cdot\mathrm{tr}\Big\{\lim_{\boldsymbol{r}'\to\boldsymbol{r}}\tfrac{1}{2i}\left(\nabla-\nabla'\right)\gamma(\boldsymbol{r};\boldsymbol{r}')\Big\}\\ &-\mu_\mathrm{B}\boldsymbol{B}\left(\boldsymbol{r}\right)\cdot\mathrm{tr}\{\boldsymbol{\sigma}\gamma(\boldsymbol{r};\boldsymbol{r})\}\\ &+\left(\tfrac{1}{2c^2}|\boldsymbol{A}(\boldsymbol{r})\,|^2+V(\boldsymbol{r})-\mu\right)\mathrm{tr}\{\gamma(\boldsymbol{r};\boldsymbol{r})\}\,\Big),\end{aligned} \tag{2.47}$$

where we introduced $\mathrm{tr}\,\{\ldots\}$ to indicate the trace over the internal (spin) degree of freedom as opposed to the trace over Fock space denoted by $\mathrm{Tr}\,\{\ldots\}$. Eq. (2.47) emphasizes that the non-local nature of the 1RDM makes it the conjugated density to all single-particle contributions of the Hamiltonian. It follows that the universal functional $W[\gamma]$ only includes contributions due to particle-particle interactions. Most notably, in contrast to the original DFT, the kinetic energy is explicitly known as a functional of the 1RDM

$$T[\gamma] = \tfrac{1}{2}\int \mathrm{d}^3r\;\mathrm{tr}\Big\{\lim_{\boldsymbol{r}'\to\boldsymbol{r}}\nabla'\cdot\nabla\gamma(\boldsymbol{r};\boldsymbol{r}')\Big\}\,. \tag{2.48}$$

The 1RDM itself can be viewed as an operator acting in the single-particle Hilbert space. Its hermiticity can readily be derived from Eq. (2.44). Accordingly it can be represented by its spectral decomposition,

$$\gamma(\boldsymbol{r};\boldsymbol{r}') = \sum_j n_j \Phi_j(\boldsymbol{r})\, \Phi_j^\dagger(\boldsymbol{r}')\,, \tag{2.49}$$

with $\Phi_j(\boldsymbol{r})$ being two-component Pauli spinors. The eigenvalues n_j are usually called occupation numbers and the eigenstates $\Phi_j(\boldsymbol{r})$ natural orbitals. The 1RDM is a non-local 2×2 matrix in spin space. Its spatial diagonal contains the charge density and the spin-magnetization,

$$\rho(\boldsymbol{r}) = \gamma(\boldsymbol{r};\boldsymbol{r}) = \tfrac{1}{2}\begin{pmatrix} n(\boldsymbol{r}) - m_3(\boldsymbol{r}) & -m_1(\boldsymbol{r}) + \imath m_2(\boldsymbol{r}) \\ -m_1(\boldsymbol{r}) - \imath m_2(\boldsymbol{r}) & n(\boldsymbol{r}) + m_3(\boldsymbol{r}) \end{pmatrix} = \tfrac{1}{2}\rho_\alpha(\boldsymbol{r})\,\sigma^\alpha, \tag{2.50}$$

with $\alpha = 0,1,2,3$. Coleman derived necessary and sufficient conditions for an 1RDM to be ensemble N-representable [Col63]. Quite naturally for an $\mathcal{N}$-particle system the occupation numbers have to sum up to $\mathcal{N}$, and for fermionic systems each occupation number has to be between zero and one, i.e. ,

$$\begin{aligned} &\gamma(\boldsymbol{r};\boldsymbol{r}') = \sum_j n_j \Phi_j(\boldsymbol{r})\, \Phi_j^\dagger(\boldsymbol{r}') \quad , \quad \sum_j n_j = \mathcal{N} \quad , \quad n_j \in [0,1] \\ &\Longleftrightarrow \\ &\gamma(\boldsymbol{r};\boldsymbol{r}') = -\operatorname{Tr}\Big\{\hat{\mathcal{D}} :\hat{\Phi}(\boldsymbol{r})\,\hat{\Phi}^\dagger(\boldsymbol{r}'):\Big\}\,. \end{aligned} \tag{2.51}$$

An important concept for 1RDMs is the notion of a pinned state. Pinned states are natural orbitals with occupation number equal to zero or one. In fact the corresponding natural orbitals are only defined up to a unitary transformation among themselves, since they form a set of states with degenerate eigenvalues. From Coleman's proof it is evident that natural orbitals with occupation number equal to one, are orbitals that appear in every Slater determinant present in the expansion of the states comprising the statistical operator. Similarly natural orbitals with occupation number equal to zero do not appear in any Slater determinant contributing to $\hat{\mathcal{D}}$. The simplest example for $\hat{\mathcal{D}}$ would be a projection on a single Slater determinant. Since the N-particle ground state of a non-interacting system can be written as a single Slater determinant, a non-interacting 1RDM can be written as

$$\gamma_s(\boldsymbol{r};\boldsymbol{r}') = \sum_{j\ \mathrm{occ.}} \Phi_j(\boldsymbol{r})\, \Phi_j^\dagger(\boldsymbol{r}')\,. \tag{2.52}$$

The non-interacting ground-state Slater determinant consists of the lowest N eigenstates of the Hamiltonian. We conclude that:

1) A non-interacting 1RDM has only pinned states.

2) The ambiguity w.r.t. the natural orbitals can be resolved for non-interacting systems by recognizing that the natural orbitals can be chosen to be simultaneous eigenstates of $\hat{\mathcal{H}}_0$. Clearly, in this way, the ambiguity can only be removed for non-degenerate eigenstates of $\hat{\mathcal{H}}_0$.
3) A non-interacting 1RDM is idempotent, i.e. ,

$$\int \mathrm{d}^3 r'' \; \gamma_s(\boldsymbol{r};\boldsymbol{r}'')\,\gamma_s(\boldsymbol{r}'';\boldsymbol{r}') = \gamma_s(\boldsymbol{r};\boldsymbol{r}')\,. \tag{2.53}$$

The idempotency of γ_s can be used to construct an explicit counter-example to the one-to-one correspondence between non-local potentials and 1RDMs. Assume that γ_s is the ground-state 1RDM for some Hamiltonian $\hat{\mathcal{H}}_0$. Now construct a Hamiltonian $\hat{\mathcal{H}}_0' = \hat{\mathcal{H}}_0 - \hat{\mathcal{U}}$, by subtracting a non-local potential of the form

$$U(\boldsymbol{r}';\boldsymbol{r}) = U\gamma_s(\boldsymbol{r}';\boldsymbol{r})\,. \tag{2.54}$$

Since $\hat{\mathcal{H}}_0$ and $\hat{\mathcal{U}}$ are diagonalized by the same set of orbitals, also $\hat{\mathcal{H}}_0'$ shares the set of eigenstates (and thereby natural orbitals) with $\hat{\mathcal{H}}_0$. Only the N-lowest eigenstates are shifted by U, i.e. , we found a ground state 1RDM γ_s that corresponds to two different non-local potentials (single-particle Hamiltonians) H_0 and H_0'.

Chapter 3

Aspects of Density-Functional Theories

The great success of DFTs can largely be attributed to an ingenious idea due to Kohn and Sham [KS65]. They proposed the introduction of a fictitious non-interacting system, that has the same ground-state density as the interacting system under investigation. Since non-interacting systems can be treated numerically exactly, only the difference of the universal functional for interacting systems and the universal functional for non-interacting systems (i.e. , the kinetic energy) has to be approximated. This difference is the so-called Hartree-exchange-correlation-energy functional. Excluding from this difference furthermore the Hartree contribution, which is explicitly known in terms of the density, the exchange-correlation (xc) functional is readily defined. The xc energy is a much smaller quantity than the full universal kinetic-plus-interaction energy. In addition the Kohn-Sham scheme provides an efficient algorithm to minimize the energy functional by self-consistently solving a single-particle Schrödinger equation. Furthermore the Kohn-Sham system may be interpreted as a crude approximation to functionals for all observables implied by an energy functional. In fact it is common practice to discuss and analyze the band structure or density of states of the Kohn-Sham system. This chapter is intended to provide an overview of the Kohn-Sham system by focusing on the three aforementioned features. Moreover we discuss the peculiarities of RDMFT compared to common DFTs, because one may view the absence of a Kohn-Sham system as the most notable difference between DFT and RDMFT for practical implementations.

3.1 The Kohn-Sham System

In Chapter 2 we introduced the energy functional

$$E[n] = F[n] + \int \mathrm{d}^3 r \; V(\boldsymbol{r})\, n(\boldsymbol{r})\,, \tag{3.1}$$

for interacting systems. Similarly we can introduce an energy functional for non-interacting systems,

$$E_s[n] = T_s[n] + \int \mathrm{d}^3 r \; V_s(\boldsymbol{r})\, n(\boldsymbol{r})\,, \tag{3.2}$$

$$T_s[n] = \inf_{\hat{\mathcal{D}}\to n} \mathrm{Tr}\Big\{\hat{\mathcal{D}}\hat{\mathcal{T}}\Big\}\,. \tag{3.3}$$

In their seminal paper [KS65] Kohn and Sham proposed to consider a non-interacting system, dubbed the Kohn-Sham (KS) system, that has the same ground-state density n_0 as the interacting system. Imposing that the variation of the interacting and the non-interacting energy functional both vanish at the common ground-state density, a relation between the potential of the non-interacting system V_s, the KS potential, and the potential of the interacting system V is readily obtained,

$$\begin{aligned}
\frac{\delta E[n_0]}{\delta n(\boldsymbol{r})} &= \frac{\delta E_s[n_0]}{\delta n(\boldsymbol{r})} = 0 \\
\frac{\delta F[n_0]}{\delta n(\boldsymbol{r})} + V(\boldsymbol{r}) &= \frac{\delta T_s[n_0]}{\delta n(\boldsymbol{r})} + V_s(\boldsymbol{r})\,, \\
\Rightarrow \quad V_s(\boldsymbol{r}) &= V(\boldsymbol{r}) + v_{Hxc}\,(\boldsymbol{r})\,, \qquad (3.4)\\
v_{Hxc}(\boldsymbol{r}) &= \frac{\delta E_{Hxc}[n_0]}{\delta n(\boldsymbol{r})} \qquad (3.5)\\
E_{Hxc}[n] &= F[n] - T_s[n]\,. \qquad (3.6)
\end{aligned}$$

In Eq. (3.6) we defined the Hartree-exchange-correlation energy functional. Furthermore its functional derivative, the Hartree-xc potential Eq. (3.5), was used in Eq. (3.4) to relate the external potential V of the interacting system to the external potential V_s of the KS system. Commonly the classical contribution due to interactions is separated out, because it is an explicitly known and large contribution to $E_{Hxc}[n]$. For Coulomb-interacting electrons this corresponds to the Hartree energy,

$$E_H[n] = \tfrac{1}{2} \iint \mathrm{d}^3 r \mathrm{d}^3 r' \; \frac{n(\boldsymbol{r})\, n(\boldsymbol{r}')}{|\boldsymbol{r} - \boldsymbol{r}'|}. \tag{3.7}$$

Therefore the energy functional Eq. (3.1) has been split into the contributions,

$$E[n] = T_s[n] + \int \mathrm{d}^3 r \; V(\boldsymbol{r})\, n(\boldsymbol{r}) + E_H[n] + E_{xc}[n]\,, \tag{3.8}$$

where we have introduced the xc-energy functional $E_{xc}[n] = E_{Hxc}[n] - E_H[n]$ which has to be approximated in practice. All other contributions are either explicitly known as functionals of the density ($E_H[n]$) or implicitly given in terms of an algorithm ($T_s[n]$). Though being a small contribution to the energy, $E_{xc}[n]$ is critical for the description of the electronic structure of interacting systems. Hence in the past decades enormous effort went into the construction of approximations to the xc-energy functional.

3.2 Representability and derivative discontinuities

Equating the variation of the non-interacting energy functional with the variation of the interacting energy functional in Eq. (3.4) requires some caution. We implicitly assume that both functionals are defined over the same set of densities. Following Hohenberg and Kohn [HK64] the functionals are defined over the set of ground-state densities of non-interacting and interacting systems, respectively. Densities that come from the ground state of some local external potential are called V-representable. The KS scheme is based on the assumption that the sets of non-interacting V-representable and interacting V-representable densities are identical.

In Eq. 3.3 we have employed the constrained-search formalism to define the non-interacting kinetic energy functional $T_s[n]$. This approach to derive an energy functional is always defined over ensemble N-representable densities (cf. Sec. 2.3) and therefore the domains of the non-interacting energy functional and the interacting energy functional are the same. Hence we can relate an external potential U of a non-interacting system to an external potential V of an interacting system, by requiring that the variations of the respective energy functionals are equal for all ensemble N-representable densities, i.e. ,

$$\frac{\delta E_V[n]}{\delta n(\boldsymbol{r})} = \frac{\delta E_{s,U[n]}[n]}{\delta n(\boldsymbol{r})}, \tag{3.9}$$

$$U_V[n](\boldsymbol{r}) = V(\boldsymbol{r}) + v_H[n](r) + v_{xc}[n](\boldsymbol{r})\,, \tag{3.10}$$

$$v_H[n](\boldsymbol{r}) = \frac{\delta E_H[n]}{\delta n(\boldsymbol{r})} = \int \mathrm{d}^3 r' \, \frac{n(\boldsymbol{r}')}{|\boldsymbol{r} - \boldsymbol{r}'|}, \tag{3.11}$$

$$v_{xc}[n](\boldsymbol{r}) = \frac{\delta E_{xc}[n]}{\delta n(\boldsymbol{r})}. \tag{3.12}$$

In the previous equations we indicate implied dependencies on densities and potentials carefully. The functional on the r.h.s. of Eq. (3.9) depends only on the density, whereas the l.h.s. also depends on the external potential V. Therefore Eq. (3.9) defines U as a functional of V and n. As can be seen from Eq. (3.10) the functional dependence on V is simple. The n-dependent part of U can be split further into the functional derivative of the Hartree energy and the functional derivative of the xc-energy, the so-called exchange-correlation potential. Evaluated

at the ground-state density n_0 of V we get

$$U_V[n_0](\boldsymbol{r}) = V_s[n_0](\boldsymbol{r})\,, \tag{3.13}$$

i.e. , the KS potential.

A second subtlety is related to the use of functional derivatives. In fact, at least for functionals defined over the ensemble N-representable densities, we have already seen that the energy exhibits kinks (cf. Fig. 2.1 in Sec. 2.2). This means that for variations within the set of densities represented by the ground-state ensemble Eq. (2.17), the functional derivative of the universal functional behaves discontinuously. We can parameterize these variations by

$$n_\delta(\boldsymbol{r}) = \Theta(-\delta)\,|\delta| n_-(\boldsymbol{r}) + (1-|\delta|)\,n_0(\boldsymbol{r}) + \Theta(\delta)\,|\delta| n_+(\boldsymbol{r})\,, \tag{3.14}$$

where n_-,n_0 and n_+ are the $(N-1)$-, N- and $(N+1)$-particle ground-state densities, respectively, and $\Theta(x)$ is the Heaviside step function. Having parameterized the functional variation in terms of $\delta \in [-1,1]$, we note that for a non-interacting system the energy change is proportional to the energy of the highest occupied orbital ϵ_{HOMO} for $\delta \in (-1,0)$ and to the energy of the lowest unoccupied orbital ϵ_{LUMO} for $\delta \in (0,1)$ of the N-particle system, respectively. Accordingly, the non-interacting energy functional exhibits a derivative discontinuity at $\delta = 0$, or equivalently at an integer number of particles, i.e. ,

$$\begin{aligned}\Delta_s &= \left.\frac{\delta E_s[n]}{\delta n(\boldsymbol{r})}\right|_{\delta\to 0^+} - \left.\frac{\delta E_s[n]}{\delta n(\boldsymbol{r})}\right|_{\delta\to 0^-} \\ &= \left.\frac{\delta T_s[n]}{\delta n(\boldsymbol{r})}\right|_{\delta\to 0^+} - \left.\frac{\delta T_s[n]}{\delta n(\boldsymbol{r})}\right|_{\delta\to 0^-} = \epsilon_{\mathrm{LUMO}} - \epsilon_{\mathrm{HOMO}}.\end{aligned} \tag{3.15}$$

Similarly we can analyze the change of the interacting energy functional under the variations defined in Eq. (3.14). Now the energy change is proportional to the energy difference between the ground-state energy of the N- and the $(N-1)$-particle system, i.e. , the negative ionization potential $-I = \mathcal{E}(N) - \mathcal{E}(N-1)$, for $\delta \in (-1,0)$ and to the energy difference of the $(N+1)$- and the N-particle system, i.e. the negative electron affinity $-A = \mathcal{E}(N+1) - \mathcal{E}(N)$, for $\delta \in (0,1)$. The derivative discontinuity of the interacting energy functional at $\delta = 0$, the so-called fundamental gap, is given by

$$\begin{aligned}\Delta &= \left.\frac{\delta E[n]}{\delta n(\boldsymbol{r})}\right|_{\delta\to 0^+} - \left.\frac{\delta E[n]}{\delta n(\boldsymbol{r})}\right|_{\delta\to 0^-} = I - A \\ &= \Delta_s + \left.\frac{\delta E_{xc}[n]}{\delta n(\boldsymbol{r})}\right|_{\delta\to 0^+} - \left.\frac{\delta E_{xc}[n]}{\delta n(\boldsymbol{r})}\right|_{\delta\to 0^-} \\ &= \Delta_s + \Delta_{xc}.\end{aligned} \tag{3.16}$$

In Eq. (3.16) we introduced the derivative discontinuity of the xc-energy functional. It was first discussed by Perdew et al. in 1982 [PPLB82]. The derivative discontinuity is important

if one aims at a quantitative prediction of the fundamental gap using DFT. This is reflected by the fact the fundamental gap obtained from approximations to the xc functional that do not exhibit a derivative discontinuity are systematically too small. A prominent example of materials where the derivative discontinuity is essential are the so-called Mott insulators. These are extended systems predicted to be conductors by band theory, an effective non-interacting theory, but are known to be insulators experimentally. The physical mechanism behind this is an interaction-induced localization of the electrons. In the framework of DFTs Mott insulators can be understood in terms of the decomposition of the fundamental gap into the KS gap Δ_s and the xc gap Δ_{xc}. Systems with a vanishing KS gap but a non-vanishing Δ_{xc} are the reflection of the aforementioned characteristics of a Mott insulator in the context of KS DFTs. The vanishing KS gap implies that the non-interacting systems, yielding the same ground-state density as the interacting system, is a conductor but the non-vanishing xc gap ensures that the true fundamental gap is finite. An approximate xc-energy functional, devised to properly describe strongly correlated systems, should therefore show a derivative discontinuity.

Finally we remark that the existence of the functional derivative of the universal functional was established on the set of non-interacting V-representable densities by Englisch and Englisch [EE84a, EE84b] if only finite dimensional Hilbert spaces are considered. Together with the results in [CCR85] that on a lattice each ensemble N-representable density is arbitrary close to a non-interacting V-representable density, on might consider the representability question to be settled for all practical purposes, because a numerical implementation of the KS scheme will always discretize the single-particle Hilbert space. For a detailed study of the V-representability issue in DFTs the interested reader is referred to the work of Lammert (e.g. [Lam10] and references therein).

3.3 The self-consistent Kohn-Sham scheme

The introduction of the KS system suggests a neat way to find the ground-state density for an interacting system exposed to an external potential V. Given an approximation for the xc-energy functional we can compute the variation of the energy functional at a trial density $n^{(k)}(\boldsymbol{r})$. We determine the potential $U^{(k)}(\boldsymbol{r})$ of a non-interacting system for which the variation of the non-interacting energy functional equals to the variation of the interacting energy functional. This is precisely the potential defined in Eq. (3.10). It is given in terms of the variation of the xc-energy functional (cf. Eq. (3.12)). Then the non-interacting ground-state density $n^{(k+1)}(\boldsymbol{r})$ corresponding to the potential $U^{(k)}$ is obtained by solving the Schrödinger equation for the non-interacting problem. This density $n^{(k+1)}(\boldsymbol{r})$ is used as new guess for the ground-state density of the interacting system. Again, for this new trial density the variation

of the interacting energy functional can be evaluated, which in turn yields a new potential $U^{(k+1)}$. Repeating this cycle until self-consistency yields a density that produces a potential U via Eq. (3.10), to which the density itself is the corresponding ground-state density. This scheme is illustrated in Fig. 3.1. The self-consistent potential is the KS potential V_s and the self-consistent density is the ground-state density n_0 of the interacting system characterized by the external potential V. Hence we can find the ground-state density and energy of an interacting system by a self-consistent solution of a non-interacting system,

$$\left(-\tfrac{1}{2}\nabla\cdot\nabla + V_s[n](\boldsymbol{r})\right)\Phi_k^s(\boldsymbol{r}) = \epsilon_k\Phi_k^s(\boldsymbol{r})\,, \tag{3.17}$$

$$\sum_{k=1}^{N}\Phi_k^{s\,\dagger}(\boldsymbol{r})\,\Phi_k^s(\boldsymbol{r}) = n(\boldsymbol{r})\,, \tag{3.18}$$

$$V_s[n](\boldsymbol{r}) = V(\boldsymbol{r}) + v_H[n](\boldsymbol{r}) + v_{xc}[n](\boldsymbol{r})\,, \tag{3.19}$$

$$v_{xc}[n](\boldsymbol{r}) = \frac{\delta E_{xc}[n]}{\delta n(\boldsymbol{r})}. \tag{3.20}$$

Since derivatives of the energy functional are used, the KS scheme might be viewed as a gradient algorithm to minimize (approximations to) the non-linear energy functional. The KS scheme is the most widely used implementation of DFTs nowadays. It yields a non-interacting ground state which reproduces the interacting densities. Hence it is possible to determine any observable by simply evaluating the expectation value of the corresponding operator using the KS ground state. The expectation values themselves have to be taken with caution, because they are always expectation values of a single Slater determinant. It is imperative to realize that even for the exact energy functional only those expectation values that are explicitly obtained from the fundamental densities are exact. The KS scheme is not a shortcut to obtain arbitrary expectation values as a functional of the density. Only if the system under investigation is weakly correlated, i.e. , in the expansion of the ground state one Slater determinant is dominant, and the dominant Slater determinant is very close to the KS Slater determinant, expectation values of the KS ground state may be good approximations to the true expectation values.

3.4 Peculiarities of Reduced-Density-Matrix-Functional Theory

RDMFT, which was introduced in the previous chapter as the most general DFT, shows some peculiarities if one tries to devise a KS scheme. It was already pointed out (cf. Sec. 2.5) that it is not possible to establish a one-to-one correspondence between the 1RDM and the single-particle contribution $\hat{\mathcal{H}}_0$ to the Hamiltonian $\hat{\mathcal{H}}$. In addition it was realized by Coleman [Col63]

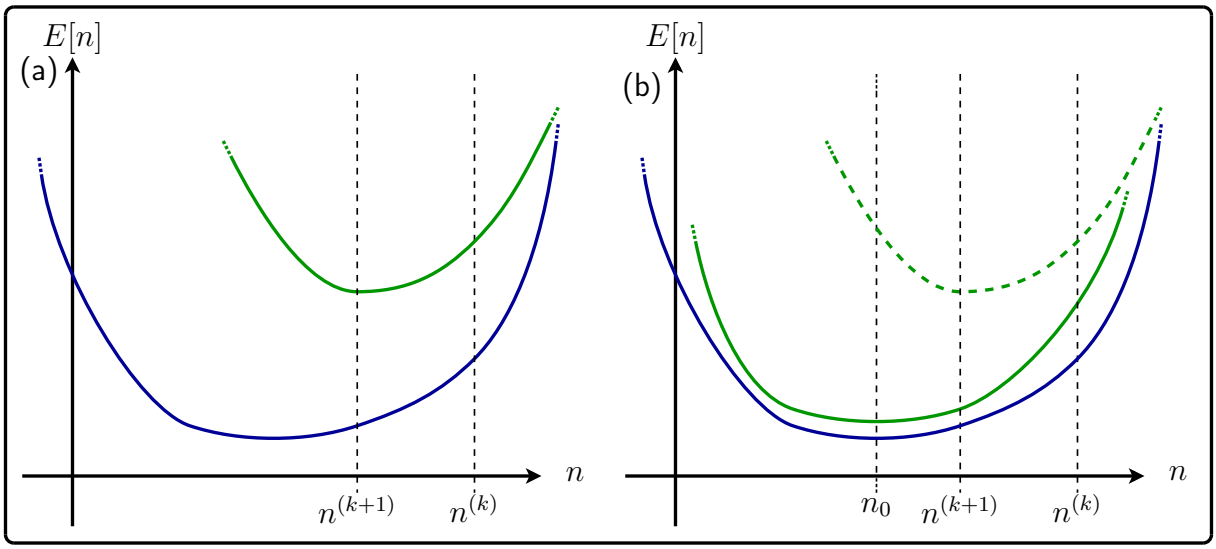

Figure 3.1: Visualization of the KS minimization procedure. The interacting energy functional is depicted by the blue curve.
Panel (a): A non-interacting system is found for which the corresponding non-interacting energy functional (green curve) has the same variation (slope) as the interacting energy functional at the trial density $n^{(k)}$. The determination of the ground-state density of this non-interacting system via the solution of the single-particle Schrödinger equation yields a new trial density $n^{(k+1)}$.
Panel (b): The energy functional of the non-interacting system obtained in the previous minimization step is shown as the dashed green curve. A new non-interacting system whose energy functional has the same slope as the interacting system at density $n^{(k+1)}$ is found (green curve). In the presented example the solution of the Schrödinger equation for the new non-interacting system yields the ground-state density n_0 of the interacting system.

that an interacting 1RDM cannot be equal to a non-interacting 1RDM. The eigenstates of a non-interacting system are always single Slater determinants, whereas eigenstates of interacting systems are superpositions of Slater determinants. Any single Slater determinant, however, yields an idempotent 1RDM (cf. Eq. (2.53)), i.e. , a 1RDM with occupation numbers either 0 or 1. An interacting eigenstate always produces an 1RDM with occupation numbers $n_j \in [0,1]$. Therefore the construction of a KS scheme along the lines outlined before is not possible. It fails because non-interacting V-representable 1RDMs do not overlap with interacting V-representable 1RDMs. As a consequence the minimization of the energy functional in RDMFT, i.e. ,

$$E[\gamma] = \iint \mathrm{d}^3r \mathrm{d}^3r' \; H_0(\boldsymbol{r}';\boldsymbol{r})\,\gamma(\boldsymbol{r};\boldsymbol{r}') + W[\gamma]\,, \tag{3.21}$$

has to be carried out directly. In order to ensure that the variations of the energy functional Eq. (3.21) are taken only over ensemble N-representable 1RDMs, one usually rewrites the functional in terms of the occupation numbers and natural orbitals defined in Eqs. (2.49),(2.51), i.e.

$$E[\{n_j, \Phi_j\}] = \sum_j n_j \int \mathrm{d}^3 r \; \Phi_j^\dagger(\boldsymbol{r}) \left\{ \tfrac{1}{2} \overleftarrow{\nabla} \cdot \overrightarrow{\nabla} + V(\boldsymbol{r}) \right\} \Phi_j(\boldsymbol{r}) + W[\{n_j, \Phi_j\}] \,. \tag{3.22}$$

Then one varies over the occupation numbers $\{n_j\}$, while ensuring the ensemble N-representability constraints $0 \leq n_j \leq 1$ and $\sum_j n_j = \mathcal{N}$, and over the natural orbitals. Since the natural orbitals are eigenstates of the hermitian operator $\gamma(\boldsymbol{r}; \boldsymbol{r}')$, they have to stay orthogonal under variations in order to ensure ensemble N-representability of the variation.

Chapter 4

Functionals in Density-Functional Theories

The applicability of DFTs depends crucially on the derivation of good approximation to the xc-energy functional. Already in their paper [KS65] introducing the KS scheme Kohn and Sham suggested an approximation for $E_{xc}[n]$, the so-called Local-Density Approximation. In subsequent years a plethora of functionals of increasing complexity was derived. In this chapter we briefly discuss various types of approximations. It will become clear that concerning functionals there will be a tradeoff between accuracy and complexity. Explicit density functionals are easier to implement and the numerical effort is small enough to investigate large systems, e.g. complex molecules or compound materials. Implicit functionals, that rely on the Kohn Sham implementation of DFTs tend to provide more accurate energies and exhibit exact features like derivative discontinuities, usually not present in explicit density functionals. Accordingly they are better suited for the description of systems where correlations play an important role, but the numerical effort is much bigger than for explicit density functionals. Finally we see that, again, RDMFT shows peculiarities when compared to standard DFTs. As already mentioned in Sec. 3.4 it is not possible to devise a Kohn-Sham scheme for RDMFT, so one might suspect that all functionals should be explicit functionals of the 1RDM. Nonetheless most approximate functionals known to date are implicit functionals of the 1RDM, because the spectral decomposition of the 1RDM (cf. Eq. (2.49)) suggest to represent the 1RDM in terms of the natural orbitals and occupation numbers.

4.1 Local and semi-local approximations

Kohn and Sham proposed a first approximation for the xc-energy functional in their seminal paper [KS65] introducing the KS construction. It can be motivated as follows. We choose to write the xc-energy in terms of an xc-energy density $\tilde{\varepsilon}_{xc}$,

$$E_{xc}[n] = \int \mathrm{d}^3 r \; \tilde{\varepsilon}_{xc}(\boldsymbol{r}) = \int \mathrm{d}^3 r \; n(\boldsymbol{r})\, \varepsilon_{xc}(\boldsymbol{r})\,. \tag{4.1}$$

In Eq. (4.1) we further decided to write the xc-energy density in terms of the xc-energy per particle ε_{xc} times the density, because the density is our fundamental variable. The energy per particle at position $\boldsymbol{r}$ is determined from a reference system where the density has the same value everywhere in space. This is the uniform electron gas, i.e. , a system of interacting electrons exposed to a constant external potential. The constant potential determines the number of electrons per unit volume and therefore by varying the constant potential and calculating the xc-energy per particle one obtains $\varepsilon_{xc}^{\mathrm{unif}}(n)$. The so-called Local-Density Approximation (LDA) is defined by evaluating $\varepsilon_{xc}^{\mathrm{unif}}(n)$ at the local value of the electron density, i.e. ,

$$E_{xc}^{\mathrm{LDA}}[n] = \int \mathrm{d}^3 r \; n(\boldsymbol{r})\, \varepsilon_{xc}^{\mathrm{unif}}(n(\boldsymbol{r}))\,. \tag{4.2}$$

The application of the LDA depends on the availability of the function $\varepsilon_{xc}^{\mathrm{unif}}(n)$. Being the prototypical interacting system, the uniform electron gas is probably one of the most studied systems in condensed matter physics. Seminal contributions were the calculation of its ground-state energy by means of perturbation theory pioneered by Macke [Mac50], Pines [Pin53] and Gell-Mann and Brueckner [GMB57], which is referred to as the Random-Phase Approximation (RPA). Though being perturbative in nature, derived from the assumed smallness of the interaction contribution, the ground breaking idea was to resum the most divergent terms in the perturbation series. This led to a renormalization of the contributions that are second order in the interaction. Thereby the divergence of the second order contribution was eliminated by grouping it with the most divergent terms of higher order contributions to the perturbation series. In the following years various attempts were made to improve the results by including more diagrams in the expansion for the ground-state energy of the uniform electron gas. In 1980 the Quantum Monte Carlo approach was used by Ceperley and Alder [CA80] to obtain the exact dependence of the energy per particle as a function of the density.

In order to improve the LDA one usually tries to determine the local xc-energy per particle not just from the density of the system at position $\boldsymbol{r}$, but also from the density around position $\boldsymbol{r}$. Viewing the density around position $\boldsymbol{r}$ as given through its Taylor expansion, it is evident that this corresponds to the determination of ε_{xc} through the density and its gradients. First

attempts using perturbative techniques to devise gradient-dependent functionals, the so-called gradient-expansion approximations (GEAs) failed in practice. This might be compared to the divergence of the xc-energy of the uniform electron gas if the perturbative expansion is cut at low orders. In many-body perturbation theory this is overcome by resumming the most divergent terms. For the construction of gradient-dependent xc-functionals a solution was obtained in a different way, but it may be viewed as the analogon of a resummation.

A heavily used concept in the construction of functionals is the so-called xc-hole. Assuming a rescaled interaction $\lambda\hat{\mathcal{W}}$, and a λ-dependent external potential that is supposed to guarantee that the same ground-state density is obtained for any value of λ, the Hartree-xc energy can be written in terms of a coupling constant integration by employing the Hellmann-Feynmann theorem,

$$E_{Hxc}[n] = \tfrac{1}{2}\int_0^1 \mathrm{d}\lambda \iint \mathrm{d}^3r_1\mathrm{d}^3r_2 \, \frac{P_\lambda\,[n](\boldsymbol{r}_1,\boldsymbol{r}_2)}{|\boldsymbol{r}_1-\boldsymbol{r}_2|}, \tag{4.3}$$

$$P_\lambda\,[n]\,(\boldsymbol{r}_1,\boldsymbol{r}_2) = \mathrm{Tr}\Big\{\hat{\mathcal{D}}_0^{(\lambda)}[n]\,\hat{\phi}^\dagger(\boldsymbol{r}_1)\,\hat{\phi}^\dagger(\boldsymbol{r}_2)\,\hat{\phi}(\boldsymbol{r}_2)\,\hat{\phi}(\boldsymbol{r}_1)\Big\}, \tag{4.4}$$

$$g_\lambda[n](\boldsymbol{r}_1,\boldsymbol{r}_2) = \frac{P_\lambda\,[n]\,(\boldsymbol{r}_1,\boldsymbol{r}_2)}{n(\boldsymbol{r}_1)\,n(\boldsymbol{r}_2)}, \tag{4.5}$$

where $P_\lambda\,[n]\,(\boldsymbol{r}_1,\boldsymbol{r}_2)$ is the pair density and $g_\lambda[n](\boldsymbol{r}_1,\boldsymbol{r}_2)$ the pair correlation function determined from the ground-state statistical operator $\hat{\mathcal{D}}_0^{(\lambda)}$ corresponding to the density n at interaction strength λ implied by the Hohenberg-Kohn theorem. Excluding the Hartree contribution we obtain the xc-energy functional expressed through the xc-hole n_{xc},

$$\begin{aligned} E_{xc}[n] &= \tfrac{1}{2}\int_0^1 \mathrm{d}\lambda \iint \mathrm{d}^3r_1\mathrm{d}^3r_2 \, \frac{n(\boldsymbol{r}_1)\,n(\boldsymbol{r}_2)}{|\boldsymbol{r}_1-\boldsymbol{r}_2|}\,(g_\lambda[n](\boldsymbol{r}_1,\boldsymbol{r}_2)-1) \\ &= \tfrac{1}{2}\int \mathrm{d}^3r\; n(\boldsymbol{r}) \int \mathrm{d}^3u \, \frac{n_{xc}[n](\boldsymbol{r},\boldsymbol{r}+\boldsymbol{u})}{u}, \end{aligned} \tag{4.6}$$

$$n_{xc}[n](\boldsymbol{r},\boldsymbol{r}+\boldsymbol{u}) = \int_0^1 \mathrm{d}\lambda\; n(\boldsymbol{r}+\boldsymbol{u})\,(g_\lambda[n](\boldsymbol{r},\boldsymbol{r}+\boldsymbol{u})-1)\,, \tag{4.7}$$

$$n_x[n](\boldsymbol{r},\boldsymbol{r}+\boldsymbol{u}) = n(\boldsymbol{r}+\boldsymbol{u})\,(g_0[n](\boldsymbol{r},\boldsymbol{r}+\boldsymbol{u})-1)\,, \tag{4.8}$$

$$n_c[n](\boldsymbol{r},\boldsymbol{r}+\boldsymbol{u}) = n_{xc}[n](\boldsymbol{r},\boldsymbol{r}+\boldsymbol{u}) - n_x[n](\boldsymbol{r},\boldsymbol{r}+\boldsymbol{u})\,. \tag{4.9}$$

In Eqs. (4.8),(4.9) we furthermore defined the partitioning of the xc-hole into the exchange hole n_x and the correlation hole n_c. Eq. (4.6) suggests the notion of the xc-energy being the interaction of the density with its surrounding xc-hole. From the sum rule (cf. Appendix 4 of [GV05]) of the pair correlation function $g(\boldsymbol{r}_1,\boldsymbol{r}_2)$ the following exact properties can be

derived,

$$n_x(\boldsymbol{r}, \boldsymbol{r}+\boldsymbol{u}) \leq 0, \tag{4.10}$$

$$\int \mathrm{d}^3u\; n_x(\boldsymbol{r}, \boldsymbol{r}+\boldsymbol{u}) = -1, \tag{4.11}$$

$$\int \mathrm{d}^3u\; n_c(\boldsymbol{r}, \boldsymbol{r}+\boldsymbol{u}) = 0. \tag{4.12}$$

The LDA is obtained by approximating n_{xc} by the xc-hole of the uniform electron gas

$$n_{xc}[n](\boldsymbol{r}, \boldsymbol{r}+\boldsymbol{u}) \approx n_{xc}^{\mathrm{unif}}(\boldsymbol{u}; n(\boldsymbol{r}))\,. \tag{4.13}$$

Since, in this case, n_{xc} is approximated by the xc-hole of a physical system, this approximation fulfills conditions Eqs. (4.10),(4.11),(4.12). The GEAs improved the small $\boldsymbol{u}$ behavior compared to the LDA approximation Eq. (4.13), but lead to an oscillatory behavior for large $\boldsymbol{u}$ which results in the violation of Eqs. (4.10),(4.11),(4.12). This is resolved in the so-called generalized gradient approximations (GGAs) by cutting off the spurious large-$\boldsymbol{u}$ limit. First steps in this direction were taken by Langreth and Perdew [LP80] and culminated in, among others, the PBE [PBE96] and the BLYP [Bec88, LYP88] xc-energy functionals. Independent on how the specific approximation is obtained, GGAs can be casted into the functional form

$$\begin{aligned} E_{xc}^{\mathrm{GGA}}[n] &= \int \mathrm{d}^3r\; n(\boldsymbol{r})\, \varepsilon_{xc}^{\mathrm{GGA}}(n(\boldsymbol{r})\,, |\nabla n(\boldsymbol{r})\,|) \\ &= \int \mathrm{d}^3r\; n(\boldsymbol{r})\, \varepsilon_{xc}^{\mathrm{unif}}(n(\boldsymbol{r}))\,(1 + G_{xc}(n(\boldsymbol{r})\,, |\nabla n(\boldsymbol{r})\,|))\,, \end{aligned} \tag{4.14}$$

where we introduced the function $G_{xc}(n, |\nabla n|)$ denoting the gradient corrections w.r.t. the LDA Eq. (4.2).

4.2 Orbital functionals

The functionals introduced so far are explicit functionals of the fundamental densities. Using the KS scheme introduced in the previous section we can define energy functionals that are implicit functionals of the fundamental densities, because they are defined in terms of properties of the KS system. Usually this means that the functional is defined in terms of the KS orbitals Φ_j^s and therefore these functionals are dubbed orbital functionals (cf. [GKKG00] for a review). A specific example is the exact-exchange-energy functional (EXX),

$$E_{xc}^{\mathrm{EXX}}[n] = -\tfrac{1}{2}\sum_{j=1}^{N}\sum_{k=1}^{N} \iint \mathrm{d}^3r_1 \mathrm{d}^3r_2\; \frac{\left(\Phi_j^{s\dagger}(\boldsymbol{r}_1)\,\Phi_k^s(\boldsymbol{r}_1)\right)\left(\Phi_k^{s\,\dagger}(\boldsymbol{r}_2)\,\Phi_j^s(\boldsymbol{r}_2)\right)}{|\boldsymbol{r}_1 - \boldsymbol{r}_2|}. \tag{4.15}$$

4.2.1 The optimized-effective-potential method

Since orbital functionals depend only implicitly on the density the evaluation of the xc-potential is rather involved compared to explicit density functionals. The result for the xc-potential stemming from the EXX functional Eq. (4.15) was first obtained by Sharp and Horton and numerically evaluated by Talman and Shadwick [TS76]. The first calculation going beyond exact-exchange were performed by Grabo and Gross [GG95]. Here we shall restrict ourselves to the spin-independent derivation,

$$\begin{aligned} v_{xc}(\boldsymbol{r}) &= \frac{\delta E_{xc}[n]}{\delta n(\boldsymbol{r})} \\ &= \sum_k \int \mathrm{d}^3x \, \left(\frac{\delta E_{xc}[n]}{\delta \phi_k^s(\boldsymbol{x})} \frac{\delta \phi_k^s(\boldsymbol{x})}{\delta n(\boldsymbol{r})} + h.c. \right) \\ &= \sum_k \iint \mathrm{d}^3x \mathrm{d}^3y \, \left(\frac{\delta E_{xc}[n]}{\delta \phi_k^s(\boldsymbol{x})} \frac{\delta \phi_k^s(\boldsymbol{x})}{\delta V_s(\boldsymbol{y})} + h.c. \right) \frac{\delta V_s(\boldsymbol{y})}{\delta n(\boldsymbol{r})}, \end{aligned} \tag{4.16}$$

where we recognize $\frac{\delta V_s(\boldsymbol{y})}{\delta n(\boldsymbol{r})}$ as the inverse of the static density-density response function of the KS system. From first order perturbation theory we get

$$\begin{aligned} \frac{\delta \phi_k^s(\boldsymbol{x})}{\delta V_s(\boldsymbol{r})} &= \sum_{j \neq k} \frac{\phi_j^s(\boldsymbol{x}) \, \phi_j^{s\dagger}(\boldsymbol{r})}{\epsilon_k - \epsilon_j} \phi_k^s(\boldsymbol{r}) \\ \Rightarrow \quad \chi_s(\boldsymbol{x}, \boldsymbol{r}) &= \frac{\delta n(\boldsymbol{x})}{\delta V_s(\boldsymbol{r})} \\ &= \sum_{k=1}^{N} \left(\phi_k^{s\dagger}(\boldsymbol{x}) \, \frac{\delta \phi_k^s(\boldsymbol{x})}{\delta V_s(\boldsymbol{r})} + \frac{\delta \phi_k^{s\dagger}(\boldsymbol{x})}{\delta V_s(\boldsymbol{r})} \phi_k^s(\boldsymbol{x}) \right) \\ &= \sum_{k=1}^{N} \sum_{j \neq k} \left(\frac{\phi_k^{s\dagger}(\boldsymbol{x}) \, \phi_j^s(\boldsymbol{x}) \, \phi_j^{s\dagger}(\boldsymbol{r}) \, \phi_k^s(\boldsymbol{r})}{\epsilon_k - \epsilon_j} + h.c. \right). \end{aligned} \tag{4.17}$$

Multiplying Eq. (4.16) by $\int \mathrm{d}^3r \, \chi_s(\boldsymbol{r}, \boldsymbol{r}')$ and bringing all terms on one side we finally arrive at the so-called optimized-effective-potential (OEP) equations,

$$0 = \sum_{k=1}^{N} \left(\phi_k^{s\dagger}(\boldsymbol{r}) \, \psi_k(\boldsymbol{r}) + h.c. \right), \tag{4.18}$$

$$\psi_k(\boldsymbol{r}) = \sum_{j \neq k} \frac{\phi_j^s(\boldsymbol{r})}{\epsilon_k - \epsilon_j} \int \mathrm{d}^3r' \, \left(\phi_j^{s\dagger}(\boldsymbol{r}') \, v_{xc}(\boldsymbol{r}') \, \phi_k^s(\boldsymbol{r}') - \phi_j^{s\dagger}(\boldsymbol{r}') \, \frac{\delta E_{xc}[n]}{\delta \phi_k^{s\dagger}(\boldsymbol{r}')} \right), \tag{4.19}$$

where we introduced the orbital shifts ψ_k. An alternative derivation of the OEP equations can be obtained by considering a generic energy functional given in terms of single-particle orbitals $\{\phi_k\}$ that result from a non-interacting system characterized by some external potential $\hat{\mathcal{V}}$. If we minimize this energy functional w.r.t. the external potential $\hat{\mathcal{V}}$, an optimized-effective

potential $V_{\mathrm{OEP}}(\boldsymbol{r})$ is determined requiring

$$\left.\frac{\delta E_{\mathrm{OEP}}[\{\phi_k\,[V]\}]}{\delta V(\boldsymbol{r})}\right|_{V=V_{\mathrm{OEP}}} = 0, \tag{4.20}$$

hence the name optimized-effective-potential method.

The total energy functional in the EXX approximation Eq. (4.15) is formally equivalent to the Hartree-Fock (HF) energy expression, which is obtained by evaluating the expectation value of the interacting Hamiltonian $\hat{\mathcal{H}}$ using a single Slater determinant $|\Phi_0\rangle$ constructed from the single-particle orbitals Φ_j,

$$E_{\mathrm{HF}}[\{\Phi_j\}] = \langle\Phi_0|\,\hat{\mathcal{H}}\,|\Phi_0\rangle = \langle\Phi_0|\,\hat{\mathcal{T}}+\hat{\mathcal{V}}\,|\Phi_0\rangle + \langle\Phi_0|\,\hat{\mathcal{W}}\,|\Phi_0\rangle \tag{4.21}$$

$$= \sum_{j=1}^{N}\int \mathrm{d}^3r\;\Phi_j^\dagger(\boldsymbol{r})\left(\tfrac{1}{2}\overleftarrow{\nabla}\cdot\overrightarrow{\nabla}+V(\boldsymbol{r})\right)\Phi_j(\boldsymbol{r}) \tag{4.22}$$

$$+\tfrac{1}{2}\sum_{j=1}^{N}\sum_{k=1}^{N}\iint \mathrm{d}^3r_1\mathrm{d}^3r_2\;\frac{\left(\Phi_j^\dagger(\boldsymbol{r}_1)\,\Phi_j(\boldsymbol{r}_1)\right)\left(\Phi_k^\dagger(\boldsymbol{r}_2)\,\Phi_k(\boldsymbol{r}_2)\right)}{|\boldsymbol{r}_1-\boldsymbol{r}_2|} \tag{4.23}$$

$$-\tfrac{1}{2}\sum_{j=1}^{N}\sum_{k=1}^{N}\iint \mathrm{d}^3r_1\mathrm{d}^3r_2\;\frac{\left(\Phi_j^\dagger(\boldsymbol{r}_1)\,\Phi_k(\boldsymbol{r}_1)\right)\left(\Phi_k^\dagger(\boldsymbol{r}_2)\,\Phi_j(\boldsymbol{r}_2)\right)}{|\boldsymbol{r}_1-\boldsymbol{r}_2|}. \tag{4.24}$$

In Eq. (4.23) we identify the Hartree energy, already introduced in Eq. (3.7) in the framework of DFT, for a density given in terms of the orbitals comprising the single Slater determinant $|\Phi_0\rangle$, i.e. ,

$$n(\boldsymbol{r}) = \langle\Phi_0|\,\hat{\Phi}^\dagger(\boldsymbol{r})\,\hat{\Phi}(\boldsymbol{r})\,|\Phi_0\rangle = \sum_{j=1}^{N}\Phi_j^\dagger(\boldsymbol{r})\,\Phi_j(\boldsymbol{r})\,.$$

The crucial difference between Eq. (4.15) and Eqs. (4.22), (4.23), (4.24) is that the Φ_j^s are orbitals of a non-interacting Hamiltonian with a local external potential, whereas the orbitals Φ_j in HF theory are obtained by minimizing $E_{HF}[\{\Phi_j\}]$ only under the constraint that the orbitals are normalized, i.e. ,

$$0 = \frac{\delta}{\delta\Phi_j^\dagger(\boldsymbol{r})}\left(E_{HF}[\{\Phi_j\}] - \sum_{k=1}^{N}\epsilon_k\int \mathrm{d}^3r'\;\Phi_k^\dagger(\boldsymbol{r}')\,\Phi_k(\boldsymbol{r}')\right). \tag{4.25}$$

Carrying out the functional derivative w.r.t. the orbitals we obtain

$$\begin{aligned}\epsilon_j \Phi_j(\boldsymbol{r}) &= \left(-\tfrac{1}{2}\nabla^2 + V(\boldsymbol{r})\right) \Phi_j(\boldsymbol{r}) + V_H(\boldsymbol{r})\, \Phi_j(\boldsymbol{r}) \\ &\quad - \int \mathrm{d}^3 r'\; U_F(\boldsymbol{r};\boldsymbol{r}')\, \Phi_j(\boldsymbol{r}')\,, \qquad (4.26)\end{aligned}$$

$$V_H(\boldsymbol{r}) = \sum_{k=1}^{N} \int \mathrm{d}^3 r'\; \frac{\Phi_k^\dagger(\boldsymbol{r}')\, \Phi_k(\boldsymbol{r}')}{|\boldsymbol{r} - \boldsymbol{r}'|}, \qquad (4.27)$$

$$U_F(\boldsymbol{r};\boldsymbol{r}') = \sum_{k=1}^{N} \frac{\Phi_k(\boldsymbol{r})\, \Phi_k^\dagger(\boldsymbol{r}')}{|\boldsymbol{r} - \boldsymbol{r}'|}. \qquad (4.28)$$

Eq. (4.26) is the single-particle HF equation which has to be solved self-consistently in order to find stationary points of the HF-energy functional. This single-particle Schrödinger equation is similar to the Kohn-Sham equation introduced in the previous chapter (cf. Eq. (3.17)). However, the effective potential in HF theory contains the Fock potential $U_F(\boldsymbol{r};\boldsymbol{r}')$, which is a non-local external potential. Orthogonality of the orbitals can be inferred *a posteriori*, because the single-particle Hamiltonian Eq. (4.26) is still a hermitian operator. Since the EXX-energy functional is minimized under an additional constraint, i.e. , that the orbitals are restricted to be eigenstates of an effective Hamiltonian with a *local* potential, it possibly yields a higher total energy than the HF-energy functional.

4.3 Functionals in Reduced-Density-Matrix-Functional Theory

Remembering that the 1RDM obtained from a single Slater determinant $|\Phi_0\rangle$ is idempotent, i.e. , the occupation numbers are either 0 or 1, we can replace $\sum_{j=1}^{N} \to \sum_j n_j$ in the definition of the HF-energy functional Eq. (4.21),

$$\begin{aligned}E_{\mathrm{HF}}[\{n_j, \Phi_j\}] &= \sum_j n_j \int \mathrm{d}^3 r\; \Phi_j^\dagger(\boldsymbol{r}) \left(\tfrac{1}{2}\overleftarrow{\nabla}\cdot\overrightarrow{\nabla} + V(\boldsymbol{r})\right) \Phi_j(\boldsymbol{r}) \\ &\quad + \tfrac{1}{2}\sum_{j,k} n_j n_k \iint \mathrm{d}^3 r_1 \mathrm{d}^3 r_2\; \frac{\left(\Phi_j^\dagger(\boldsymbol{r}_1)\, \Phi_j(\boldsymbol{r}_1)\right)\left(\Phi_k^\dagger(\boldsymbol{r}_2)\, \Phi_k(\boldsymbol{r}_2)\right)}{|\boldsymbol{r}_1 - \boldsymbol{r}_2|} \\ &\quad - \tfrac{1}{2}\sum_{j,k} n_j n_k \iint \mathrm{d}^3 r_1 \mathrm{d}^3 r_2\; \frac{\left(\Phi_j^\dagger(\boldsymbol{r}_1)\, \Phi_k(\boldsymbol{r}_1)\right)\left(\Phi_k^\dagger(\boldsymbol{r}_2)\, \Phi_j(\boldsymbol{r}_2)\right)}{|\boldsymbol{r}_1 - \boldsymbol{r}_2|}. \qquad (4.29)\end{aligned}$$

Moreover from the spectral decomposition of the 1RDM Eq. (2.49) we can write the HF energy functional as an explicit functional of the 1RDM,

$$\begin{aligned} E_{\mathrm{HF}}[\gamma] = &\iint \mathrm{d}^3 r \mathrm{d}^3 r' \ \mathrm{tr}\{H_0(\boldsymbol{r}';\boldsymbol{r})\,\gamma(\boldsymbol{r};\boldsymbol{r}')\} \\ &+ \tfrac{1}{2} \iint \mathrm{d}^3 r_1 \mathrm{d}^3 r_2 \ \frac{\mathrm{tr}\{\gamma(\boldsymbol{r}_1;\boldsymbol{r}_1)\}\,\mathrm{tr}\{\gamma(\boldsymbol{r}_2;\boldsymbol{r}_2)\}}{|\boldsymbol{r}_1-\boldsymbol{r}_2|} \\ &- \tfrac{1}{2} \iint \mathrm{d}^3 r_1 \mathrm{d}^3 r_2 \ \frac{\mathrm{tr}\{\gamma(\boldsymbol{r}_1;\boldsymbol{r}_2)\,\gamma(\boldsymbol{r}_2;\boldsymbol{r}_1)\}}{|\boldsymbol{r}_1-\boldsymbol{r}_2|}. \end{aligned} \tag{4.30}$$

In fact it has been proved by Bach et al. [BLLS94] that minimization of the RDMFT HF-energy functional Eq. (4.30) yields exactly the 1RDM corresponding to the HF ground state $|\Phi_0\rangle$, even if the domain of $E_{\mathrm{HF}}[\gamma]$ is taken to be the ensemble N-representable 1RDMs. Most RDMFT functionals are structurally similar to the HF functional. It is usually the quadratic dependence on the occupation numbers in the Fock term that is modified, and the functionals can be casted into the form

$$E[\gamma] = H_0[\gamma] + E_H[\gamma] + E_{xc}[\gamma] \tag{4.31}$$

$$E_{xc}[\gamma] = \tfrac{1}{2} \sum_{j,k} F(n_j, n_k) \iint \mathrm{d}^3 r_1 \mathrm{d}^3 r_2 \ \frac{\left(\Phi_j^\dagger(\boldsymbol{r}_1)\,\Phi_k(\boldsymbol{r}_1)\right)\left(\Phi_k^\dagger(\boldsymbol{r}_2)\,\Phi_j(\boldsymbol{r}_2)\right)}{|\boldsymbol{r}_1-\boldsymbol{r}_2|}, \tag{4.32}$$

with the specific form of $F(n_j, n_k)$ determining the functional at hand.

In Table 4.1 we collect a representative selection of functionals for RDMFT. The non-quadratic dependence on the occupation numbers in $F(n_j, n_k)$ is responsible for minimizing the corresponding energy functional with a non-idempotent 1RDM. At first sight it seems that we have a contradiction, because in the previous section we realized that there is no non-interacting system that yields the 1RDM of an interacting system, but we just identified the Hartree-Fock theory with an approximation to the energy functional in RDMFT. The key to solve this issue is to realize that the HF-functional represents an approximation to the exact RDMFT energy functional. This specific approximation is responsible for the fact that the minimizing 1RDM is idempotent, i.e. , corresponds to a single Slater determinant. Approximations that are minimized by a correlated 1RDM cannot be obtained from an effective single-particle Schrödinger equation. The only way around this would be to consider an effective single-particle theory with a huge number of degenerate eigenstates. Then one could construct an ensemble of the degenerate non-interacting ground states that reproduces the 1RDM of the interacting system. In fact if one tries to derive a single-particle scheme from the variational equations in RDMFT one obtains a single-particle Hamiltonian with a non-local external potential, that ensures that all un-pinned natural orbitals are eigenstates of the single-particle Hamiltonian with eigenvalue μ, i.e. , all un-pinned natural orbitals have

$F(n_j, n_k)$	remarks	reference
$-n_j n_k$	no correlation	[Har28, Foc30]
$-\sqrt{n_j n_k}$		[Mül84, BB02]
$-\sqrt{n_j n_k} + \delta_{jk}\left(n_j - n_j^2\right)$	self-interaction correction to Müller	[GU98]
$-\frac{1}{2} n_j n_k$ $-\frac{1}{2}\sqrt{n_j\left(2-n_j\right) n_k\left(2-n_k\right)}$		[CGA02]
$\begin{cases} \sqrt{n_j n_k}, & \text{for } j \neq k \text{ and } \Phi_j, \Phi_k \in W \\ -\sqrt{n_j n_k}, & \text{otherwise} \end{cases}$	W: occ. orbitals in HF	[GPB05]
$\begin{cases} \sqrt{n_j n_k}, & \text{for } j \neq k \text{ and } \Phi_j, \Phi_k \in W \\ -n_j n_k, & \text{for } j \neq k \text{ and } \Phi_j, \Phi_k \in S \\ -\sqrt{n_j n_k}, & \text{otherwise} \end{cases}$	S: unocc. orbitals in HF	[GPB05]
$-\sqrt{n_j n_k} + \delta_{jk}\left(n_j - n_j^2\right)$ $+2\Theta\left(\frac{1}{2} - n_j\right)\Theta\left(\frac{1}{2} - n_k\right)\sqrt{n_j n_k}$ $-\Theta\left(n_j - \frac{1}{2}\right)\Theta\left(n_k - \frac{1}{2}\right)\sqrt{\left(1-n_j\right)\left(1-n_k\right)}$	$\Theta(x)$: Heaviside step function	[Pir05]
$-\left(n_j n_k\right)^{\alpha}$	$\alpha \approx 0.55$	[SDLG08]
$-\left(n_j n_k\right)\frac{a_0 + a_1(n_j n_k)}{1 + b_1(n_j n_k)}$	$\{a_0, a_1, b_1\}$ optimized for a selection of molecules	[ML08]

Table 4.1: Table of RDMFT functionals (not exhaustive).

an effective single-particle energy equal to the chemical potential. The admission of non-local potentials makes the development of degeneracies possible since state-dependent potentials, i.e. , potentials shifting the eigenvalue of a single state, are allowed. This not only destroys the intuitive notion of the energy of a state being a compromise between the kinetic energy and a local potential energy, but also makes this effective system useless as a numerical minimization algorithm for RDMFT functionals. Hence in RDMFT the energy functional has to be minimized directly, usually by employing gradient based algorithms for high dimensional optimization problems, while enforcing the ensemble N-representable constraints.

Chapter 5

The uniform electron gas

The uniform electron gas is the paradigm of interacting metallic systems [GV05]. It is described by an interacting Hamiltonian with a constant external potential. This seemingly trivial model exhibits already a variety of features arising due to interactions between the electrons, e.g. spontaneous symmetry breaking. Although one might suspect that the translational invariance of the Hamiltonian is reflected in all expectation values of the interacting system, interactions induce correlations in the probability of finding an electron as position $\boldsymbol{r}_1$ and another electron at position $\boldsymbol{r}_2$. The joint probability is referred to as the two-particle or pair density. Due to the indistinguishability of the electrons and their fermionic character there is already a fundamental correlation in the two-particle density even when the particles are non-interacting. In the world of physics, however, there is the convention that talking about correlations means to talk about the additional correlation due to the interaction between the electrons. In order to illustrate the complexity of interacting electrons we consider the uniform electron gas in two extreme limits. For a very dense electron gas the kinetic energy is the dominant contribution to the total energy and therefore the ground state will minimize the kinetic energy. This means that the electrons will occupy completely delocalized orbitals, i.e. , plane waves states. On the other hand, as first suggested by Wigner [Wig34], the long-range Coulomb repulsion is the dominant contribution for a very dilute electron gas and therefore the ground state will minimize the energy by keeping the electrons as far apart as possible. This implies that the electrons tend to localize and form the so-called Wigner crystal. Then the ground state energy is essentially given by the classical Coulomb energy of charges localized on a periodic lattice. Accordingly the two-particle density will be strongly peaked for $\boldsymbol{r}_1 - \boldsymbol{r}_2$ being the lattice vectors of the Wigner crystal. In the intermediate regime the electron gas has to find an optimal balance between the kinetic and the interaction energy which is reflected in the structure of the two-particle density. Even if, by means of the Quantum Monte Carlo method [Cep04], it is possible to compute the interacting ground-state

energy exactly, one has to make some assumptions on the specific nature (or symmetry) of the ground state (e.g. spin-unpolarized uniform, spin-unpolarized Wigner crystal, partially spin-polarized, fully spin-polarized, superconducting, ...). In practice one forces the electron gas into a specific state by applying a symmetry-breaking external potential. Then one compares the resulting ground-state energy for different states, excluding the energy contribution due to the symmetry-breaking fields, in order to determine the lowest energy configuration. In the present chapter we review the basic properties of the uniform electron gas with unbroken symmetries.

5.1 Hamiltonian

The grand-canonical Hamiltonian of the uniform electron gas is given by

$$\begin{aligned}\hat{\mathcal{H}} &= \hat{\mathcal{T}} - \mu\hat{\mathcal{N}} + \hat{\mathcal{W}} \\ &= \int \mathrm{d}^3 r\; \hat{\Phi}^\dagger(\boldsymbol{r}) \left(\tfrac{1}{2} \overleftarrow{\nabla} \cdot \overrightarrow{\nabla} - \mu \right) \hat{\Phi}(\boldsymbol{r}) \\ &+ \tfrac{1}{2} \iint \mathrm{d}^3 r_1 \mathrm{d}^3 r_2\; \hat{\Psi}^\dagger(\boldsymbol{r}_1, \boldsymbol{r}_2)\, W(\boldsymbol{r}_1 - \boldsymbol{r}_2)\, \hat{\Psi}(\boldsymbol{r}_1, \boldsymbol{r}_2)\,, \end{aligned} \tag{5.1}$$

where we introduced the composed two-particle field $\hat{\Psi}$. It is given in terms of the components of the fundamental Pauli field $\hat{\Phi}$,

$$\hat{\Psi}(\boldsymbol{r}_1, \boldsymbol{r}_2) = \begin{pmatrix} \psi_{s,0}(\boldsymbol{r}_1.\boldsymbol{r}_2) \\ \psi_{t,1}(\boldsymbol{r}_1.\boldsymbol{r}_2) \\ \psi_{t,0}(\boldsymbol{r}_1.\boldsymbol{r}_2) \\ \psi_{t,-1}(\boldsymbol{r}_1.\boldsymbol{r}_2) \end{pmatrix} = \begin{pmatrix} \frac{1}{\sqrt{2}} \left(\hat{\phi}_\uparrow(\boldsymbol{r}_1)\, \hat{\phi}_\downarrow(\boldsymbol{r}_2) - \hat{\phi}_\downarrow(\boldsymbol{r}_1)\, \hat{\phi}_\uparrow(\boldsymbol{r}_2) \right) \\ \hat{\phi}_\uparrow(\boldsymbol{r}_1)\, \hat{\phi}_\uparrow(\boldsymbol{r}_2) \\ \frac{1}{\sqrt{2}} \left(\hat{\phi}_\uparrow(\boldsymbol{r}_1)\, \hat{\phi}_\downarrow(\boldsymbol{r}_2) + \hat{\phi}_\downarrow(\boldsymbol{r}_1)\, \hat{\phi}_\uparrow(\boldsymbol{r}_2) \right) \\ \hat{\phi}_\downarrow(\boldsymbol{r}_1)\, \hat{\phi}_\downarrow(\boldsymbol{r}_2) \end{pmatrix}. \tag{5.2}$$

The components of the field $\hat{\Psi}$ correspond to the spin-0 singlet and spin-$(1, 0, -1)$ triplet states. Together with the definition of the Coulomb interaction

$$W(\boldsymbol{r}_1 - \boldsymbol{r}_2) = \frac{1}{|\boldsymbol{r}_1 - \boldsymbol{r}_2|} \begin{pmatrix} 1 & 0 & 0 & 0 \\ 0 & 1 & 0 & 0 \\ 0 & 0 & 1 & 0 \\ 0 & 0 & 0 & 1 \end{pmatrix}, \tag{5.3}$$

one arrives at the more common representation of the interaction

$$\hat{\mathcal{W}} = \tfrac{1}{2} \sum_{\sigma_1 \sigma_2} \iint \mathrm{d}^3 r_1 \mathrm{d}^3 r_2\; \hat{\phi}^\dagger_{\sigma_1}(\boldsymbol{r}_1)\, \hat{\phi}^\dagger_{\sigma_2}(\boldsymbol{r}_2)\, \frac{1}{|\boldsymbol{r}_1 - \boldsymbol{r}_2|} \hat{\phi}_{\sigma_2}(\boldsymbol{r}_2)\, \hat{\phi}_{\sigma_1}(\boldsymbol{r}_1)\,. \tag{5.4}$$

Writing the interaction $\hat{\mathcal{W}}$ as in Eq. (5.1) using the interaction Eq. (5.3) emphasizes that the Coulomb interaction does not scatter between different spin channels. It is convenient to rewrite the fields and the Coulomb interaction in terms of their Fourier components,

$$\hat{\Phi}(\boldsymbol{r}) = \frac{1}{\sqrt{2\pi}^3} \int \mathrm{d}^3k \; e^{\imath \boldsymbol{k}\cdot\boldsymbol{r}} \hat{\Phi}(\boldsymbol{k}) \,, \tag{5.5}$$

$$\hat{\Psi}(\boldsymbol{r}_1, \boldsymbol{r}_2) = \frac{1}{(2\pi)^3} \iint \mathrm{d}^3k_1 \mathrm{d}^3k_2 \; e^{\imath \boldsymbol{k}_1\cdot\boldsymbol{r}_1} e^{\imath \boldsymbol{k}_2\cdot\boldsymbol{r}_2} \hat{\Psi}(\boldsymbol{k}_1, \boldsymbol{k}_2) \,, \tag{5.6}$$

$$W(\boldsymbol{r}_1 - \boldsymbol{r}_2) = \frac{1}{(2\pi)^3} \int \mathrm{d}^3q \; e^{\imath \boldsymbol{q}\cdot(\boldsymbol{r}_1 - \boldsymbol{r}_2)} \underbrace{\frac{4\pi}{q^2} \operatorname{diag}(1,1,1,1)}_{=W(q)}, \tag{5.7}$$

leading to

$$\hat{\mathcal{H}} = \int \mathrm{d}^3k \; \hat{\Phi}^\dagger(\boldsymbol{k}) \left(\frac{k^2}{2} - \mu \right) \hat{\Phi}(\boldsymbol{k}) \tag{5.8}$$

$$+ \tfrac{1}{2} \frac{1}{(2\pi)^3} \iiint \mathrm{d}^3k_1 \mathrm{d}^3k_2 \mathrm{d}^3q \; \hat{\Psi}^\dagger(\boldsymbol{k}_1 + \boldsymbol{q}, \boldsymbol{k}_2 - \boldsymbol{q}) \, W(q) \, \hat{\Psi}(\boldsymbol{k}_1, \boldsymbol{k}_2) \,. \tag{5.9}$$

5.2 The non-interacting ground state

Considering only the single-particle contribution Eq. (5.8), it is straight forward to construct the ground state of the non-interacting electron gas

$$|\Phi_0\rangle = \prod_{k \le k_\mathrm{F}} \hat{\phi}^\dagger_\downarrow(\boldsymbol{k}) \, \hat{\phi}^\dagger_\uparrow(\boldsymbol{k}) \, |\Omega\rangle \tag{5.10}$$

$$= \prod_{\epsilon(\boldsymbol{k}) \le 0} \hat{\phi}^\dagger_\downarrow(\boldsymbol{k}) \, \hat{\phi}^\dagger_\uparrow(\boldsymbol{k}) \, |\Omega\rangle \,. \tag{5.11}$$

The non-interacting ground state $|\Phi_0\rangle$ is obtained by filling the vacuum $|\Omega\rangle$ successively with spin-up and spin-down electrons in momentum eigenstates labeled by $\boldsymbol{k}$ up to a maximum momentum k_F, the so-called Fermi wave vector. The Fermi wave vector is determined by the constant density, i.e. , the number of electrons per unit volume. The constant density n of the uniform electron gas is commonly specified in terms of the Wigner-Seitz radius r_s. It is defined by assigning each electron a spherical volume with radius r_s, i.e.

$$n = \frac{1}{\frac{4}{3}\pi r_s^3}. \tag{5.12}$$

Alternatively we can compute the density by calculating the expectation value of the density operator,

$$\begin{aligned} n &= \langle \Phi_0 | \, \hat{\Phi}^\dagger(\boldsymbol{r}) \, \hat{\Phi}(\boldsymbol{r}) \, | \Phi_0 \rangle \\ &= \frac{1}{(2\pi)^3} \iint \mathrm{d}^3k \mathrm{d}^3k' \; e^{\imath \boldsymbol{k}\cdot\boldsymbol{r}} e^{-\imath \boldsymbol{k}'\cdot\boldsymbol{r}} \, \langle \Phi_0 | \, \hat{\Phi}^\dagger(\boldsymbol{k}') \, \hat{\Phi}(\boldsymbol{k}) \, | \Phi_0 \rangle \,. \end{aligned} \tag{5.13}$$

The expectation value $\langle\Phi_0|\,\hat{\Phi}^\dagger(\boldsymbol{k}')\,\hat{\Phi}(\boldsymbol{k})\,|\Phi_0\rangle$ is equal to 1 if the two momenta are equal and if the state with momentum $\boldsymbol{k}$ is present in the ground-state Slater determinant $|\Phi_0\rangle$,

$$\begin{aligned}\langle\Phi_0|\,\hat{\Phi}^\dagger(\boldsymbol{k}')\,\hat{\Phi}(\boldsymbol{k})\,|\Phi_0\rangle &= \langle\Phi_0|\left(\hat{\phi}^\dagger_\uparrow(\boldsymbol{k}')\,\hat{\phi}_\uparrow(\boldsymbol{k}) + \hat{\phi}^\dagger_\downarrow(\boldsymbol{k}')\,\hat{\phi}_\downarrow(\boldsymbol{k})\right)|\Phi_0\rangle \\ &= \delta(\boldsymbol{k}-\boldsymbol{k}')\left(\Theta(k_\mathrm{F}-k)+\Theta(k_\mathrm{F}-k)\right).\end{aligned}$$

Accordingly the Fermi wave vector can be related to the density or equivalently the Wigner-Seitz radius,

$$n = \frac{1}{3\pi^2}k_\mathrm{F}^3 = \frac{1}{\frac{4}{3}\pi r_s^3} \quad \Rightarrow \quad k_\mathrm{F} = \left(\frac{9\pi}{4}\right)^{1/3}\frac{1}{r_s}. \tag{5.14}$$

As already indicated in Eq. (5.11) an alternative prescription to construct the non-interacting ground state is to fill the vacuum with single-particle states that have a negative energy. From $\epsilon(\boldsymbol{k}) = \frac{k^2}{2} - \mu$ it is clear that the chemical potential μ determines how many single-particle state have a negative energy and therefore the density of the uniform electron gas. This prescription is more general than the prescription to fill all states with a momentum less than k_F, since it also applies for non-isotropic dispersions $\epsilon(\boldsymbol{k})$.

5.3 The Hartree-Fock ground-state energy

The first order correction to the ground-state energy due to the interactions is obtained by evaluating the expectation value of $\hat{\mathcal{W}}$ w.r.t. the non-interacting ground state $|\Phi_0\rangle$. Similarly to the computation of density (cf. (5.13)) one has to calculate

$$\langle\Phi_0|\,\hat{\phi}^\dagger_{\sigma_1}(\boldsymbol{k}_1+\boldsymbol{q})\,\hat{\phi}^\dagger_{\sigma_2}(\boldsymbol{k}_2-\boldsymbol{q})\,\hat{\phi}_{\sigma_2}(\boldsymbol{k}_2)\,\hat{\phi}_{\sigma_1}(\boldsymbol{k}_1)\,|\Phi_0\rangle\,.$$

In contrast to the evaluation of the quadratic terms in the fundamental fields, there are two possibilities for a non-vanishing contribution. The first is that the outer annihilation/creation operators remove/insert an electron into the same state and the inner annihilation/creation operators remove/insert an electron into the same state. Both processes require that $\boldsymbol{q}$ vanishes. The second possibility is that the outer/inner annihilation/creation operators remove/insert an electron into the same state and vice-versa. These processes both require that $\boldsymbol{q} = \boldsymbol{k}_2 - \boldsymbol{k}_1$ and additionally that $\sigma_1 = \sigma_2$. Furthermore $\boldsymbol{k}_1$ and $\boldsymbol{k}_2$ have to be occupied in Φ_0. Due to the anti-symmetry of fermionic states the second term acquires an additional minus sign,

$$\begin{aligned}&\langle\Phi_0|\,\hat{\phi}^\dagger_{\sigma_1}(\boldsymbol{k}_1+\boldsymbol{q})\,\hat{\phi}^\dagger_{\sigma_2}(\boldsymbol{k}_2-\boldsymbol{q})\,\hat{\phi}_{\sigma_2}(\boldsymbol{k}_2)\,\hat{\phi}_{\sigma_1}(\boldsymbol{k}_1)\,|\Phi_0\rangle \\ &= \left(\delta(\boldsymbol{q})\,\delta(\boldsymbol{q}) - \delta(\boldsymbol{k}_1+\boldsymbol{q}-\boldsymbol{k}_2)\,\delta(\boldsymbol{k}_1+\boldsymbol{q}-\boldsymbol{k}_2)\,\delta_{\sigma_1\sigma_2}\delta_{\sigma_1\sigma_2}\right)\Theta(k_\mathrm{F}-k_1)\,\Theta(k_\mathrm{F}-k_2) \\ &= \frac{1}{(2\pi)^3}\left(\delta(\boldsymbol{q}) - \delta(\boldsymbol{k}_1+\boldsymbol{q}-\boldsymbol{k}_2)\,\delta_{\sigma_1\sigma_2}\right)\Theta(k_\mathrm{F}-k_1)\,\Theta(k_\mathrm{F}-k_2)\,.\end{aligned} \tag{5.15}$$

This result can also be obtained employing the methods of Many-Body-Perturbation Theory, i.e. , by evaluating the first order Feynmann diagrams derived employing Wick's theorem [FV71, GRH91]. Starting from Eq. (5.4) the expectation value of the interaction $\hat{\mathcal{W}}$ w.r.t. the interacting ground state $|\Psi_0\rangle$ is

$$\begin{aligned}
\langle\Psi_0|\,\hat{\mathcal{W}}\,|\Psi_0\rangle &= \tfrac{1}{2}\sum_{\sigma_1\sigma_2}\iint \mathrm{d}^3r_1\mathrm{d}^3r_2\;\frac{1}{|\boldsymbol{r}_1-\boldsymbol{r}_2|}\\
&\times\Big(\langle\Phi_0|\,\hat{\phi}^\dagger_{\sigma_1}(\boldsymbol{r}_1)\,\hat{\phi}_{\sigma_1}(\boldsymbol{r}_1)\,|\Phi_0\rangle\,\langle\Phi_0|\,\hat{\phi}^\dagger_{\sigma_2}(\boldsymbol{r}_2)\,\hat{\phi}_{\sigma_2}(\boldsymbol{r}_2)\,|\Phi_0\rangle\\
&\quad-\langle\Phi_0|\,\hat{\phi}^\dagger_{\sigma_2}(\boldsymbol{r}_2)\,\hat{\phi}_{\sigma_1}(\boldsymbol{r}_1)\,|\Phi_0\rangle\,\langle\Phi_0|\,\hat{\phi}^\dagger_{\sigma_1}(\boldsymbol{r}_1)\,\hat{\phi}_{\sigma_2}(\boldsymbol{r}_2)\,|\Phi_0\rangle\Big)+\mathcal{O}\big(W^2\big)\\
&= \tfrac{1}{2}\sum_{\sigma_1\sigma_2}\iint \mathrm{d}^3r_1\mathrm{d}^3r_2\;\frac{1}{|\boldsymbol{r}_1-\boldsymbol{r}_2|}\\
&\times\left(n_{\sigma_1}(\boldsymbol{r}_1)\,n_{\sigma_2}(\boldsymbol{r}_2)-\gamma_{\sigma_1\sigma_2}(\boldsymbol{r}_1;\boldsymbol{r}_2)\,\gamma_{\sigma_2\sigma_1}(\boldsymbol{r}_2;\boldsymbol{r}_1)\right). \qquad (5.16)
\end{aligned}$$

We recognize that the interaction energy, up to first order, appears to be the same as the approximation to the interaction energy within Hartree-Fock theory (cf. Eq. (4.30)). However, in Hartree-Fock theory the 1RDM is constructed from orbitals diagonalizing the effective single-particle Hamiltonian Eq. (4.26) whereas in Eq. (5.16) the 1RDM is obtained from orbitals diagonalizing the single-particle contribution to the interacting Hamiltonian $\hat{\mathcal{H}}$. It turns out that for the uniform electron gas the orbitals diagonalizing the non-interacting part $\hat{\mathcal{H}}_0$ and the orbitals diagonalizing the Hartree-Fock Hamiltonian $\hat{\mathcal{H}}_{\mathrm{HF}}$ are identical and therefore the ground-state energy in first-order perturbation theory and Hartree-Fock theory are identical. A caveat, when evaluating this ground-state energy, is that the direct term, i.e. , the Hartree energy, in Eq. (5.16) diverges due to the long-range character of the Coulomb interaction. This divergence is canceled by exposing the electrons to a uniform positive background charge with a density equal to the electron density. Because of this uniform background charge, the uniform electron gas is sometimes referred to as the Jellium model. Excluding furthermore the energy contribution due to the chemical potential, the internal energy per unit volume is

$$\begin{aligned}
E_{\mathrm{HF}} &= \tfrac{1}{2}\sum_{\sigma}\iint \mathrm{d}^3r\mathrm{d}^3k\;\Theta(k_{\mathrm{F}}-k)\,\frac{e^{-\imath\boldsymbol{k}\cdot\boldsymbol{r}}}{(2\pi)^3}\overleftarrow{\nabla}\cdot\overrightarrow{\nabla}\frac{e^{\imath\boldsymbol{k}\cdot\boldsymbol{r}}}{(2\pi)^3}\\
&\quad-\tfrac{1}{2}\sum_{\sigma_1\sigma_2}\iint \mathrm{d}^3r_1\mathrm{d}^3r_2\;\frac{\gamma_{\sigma_1\sigma_2}(\boldsymbol{r}_1;\boldsymbol{r}_2)\,\gamma_{\sigma_2\sigma_1}(\boldsymbol{r}_2;\boldsymbol{r}_1)}{|\boldsymbol{r}_1-\boldsymbol{r}_2|}\\
&= \frac{1}{(2\pi)^3}\int \mathrm{d}^3k\;\Theta(k_{\mathrm{F}}-k)\,k^2\\
&\quad-\frac{1}{(2\pi)^6}\iint \mathrm{d}^3k_1\mathrm{d}^3k_2\;\Theta(k_{\mathrm{F}}-k_1)\,\frac{4\pi}{(\boldsymbol{k}_1-\boldsymbol{k}_2)^2}\Theta(k_{\mathrm{F}}-k_2)\,. \qquad (5.17)
\end{aligned}$$

The remaining integrals can be solved analytically and yield the well-known Hartree-Fock result for the energy per electron in terms of the Wigner-Seitz radius

$$\epsilon_{\mathrm{HF}}^{\mathrm{unif}}(r_s) = \underbrace{\frac{3}{10}\left(\frac{9\pi}{4}\right)^{2/3}}_{\approx 1.10}\frac{1}{r_s^2} - \underbrace{\frac{3}{4\pi}\left(\frac{9\pi}{4}\right)^{1/3}}_{\approx 0.45}\frac{1}{r_s}. \tag{5.18}$$

We complete our discussion of the uniform electron gas within Hartree-Fock theory by calculating the effective Hartree-Fock potential defined in Eq. (4.28),

$$\begin{aligned} U_F(\boldsymbol{r};\boldsymbol{r}') &= \frac{1}{(2\pi)^3}\int \mathrm{d}^3k'\ \Theta(k_{\mathrm{F}}-k')\,\frac{e^{\imath\boldsymbol{k}'\cdot(\boldsymbol{r}-\boldsymbol{r}')}}{|\boldsymbol{r}-\boldsymbol{r}'|} \\ &= \frac{1}{(2\pi)^6}\iint \mathrm{d}^3k\mathrm{d}^3k'\ \Theta(k_{\mathrm{F}}-k')\,\frac{4\pi e^{\imath(\boldsymbol{k}+\boldsymbol{k}')\cdot(\boldsymbol{r}-\boldsymbol{r}')}}{k^2} \\ &= \frac{1}{(2\pi)^3}\int \mathrm{d}^3k\ e^{\imath\boldsymbol{k}\cdot(\boldsymbol{r}-\boldsymbol{r}')}\frac{1}{(2\pi)^3}\int \mathrm{d}^3k'\ \frac{4\pi\Theta(k_{\mathrm{F}}-k')}{(\boldsymbol{k}-\boldsymbol{k}')^2}. \end{aligned} \tag{5.19}$$

From Eq. (5.19) we can extract the shift of the single-particle dispersion in the effective Hartree-Fock Hamiltonian compared to the non-interacting dispersion, i.e.

$$\begin{aligned} U(\boldsymbol{k}) &= \frac{1}{(2\pi)^3}\int \mathrm{d}^3k'\ \frac{4\pi\Theta(k_{\mathrm{F}}-k')}{(\boldsymbol{k}-\boldsymbol{k}')^2} \\ &= \frac{k_{\mathrm{F}}}{\pi}\left(1+\frac{k^2-k_{\mathrm{F}}^2}{4k}\ln\left(\frac{(k_{\mathrm{F}}-k)^2}{(k_{\mathrm{F}}+k)^2}\right)\right). \end{aligned} \tag{5.20}$$

Now we can understand why the Hartree-Fock result is equivalent to the result from first-order perturbation theory. The shift in the dispersion $-U(\boldsymbol{k})$ depends, just like the non-interacting dispersion, only on the magnitude of $\boldsymbol{k}$. The dispersion remains isotropic. Furthermore $-U(\boldsymbol{k})$ is a monotonically increasing function and therefore the energetical ordering of the plane wave states is unchanged. Hence the minimizing Slater determinant is equivalent to the non-interacting Slater determinant.

5.4 Reduced-Density-Matrix-Functional Theory for the uniform electron gas

An important step to go beyond the Hartree-Fock approximation was taken by Gell-Mann and Brueckner in 1957 [GMB57]. They employed the Random-Phase Approximation (RPA), which represents a resummantion of the most divergent terms of the perturbation expansion, to obtain the leading order corrections to the Hartree-Fock result. In the small r_s, i.e. , the

high density limit, it is given by

$$\epsilon^{\mathrm{unif}}(r_s) = \epsilon^{\mathrm{unif}}_{\mathrm{HF}}(r_s) + \alpha \ln(r_s) - \beta + \mathcal{O}(r_s \ln(r_s)) \,, \qquad (5.21)$$
$$\alpha \approx 0.031 \quad , \quad \beta \approx 0.047.$$

The constant contribution β stems from the second-order exchange diagram and the $\ln(r_s)$-dependence comes from the screened second-oder bubble diagram. In 1980 numerically exact ground-state energies became available due to the Quantum Monte Carlo calculations by Ceperley and Alder [CA80]. These exact results cannot only directly be used to construct the LDA (cf. Sec. 4.1) but also serve as a benchmark for the developments of functionals in RDMFT. Since most RMDFT functionals are variations of the Hartree-Fock functional (cf. Sec. 4.3), we can immediately write down the energy functional,

$$\begin{aligned} E[\gamma] &= \sum_\sigma \int \mathrm{d}^3k \, \frac{n_\sigma(k)}{(2\pi)^3} \left(\frac{k^2}{2} - \mu \right) \\ &\quad - \tfrac{1}{2} \sum_\sigma \iint \mathrm{d}^3k_1 \mathrm{d}^3k_2 \, \frac{F(n_\sigma(k_1)\,, n_\sigma(k_2))}{(2\pi)^6} \frac{1}{(\boldsymbol{k}_1 - \boldsymbol{k}_2)^2}, \qquad (5.22) \\ \gamma(\boldsymbol{r};\boldsymbol{r}') &= \int \mathrm{d}^3k \, \left(n_\uparrow(\boldsymbol{k}) \, \Phi^\dagger_{\boldsymbol{k}\uparrow}(\boldsymbol{r}') \, \Phi_{\boldsymbol{k}\uparrow}(\boldsymbol{r}) + n_\downarrow(\boldsymbol{k}) \, \Phi^\dagger_{\boldsymbol{k}\downarrow}(\boldsymbol{r}') \, \Phi_{\boldsymbol{k}\downarrow}(\boldsymbol{r}) \right) \\ &= \frac{1}{(2\pi)^3} \int \mathrm{d}^3k \, \begin{pmatrix} n_\uparrow(\boldsymbol{k}) \, e^{\imath \boldsymbol{k}\cdot(\boldsymbol{r}-\boldsymbol{r}')} & 0 \\ 0 & n_\downarrow(\boldsymbol{k}) \, e^{\imath \boldsymbol{k}\cdot(\boldsymbol{r}-\boldsymbol{r}')} \end{pmatrix}. \qquad (5.23) \end{aligned}$$

We included the chemical potential in the energy functional, because it acts as a Langrangian multiplier to fix the density when minimizing the energy functional directly. In Eq. (5.23) the natural orbitals are taken to be pure spin-up and pure spin-down plane waves. Assuming furthermore that the occupation numbers are spherically symmetric, we can discretize the momentum space into spherical volume elements Ω_j. Averaging the occupation numbers over the volume elements Ω_j, i.e. ,

$$n_{j\sigma} = \int_{\Omega_j} \mathrm{d}^3k \; n_\sigma(k) \,, \qquad (5.24)$$

and defining the integral weights

$$\mathrm{DWI}_j = \int_{\Omega_j} \mathrm{d}^3k \, \frac{1}{(2\pi)^3}, \qquad (5.25)$$

$$\mathrm{DKI}_j = \int_{\Omega_j} \mathrm{d}^3k \, \frac{1}{(2\pi)^3} \frac{k^2}{2}, \qquad (5.26)$$

$$\mathrm{DXI}_{jk} = \int_{\Omega_j} \int_{\Omega_k} \mathrm{d}^3k_1 \mathrm{d}^3k_2 \, \frac{1}{(2\pi)^6} \frac{4\pi}{(\boldsymbol{k}_1 - \boldsymbol{k}_2)}, \qquad (5.27)$$

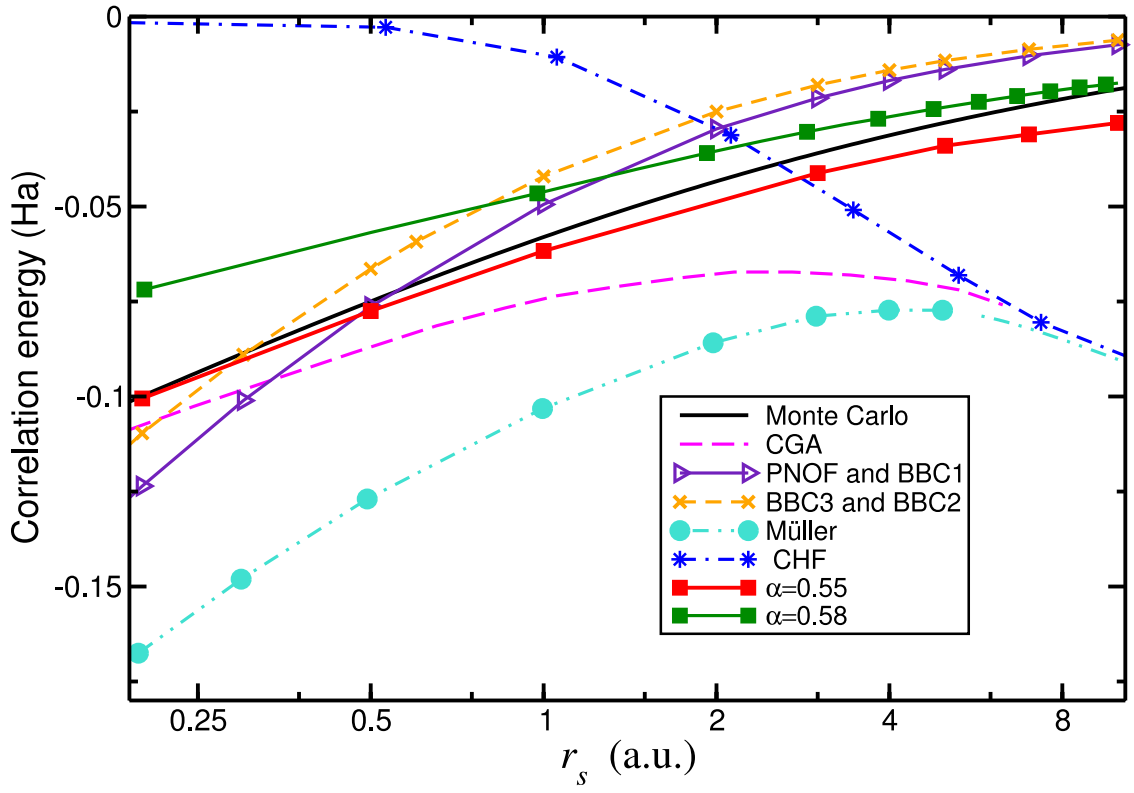

Figure 5.1: Correlation energy as a function of the Wigner-Seitz radius r_s for various functionals (Fig. taken from [LSD$^+$09]). The Monte Carlo results are obtained fitting the Perdew Wang parameterization [PW92] to the Diffusion Monte Carlo data of Ortiz and Ballone [OHB99].

the discretized version of the energy functional reads

$$E[\{n_j\}] = \sum_{j\sigma} n_{j\sigma}\mathrm{DKI}_j - \mu \sum_{j\sigma} n_{j\sigma}\mathrm{DWI}_j - \tfrac{1}{2}\sum_{jk\sigma} F(n_{j\sigma}; n_{k\sigma})\,\mathrm{DXI}_{jk}. \tag{5.28}$$

The minimization of the functional Eq. (5.28) is a high dimensional non-linear optimization problem in terms of the occupation numbers $\{n_j\}$. The chemical potential μ ensures as Lagrangian multiplier that the minimum configuration $\{n_j\}_0$ is normalized to the required density $n = \sum_{j\sigma} (n_{j\sigma})_0\,\mathrm{DWI}_i$. The minimization is carried out using a steepest descent algorithm. In each minimization step the occupation numbers are constrained to be $n_j \in [0, 1]$ in order to ensure ensemble-N representability. In addition, the volume elements Ω_j can be adjusted to be finer in regions of high variance in $n(\boldsymbol{k})$ and coarser in regions where $n(\boldsymbol{k})$ is almost constant. The results for the xc-energy obtained by minimizing various functionals are compiled in Fig. 5.1. The Power-functional [SDLG08] yields very accurate correlation energies for the uniform electron gas in the range of metallic densities $1 \leq r_s \leq 10$ for an optimal value of $\alpha = 0.55$. In [LSD$^+$09] we find that the optimal value for α determined from the disso-

ciation of the Hydrogen molecule ($\alpha = 0.525$) and determined from a set of small molecules ($\alpha = 0.578$) are very close to the optimal value determined from the uniform electron gas. All functionals are minimized by momentum distributions $n(\boldsymbol{k})$ that are smoothened out compared to the non-interacting momentum distribution $n(\boldsymbol{k}) = \Theta(\mu - \epsilon(\boldsymbol{k}))$. The momentum distributions exhibit a discontinuity at the Fermi energy $\epsilon(\boldsymbol{k}_\mathrm{F}) = \mu$ only if the definition of $F(n_i, n_j)$ contains an explicit sign change, as for example the corrections to the Müller functional proposed in [GPB05]. The step in the momentum distribution defines the Fermi surface of the system. Functionals that smoothly vary between occupied and unoccupied states therefore seem to dissolve the Fermi surface. Hence one might view the action of the xc-contribution in the energy functional Eq. (5.28) as a thermalization of the electrons with each other. In this picture the momentum distribution would correspond to the statistical weights $n(\boldsymbol{k})$ associated to the states $|\phi_{\boldsymbol{k}}\rangle$. Their specific value is determined by the minimizing momentum distribution $n_0(\boldsymbol{k})$ of the employed functional. However, from Landau's theory of the Fermi liquid, is is expected that the momentum distribution exhibits a discontinuity at the Fermi surface. The size of the discontinuity is directly related to the effective mass of the quasi-electron in the normal Fermi liquid. Momentum distributions can be obtained to high accuracy by Quantum Monte Carlo methods [HBP$^+$11] or other many-body techniques [Lam71, Ove71, TY91]. They all agree that the discontinuity decreases with decreasing density which signals the break-down of the quasi-electron concept for very dilute systems. Unfortunately the functionals yielding discontinuous momentum distributions show the opposite trend for the discontinuity as a function of the density (cf. Fig. 5.2). For all DFTs it is desirable that the energy functional not only yields the correct ground-state energy, but also the correct fundamental density, i.e. , the correct momentum distribution in the case of RDMFT for the uniform electron gas. The universal functional within RDMFT for all uniform systems can be defined as

$$E_{xc}^{\mathrm{unif}}[\{n(\boldsymbol{k})\}] = \inf_{\hat{\mathcal{D}} \to n(\boldsymbol{k})} \mathrm{Tr}\Big\{\hat{\mathcal{D}}\hat{\mathcal{W}}'\Big\}\,, \tag{5.29}$$

where the prime indicates that the Hartree contribution has been canceled from the interaction. A numerically exact construction seems to be possible employing Quantum Monte Carlo methods. Since the Quantum Monte Carlo methods are wave-function or propagator based methods, they provide a momentum distribution $n(\boldsymbol{k})$ together with the corresponding value of xc-energy $E_{xc}^{\mathrm{QMC}}[\{n(\boldsymbol{k})\}]$. The momentum distribution is implicitly determined by the single particle dispersion $\epsilon(\boldsymbol{k})$. Usually this is taken to be $\epsilon(\boldsymbol{k}) = \frac{1}{2}k^2 - \mu$, but one could add an external, translationally invariant, non-local potential $\Sigma(\boldsymbol{k})$, acting as Lagrangian multiplier, in order to impose a specific momentum distribution. This is surely a formidable task, since the momentum distribution is an almost arbitrary positive function. It might be possible to streamline this procedure via a parameterization of the Lagrangian multiplier $\Sigma(\boldsymbol{k})$ in terms

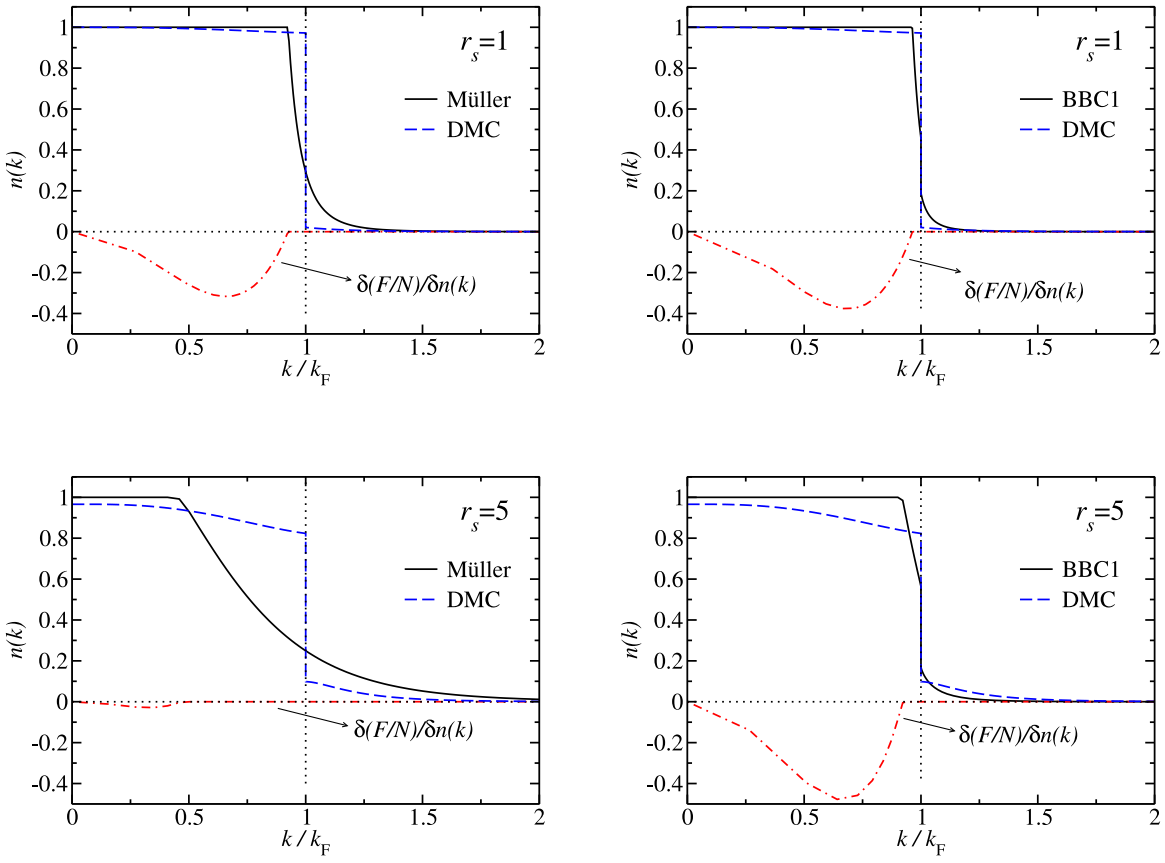

Figure 5.2: Momentum distributions for the uniform electron gas for the Müller [Mül84] and the BBC1 [GPB05] functional (Figs. taken from [LHG07]). The upper panels show the momentum distribution at $r_s = 1$ and the lower panels at $r_s = 5$. The discontinuous dependency on the occupation numbers in the BBC1 functional (cf. Table 4.1) yields a step of the momentum distribution at the Fermi wave vector k_{F}. The size of the step is smaller for higher densities (lower r_s) in contrast to the expectations from Landau's theory of the Fermi liquid. The dashed red line is the variation of the occupation numbers at the minimum. Deviation from zero indicates that the corresponding occupation number is pinned, i.e. , it is optimal at 1, the upper limit of its allowed range.

of a parameter ω. For a set of $\{\omega_i\}$ one could employ the Quantum Monte Carlo methods to determine

$$E^{\mathrm{unif}}(\omega) = \min\left\{ \frac{1}{(2\pi)^3} \int \mathrm{d}^3k \ \left(\tfrac{1}{2}k^2 - \mu + \Sigma_\omega(\boldsymbol{k})\right) n(\boldsymbol{k}) - E_{xc}^{\mathrm{QMC}}[\{n(\boldsymbol{k})\}] \right\} \tag{5.30}$$

The parametrical dependence of $\Sigma_\omega(\boldsymbol{k})$ on ω should be chosen such, that a relevant set of momentum distributions is sampled by the set $\{\omega_i\}$. Furthermore a unique prescription $\{n(\boldsymbol{k})\} \to \{\omega_i\}$ has to be given in order to extrapolate the results, obtained via Eq. (5.30), to all ensemble-N representable $n(\boldsymbol{k})$. Then the resulting mapping $\varepsilon_{xc}^{\mathrm{QMC}}[n(\boldsymbol{k})]$ could be used to define the RDMFT analogy to the LDA by employing the Wigner transform

$$n_{\boldsymbol{R}}(\boldsymbol{k}) = \frac{1}{\sqrt{2\pi}^3} \int \mathrm{d}^3s \ e^{-\imath \boldsymbol{k}\cdot\boldsymbol{s}} \gamma(\boldsymbol{R} + \boldsymbol{s}/2; \boldsymbol{R} - \boldsymbol{s}/2) \,, \tag{5.31}$$

$$E_{xc}^{\mathrm{LMDA}}[\gamma] = \int \mathrm{d}^3R \ \gamma(\boldsymbol{R}; \boldsymbol{R}) \, \varepsilon[n_{\boldsymbol{R}}(\boldsymbol{k})] \,, \tag{5.32}$$

i.e. , the Local-Momentum-Distribution Approximation (LMDA). The implementation of the proposed construction should be guided by physical considerations when constructing the path to be explored using Quantum Monte Carlo techniques via explicit expressions for $\Sigma_\omega(\boldsymbol{k})$. It remains to be seen whether a functional along the lines of proposition Eq. (5.32) can compete with the comparatively simple functionals (cf. Table 4.1), since these orbital functionals are fundamentally non-local in nature whereas the LMDA imposes a somewhat local picture of the xc-energy functional.

Chapter 6

Overhauser's spin-spiral-wave state

In his seminal paper [Ove62] Overhauser proved that the paramagnetic solution of the uniform electron gas within Hartree-Fock theory is always unstable w.r.t. the formation of a charge-density wave (CDW) or spin-density wave (SDW). This in not in contradiction with the result of the Sec. 5.3 that the paramagnetic state is a self-consistent solution of the Hartree-Fock equations, because the Hartree-Fock equations are derived from the stationarity of the Hartree-Fock energy functional under variations of the orbitals constituting the Hartree-Fock state. Self-consistent solutions of the Hartree-Fock equation therefore might be saddle points of the energy. The possibility for multiple stationary points is a reflection of the non-linearity in self-consistent theories. In other words, the interaction between the electrons leads to a rich structure of the energy landscape with various stationary points representing different phases of the system. These various phases are characterized by a state that breaks the symmetry of the Hamiltonian. Furthermore the symmetry breaking state yields a non-vanishing expectation value of a characteristic observable called the order parameter. Hence self-consistent theories are tools to explore the different phases and reveal their corresponding order parameters. In this chapter we investigate the spin-spiral-wave (SSW) state, introduced by Overhauser as an explicit example for a self-consistent solution of the Hartree-Fock equations for the Jellium model. The SSW state has a spatially rotating spin magnetization

$$\boldsymbol{m}(\boldsymbol{r}) = n\chi \begin{pmatrix} s\cos(\boldsymbol{q}\cdot\boldsymbol{r}) \\ s\sin(\boldsymbol{q}\cdot\boldsymbol{r}) \\ \sqrt{1-s^2} \end{pmatrix}, \tag{6.1}$$

with a SSW wave vector $\boldsymbol{q}$, relative spin magnetization χ and the azimuthal angle $s = \sin(\theta)$. It is a specific realization of a SDW state proved to have a lower energy than the paramagnetic state. The results presented in this chapter have been published in [EKP+10].

6.1 Uniformly polarized electron gas in Hartree-Fock theory

Before considering the spin-spiral-wave state we discuss the uniformly polarized state as an introductory example of a broken-symmetry solution to the HF equations. Modifying the single-particle contribution to the Jellium Hamiltonian Eq. (5.1) by a constant magnetic field $\boldsymbol{B} = B\boldsymbol{e}_3$ along the z-axis, we get

$$\hat{\mathcal{H}}_0 = \int \mathrm{d}^3k \; \hat{\Phi}^\dagger(\boldsymbol{k}) \begin{pmatrix} \frac{1}{2}k^2 - \mu - \frac{1}{2}B & 0 \\ 0 & \frac{1}{2}k^2 - \mu + \frac{1}{2}B \end{pmatrix} \hat{\Phi}(\boldsymbol{k}) \,. \tag{6.2}$$

The application of a constant external magnetic field can be viewed as the application of a chemical potential $\mu_\uparrow = \mu + \frac{1}{2}B$ for spin-up electrons and a chemical potential $\mu_\downarrow = \mu - \frac{1}{2}B$ for the spin-down electrons. Defining the relative spin-polarization

$$\chi = \frac{n_\uparrow - n_\downarrow}{n} \in [-1, 1] \,, \tag{6.3}$$

we obtain spin-resolved Fermi vectors via

$$\begin{aligned} n_{\uparrow/\downarrow} &= n\frac{1 \pm \chi}{2} = \frac{1}{3\pi^2}k_\mathrm{F}^3\frac{1 \pm \chi}{2} = \frac{1}{(2\pi)^3}\int_{k \le k_{\mathrm{F}\uparrow/\downarrow}} \mathrm{d}^3k \\ \Rightarrow \quad k_{\mathrm{F}\uparrow/\downarrow} &= k_\mathrm{F}\left(1 \pm \chi\right)^{1/3} . \end{aligned} \tag{6.4}$$

Since in the Hartree-Fock energy for the uniformly polarized case the spin-up and spin-down channels are decoupled, one can obtain the spin-resolved Hartree-Fock energy per electron (excluding the contribution due to the external magnetic field) from the result for the unpolarized electron gas (cf. Eq. (5.18)),

$$\begin{aligned} \epsilon_\mathrm{HF}^\mathrm{unif}(r_s, \chi) = \frac{3}{10}\left(\frac{9\pi}{4}\right)^{2/3}\frac{1}{r_s^2}\frac{\left((1+\chi)^{5/3} + (1-\chi)^{5/3}\right)}{2} \\ - \frac{3}{4\pi}\left(\frac{9\pi}{4}\right)^{1/3}\frac{1}{r_s}\frac{\left((1+\chi)^{4/3} + (1-\chi)^{4/3}\right)}{2} . \end{aligned} \tag{6.5}$$

The energy is a symmetric function of χ and furthermore concave in $\chi \in [0, 1]$. Accordingly its minimum as a function of χ is either at $\chi = 0$, i.e. , the unpolarized (paramagnetic) state, or at $\chi = 1$, i.e. , the fully polarized (ferromagnetic) state. Whether the paramagnetic or the ferromagnetic configuration is lower in energy is determined by the relative weight of the kinetic energy w.r.t. the exchange energy and therefore the density. For a density less than a critical density, specified by

$$r_s = r_c = \frac{2\pi}{5}\left(\frac{9\pi}{4}\right)^{1/3}\frac{2^{2/3} - 1}{2^{1/3} - 1} \approx 5.45, \tag{6.6}$$

the electron gas prefers to be in the fully polarized state even if no external magnetic field is applied.

6.2 The Overhauser instability of the uniform electron gas

Now we turn to the SSW state that Overhauser introduced as an explicit example for the instability of the uniform electron gas w.r.t. the formation of a charge- or spin-density waves [Ove62]. His idea was to assume a coupling $g(\boldsymbol{k})$ of spin-up plane waves with wave vector $\boldsymbol{k}-\frac{1}{2}\boldsymbol{q}$ to spin-down plane waves with wave vector $\boldsymbol{k}+\frac{1}{2}\boldsymbol{q}$ in the effective single-particle Hamiltonian (cf. Eq. (4.26)), i.e. ,

$$\hat{\mathcal{H}}_{\mathrm{HF}} = \int \mathrm{d}^3k \, \begin{pmatrix} \hat{\phi}^\dagger_\uparrow\big(\boldsymbol{k}-\frac{1}{2}\boldsymbol{q}\big) & \hat{\phi}^\dagger_\downarrow\big(\boldsymbol{k}+\frac{1}{2}\boldsymbol{q}\big) \end{pmatrix} \mathrm{H}_{\mathrm{SSW}} \begin{pmatrix} \hat{\phi}_\uparrow\big(\boldsymbol{k}-\frac{1}{2}\boldsymbol{q}\big) \\ \hat{\phi}_\downarrow\big(\boldsymbol{k}+\frac{1}{2}\boldsymbol{q}\big) \end{pmatrix}. \tag{6.7a}$$

$$\mathrm{H}_{\mathrm{SSW}} = \begin{pmatrix} \frac{1}{2}\left(\boldsymbol{k}-\frac{1}{2}\boldsymbol{q}\right)^2 - U_\uparrow\big(\boldsymbol{k}-\frac{1}{2}\boldsymbol{q}\big) - \mu & -\frac{1}{2}g(\boldsymbol{k}) \\ -\frac{1}{2}g^\dagger(\boldsymbol{k}) & \frac{1}{2}\left(\boldsymbol{k}+\frac{1}{2}\boldsymbol{q}\right)^2 - U_\downarrow\big(\boldsymbol{k}+\frac{1}{2}\boldsymbol{q}\big) - \mu \end{pmatrix}. \tag{6.7b}$$

Defining $\epsilon_\sigma(\boldsymbol{k}) = \frac{1}{2}k^2 - U_\sigma(\boldsymbol{k})$ one can readily diagonalize

$$\mathrm{H}_{\mathrm{SSW}} = \mathcal{U}^\dagger(\boldsymbol{k}) \begin{pmatrix} \epsilon_-(\boldsymbol{k}) - \mu & 0 \\ 0 & \epsilon_+(\boldsymbol{k}) - \mu \end{pmatrix} \mathcal{U}(\boldsymbol{k}), \tag{6.8}$$

$$\epsilon_\mp(\boldsymbol{k}) = \epsilon(\boldsymbol{k}) \mp \tfrac{1}{2}\sqrt{|D(\boldsymbol{k})|^2 + |g(\boldsymbol{k})|^2}, \tag{6.9}$$

$$\mathcal{U}(\boldsymbol{k}) = \begin{pmatrix} \cos\big(\frac{1}{2}\theta(\boldsymbol{k})\big) & -\sin\big(\frac{1}{2}\theta(\boldsymbol{k})\big) \\ \sin\big(\frac{1}{2}\theta(\boldsymbol{k})\big) & \cos\big(\frac{1}{2}\theta(\boldsymbol{k})\big) \end{pmatrix}, \tag{6.10}$$

where we introduced the two energies

$$\begin{aligned} \epsilon(\boldsymbol{k}) &= \tfrac{1}{2}\left(\epsilon_\uparrow\big(\boldsymbol{k}-\tfrac{1}{2}\boldsymbol{q}\big) + \epsilon_\downarrow\big(\boldsymbol{k}+\tfrac{1}{2}\boldsymbol{q}\big)\right) \\ &= \tfrac{1}{2}k^2 + \tfrac{1}{8}q^2 - \tfrac{1}{2}\left(U_\uparrow\big(\boldsymbol{k}-\tfrac{1}{2}\boldsymbol{q}\big) + U_\downarrow\big(\boldsymbol{k}+\tfrac{1}{2}\boldsymbol{q}\big)\right), \end{aligned} \tag{6.11}$$

$$\begin{aligned} D(\boldsymbol{k}) &= -\left(\epsilon_\uparrow\big(\boldsymbol{k}-\tfrac{1}{2}\boldsymbol{q}\big) - \epsilon_\downarrow\big(\boldsymbol{k}+\tfrac{1}{2}\boldsymbol{q}\big)\right) \\ &= \boldsymbol{k}\cdot\boldsymbol{q} + U_\uparrow\big(\boldsymbol{k}-\tfrac{1}{2}\boldsymbol{q}\big) - U_\downarrow\big(\boldsymbol{k}+\tfrac{1}{2}\boldsymbol{q}\big). \end{aligned} \tag{6.12}$$

Furthermore the angle $\theta(\boldsymbol{k})$ is defined via

$$\cos(\theta(\boldsymbol{k})) = \frac{D(\boldsymbol{k})}{\sqrt{|D(\boldsymbol{k})|^2 + |g(\boldsymbol{k})|^2}}, \tag{6.13a}$$

$$\sin(\theta(\boldsymbol{k})) = \frac{g(\boldsymbol{k})}{\sqrt{|D(\boldsymbol{k})|^2 + |g(\boldsymbol{k})|^2}}, \tag{6.13b}$$

$$\Rightarrow \quad \theta(\boldsymbol{k}) = \arctan\left(\frac{g(\boldsymbol{k})}{D(\boldsymbol{k})}\right). \tag{6.13c}$$

We introduce the SSW field $\hat{\Xi}(\boldsymbol{k})$ in terms of the components of the fundamental Pauli field in momentum space,

$$\hat{\Xi}(\boldsymbol{k}) = \begin{pmatrix} \hat{\xi}_-(\boldsymbol{k}) \\ \hat{\xi}_+(\boldsymbol{k}) \end{pmatrix} = \mathcal{U}(\boldsymbol{k}) \begin{pmatrix} \hat{\phi}_\uparrow\big(\boldsymbol{k} - \frac{1}{2}\boldsymbol{q}\big) \\ \hat{\phi}_\uparrow\big(\boldsymbol{k} + \frac{1}{2}\boldsymbol{q}\big) \end{pmatrix}, \tag{6.14}$$

in order to write the Hamiltonian Eq. (6.7a) in its spectral decomposition,

$$\hat{\mathcal{H}}_{\mathrm{HF}} = \int \mathrm{d}^3k\, \hat{\Xi}^\dagger(\boldsymbol{k}) \begin{pmatrix} \epsilon_-(\boldsymbol{k}) - \mu & 0 \\ 0 & \epsilon_+(\boldsymbol{k}) - \mu \end{pmatrix} \hat{\Xi}(\boldsymbol{k})\,. \tag{6.15}$$

The corresponding creation operators $\hat{\xi}^\dagger_-(\boldsymbol{k})$, $\hat{\xi}^\dagger_+(\boldsymbol{k})$ insert an electron in the single-particle orbitals

$$\xi_{\boldsymbol{k}-}(\boldsymbol{r}) = \begin{pmatrix} \cos\big(\frac{1}{2}\theta(\boldsymbol{k})\big)\, e^{-\frac{\imath}{2}\boldsymbol{q}\cdot\boldsymbol{r}} \\ \sin\big(\frac{1}{2}\theta(\boldsymbol{k})\big)\, e^{\frac{\imath}{2}\boldsymbol{q}\cdot\boldsymbol{r}} \end{pmatrix} \frac{e^{\imath\boldsymbol{k}\cdot\boldsymbol{r}}}{\sqrt{2\pi}^3}, \tag{6.16a}$$

$$\xi_{\boldsymbol{k}+}(\boldsymbol{r}) = \begin{pmatrix} -\sin\big(\frac{1}{2}\theta(\boldsymbol{k})\big)\, e^{-\frac{\imath}{2}\boldsymbol{q}\cdot\boldsymbol{r}} \\ \cos\big(\frac{1}{2}\theta(\boldsymbol{k})\big)\, e^{\frac{\imath}{2}\boldsymbol{q}\cdot\boldsymbol{r}} \end{pmatrix} \frac{e^{\imath\boldsymbol{k}\cdot\boldsymbol{r}}}{\sqrt{2\pi}^3}, \tag{6.16b}$$

respectively. Having diagonalized the effective Hartree-Fock Hamiltonian Eq. (6.7a) by means of the SSW orbitals Eq. (6.16) we can compute the non-local effective potential defined in Eq. (4.28),

$$\begin{aligned} U_F(\boldsymbol{r};\boldsymbol{r}') &= \sum_{b=-,+} \int \mathrm{d}^3k'\; n_b(\boldsymbol{k}')\, \frac{\xi_{\boldsymbol{k}'b}(\boldsymbol{r})\, \xi^\dagger_{\boldsymbol{k}'b}(\boldsymbol{r}')}{|\boldsymbol{r} - \boldsymbol{r}'|} \\ &= \sum_{b=-,+} \int \mathrm{d}^3k'\; n_b(\boldsymbol{k}')\, \xi_{\boldsymbol{k}'b}(\boldsymbol{r})\, \xi^\dagger_{\boldsymbol{k}'b}(\boldsymbol{r}')\, \frac{1}{(2\pi)^3} \int \mathrm{d}^3k\; \frac{4\pi e^{\imath\boldsymbol{k}\cdot(\boldsymbol{r}-\boldsymbol{r}')}}{k^2} \\ &= \sum_{b=-,+} \int \mathrm{d}^3k'\; n_b(\boldsymbol{k}')\, \xi_{\boldsymbol{k}'b}(\boldsymbol{r})\, \xi^\dagger_{\boldsymbol{k}'b}(\boldsymbol{r}')\, \frac{1}{(2\pi)^3} \int \mathrm{d}^3k\; \frac{4\pi e^{\imath(\boldsymbol{k}-\boldsymbol{k}')\cdot(\boldsymbol{r}-\boldsymbol{r}')}}{(\boldsymbol{k} - \boldsymbol{k}')^2} \\ &= \frac{1}{(2\pi)^3} \int \mathrm{d}^3k\; e^{\imath\boldsymbol{k}\cdot(\boldsymbol{r}-\boldsymbol{r}')} \frac{1}{(2\pi)^3} \int \mathrm{d}^3k'\; \frac{4\pi}{(\boldsymbol{k} - \boldsymbol{k}')^2} \\ &\times \tfrac{1}{2} \begin{pmatrix} (n(\boldsymbol{k}') + B(\boldsymbol{k}'))\, e^{-\imath\frac{1}{2}\boldsymbol{q}\cdot(\boldsymbol{r}-\boldsymbol{r}')} & A(\boldsymbol{k}')\, e^{-\imath\frac{1}{2}\boldsymbol{q}\cdot(\boldsymbol{r}+\boldsymbol{r}')} \\ A(\boldsymbol{k}')\, e^{\imath\frac{1}{2}\boldsymbol{q}\cdot(\boldsymbol{r}+\boldsymbol{r}')} & (n(\boldsymbol{k}') - B(\boldsymbol{k}'))\, e^{\imath\frac{1}{2}\boldsymbol{q}\cdot(\boldsymbol{r}-\boldsymbol{r}')} \end{pmatrix}. \end{aligned} \tag{6.17}$$

In Eq. (6.17) we introduced the abbreviations

$$n(\boldsymbol{k}) = (n_-(\boldsymbol{k}) + n_+(\boldsymbol{k}))\,, \tag{6.18}$$

$$B(\boldsymbol{k}) = (n_-(\boldsymbol{k}) - n_+(\boldsymbol{k}))\cos(\theta(\boldsymbol{k}))\,, \tag{6.19}$$

$$A(\boldsymbol{k}) = (n_-(\boldsymbol{k}) - n_+(\boldsymbol{k}))\sin(\theta(\boldsymbol{k}))\,. \tag{6.20}$$

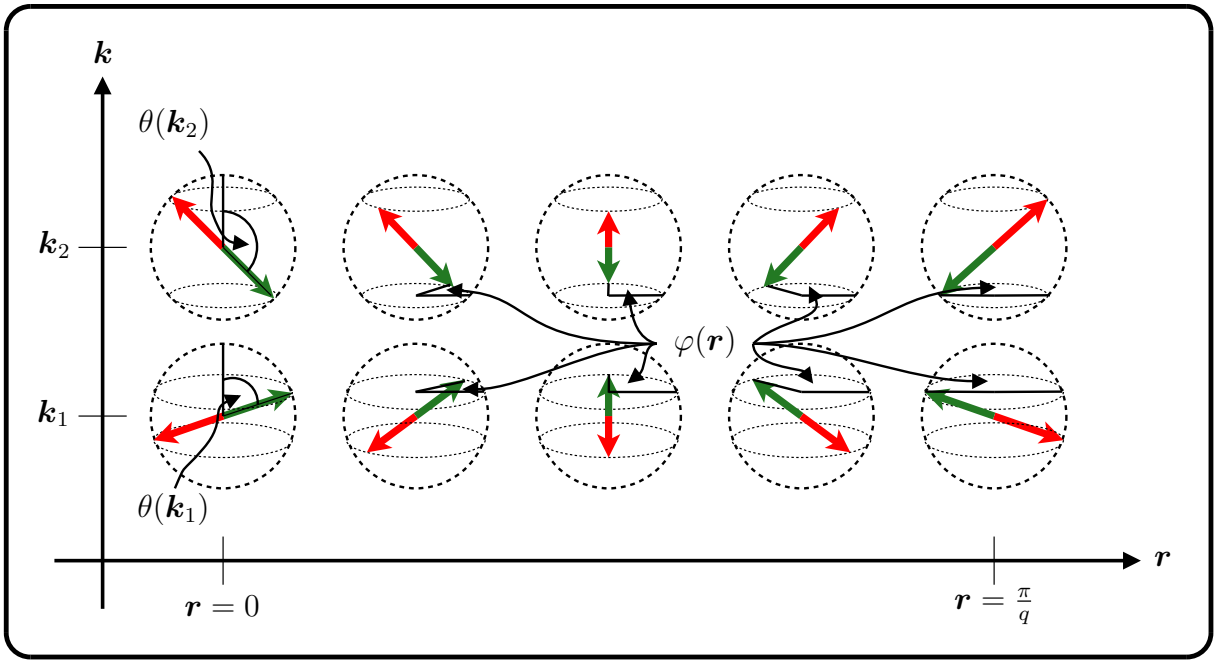

Figure 6.1: The effect of the spin rotation $\mathcal{U}(\boldsymbol{r},\boldsymbol{k})$ on pure spin-up (green arrow) or pure spin-down (red arrow) plane waves for two momenta $\boldsymbol{k}_{1/2}$. The angle $\theta(\boldsymbol{k})$ specifies the cone on which the spin is rotating. The position on the cone is given by the angle $\varphi(\boldsymbol{r}) = \boldsymbol{q}\cdot\boldsymbol{r}$, which is the same for all plane waves.

Moreover, comparing Eqs. (6.17) and (6.7b) we can identify the Hartree-Fock self-consistency conditions,

$$U_\uparrow\left(\boldsymbol{k}-\tfrac{1}{2}\boldsymbol{q}\right) = \frac{1}{(2\pi)^3}\int \mathrm{d}^3k'\,\frac{4\pi}{(\boldsymbol{k}-\boldsymbol{k}')^2}\tfrac{1}{2}\left(n(\boldsymbol{k}')+B(\boldsymbol{k}')\right), \tag{6.21a}$$

$$U_\downarrow\left(\boldsymbol{k}+\tfrac{1}{2}\boldsymbol{q}\right) = \frac{1}{(2\pi)^3}\int \mathrm{d}^3k'\,\frac{4\pi}{(\boldsymbol{k}-\boldsymbol{k}')^2}\tfrac{1}{2}\left(n(\boldsymbol{k}')-B(\boldsymbol{k}')\right), \tag{6.21b}$$

$$g(\boldsymbol{k}) = \frac{1}{(2\pi)^3}\int \mathrm{d}^3k'\,\frac{4\pi}{(\boldsymbol{k}-\boldsymbol{k}')^2}A(\boldsymbol{k}')\,. \tag{6.21c}$$

Eqs. (6.21a), (6.21b), (6.21c) determine the effective potentials $U_\uparrow$, $U_\downarrow$ and g in terms of the occupation numbers n_b, or equivalently the Fermi surface, and the angles θ. The Fermi surface and the angles in turn depend on the effective potentials $U_\uparrow$, $U_\downarrow$ and g (cf. Eqs. (6.11)-(6.13c)). Accordingly those equations have to be solved self-consistently in order to determine the optimal potentials, Fermi surface and angles. It is important to emphasize that all equations derived in this section intrinsically depend on the SSW wave vector $\boldsymbol{q}$. The energy contribution due to the pairing potential $g(\boldsymbol{k})$ favors a hybridization of spin-up and spin-down plane waves differing by $\boldsymbol{q}$ in their momenta. The orbital angles $\theta(\boldsymbol{k})$ (cf. (6.16)) describe this hybridization. Another way of looking at the orbital angles $\theta(\boldsymbol{k})$ is to consider them, together with the angles

$\varphi(\boldsymbol{r}) = \boldsymbol{q} \cdot \boldsymbol{r}$, as angles defining a rotation in spin space represented by

$$\begin{aligned} \mathcal{U}(\boldsymbol{r}, \boldsymbol{k}) &= e^{-\imath\varphi(\boldsymbol{r})\sigma^3} e^{-\imath\theta(\boldsymbol{k})\sigma^2} \\ &= \begin{pmatrix} \cos\left(\frac{1}{2}\theta(\boldsymbol{k})\right) e^{-\frac{\imath}{2}\boldsymbol{q}\cdot\boldsymbol{r}} & -\sin\left(\frac{1}{2}\theta(\boldsymbol{k})\right) e^{-\frac{\imath}{2}\boldsymbol{q}\cdot\boldsymbol{r}} \\ \sin\left(\frac{1}{2}\theta(\boldsymbol{k})\right) e^{\frac{\imath}{2}\boldsymbol{q}\cdot\boldsymbol{r}} & \cos\left(\frac{1}{2}\theta(\boldsymbol{k})\right) e^{\frac{\imath}{2}\boldsymbol{q}\cdot\boldsymbol{r}} \end{pmatrix}. \end{aligned} \tag{6.22}$$

The orbitals of Eq. (6.16a)/(6.16b) can then be thought of as being constructed by transforming pure spin-up/spin-down plane waves in spin space according to the rotation Eq. (6.22). First the plane wave is rotated around the y-axis by an angle $\theta(\boldsymbol{k})$, i.e. , an angle depending on its momentum. Then it is rotated around the z-axis by an angle $\varphi(\boldsymbol{r}) = \boldsymbol{q} \cdot \boldsymbol{r}$, which is the same for all plane waves, but depends on the spatial position (see Fig. 6.1). With this consideration it is clear that the angle $\theta(\boldsymbol{k})$ has to be restricted to the interval $[0, \pi]$ (or $[-\pi, 0]$) in order to assign a unique azimuthal rotation angle.

6.3 Spin spirals in Reduced-Density-Matrix-Functional Theory

In order to determine the SSW state we will not solve the Hartree-Fock self-consistent integral equations introduced in the previous section, but we will employ the theoretical framework of RDMFT, introduced in Secs. 2.5, 3.4 and 4.1. As already mentioned, Hartree-Fock theory can be viewed as a specific approximation for an energy functional in RDMFT. This will enable us to not only find the Hartree-Fock SSW state, but also to investigate the effect of the inclusion of correlations, by means of an xc-energy functional, on the SSW state and the Overhauser instability in general. Overhauser proved that the SSW state is lower in energy than the paramagnetic state assuming a wave vector $q \approx 2k_\mathrm{F}$. In our numerical investigation we determine the optimal value of q for a given density. We will see that q in fact varies from $2k_\mathrm{F} \to 1k_\mathrm{F}$, at the Hartree-Fock level, as the density decreases. We choose the Power-functional [SDLG08] (cf. Table 4.1), since it reduces to the Hartree-Fock functional for $\alpha = 1$ on one hand, excluding correlation effects, and on the other hand for $\alpha = 0.5$ coincides with the Müller functional, which is known to over-correlate. Furthermore for $\alpha \approx 0.6$ it yields very good correlation energies for the symmetry unbroken electron gas as discussed in Sec. 5.4. The implementation of RDMFT for the SSW state follows closely the treatment of the symmetry unbroken uniform electron gas outlined in the aforementioned section. There we assumed that the 1RDM exhibits the symmetries present in the Hamiltonian, i.e. , the natural orbitals are pure spin-up/spin-down plane waves, while here we use orbitals of the form of Eq. (6.16) as ansatz for the natural orbitals for our RDMFT treatment of the uniform electron gas. The spin-

spiral wave vector $\boldsymbol{q}$ and the hybridization angle $\theta(\boldsymbol{k})$ will be treated as variational parameters for the natural orbitals. It can easily be verified that the SSW orbitals of Eq. (6.16) form a complete and orthonormal set. The 1RDM, with the SSW ansatz for the natural orbitals, is given by

$$\begin{aligned}\gamma_{\mathrm{SSW}}(\boldsymbol{r};\boldsymbol{r}') &= \sum_{b=-,+}\int \mathrm{d}^3k\; n_b(\boldsymbol{k})\,\xi_{\boldsymbol{k}b}(\boldsymbol{r})\,\xi^{\dagger}_{\boldsymbol{k}b}(\boldsymbol{r}') \\ &= \frac{1}{(2\pi)^3}\int \mathrm{d}^3k\; e^{\imath\boldsymbol{k}\cdot(\boldsymbol{r}-\boldsymbol{r}')} \\ &\times \tfrac{1}{2}\begin{pmatrix} (n(\boldsymbol{k})+B(\boldsymbol{k}))\,e^{-\imath\frac{1}{2}\boldsymbol{q}\cdot(\boldsymbol{r}-\boldsymbol{r}')} & A(\boldsymbol{k})\,e^{-\imath\frac{1}{2}\boldsymbol{q}\cdot(\boldsymbol{r}+\boldsymbol{r}')} \\ A(\boldsymbol{k})\,e^{\imath\frac{1}{2}\boldsymbol{q}\cdot(\boldsymbol{r}+\boldsymbol{r}')} & (n(\boldsymbol{k})-B(\boldsymbol{k}))\,e^{\imath\frac{1}{2}\boldsymbol{q}\cdot(\boldsymbol{r}-\boldsymbol{r}')}\end{pmatrix}. \end{aligned} \tag{6.23}$$

From the spatial diagonal $\boldsymbol{r}=\boldsymbol{r}'$ we see that the corresponding electron density n is spatially constant, i.e. , CDWs are not described within this ansatz. The magnetization of the uniform electron gas is

$$\boldsymbol{m}\,(\boldsymbol{r}) = n\chi\begin{pmatrix} s\cos(\boldsymbol{q}\cdot\boldsymbol{r}) \\ s\sin(\boldsymbol{q}\cdot\boldsymbol{r}) \\ \sqrt{1-s^2}\end{pmatrix}, \tag{6.24a}$$

$$n\chi s = -\frac{1}{(2\pi)^3}\int \mathrm{d}^3k\; A(\boldsymbol{k})\,, \tag{6.24b}$$

$$n\chi\sqrt{1-s^2} = -\frac{1}{(2\pi)^3}\int \mathrm{d}^3k\; B(\boldsymbol{k})\,. \tag{6.24c}$$

The x- and y-components of the magnetization rotate in space along the direction of $\boldsymbol{q}$ with a periodicity given by the wavelength $q=|\boldsymbol{q}|$.

6.4 Numerical Implementation

Having chosen a functional and having made an ansatz for the natural orbitals, we minimize the functional for the ground-state energy. The functional depends on $n_b(\boldsymbol{k})$, $\theta(\boldsymbol{k})$ and the SSW wave vector $\boldsymbol{q}$. Since the density of the SSW state remains constant the Hartree contribution to the energy is cancelled by the uniform background charge. Accordingly the energy per electron reads

$$e_\alpha[n_b,\theta]\,(\boldsymbol{q}) = t\,[n_b,\theta]\,(\boldsymbol{q}) - w_{\alpha 1}[n_b,\theta] - w_{\alpha 2}[n_b,\theta]\,, \tag{6.25}$$

with the kinetic energy per electron

$$t[n_b,\theta]\left(\boldsymbol{q}\right)=\frac{1}{2n}\frac{1}{\left(2\pi\right)^3}\int\mathrm{d}^3k\,\Big(\left(n_-(\boldsymbol{k})+n_+(\boldsymbol{k})\right)k^2 - \boldsymbol{q}\cdot\boldsymbol{k}\left(n_-(\boldsymbol{k})-n_+(\boldsymbol{k})\right)\cos(\theta(\boldsymbol{k}))\Big)+\frac{q^2}{8}, \tag{6.26}$$

the energy contribution from exchange-like terms of orbitals with the same b (intra-band exchange)

$$w_{\alpha1}[n_b,\theta]=\frac{1}{2n}\frac{1}{\left(2\pi\right)^6}\iint\mathrm{d}^3k_1\mathrm{d}^3k_2\;\frac{4\pi}{\left(\boldsymbol{k}_1-\boldsymbol{k}_2\right)^2} \times\Big(\left(n_-(\boldsymbol{k}_1)\,n_-(\boldsymbol{k}_2)\right)^\alpha+\left(n_+(\boldsymbol{k}_1)\,n_+(\boldsymbol{k}_2)\right)^\alpha\Big)\cos^2\left(\frac{\theta(\boldsymbol{k}_1)-\theta(\boldsymbol{k}_2)}{2}\right), \tag{6.27}$$

and the energy contribution from exchange-like terms of orbitals with opposite b (inter-band exchange)

$$w_{\alpha1}[n_b,\theta]=\frac{1}{2n}\frac{1}{\left(2\pi\right)^6}\iint\mathrm{d}^3k_1\mathrm{d}^3k_2\;\frac{4\pi}{\left(\boldsymbol{k}_1-\boldsymbol{k}_2\right)^2} \times\Big(\left(n_-(\boldsymbol{k}_1)\,n_+(\boldsymbol{k}_2)\right)^\alpha+\left(n_+(\boldsymbol{k}_1)\,n_-(\boldsymbol{k}_2)\right)^\alpha\Big)\sin^2\left(\frac{\theta(\boldsymbol{k}_1)-\theta(\boldsymbol{k}_2)}{2}\right). \tag{6.28}$$

The symmetry is only broken along the direction of $\boldsymbol{q}$, which is chosen to be parallel to the z-axis. Since we are not considering spin-orbit coupling the plane in which the spin magnetizations rotates can be chosen as the x-y plane. Accordingly we can use cylindrical coordinates in momentum space, i.e. , $n_b(\boldsymbol{k})=n_b(k_\rho,k_z)$ and $\theta(\boldsymbol{k})=\theta(k_\rho,k_z)$. In order to minimize the gain in the kinetic energy (cf. (6.26)) by forming a spin spiral $\left(n_-(\boldsymbol{k})-n_+(\boldsymbol{k})\right)\cos(\theta(\boldsymbol{k}))$ should be an odd function w.r.t. k_z. Therefore we impose the following restrictions:

$$n_b(k_\rho,-k_z)=n_b(k_\rho,k_z)\quad,\quad n_-(\boldsymbol{k})\geq n_+(\boldsymbol{k})\,, \tag{6.29}$$

$$\theta(k_\rho,\pm|k_z|)=\frac{\pi}{2}\left(1\mp a(k_\rho,|k_z|)\right), \tag{6.30}$$

with $0\leq a(\boldsymbol{k})\leq1$. The z-component of the magnetization vanishes for these symmetry restrictions and the ansatz Eqs. (6.29),(6.30) describes a planar SSW. The configurations

$$\begin{aligned} &n_-^{\mathrm{PM}}(\boldsymbol{k})=\Theta\left(|\boldsymbol{k}-k_{\mathrm{F}}\boldsymbol{e}_3|-k_{\mathrm{F}}\right)+\Theta\left(|\boldsymbol{k}+k_{\mathrm{F}}\boldsymbol{e}_3|-k_{\mathrm{F}}\right),\\ &n_+^{\mathrm{PM}}(\boldsymbol{k})=0\;,\;a^{\mathrm{PM}}(\boldsymbol{k})=1\;,\;\boldsymbol{q}=2k_{\mathrm{F}}\boldsymbol{e}_3 \end{aligned} \tag{6.31a}$$

and

$$\begin{aligned} &n_-^{\mathrm{FM}}(\boldsymbol{k})=\Theta\left(|\boldsymbol{k}-2^{1/3}k_{\mathrm{F}}|\right),\\ &n_+^{\mathrm{FM}}(\boldsymbol{k})=0\;,\;a^{\mathrm{FM}}(\boldsymbol{k})=0\;,\;\boldsymbol{q}=0, \end{aligned} \tag{6.31b}$$

which are compatible with Eqs. (6.29),(6.30), correspond to the paramagnetic (PM) and ferromagnetic (FM) state of the uniform electron gas, respectively. Analogous to the discretization procedure described in Sec. 5.4 we assume that the occupation numbers $n_b(\boldsymbol{k})$ and the angles $a(\boldsymbol{k})$ are constant within annular regions Ω_j in $\boldsymbol{k}$-space,

$$\Omega_j = \left\{ \boldsymbol{k} \;\middle|\; k_\rho^{j-} \leq k_\rho \leq k_\rho^{j+} \;;\; k_z^{j-} \leq k_z \leq k_z^{j+} \right\}. \tag{6.32}$$

Then the discretized energy contributions are

$$\begin{aligned} t[n_b, \theta]\,(q) =& \sum_{bj} n_{bj} \mathrm{DKI}_j + \frac{q^2}{8} \\ & - q \sum_j \left(n_{-j} - n_{+j}\right) \cos(\theta_j)\, \mathrm{DQI}_j, \end{aligned} \tag{6.33a}$$

$$w_{\alpha 1}[n_b, \theta] = \frac{1}{2} \sum_{bjk} \left(n_{bj} n_{bk}\right)^\alpha \cos^2\left(\frac{\theta_j - \theta_k}{2}\right) \mathrm{DXI}_{jk}, \tag{6.33b}$$

$$w_{\alpha 2}[n_b, \theta] = \sum_{jk} \left(n_{-j} n_{+k}\right)^\alpha \sin^2\left(\frac{\theta_j - \theta_k}{2}\right) \mathrm{DXI}_{jk}, \tag{6.33c}$$

where the integral weights are given by

$$\mathrm{DKI}_j = \frac{1}{8\pi^2 n} \iint_{\Omega_j} \mathrm{d}k_\rho \mathrm{d}k_z \;\; \left(k_\rho^3 + k_\rho k_z^2\right) \tag{6.34a}$$

$$\mathrm{DQI}_j = \frac{1}{8\pi^2 n} \iint_{\Omega_j} \mathrm{d}k_\rho \mathrm{d}k_z \;\; \left(k_\rho k_z\right) \tag{6.34b}$$

$$\begin{aligned} \mathrm{DXI}_{jk} = & \frac{1}{2n} \frac{1}{(2\pi)^6} \iiint_{\Omega_j} \mathrm{d}k_{\rho 1} \mathrm{d}k_{z1} \mathrm{d}\phi_1 \;\; \iiint_{\Omega_k} \mathrm{d}k_{\rho 2} \mathrm{d}k_{z2} \mathrm{d}\phi_2 \\ & \times \frac{4\pi k_{\rho 1} k_{\rho 2}}{k_{\rho 1}^2 + k_{\rho 2}^2 + \left(k_{z1} - k_{z2}\right)^2 - 2k_{\rho 1} k_{\rho 2} \cos(\phi_1 - \phi_2)}. \end{aligned} \tag{6.34c}$$

The integrals (6.34a) and (6.34b) are readily solved and the integrals (6.34c) can ultimately be reduced to elliptic integrals (cf. App. A), which are numerically accessible with high accuracy. Since the momenta are treated as continuous variables we stay in the thermodynamic limit. Thus all energies obtained numerically are variational. The error introduced by the discretization is solely due to the assumption that the $n_b(\boldsymbol{k})$ and $\theta(\boldsymbol{k})$ are constant within the elementary volume elements Ω_j and can systematically be reduced by increasing the number of discretization points.

After having discretized the problem, the minimization of the energy functional of Eq. (6.25) becomes a high-dimensional optimization problem. We use a steepest descent algorithm for the minimization and ensure that the N-representability conditions (cf. Sec. 2.5 Eq. (2.51)), are satisfied during the minimization process. Starting from some initial 1RDM and some initial discretization in momentum space the energy is minimized for a fixed spin-spiral wave

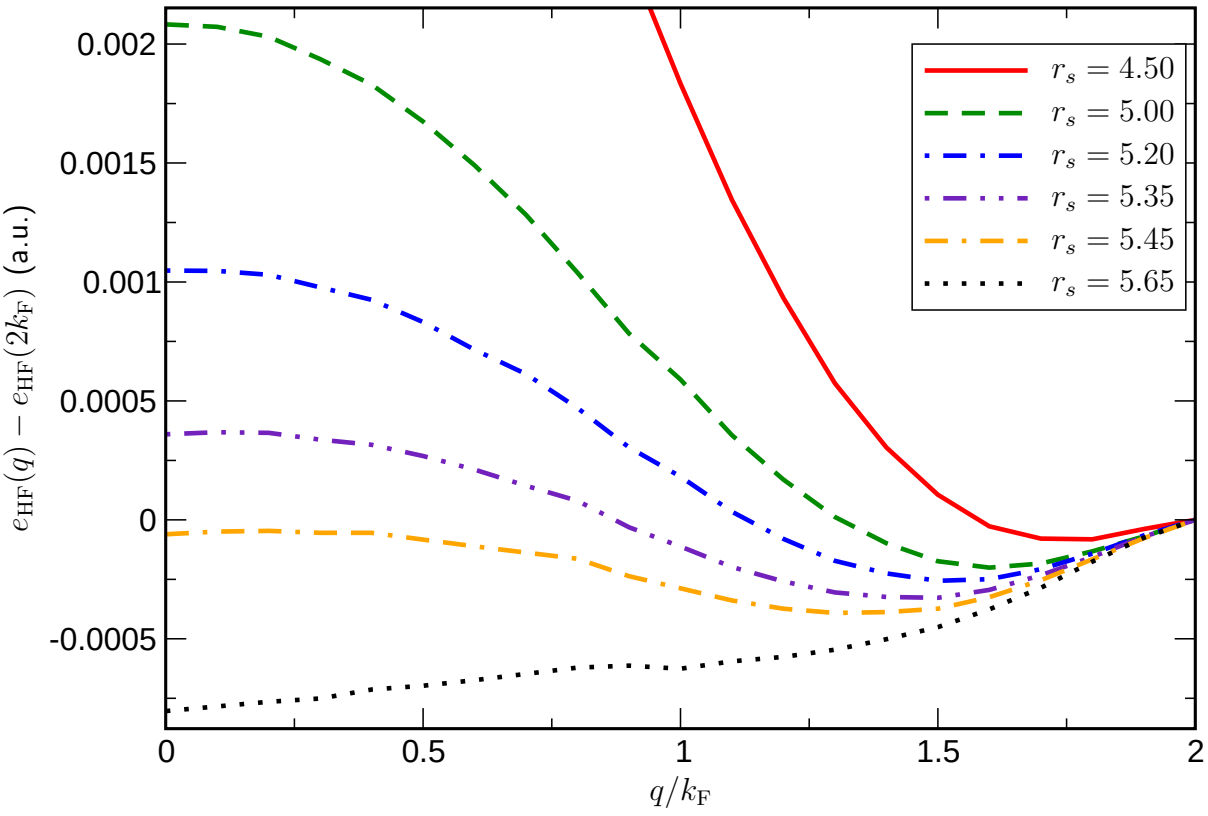

Figure 6.2: Hartree-Fock total energy per electron of the SSW state as function of the SSW wave vector q at various r_s. The value $e_{\mathrm{HF}}(q = 2k_{\mathrm{F}})$ is subtracted in order to emphasize the behavior of the minimum at different densities. For increasing density (decreasing r_s) the minimum shifts to higher values of q_{opt} and the energy gain compared to the paramagnetic state by forming a spin spiral decreases.

vector $\boldsymbol{q}$. Then the discretization is refined in those regions of momentum space where the n_{bj} and/or the a_j show the largest variations. The minimization on the refined momentum space mesh starts from a re-initialized 1RDM in order to prevent dependencies on the result of the minimization on the coarser grid. Finally we compare the total energies at different $\boldsymbol{q}$ in order to determine the optimal SSW wave vector $\boldsymbol{q}_{\mathrm{opt}}$ for various densities.

6.5 Results within Hartree-Fock theory

We first use our numerical implementation to investigate Overhauser's SSW state in the Hartree-Fock approximation or equivalently the Power functional with $\alpha = 1$. From the considerations in Eqs. (6.31) we see that it is sufficient to minimize w.r.t. a 1RDM whose occupation numbers are only non-zero for orbitals with $b = -$ and $|\boldsymbol{q}| \in [0, 2k_{\mathrm{F}}]$ since both the

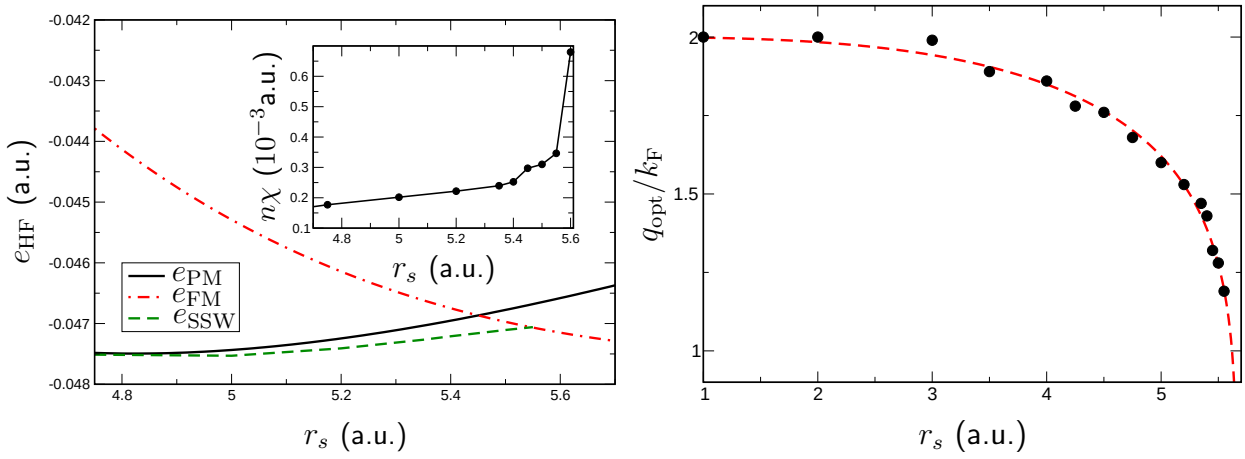

Figure 6.3:
Left panel: Dependence of the energy per electron on r_s, within the Hartree-Fock approximation, for the paramagnetic, ferromagnetic and SSW phase in the region of the paramagnetic-ferromagnetic crossover. The inset shows the behavior of the amplitude $n\chi$, defined in Eq. (6.24a), at the optimal spin-spiral wave vector.
Right panel: Dependence of the Hartree-Fock optimal spin-spiral wave vector $q_{\rm opt}$ on the density, given by r_s. The proposed approximation by a simple scaling law Eq. (6.35) is shown as the dashed line.

paramagnetic and the ferromagnetic Hartree-Fock solutions are accessible under these conditions. The minimization at $q = 0$ and $q = 2k_{\rm F}$ yields exactly the occupation numbers n_{bj} and angle parameters a_j given in Eqs. (6.31b) and (6.31a), respectively. Therefore we can read the total energy per particle as function of the spin-spiral wave vector in the following way: $e_{\rm HF}(q = 0)$ is the energy of the ferromagnetic state, $e_{\rm HF}(q = 2k_{\rm F})$ corresponds to the energy of the paramagnetic state. For intermediate values, $0 < q < 2k_{\rm F}$, $e_{\rm HF}(q)$ corresponds to a SSW configuration with $m_3 = 0$ (planar spiral). Overhauser's statement can then be expressed as $\partial_q e_{\rm HF}(q)|_{q=2k_{\rm F}} > 0$, i.e. , the paramagnetic configuration is unstable w.r.t. the formation of a SSW.

In Fig. 6.2 we show the dependence of the total energy per particle on the spin-spiral wave vector $\boldsymbol{q}$ for various densities. Consistent with Overhauser's proof, the derivative of $e_{\rm HF}(q)$ is positive at $q = 2k_{\rm F}$. It is clear from Fig. 6.2 that the optimal SSW wave vector moves away from the paramagnetic configuration ($q = 2k_{\rm F}$) as the density decreases. Furthermore the difference between the total energy at the minimum and the total energy at $q = 2k_{\rm F}$ increases with increasing r_s, i.e. , the instability is more pronounced at lower densities. Below some critical density, however, the ferromagnetic state ($q = 0$) becomes the most stable solution.

This is not in contradiction with Overhauser's statement since the SSW state is still lower in energy than the paramagnetic state. A comparison of the energy per electron in the paramagnetic, ferromagnetic and SSW phase is depicted in Fig. 6.3. Our results for the non-collinear magnetic states of the uniform electron gas extend the picture given by Zhang and Ceperley [ZC08]. They employed a Monte Carlo algorithm that samples only single Slater determinants in order to investigate a combined CDW/SDW state, staying however in the collinear regime. It seems that the gain in energy by forming a collinear SDW/CDW state (cf. Ref. [ZC08] for details) is larger compared to the energy gain by forming an SSW. This is consistent with the qualitative argument already given by Overhauser, that the superposition of a left- and right-rotating SSW yielding a collinear SDW will increase the gain in energy.

To describe the resulting behavior of the optimal wave vector $q_{\mathrm{opt}}(r_s)$ for the non-collinear SSW we propose a simple, empirical scaling law:

$$q_{\mathrm{opt}}(r_s) = 2k_{\mathrm{F}} \left(1 - \left(\frac{r_s}{r_0} \right)^3 \right)^{\beta}, \tag{6.35}$$

where $r_0 \approx 5.7$ and $\beta \approx 0.2$. The proposed scaling behavior of q_{opt} reproduces the numerical data very accurately as can be seen in Fig. 6.3. It should be emphasized that we do not find any optimal spin-spiral wave vector $q_{opt} < k_{\mathrm{F}}$. Note that for densities close to the transition to the ferromagnetic state the optimum wave vector q_{opt} can be quite different from $2k_{\mathrm{F}}$ while for higher densities it is very close to this value. The results in Ref. [ZC08] indicate a different behavior of the dominant wave vector at high densities. This can be understood by considering that in Ref. [ZC08] a general superposition of collinear SDWs and CDWs was considered while in our work we investigate the broken-symmetry solution due to a single non-collinear SSW.

The effect of the refinement of the discretization in momentum space is shown in Fig. 6.4. By sampling n_{bj} and a_j more often in regions of higher variations we both lower the energy and reduce the numerical noise in $e_{\mathrm{HF}}(q)$. The convergence of the total energy can be inferred from the values $e_{\mathrm{HF}}(q = 2k_{\mathrm{F}})$ at different discretizations and comparing to the analytic paramagnetic energy. For the case of $r_s = 5.0$ we obtain an SSW energy that is lower than the analytic paramagnetic energy at the optimal value of the SSW wave vector. At higher densities (lower r_s) the energy gain by forming a SSW is lower, so we would need a very fine discretization to obtain numerical results lower than the analytic paramagnetic energy. However, considering the numerical value of the paramagnetic energy at the same discretization is sufficient to demonstrate the instability w.r.t. a SSW formation, because the computed energies are variational as discussed in Sec. 6.4. In order to determine the dependence of the optimal spin-spiral wave vector q_{opt} on the density, we therefore refine the momentum space discretization until q_{opt} is converged.

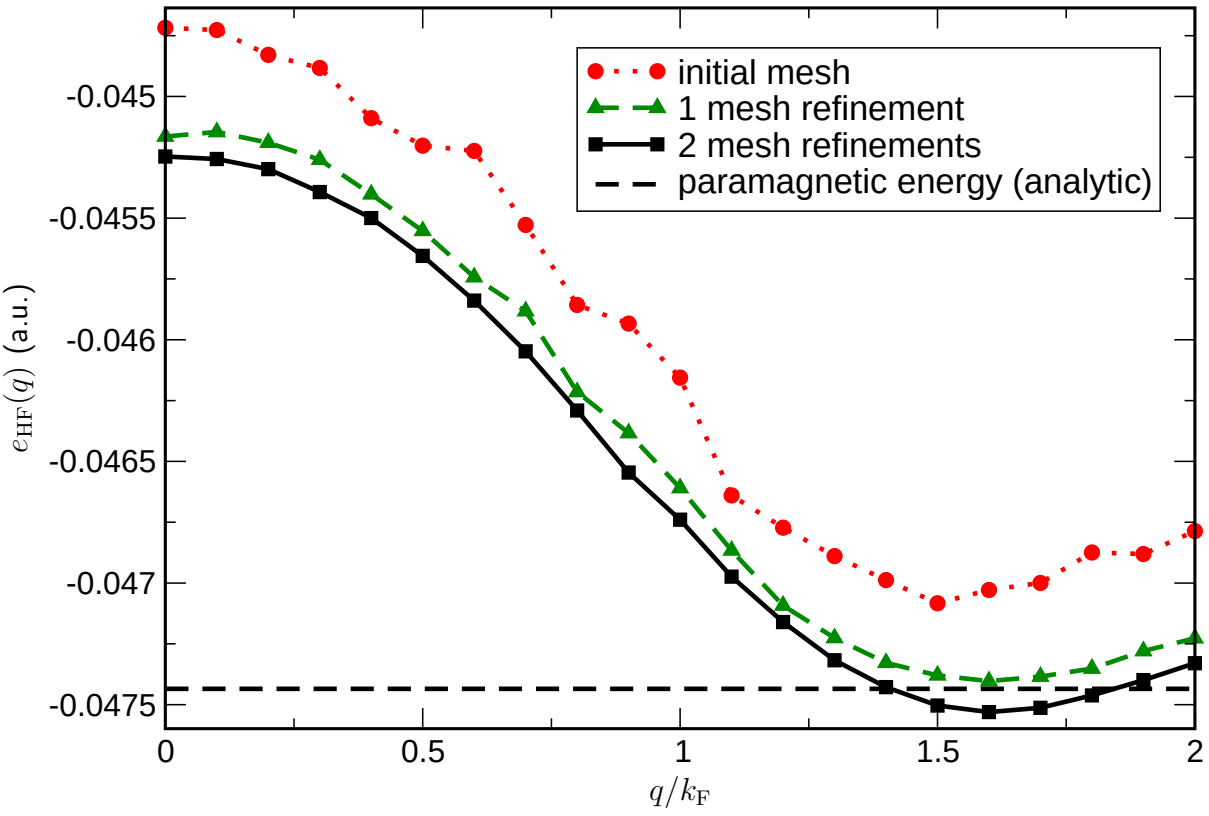

Figure 6.4: Hartree-Fock total energy per electron as function of the spin-spiral wave vector q at the density corresponding to $r_s = 5.0$. The data sets represent results at different discretizations. The dashed horizontal line visualizes the analytic value of the paramagnetic ground state energy. The optimal SSW wave vector is $q_{\mathrm{opt}} \approx 1.6 k_{\mathrm{F}}$.

For our numerical results we have verified that the occupation numbers and the angular parameters a_j satisfy Overhauser's self-consistency equations Eq. (6.21) by iterating them only once. The difference between the angles a_j in the occupied regions before and after the iteration is numerically zero for all values of $\boldsymbol{q}$. This means that choosing a spin-spiral wave vector we can always find a solution of the self-consistency equations derived by Overhauser. Since the total energy does not depend on the a_j in regions where $n_{bj} = 0$, one self-consistency loop furthermore fixes the angles a_j in unoccupied regions of $\boldsymbol{k}$-space. This is necessary to construct the proper Hartree-Fock dispersions (cf. Fig. 6.5) also for the unoccupied states.

At the single-particle level we have an intuitive understanding of the instability: as the two distinct spin-up and spin-down regions of the paramagnetic state are squeezed into each other, the orbitals in the overlapping region hybridize. This hybridization then leads to the opening of a direct gap between the Hartree-Fock single-particle dispersions corresponding to $b = -, +$ at $k_z = 0$ as well as to a lowering of both the symmetry and the total energy of the system. The mixing of the spin-up and spin-down orbitals is given by the orbital angles $\theta(\boldsymbol{k})$, capable

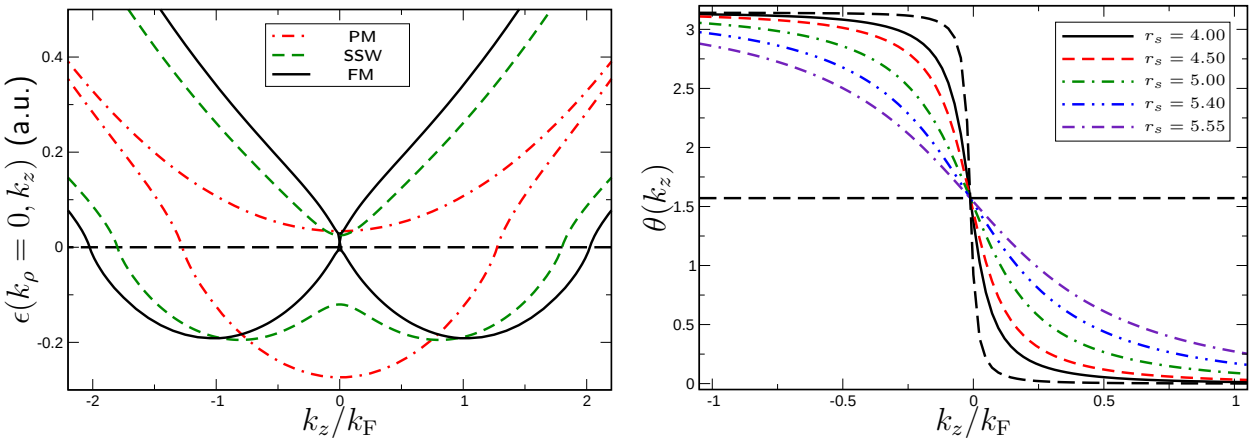

Figure 6.5:
Left panel: Hartree-Fock single-particle dispersion $(k_\rho = 0)$ at $r_s = 5.0$ for the paramagnetic $(q \geq 2k_\mathrm{F})$, ferromagnetic $(q = 0)$ and the SSW state $(q_\mathrm{opt} = 1.6k_\mathrm{F})$. The difference between the two symmetric minima corresponds to the SSW wave vector q. The paramagnetic dispersion may also be viewed as an SSW dispersion with the origin in momentum space shifted by $\pm q$ for the different spin channels (cf. Eqs. (6.31)).
Right panel: Orbital angles $\theta(k_\rho = 0, k_z)$ for various densities, specified by r_s, at the optimal SSW wave vector. The horizontal dashed line corresponds to the orbital angles at $q = 0$ (ferromagnetic) and the step-like dashed line corresponds to $q = 2k_\mathrm{F}$ (paramagnetic). For increasing r_s the optimal spin-spiral wave vector becomes smaller, such that the Fermi spheres, separated at $q = 2k_\mathrm{F}$, begin to overlap. In order to gain energy the spin-up and spin-down orbitals in the overlapping region hybridize and the orbital angle θ describes the mixing of the spin-up and spin-down states.

of describing a continuous transition between the paramagnetic and the ferromagnetic state (cf. Eqs. (6.31a) and (6.31b) respectively). The behavior of the orbital angles at the optimal spin-spiral wave vector is shown in Fig. 6.5.

6.6 Results within Reduced-Density-Matrix-Functional Theory

As discussed above the Power functional reduces to the uncorrelated Hartree-Fock approximation for $\alpha = 1$ and to the Müller functional for $\alpha = 0.5$. The latter one is known [LHG07] to over-correlate and therefore one expects that decreasing α from $1 \to 0.5$ increases the amount of correlation in the system. This picture was verified in Ref. [LSD$^+$09], where an optimal value of $\alpha \approx 0.6$ was found in the regions of metallic densities for the paramagnetic uniform

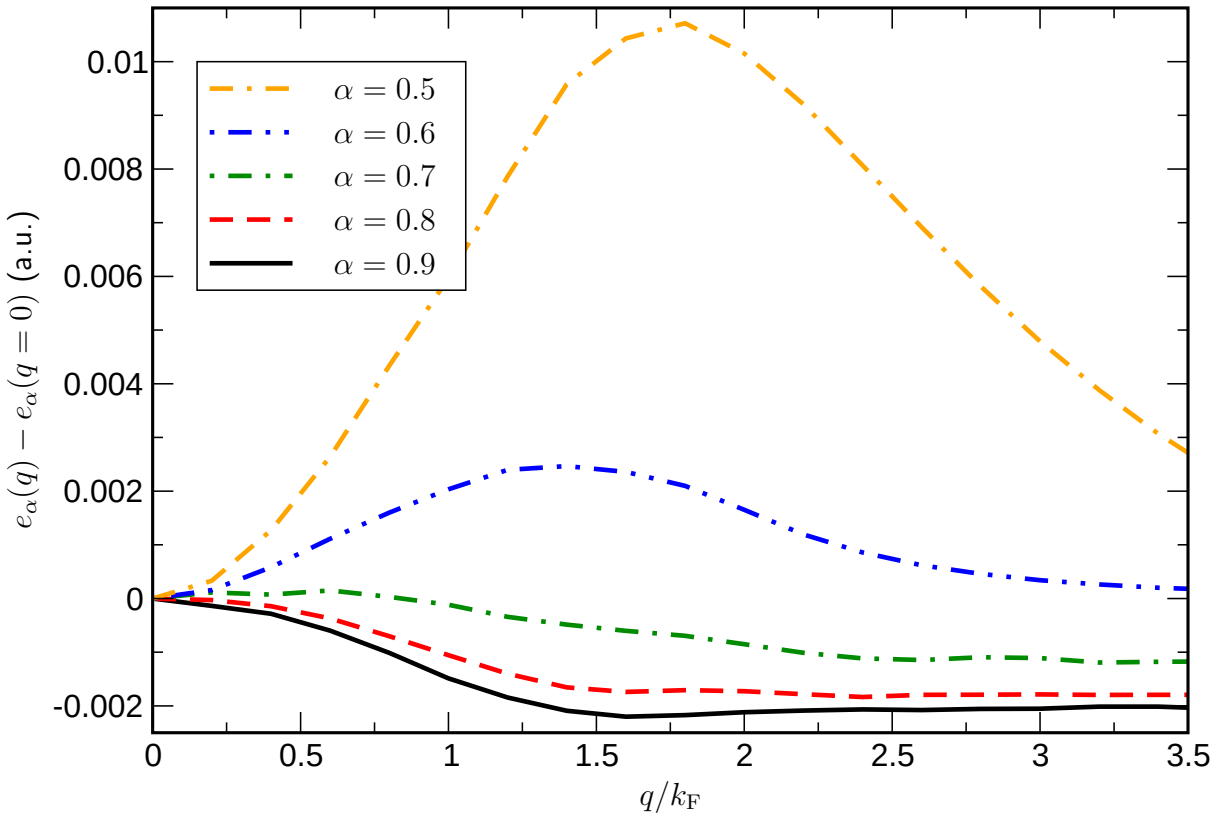

Figure 6.6: Total energies per electron of the SSW state described with the density-matrix-power functional as a function of the spin-spiral wave vector q for various values of α at $r_s = 5.0$. The total energy per electron at $q = 0$ is subtracted in order to emphasize the behavior with increasing q.

electron gas (cf. Sec. 5.4). In Fig. 6.6 the dependence of the total energy per particle at $r_s = 5.0$ is shown for various α. It should be noted that the configuration for $q > 2k_\mathrm{F}$ cannot be interpreted as the paramagnetic state in the correlated case. This is due to the fact that correlations smear out the sharp step found for the uncorrelated case in the momentum distribution around the Fermi surface as discussed in Sec. 5.4. Therefore at $q = 2k_\mathrm{F}$ the fractionally occupied regions in momentum space are not necessarily disjoint. Only when the occupied regions separate into two parts the configuration corresponds to the paramagnetic state. However, the configuration at $q = 0$ may still be interpreted as the ferromagnetic state. From Fig. 6.6 it is clear that the instability w.r.t. a SSW is still present for $\alpha = 0.9$. For higher values of α the instability disappears and for $\alpha = 0.5, 0.6$ the energy has a maximum in the SSW region. Thus for values of α which provide good correlation energies for the uniform electron gas in the paramagnetic regime there is no SSW formation. In order to understand the reason for this it is instructive to look at various contributions to the total energy. In Fig. 6.7 we compare the correlation energy contribution with the contribution coming from

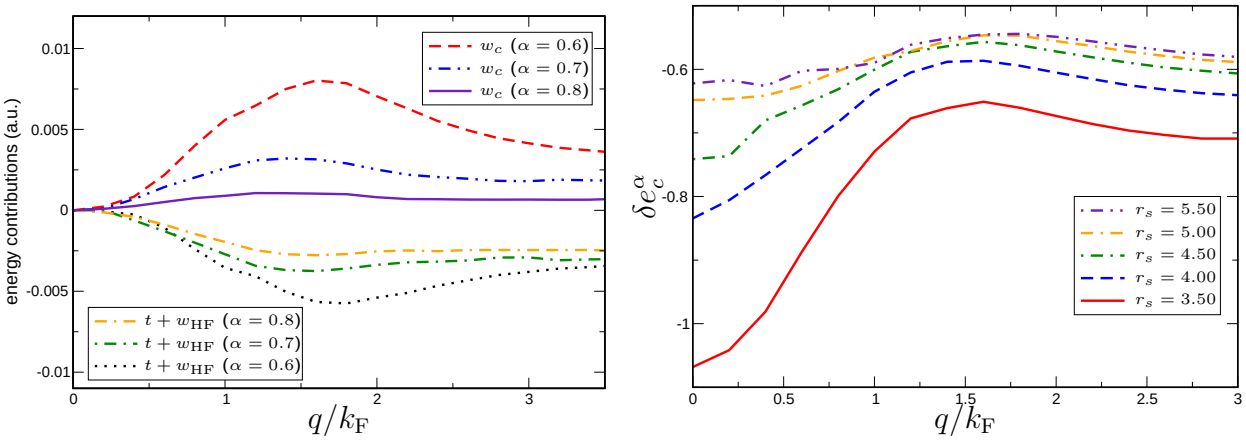

Figure 6.7:
Right panel: Comparison of the correlation energy with the contribution from kinetic plus exchange terms $t + w_{\mathrm{HF}}$ for $\alpha = 0.6, 0.7, 0.8$ at $r_s = 5.0$. All energy contributions are shifted such that the value at $q = 0$ is zero. For decreasing α the minimum in $t + w_{\mathrm{HF}}$ shifts to higher values of q. The correlation contribution $w_c = w_\alpha - w_{\mathrm{HF}}$ however damps out this instability for values of α that yield good total energies at metallic densities.
Left panel: Relative correlation energy as a function of the spin-spiral wave vector q for various r_s at $\alpha = 0.6$. Correlations are more important around the ferromagnetic configuration. In the region of the Hartree-Fock SSW instability correlations have the smallest effect. This indicates why the instability is not sustained when correlations are included at the level of the density-matrix-power functional.

the kinetic and exchange terms. The minimum is still present considering only kinetic and exchange contributions, but for decreasing α the correlation contribution damps out the instability more and more. One might suspect that at high densities, where exchange dominates correlations, the instability sustains. Our findings in Sec. 6.5 show that in the Hartree-Fock approximation the energy gain decreases when the density increases, which is consistent with an analytic argument given by Giuliani and Vignale [GV08] that at high densities the energy gain by forming a SDW and/or CDW is overcome by correlations. Furthermore our results indicate that correlation effects dominate the SSW instability also at intermediate densities. In order to gain some insight into the role of correlations we define the relative correlation energy δe_c as

$$\delta e_c^{\alpha} = \frac{w_\alpha - w_{\mathrm{HF}}}{|e_\alpha|} \,. \tag{6.36}$$

In Fig. 6.7 we show the dependence of this quantity on the spin-spiral wave vector for the correlation parameter $\alpha = 0.6$. The absolute value of the relative correlation is smallest in the region of the SSW instability ($q = k_{\mathrm{F}} \to 2k_{\mathrm{F}}$), which explains why the instability is no longer

present when correlations are included. Furthermore we can see that the relative correlation is dominant in the region of the ferromagnetic configuration. This can be understood by noticing that the Power functional approximates the correlation energy by a pre-factor times a Fock integral (most present-day functionals in RDMFT approximate correlations in this way, cf. Sec. 4.1). Since Fock integrals imply that equal spins are particularly correlated, we expect a similar dependence of the relative correlation energy for other RDMFT functionals.

6.7 Summary and Conclusion

We have investigated the instability of the uniform electron gas w.r.t. the formation of a spin-spiral wave within Reduced-Density-Matrix-Functional Theory, which includes the Hartree-Fock approximation as an important limiting case. To our knowledge this is the first numerical Hartree-Fock study of the non-collinear spin-spiral-wave state in the electron gas, despite the fact that Overhauser presented his analytical work on the problem five decades ago. In Overhauser's work, the optimal spin-spiral wave vector was not determined. Our study shows that, in contrast to common belief, the optimal spin-spiral wave vector is not always close to $2k_{\mathrm{F}}$. While at high densities we confirm this value for the optimal wave vector for a single non-collinear spin-spiral, for lower densities (just before the transition to the ferromagnetic state) the optimal wave vector even approaches k_{F}. Within the framework of Reduced-Density-Matrix-Functional Theory we also studied the effect of correlations on the spin-spiral-wave instability using the Power functional. Not unexpectedly, we find that the inclusion of correlations suppresses the instability, which is explained by the behavior of the correlation energy in the region of the spin-spiral wave instability.

Chapter 7

Spin-Density-Functional Theory for the spin-spiral wave

Overhauser's spin-spiral wave is as picture-book example of the intriguing feature of self-consistent theories to predict spontaneous symmetry breaking. Based on the seemingly innocent ansatz that the many-particle wave function is a single Slater determinant, Hartree-Fock theory predicts that the spin-spiral state of the uniform alectron gas is lower in energy than the paramagnetic state. As we have discussed in chapter 3 the Kohn-Sham implementation of DFT also represents a self-consistent theory. However, it is not based on an ansatz for the many-body wave function but instead is based on the Hohenberg-Kohn theorem that allows to connect the Kohn-Sham system uniquely to the interacting system via the fundamental densities, that are identical in both systems. This is of great importance if one aims at the description of symmetry breaking. If the Hartree-Fock system exhibits a broken symmetry, e.g. a non-vanishing spin magnetization, this has strictly speaking no implications for the physical, i.e. , interacting system, because it is obtained using an ansatz for the wave function. If the Kohn-Sham system exhibits a non-vanishing spin magnetization, however, this implies that the spin magnetization of the interacting system is also non-vanishing since they are identical by construction. In practice one has to be careful that bad approximations for the xc potentials may cause unphysical symmetry breaking or prevent physical symmetry breaking. Another way to illustrate the difference between Kohn-Sham DFT and Hartree-Fock theory is to look at the uniform electron gas. When treated within Kohn-Sham DFT the Kohn-Sham potential is a constant otherwise the density would not be constant. This means that the single-particle dispersion in the Kohn-Sham system is $\frac{1}{2}k^2$. Therefore one may view the effective Kohn-Sham single-particle Hamiltonian to be more physical than the effective Hartree-Fock single-particle Hamiltonian for the uniform electron gas, because it retains the $\frac{1}{2}k^2$ dispersion for the effective electrons, whereas the dispersion of the effective electrons in Hartree-Fock theory is

modified by a k-dependent term with a logarithmically diverging slope at the Fermi wave vector (cf. Sec. 5.3). This logarithmic divergence implies a vanishing density of states at the Fermi surface rendering the electron gas insulating at *all* densities. This comparison of course employs the notion that the quasi particles of the uniform electron gas are approximated by the Kohn-Sham or Hartree-Fock effective particles, respectively.

In the present chapter we investigate if the Overhauser instability is also present in the treatment of the uniform electron gas employing Spin-Density-Functional Theory (SDFT) [vBH72]. The inclusion of the spin magnetization as fundamental variable is necessary since it is the characterizing density of the spin-spiral wave. An alternative density-functional formalism for the description of general spin-density waves and anti-ferromagnetism was proposed by Capelle and Oliveira [CO00a, CO00b]. In their work the system is also described in terms of its density and spin magnetization but the x- and y-components of the spin magnetization are replaced by their non-local counterparts. This might be viewed as a hybrid theory between the completely non-local RDMFT and the completely local SDFT. The results presented in this chapter were published in [KE09].

7.1 Spin-spiral wave for local effective potentials

The crucial difference between the effective Hartree-Fock Hamiltonian and the effective Kohn-Sham Hamiltonian is that the latter only contains local external potentials, i.e. , a local external potential V_s and a local external magnetic field $\boldsymbol{B}_s$ in the case of SDFT. The Kohn-Sham Hamiltonian for the SSW state can be inferred directly from the Hamiltonian Eq. (6.7), because the requirement of local external potentials means that the only k-dependent part of the effective Hamiltonian is the kinetic contribution. This is accomplished by setting $U_\uparrow\big(\boldsymbol{k}-\frac{1}{2}\boldsymbol{q}\big)\to\frac{1}{2}B$, $U_\downarrow\big(\boldsymbol{k}+\frac{1}{2}\boldsymbol{q}\big)\to-\frac{1}{2}B$ and $g(\boldsymbol{k})\to A$ yielding

$$\hat{\mathcal{H}}_\mathrm{s}=\int\mathrm{d}^3k\,\begin{pmatrix}\hat{\phi}^\dagger_\uparrow\big(\boldsymbol{k}-\frac{1}{2}\boldsymbol{q}\big) & \hat{\phi}^\dagger_\downarrow\big(\boldsymbol{k}+\frac{1}{2}\boldsymbol{q}\big)\end{pmatrix}\mathrm{H}^s_\mathrm{SSW}\begin{pmatrix}\hat{\phi}_\uparrow\big(\boldsymbol{k}-\frac{1}{2}\boldsymbol{q}\big)\\ \hat{\phi}_\downarrow\big(\boldsymbol{k}+\frac{1}{2}\boldsymbol{q}\big)\end{pmatrix}. \tag{7.1a}$$

$$\mathrm{H}^s_\mathrm{SSW}=\begin{pmatrix}\frac{1}{2}\left(\boldsymbol{k}-\frac{1}{2}\boldsymbol{q}\right)^2-\frac{1}{2}B-\mu & -\frac{1}{2}A\\ -\frac{1}{2}A & \frac{1}{2}\left(\boldsymbol{k}+\frac{1}{2}\boldsymbol{q}\right)^2+\frac{1}{2}B-\mu\end{pmatrix}. \tag{7.1b}$$

It is straight forward to write Eq. (7.1) in terms of the fundamental Pauli fields employing a Fourier transformation,

$$\hat{\mathcal{H}}_{\mathrm{s}} = \int \mathrm{d}^3 r \; \hat{\Phi}^\dagger(\boldsymbol{r}) \left(\tfrac{1}{2} \overleftarrow{\nabla} \cdot \overrightarrow{\nabla} - \mu + \mu_{\mathrm{B}} \boldsymbol{\sigma} \cdot \boldsymbol{B}_s(\boldsymbol{r}) \right) \hat{\Phi}(\boldsymbol{r}) \,, \tag{7.2a}$$

$$\boldsymbol{B}_s(\boldsymbol{r}) = -\tfrac{1}{2\mu_{\mathrm{B}}} \begin{pmatrix} A\cos(\boldsymbol{q}\cdot\boldsymbol{r}) \\ A\sin(\boldsymbol{q}\cdot\boldsymbol{r}) \\ B \end{pmatrix}. \tag{7.2b}$$

It is not surprising that the external magnetic field $\boldsymbol{B}_s$ has the same form as the spin magnetization of the SSW. The diagonalization of the Kohn-Sham Hamiltonian Eq. (7.1) is analogous to the diagonalization of the Hartree-Fock Hamiltonian Eq. (6.7). The spectral decomposition is given by

$$\hat{\mathcal{H}}_{\mathrm{s}} = \int \mathrm{d}^3 k \; \hat{\Xi}_s^\dagger(\boldsymbol{k}) \begin{pmatrix} \epsilon_-(\boldsymbol{k}) - \mu & 0 \\ 0 & \epsilon_+(\boldsymbol{k}) - \mu \end{pmatrix} \hat{\Xi}_s(\boldsymbol{k}) \,, \tag{7.3a}$$

$$\epsilon_\mp(\boldsymbol{k}) = \tfrac{1}{2}k^2 + \tfrac{1}{8}q^2 \mp \tfrac{1}{2}\sqrt{(\boldsymbol{k}\cdot\boldsymbol{q} + B)^2 + A^2}. \tag{7.3b}$$

The Kohn-Sham orbitals corresponding to the components of the spiral field $\hat{\Xi}_s$ are determined through the angles

$$\cos(\theta(\boldsymbol{k})) = \frac{\boldsymbol{k}\cdot\boldsymbol{q} + B}{\sqrt{(\boldsymbol{k}\cdot\boldsymbol{q} + B)^2 + A^2}}, \tag{7.4a}$$

$$\sin(\theta(\boldsymbol{k})) = \frac{A}{\sqrt{(\boldsymbol{k}\cdot\boldsymbol{q} + B)^2 + A^2}}, \tag{7.4b}$$

$$\Rightarrow \quad \theta(\boldsymbol{k}) = \arctan\left(\frac{A}{\boldsymbol{k}\cdot\boldsymbol{q} + B} \right). \tag{7.4c}$$

They look formally equivalent to the Hartree-Fock spin-spiral orbitals Eq. (6.16), but it should be kept in mind that the definition of the orbital angles $\theta(\boldsymbol{k})$ differs :

$$\xi^s_{\boldsymbol{k}-}(\boldsymbol{r}) = \begin{pmatrix} \cos\left(\frac{1}{2}\theta(\boldsymbol{k})\right) e^{-\frac{\imath}{2}\boldsymbol{q}\cdot\boldsymbol{r}} \\ \sin\left(\frac{1}{2}\theta(\boldsymbol{k})\right) e^{\frac{\imath}{2}\boldsymbol{q}\cdot\boldsymbol{r}} \end{pmatrix} \frac{e^{i\boldsymbol{k}\cdot\boldsymbol{r}}}{\sqrt{2\pi}^3}, \tag{7.5a}$$

$$\xi^s_{\boldsymbol{k}+}(\boldsymbol{r}) = \begin{pmatrix} -\sin\left(\frac{1}{2}\theta(\boldsymbol{k})\right) e^{-\frac{\imath}{2}\boldsymbol{q}\cdot\boldsymbol{r}} \\ \cos\left(\frac{1}{2}\theta(\boldsymbol{k})\right) e^{\frac{\imath}{2}\boldsymbol{q}\cdot\boldsymbol{r}} \end{pmatrix} \frac{e^{i\boldsymbol{k}\cdot\boldsymbol{r}}}{\sqrt{2\pi}^3}. \tag{7.5b}$$

The expression for the Kohn-Sham 1RDM is therefore also equivalent to Eq. (6.23) (again, the difference in the definition of the angles has to be remembered) and the spin magnetization

is given by

$$\boldsymbol{m}(\boldsymbol{r}) = n\chi \begin{pmatrix} s\cos(\boldsymbol{q}\cdot\boldsymbol{r}) \\ s\sin(\boldsymbol{q}\cdot\boldsymbol{r}) \\ \sqrt{1-s^2} \end{pmatrix}, \tag{7.6a}$$

$$n\chi s = -\frac{1}{(2\pi)^3}\int \mathrm{d}^3k\ \left(n_-(\boldsymbol{k}) - n_+(\boldsymbol{k})\right) \frac{A}{\sqrt{(\boldsymbol{k}\cdot\boldsymbol{q}+B)^2 + A^2}}, \tag{7.6b}$$

$$n\chi\sqrt{1-s^2} = -\frac{1}{(2\pi)^3}\int \mathrm{d}^3k\ \left(n_-(\boldsymbol{k}) - n_+(\boldsymbol{k})\right) \frac{\boldsymbol{k}\cdot\boldsymbol{q}+B}{\sqrt{(\boldsymbol{k}\cdot\boldsymbol{q}+B)^2 + A^2}}. \tag{7.6c}$$

Note that the integration region is specified by the occupation numbers $n_b(\boldsymbol{k})$. They are either zero (for $\epsilon_b(\boldsymbol{k}) > 0$) or one (for $\epsilon_b(\boldsymbol{k}) < 0$) and determine the Fermi surface of the electron gas. The Fermi surface is not the usual Fermi sphere, because the dispersion Eq. (7.3b) breaks the spherical symmetry of the para- or ferromagnetic state of the uniform electron gas. The discussion so far is valid for SDFT in general, i.e. , considering the Kohn-Sham magnetic field Eq. (7.2b) as the sum of external and xc magnetic field. If we want to investigate whether a given approximation for the xc-energy functional favors a broken-symmetry ground state we have to establish that the effective Kohn-Sham magnetic field is only the xc-magnetic field. This condition is

$$\mu_\mathrm{B}\boldsymbol{B}_s = -\mu_\mathrm{B}\boldsymbol{B}_{xc} = -\frac{\delta E_{xc}[n,m]}{\delta \boldsymbol{m}(\boldsymbol{r})}, \tag{7.7}$$

which has to be checked for a given approximation for $E_{xc}[n,\boldsymbol{m}]$. Eq. (7.7) is the Kohn-Sham analog to the Hartree-Fock self-consistency equations (cf. Eq. (6.21)).

7.2 The exact-exchange functional in Spin-Density-Functional Theory

Since we are interested in comparing SDFT to Hartree-Fock theory we employ the exact-exchange functional, introduced in Sec. 4.2. In terms of the spin-spiral orbitals Eq. (7.5), it is given by

$$\begin{aligned} E_{xc}^{\mathrm{EXX}}[n,\boldsymbol{m}] = -\tfrac{1}{2}\sum_{b_1,b_2}\iint \mathrm{d}^3k_1\mathrm{d}^3k_2\ n_{b_1}(\boldsymbol{k}_1)\, n_{b_2}(\boldsymbol{k}_2) \\ \times \iint \mathrm{d}^3r_1\mathrm{d}^3r_2\ \frac{\left({\xi^s_{\boldsymbol{k}_1 b_1}}^\dagger(\boldsymbol{r}_1)\,\xi^s_{\boldsymbol{k}_2 b_2}(\boldsymbol{r}_1)\right)\left({\xi^s_{\boldsymbol{k}_2 b_2}}^\dagger(\boldsymbol{r}_2)\,\xi^s_{\boldsymbol{k}_1 b_1}(\boldsymbol{r}_2)\right)}{|\boldsymbol{r}_1-\boldsymbol{r}_2|}. \end{aligned} \tag{7.8}$$

The exchange-correlation potentials

$$v_{xc}(\boldsymbol{r}) = \frac{\delta E_{xc}[n,\boldsymbol{m}]}{\delta n(\boldsymbol{r})}, \tag{7.9}$$

$$\mu_{\mathrm{B}}\boldsymbol{B}_{xc}(\boldsymbol{r}) = \frac{\delta E_{xc}[n,\boldsymbol{m}]}{\delta \boldsymbol{m}(\boldsymbol{r})}, \tag{7.10}$$

have to be determined employing the OEP method (cf. Sec. 4.2.1). Here we will not follow the route taken in Sec. 4.2.1 in order to compute the Kohn-Sham potential for the charge-only DFT, but use Eq. 4.20, i.e. ,

$$0 = \frac{\delta E_{\mathrm{EXX}}}{\delta V_s(\boldsymbol{r})}, \tag{7.11}$$

$$0 = \frac{\delta E_{\mathrm{EXX}}}{\delta \boldsymbol{B}_s(\boldsymbol{r})}, \tag{7.12}$$

$$E_{\mathrm{EXX}} = T_s + V_0 + E_{xc}^{\mathrm{EXX}}. \tag{7.13}$$

The functional dependency on the potentials of E_{EXX} is implied through the dependence of the kinetic energy T_s and the exact-exchange energy E_{xc}^{EXX} on the Kohn-Sham orbitals, which in turn may be viewed as functionals of the external potential via a solution of the Kohn-Sham equation. In order to streamline the derivation of the OEP integral equations we introduce the 2×2-potential

$$\begin{aligned} v_s(\boldsymbol{r}) &= \begin{pmatrix} V_s(\boldsymbol{r}) + \mu_{\mathrm{B}} B_{s3}(\boldsymbol{r}) & \mu_{\mathrm{B}} B_{s1}(\boldsymbol{r}) - \imath \mu_{\mathrm{B}} B_{s2}(\boldsymbol{r}) \\ \mu_{\mathrm{B}} B_{s1}(\boldsymbol{r}) + \imath \mu_{\mathrm{B}} B_{s2}(\boldsymbol{r}) & V_s(\boldsymbol{r}) - \mu_{\mathrm{B}} B_{s3}(\boldsymbol{r}) \end{pmatrix} = v_\alpha(\boldsymbol{r})\,\sigma^\alpha \\ &= \left(v_\alpha^0 + v_\alpha^{xc}\right)\sigma^\alpha \quad , \quad \alpha = 0,1,2,3. \end{aligned} \tag{7.14}$$

Furthermore we define the combined index $j = (\boldsymbol{k}, b)$ such that $\sum_b \int \mathrm{d}^3k \;\to \sum_j$. Accordingly Eqs. (7.11), (7.12) are expressed as

$$\begin{aligned} 0 &= \frac{\delta E_{\mathrm{EXX}}}{\delta v_\alpha(\boldsymbol{r})} \\ &= \sum_j \int \mathrm{d}^3 r' \, \left(\frac{\delta T_s}{\delta \xi_j^s(\boldsymbol{r}')} + n_j \xi_j^{s\dagger}(\boldsymbol{r}')\, v_\alpha^0(\boldsymbol{r}')\,\sigma^\alpha + \frac{\delta E_{xc}^{\mathrm{EXX}}}{\delta \xi_j^s(\boldsymbol{r}')} \right) \frac{\delta \xi_j^s(\boldsymbol{r}')}{\delta v_\alpha(\boldsymbol{r})} + h.c. \,. \end{aligned} \tag{7.15}$$

Using the Kohn-Sham equation we can rewrite

$$\begin{aligned} \frac{\delta T_s}{\delta \xi_j^s(\boldsymbol{r}')} &= n_j \xi_j^{s\dagger}(\boldsymbol{r}') \left(-\tfrac{1}{2} \overleftarrow{\nabla} \cdot \overleftarrow{\nabla} \right) \\ &= n_j \xi_j^{s\dagger}(\boldsymbol{r}') \left(-\tfrac{1}{2} \overleftarrow{\nabla} \cdot \overleftarrow{\nabla} + v_\beta(\boldsymbol{r}')\,\sigma^\beta - v_\beta(\boldsymbol{r}')\,\sigma^\beta \right) \\ &= n_j \xi_j^{s\dagger}(\boldsymbol{r}') \left(\epsilon_j - v_\beta(\boldsymbol{r}')\,\sigma^\beta \right). \end{aligned} \tag{7.16}$$

Moreover we know from first-order perturbation theory

$$\frac{\delta\xi_j^s(\boldsymbol{r}')}{\delta v_\alpha(\boldsymbol{r})} = \sum_{k\neq j} \frac{\xi_k^{s\dagger}(\boldsymbol{r})\,\sigma^\alpha\xi_j^s(\boldsymbol{r})}{\epsilon_j-\epsilon_k}\xi_k^s(\boldsymbol{r}')\,. \tag{7.17}$$

The variation of E_{xc}^{EXX} w.r.t. $\xi_j^s(\boldsymbol{r}')$ is

$$\frac{\delta E_{xc}^{\mathrm{EXX}}}{\delta\xi_j^s(\boldsymbol{r}')} = -\sum_k n_j n_k \xi_k^{s\dagger}(\boldsymbol{r}')\int \mathrm{d}^3x\;\frac{\xi_j^{s\dagger}(\boldsymbol{x})\,\xi_k^s(\boldsymbol{x})}{|\boldsymbol{r}'-\boldsymbol{x}|}. \tag{7.18}$$

It is common practice to define the matrix elements

$$M_{kj}^\star = -\int \mathrm{d}^3r'\;\left(v_\beta^{xc}(\boldsymbol{r}')\,\xi_j^{s\dagger}(\boldsymbol{r}')\,\sigma^\beta\xi_k^s(\boldsymbol{r}') + \sum_l n_l\int \mathrm{d}^3x\;\frac{\xi_j^{s\dagger}(\boldsymbol{x})\,\xi_l^s(\boldsymbol{x})\,\xi_l^{s\dagger}(\boldsymbol{r}')\,\xi_k^s(\boldsymbol{r}')}{|\boldsymbol{r}'-\boldsymbol{x}|}\right), \tag{7.19}$$

together with the orbital shifts

$$\Psi_j(\boldsymbol{r}) = \sum_{k\neq j}\frac{M_{jk}\xi_k^s(\boldsymbol{r})}{\epsilon_j-\epsilon_k}. \tag{7.20}$$

With these definitions the OEP equations take the simple form

$$0 = \sum_j n_j\left(\Psi_j^\dagger(\boldsymbol{r})\,\sigma^\alpha\xi_j^s(\boldsymbol{r}) + \xi_j^{s\dagger}(\boldsymbol{r})\,\sigma^\alpha\Psi_j(\boldsymbol{r})\right). \tag{7.21}$$

7.2.1 Optimized effective potential equations for the spin-spiral wave

For the spin-spiral orbitals the orbital shifts are

$$\Psi_{\boldsymbol{k}\mp}(\boldsymbol{r}) = \frac{\mp\xi_{\boldsymbol{k}\pm}^s(\boldsymbol{r})}{\sqrt{(\boldsymbol{q}\cdot\boldsymbol{k}+B)^2+A^2}}\left(d(\boldsymbol{k}) - \int \mathrm{d}^3k'\;\frac{4\pi}{(\boldsymbol{k}-\boldsymbol{k}')^2}D(\boldsymbol{k},\boldsymbol{k}')\right), \tag{7.22}$$

$$d(\boldsymbol{k}) = \tfrac{1}{2}\left(A\cos(\theta(\boldsymbol{k})) - B\sin(\theta(\boldsymbol{k}))\right), \tag{7.23}$$

$$D(\boldsymbol{k},\boldsymbol{k}') = \tfrac{1}{2}\left(n_-(\boldsymbol{k}')-n_+(\boldsymbol{k}')\right)\left(\cos(\theta(\boldsymbol{k}))\sin(\theta(\boldsymbol{k}')) - \sin(\theta(\boldsymbol{k}))\cos(\theta(\boldsymbol{k}'))\right), \tag{7.24}$$

where the denominator in Eq. (7.22) is the energy difference between the lower band ($b=-$) and the upper band ($b=+$) at the same wave vector $\boldsymbol{k}$. Since the orbital shifts for the upper band are proportional to the orbitals of the lower band, and vice-versa, the OEP equation for the scalar potential, i.e. , $\alpha=0$, is trivially fulfilled. For the x- and y-components of the

magnetic field we obtain the OEP equations

$$
\begin{aligned}
0 = & \int \mathrm{d}^3k \, \frac{n_-(\boldsymbol{k}) - n_+(\boldsymbol{k})}{\sqrt{(\boldsymbol{q}\cdot\boldsymbol{k}+B)^2 + A^2}} \cos(\theta(\boldsymbol{k})) \left(A\cos(\theta(\boldsymbol{k})) - B\sin(\theta(\boldsymbol{k}))\right) \\
& - \iint \mathrm{d}^3k \mathrm{d}^3k' \, \frac{4\pi}{(\boldsymbol{k}-\boldsymbol{k}')^2} \frac{(n_-(\boldsymbol{k}) - n_+(\boldsymbol{k}))\,(n_-(\boldsymbol{k}') - n_+(\boldsymbol{k}'))}{\sqrt{(\boldsymbol{q}\cdot\boldsymbol{k}+B)^2 + A^2}} \cos(\theta(\boldsymbol{k})) \\
& \times \left(\cos(\theta(\boldsymbol{k}))\sin(\theta(\boldsymbol{k}')) - \sin(\theta(\boldsymbol{k}))\cos(\theta(\boldsymbol{k}'))\right), \qquad (7.25)
\end{aligned}
$$

where the equation for the x-component is Eq. (7.25) multiplied by $\cos(\boldsymbol{q}\cdot\boldsymbol{r})$ and the equation for the y-component is Eq. (7.25) multiplied by $\sin(\boldsymbol{q}\cdot\boldsymbol{r})$. The OEP equations hold for all $\boldsymbol{r}$ and therefore both components yield the same condition Eq. (7.25). Similarly the OEP equation for the z-component of the magnetic field is

$$
\begin{aligned}
0 = & \int \mathrm{d}^3k \, \frac{n_-(\boldsymbol{k}) - n_+(\boldsymbol{k})}{\sqrt{(\boldsymbol{q}\cdot\boldsymbol{k}+B)^2 + A^2}} \sin(\theta(\boldsymbol{k})) \left(A\cos(\theta(\boldsymbol{k})) - B\sin(\theta(\boldsymbol{k}))\right) \\
& - \iint \mathrm{d}^3k \mathrm{d}^3k' \, \frac{4\pi}{(\boldsymbol{k}-\boldsymbol{k}')^2} \frac{(n_-(\boldsymbol{k}) - n_+(\boldsymbol{k}))\,(n_-(\boldsymbol{k}') - n_+(\boldsymbol{k}'))}{\sqrt{(\boldsymbol{q}\cdot\boldsymbol{k}+B)^2 + A^2}} \sin(\theta(\boldsymbol{k})) \\
& \times \left(\cos(\theta(\boldsymbol{k}))\sin(\theta(\boldsymbol{k}')) - \sin(\theta(\boldsymbol{k}))\cos(\theta(\boldsymbol{k}'))\right). \qquad (7.26)
\end{aligned}
$$

Restricting the spin-spiral state to planar spirals, i.e. , $B = 0$, we note the following definit parities: 1) The dispersions Eq. (7.3b) are even under $\boldsymbol{k} \to -\boldsymbol{k}$, accordingly the occupations numbers are also even under $\boldsymbol{k} \to -\boldsymbol{k}$. 2) $\cos(\theta(\boldsymbol{k}))$ and $\sin(\theta(\boldsymbol{k}))$ are odd and even, respectively, under $\boldsymbol{k} \to -\boldsymbol{k}$ as can be seen from the definitions Eqs. (7.4a), (7.4b). It follows that the equation for the z-component (cf. Eq. (7.26)) is fulfilled trivially. The only remaining OEP equation for planar spin-spiral waves reads therefore

$$
\begin{aligned}
0 = & A \int \mathrm{d}^3k \, \frac{n_-(\boldsymbol{k}) - n_+(\boldsymbol{k})}{\left((\boldsymbol{q}\cdot\boldsymbol{k})^2 + A^2\right)^{3/2}} (\boldsymbol{q}\cdot\boldsymbol{k})^2 \\
& - A \iint \mathrm{d}^3k \mathrm{d}^3k' \, \frac{4\pi}{(\boldsymbol{k}-\boldsymbol{k}')^2} (\boldsymbol{q}\cdot(\boldsymbol{k}-\boldsymbol{k}')) \frac{\boldsymbol{q}\cdot\boldsymbol{k}}{(\boldsymbol{q}\cdot\boldsymbol{k})^2 + A^2} \\
& \times \frac{(n_-(\boldsymbol{k}) - n_+(\boldsymbol{k}))}{\sqrt{(\boldsymbol{q}\cdot\boldsymbol{k})^2 + A^2}} \frac{(n_-(\boldsymbol{k}') - n_+(\boldsymbol{k}'))}{\sqrt{(\boldsymbol{q}\cdot\boldsymbol{k}')^2 + A^2}}. \qquad (7.27)
\end{aligned}
$$

In the following we will evaluate the exact-exchange-energy functional for planar SSWs. For a fixed amplitude A of the external magnetic field we vary $\boldsymbol{q}$ in order to determine the optimal $\boldsymbol{q}_{\mathrm{opt}}$. Then the curves for various amplitudes are compared for the determination of the absolute minimum within the planar SSW configuration.

7.3 Direct minimization of the energy

Rather than calculating the Kohn-Sham potentials self-consistently, we use the fact that the Kohn-Sham potential $v_s(\boldsymbol{r})$ is a constant and that the Kohn-Sham magnetic field $\boldsymbol{B}_s(\boldsymbol{r})$ forms a spiral with amplitude A and wave vector $\boldsymbol{q} = q\boldsymbol{e}_q$, where $\boldsymbol{e}_q$ is chosen w.l.o.g. to be the unit vector in z-direction. We are interested in the situation of spontaneous symmetry breaking, i.e. , the Kohn-Sham magnetic field is entirely due to its exchange-correlation magnetic field. We will show later that this is indeed the case and $\boldsymbol{B}_s(\boldsymbol{r})$ is consistent within the OEP equation Eq. (7.27). We point out that the vector of the spin magnetization for the planar SSW is parallel to the Kohn-Sham magnetic field. This certainly is a consequence of the simplicity of the system under study. For more complicated systems it was shown [SDAD$^+$07] that these quantities need not be parallel in non-collinear SDFT employing the exact-exchange-energy functional. This is an important difference to the non-collinear LSDA formulation [KHSW88], where the spin magnetization and the exchange-correlation magnetic field are locally parallel by construction. In contrast to the energy functional within RDMFT (cf. Sec. 6.4) the energy functional for SDFT depends only on the three paramters of the planar SSW, i.e. , the amplitude A, the spin-spiral wave vector $\boldsymbol{q}$ and the chemical potential μ. Since we want to investigate the SSW instability for a fixed density, the chemical potential is implicitly determined through the density, specified in terms of the Wigner-Seitz radius r_s, the amplitude A and the magnitude q of the spin-spiral wave vector, i.e. , $\mu = \mu(r_s, A, q)$. For a fixed density n the energy per particle reads,

$$e_{\mathrm{EXX}}(r_s, A, q) = t(r_s, A, q) - w_1(r_s, A, q) - w_2(r_s, A, q)\,, \tag{7.28}$$

with the kinetic contribution (introducing $k = k_\rho$, $z = k_z$ and $k_\phi = \phi$)

$$\begin{aligned} t(r_s, A, q) = \frac{1}{2n}\frac{1}{(2\pi)^3}\int \mathrm{d}^3k \,\Big(\left(k^2 + z^2\right)\left(n_-(k,z) + n_+(k,z)\right) \\ - qz\left(n_-(k,z) + n_+(k,z)\right)\cos(\theta(z))\Big) + \frac{q^2}{8}, \end{aligned} \tag{7.29}$$

and the intra- and inter-band exchange contributions

$$\begin{aligned} w_1(r_s, A, q) = \frac{1}{2n}\frac{1}{(2\pi)^6}\iint \mathrm{d}^3k_1\mathrm{d}^3k_2 \,\frac{4\pi}{\left(\boldsymbol{k}_1 - \boldsymbol{k}_2\right)^2} \\ \times \left(n_-(k_1, z_1)\, n_-(k_2, z_2) + n_+(k_1, z_1)\, n_+(k_2, z_2)\right) \\ \times \left(1 + \cos(\theta(z_1))\cos(\theta(z_2)) + \sin(\theta(z_1))\sin(\theta(z_2))\right), \end{aligned} \tag{7.30a}$$

$$\begin{aligned} w_2(r_s, A, q) = \frac{1}{2n}\frac{1}{(2\pi)^6}\iint \mathrm{d}^3k_1\mathrm{d}^3k_2 \,\frac{4\pi}{\left(\boldsymbol{k}_1 - \boldsymbol{k}_2\right)^2} \\ \times \left(n_-(k_1, z_1)\, n_+(k_2, z_2) + n_+(k_1, z_1)\, n_-(k_2, z_2)\right) \\ \times \left(1 - \cos(\theta(z_1))\cos(\theta(z_2)) - \sin(\theta(z_1))\sin(\theta(z_2))\right). \end{aligned} \tag{7.30b}$$

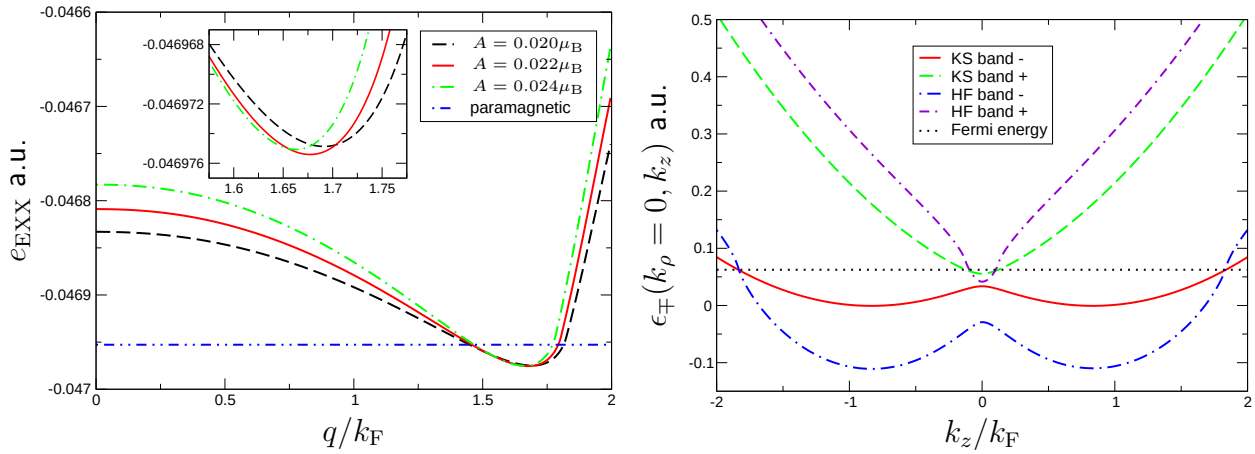

Figure 7.1:
Left panel: Energy per particle in EXX for the electron gas at $r_s = 5.4$ with spin density wave as function of q/k_{F} and different values of the amplitude A of the Kohn-Sham magnetic field. The straight line corresponds to the total energy per particle of the paramagnetic state at this density. The inset shows a magnification close to the minimum.
Right panel: Single-particle Kohn-Sham and Hartree-Fock bands at $k = 0$ for the optimized parameter values ($A = 0.022\mu_{\mathrm{B}}$ and $q/k_{\mathrm{F}} = 1.68$ at $r_s = 5.4$) mimizing the EXX total energy per particle (cf. left panel). The straight line indicates the Fermi energy and shows that close to $z/k_{\mathrm{F}} = 0$ states of the second Kohn-Sham band (green, dashed line) are occupied in the ground state. The Kohn-Sham orbitals are used to compute the Hartree-Fock Hamiltonian. The relative position of the second HF band (purple, dash-dash-dotted line) indicates that also in HF the states in both bands will be occupied.

The formal equivalence to Eqs. (6.27), (6.28) is readily established using trigonometric identities. In contrast to the RDMFT treatment we do not discretize momentum space into cylindrical volume elements, because we explicitly know the Fermi surface, specified by $n_b(\boldsymbol{k})$ or equivalently the single-particle dispersion, and the angle functionas $\theta(z)$. The exchange integrals Eq. (7.30) can be evaluated analytically (cf. App. A) up to the intergrations along z_1, z_2, which have to be carried out numerically.

In Fig. 7.1 we show the total energy per electron at $r_s = 5.4$ for a few values of A as function of q/k_{F}. The value $r_s = 5.4$ was chosen because then 1) the SSW phase is lower in energy than both the paramagnetic and ferromagnetic phases and 2) the amplitude of the SSW (or the Kohn-Sham magnetic field) is relatively high such that the resulting energy differences can easily be resolved numerically. We clearly see that for the given values of A for wavenumbers between $q/k_{\mathrm{F}} \approx 1.5$ and $q/k_{\mathrm{F}} \approx 1.75$ the energy of the SSW state is lower than the energy of the paramagnetic state. The lowest energy for this value of r_s is achieved for the parameters

$A = 0.022\mu_{\mathrm{B}}$ and $q/k_{\mathrm{F}} = 1.68$. In Fig. 7.1 we show the Kohn-Sham single-particle dispersions of Eq. (7.3b) as well as the Hartree-Fock single particle dispersions. To obtain the latter we first calculate the non-local Fock potential (which is a 2×2 matrix in spin space),

$$U_F(\boldsymbol{r};\boldsymbol{r}') = \sum_{b=-,+} \int \mathrm{d}^3k \, \frac{\xi^s_{\boldsymbol{k}b}(\boldsymbol{r})\, \xi^{s\,\dagger}_{\boldsymbol{k}b}(\boldsymbol{r}')}{|\boldsymbol{r}-\boldsymbol{r}'|}, \tag{7.31}$$

and then diagonalize the resulting Hartree-Fock single-particle Hamiltonian

$$H_{\mathrm{HF}}(\boldsymbol{r};\boldsymbol{r}') = \tfrac{1}{2}\overleftarrow{\nabla}\cdot\overrightarrow{\nabla} - U_F(\boldsymbol{r};\boldsymbol{r}')\,, \tag{7.32}$$

It is important to emphasize that we use the Kohn-Sham orbitals and orbital energies to evaluate the non-local Fock potential, i.e., we do not perform a self-consistent Hartree-Fock calculation here. In Fig. 7.1 we show the KS and HF dispersions only for the z-coordinate, i.e., we set $k = 0$. As expected, close to $z/k_{\mathrm{F}} = 0$ a direct gap opens up in the Kohn-Sham single-particle dispersions due to the presence of the mixing of the spin-up and spin-down channels. The position of the Fermi energy is such that not only states of the lower ($b = -$) band but also states of the upper ($b = +$) Kohn-Sham band are occupied in the ground state. It is evident that the Hartree-Fock single-particle direct band gap at $z/k_{\mathrm{F}} = 0$ is much larger than the corresponding Kohn-Sham gap. Moreover, the position of the second Hartree-Fock band indicates that also in the Hartree-Fock case there will be occupied states in the second band.

The occupation of states in both single-particle bands is sometimes excluded in works on the SSW in the Hartree-Fock approximation [Ove62, GV05] and also the numerical investigation in the previous chapter showed that in Hartree-Fock theory only the lowest single-particle band is occupied. This has motivated us to do the minimization of the exact-exchange-energy functional under the additional constraint that only states of the lower band are occupied. Similar to Fig. 7.1, in Fig. 7.2 we show the total energy per electron at $r_s = 5.4$ for a few values of A as function of q/k_{F}. Of course, the constrained minimization leads, for a given value of r_s, to different optimized parameter values. Surprisingly, however, we find that the minimization constraining the occupation to the lower band leads to lower total energies than the minimization obtained occupying both bands. Moreover, this lower total energy is achieved with a Slater determinant which has empty states below the Fermi level. This can be seen in the right panel of Fig. 7.2 where we show the Kohn-Sham and Hartree-Fock energy bands at $r_s = 5.4$ for the one-band minimization for the optimized parameter values of $A = 0.040\mu_{\mathrm{B}}$ and $q/k_{\mathrm{F}} = 1.33$. We see that there are states in the upper Kohn-Sham band below the Fermi energy which, due to the constraint in the minimization, remain unoccupied. We also note that for the one-band case the amplitude of the minimizing Kohn-Sham magnetic field, and

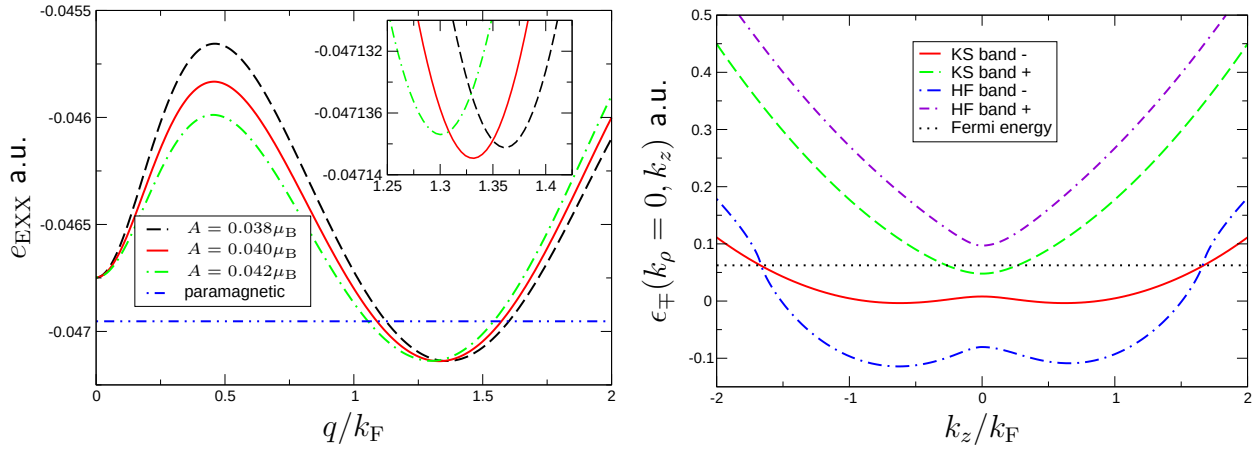

Figure 7.2:
Left panel: Same as left panel in Fig. 7.1 except that now only states in the lower band are allowed to be occupied. The total energy per particle at the minimum is lower than when states in both bands are allowed to be occupied.
Right panel: Same as right panel in Fig. 7.1 except that the optimized parameters are used which result from a minimization with occupied states in the lower Kohn-Sham band only. For $r_s = 5.4$ these values are $A = 0.040\mu_{\rm B}$ and $q/k_{\rm F} = 1.33$. Again, the straight line indicates the Fermi energy. Note that the states of the upper Kohn-Sham band (green, dashed line) remain unoccupied in this calculation, even if their single-particle energies are below the Fermi level, i.e., the resulting Slater determinant is not a ground state of the Kohn-Sham Single-particle Hamiltonian. On the other hand, the post-hoc evaluation of the Hartree-Fock bands indicates that the upper Hartree-Fock band (purple, dash-dash-dotted line) will remain unoccupied and the resulting Hartree-Fock wave function will be a ground-state Slater determinant.

therefore also the gap between the two Kohn-Sham bands at $z/k_F = 0$, is almost twice as large as in the two-band case. Compared to Fig. 7.1, the intersection of the Fermi energy with the bands $\varepsilon_b(k = 0, z)$ is shifted to a lower value of $|z|$. Again, the direct Hartree-Fock gap at $z/k_{\rm F} = 0$ is significantly larger than the Kohn-Sham gap. In contrast to the two-band case, the upper Hartree-Fock band now is energetically higher than the Fermi energy and the corresponding Hartree-Fock state, unlike the Kohn-Sham state, has no unoccupied single-particle states below the Fermi energy. Again here we have done only a post-hoc evaluation of the Hartree-Fock bands, but we have seen in Sec. 6.5 that the statement remains valid for a self-consistent Hartree-Fock calculation. We have optimized the energy per particle for a range of r_s for single-particle occupations in both energy bands and for occupations restricted to the lower band. In Fig. 7.3 we show the resulting phase diagram in the relevant density range. When allowing occupations in both bands, the SSW state (which is then

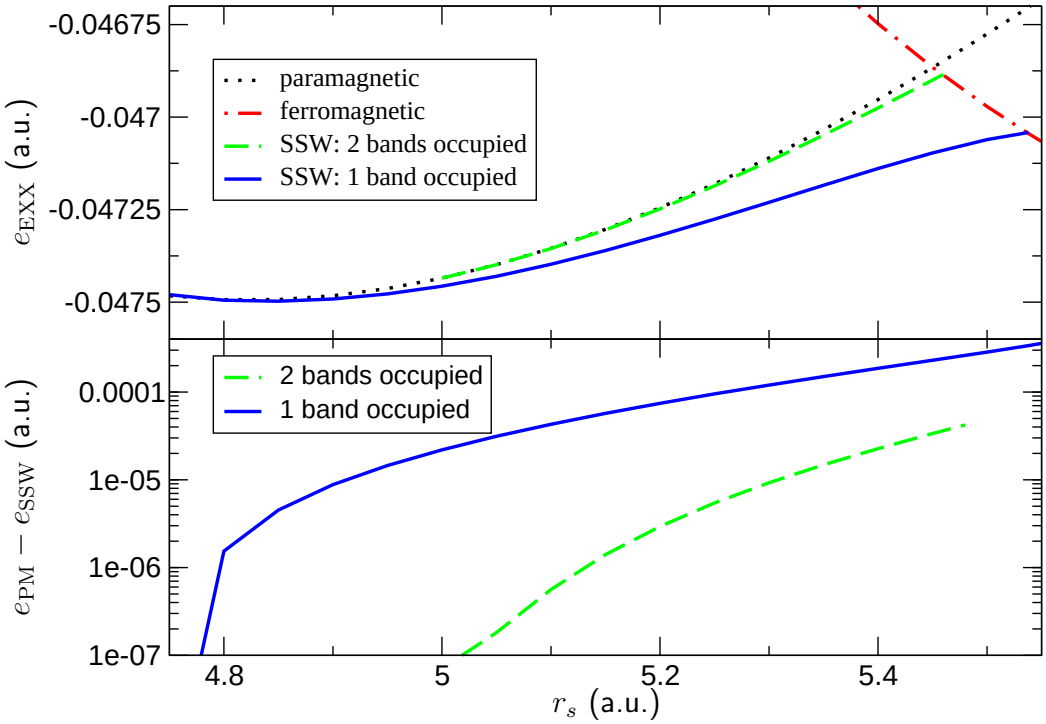

Figure 7.3:
Upper panel: Total energy per particle in EXX for different phases of the uniform electron gas as function of Wigner-Seitz radius r_s. In the SSW phase we consider two cases. In one case the occupation of single-particle states in both bands is allowed while in the other case the occupied states are restricted to the lower band.
Lower panel: Energy difference between the total energies per particle of the paramagnetic phase and the SSW phase for SSWs with occupied states in one and two bands. For the two-band case, the SSW phase is lower in energy than both the paramagnetic and the ferromagnetic phase for $5.0 \lesssim r_s \lesssim 5.46$. For the one-band case the range of stability of the SSW phase is $4.78 \lesssim r_s \lesssim 5.54$.

a ground state Slater determinant) is lower in energy than both the paramagnetic and the ferromagnetic phase for r_s in the range $5.0 \lesssim r_s \lesssim 5.46$. In this case the energies are very close to the energies of the paramagnetic phase (energy differences of less than $0.04\ \mathrm{mHa}$, c.f. lower panel of Fig. 7.3) and therefore the transition to the ferromagnetic phase occurs at an value of r_s only slightly higher than r_c where paramagnetic and ferromagnetic phase are degenerate. On the other hand, restricting the single-particle occupation to the lower band, the SSW state is more stable than para- and ferromagnetic state for $4.78 \lesssim r_s \lesssim 5.54$. In this case the energy differences between the paramagnetic and the SSW phase range to almost $0.4\mathrm{mHa}$ (lower panel of Fig. 7.3), almost an order of magnitude larger than in the two-band case. However, for all r_s values in the stability range of the SSW phase, the minimizing Slater

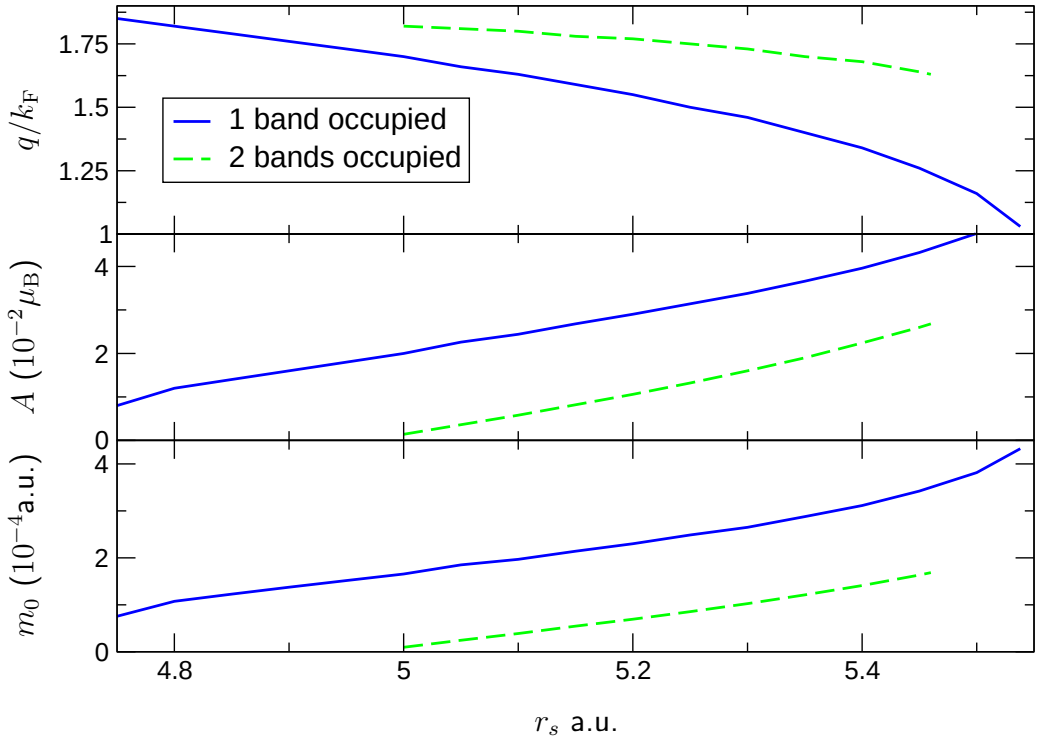

Figure 7.4: Optimized values for the parameters q (upper panel) and A (middle panel) for which the EXX energy per particle of the SSW phase is minimized. The results are shown over the range of r_s for which the SSW phase is lower in energy than both the paramagnetic and the ferromagnetic phases for the cases when both bands or only one band are occupied. Lower panel: amplitude of the SSW (Eq. (7.6b)) for the one- and two-band case.

determinant in the one-band case is not a ground state of the Kohn-Sham Hamiltonian. Both the one- and two-band cases in EXX have in common that they predict the SSW phase to be lower in energy than the paramagnetic phase only for a restricted range of r_s. This is different from the Hartree-Fock case (cf. Cap. 6) where the SSW phase is more stable than the paramagnetic phase for all values of r_s. This is not completely surprising since due to the additional constraint of local Kohn-Sham potentials v_s and $\boldsymbol{B}_s$ in the EXX minimization, the resulting energies have to be higher than the Hartree-Fock total energies. Since for small values of r_s the SSW total energies in Hartree-Fock are extremely close to the total energies of the paramagnetic phase as discussed in Sec. 6.5, the higher EXX total energies can easily lead to a more stable paramagnetic phase. In Fig. 7.4 we show the SSW parameters q (upper panel) and A (middle panel) for which the EXX total energy per particle is minimized in the one- and two-band cases for those r_s for which the SSW phase is more stable than both the paramagnetic and ferromagnetic phases. For the one-band case, the wave vector q of the spin-spiral wave covers almost the whole range between k_F and $2k_F$ while for the two-band case

this range is much narrower. The amplitudes A and $m_0 = n\chi$ of the Kohn-Sham magnetic field (middle panel) and the spin magnetization (lower panel) of the SSW are significantly smaller in the two-band case than in the case with occupied single-particle states in the lower band only. It is sometimes assumed [GV05] that the wavenumber of the SSW is close to $2k_\mathrm{F}$. Our results show that this need not be the case, as in the one-band case q approaches k_F for densities at the lower end of the stability range of the SSW phase. However, neither in EXX nor in Hartree-Fock (cf. Sec. 6.5) we ever found a stable SSW state with wavenumber lower than k_F.

7.4 Self-consistency conditions

In the previous Section we have used an ansatz for the Kohn-Sham orbitals in the SSW phase which depends on two parameters and then minimized the EXX total energy per particle with respect to these parameters. We have done this minimization once allowing single-particle states in both bands to be occupied and once for occupations only in the lower band. This is different from the usual way of applying SDFT where one calculates the exchange-correlation potentials and solves the Kohn-Sham equation self-consistently. In this section we still use the ansatz Eq. (7.5) for the Kohn-Sham orbitals and investigate if it is consistent with the OEP equation

$$\begin{aligned} J(r_s, A, q) = 0 = A \int \mathrm{d}^3k \, \frac{n_-(\boldsymbol{k}) - n_+(\boldsymbol{k})}{\left((\boldsymbol{q}\cdot\boldsymbol{k})^2 + A^2\right)^{3/2}} \left(\boldsymbol{q}\cdot\boldsymbol{k}\right)^2 \\ - A \iint \mathrm{d}^3k \mathrm{d}^3k' \, \frac{4\pi}{\left(\boldsymbol{k}-\boldsymbol{k}'\right)^2} \left(\boldsymbol{q}\cdot(\boldsymbol{k}-\boldsymbol{k}')\right) \frac{\boldsymbol{q}\cdot\boldsymbol{k}}{\left(\boldsymbol{q}\cdot\boldsymbol{k}\right)^2 + A^2} \\ \times \frac{(n_-(\boldsymbol{k}) - n_+(\boldsymbol{k}))}{\sqrt{\left(\boldsymbol{q}\cdot\boldsymbol{k}\right)^2 + A^2}} \frac{(n_-(\boldsymbol{k}') - n_+(\boldsymbol{k}'))}{\sqrt{\left(\boldsymbol{q}\cdot\boldsymbol{k}'\right)^2 + A^2}}, \end{aligned} \tag{7.33}$$

derived in Sec. 7.2.1 Eq. (7.27). In Fig. 7.5 we show $J(r_s, A, q)$ of Eq. (7.33) for $r_s = 5.4$ as function of q/k_F for different values of A both for the case of occupations in both bands (upper panel) as well as for occupations restricted to the lower band (lower panel). In the upper panel of Fig. 7.5 we choose the same values for the parameter A as used in Fig. 7.1 which all had local minima for some value of $q < 2k_\mathrm{F}$. For these values of A, however, Eq. (7.33) is not satisfied for any value of q in that range. We therefore conclude that in the two-band case the energy minimization is not consistent with the OEP equations. In the lower panel of Fig. 7.5 where only single-particle states of the lower band are occupied we choose the parameters as in Fig. 7.2. In this case, $J(r_s, A, q)$ not only crosses zero, but also does so exactly for those values of q/k_F for which we found local minima in the total energy per particle. We

therefore conclude that in the one-band case the minimization of the total energy is consistent with the OEP equation, i.e., our ansatz is self-consistent in this case. Again we emphasize that the lowest total energy is achieved when the Slater determinant is has holes below the Fermi surface. It has been shown [BLLS94] that in unrestricted Hartree-Fock theory all the single-particle levels are fully occupied up to the Fermi energy. To the best of our knowledge, a similar statement has not been proven for SDFT (even in EXX approximation) and our results indicate that it might not be true in EXX. On the other hand, the proof of Ref. [BLLS94] holds for the true, unrestricted Hartree-Fock ground state while in our case we have restricted the uniform electron gas to the SSW symmetry. It is conceivable that the fact that we find an "excited-state" Slater determinant as energy-minimizing wave function hints towards an instability of the SSW phase against further reduction of the symmetry.

7.5 Summary and Conclusions

In the present chapter we have investigated the SSW state of the uniform electron gas within the EXX approximation of non-collinear SDFT. While in the Hartree-Fock approximation the SSW state is energetically more stable than the paramagnetic state for all values of r_s, in EXX this is only true for values of r_s larger than a critical value. Using an explicit ansatz for the spinor orbitals in the SSW state, we have performed the energy minimization of the EXX total energy in two ways: (i) in the first case we used as non-interacting reference wavefunction a ground-state Slater determinant with occupied single-particle orbitals belonging to both single-particle energy bands, as long as their energy is below the Fermi energy. Then the SSW phase is more stable than both paramagnetic and ferromagnetic phases for $5.0 \lesssim r_s \lesssim 5.46$. (ii) In the second case we required all the occupied single-particle orbitals in the Slater determinant to belong to the lower band. The minimizing Slater determinant in this case turns out to be an "excited state", since orbitals with orbital energies below the Fermi energy belonging to the second band remain unoccupied. Nevertheless, for a given r_s the total energies of the minimizing SSW states are significantly lower than in case (i). The range of stability of the SSW phase with respect to both paramagnetic and ferromagnetic phases is extended to $4.78 \lesssim r_s \lesssim 5.54$. The self-consistency conditions provided by the OEP equations for non-collinear SDFT are satisfied with our ansatz for the single-particle orbitals only for case (ii). We found that for case (i) the parameter values minimizing the EXX total energy are not consistent with the OEP equations. This means that case (i) is not a solution of the OEP equations. Only case (ii) is a solution of the OEP equations and therefore yields spontaneous symmetry breaking.

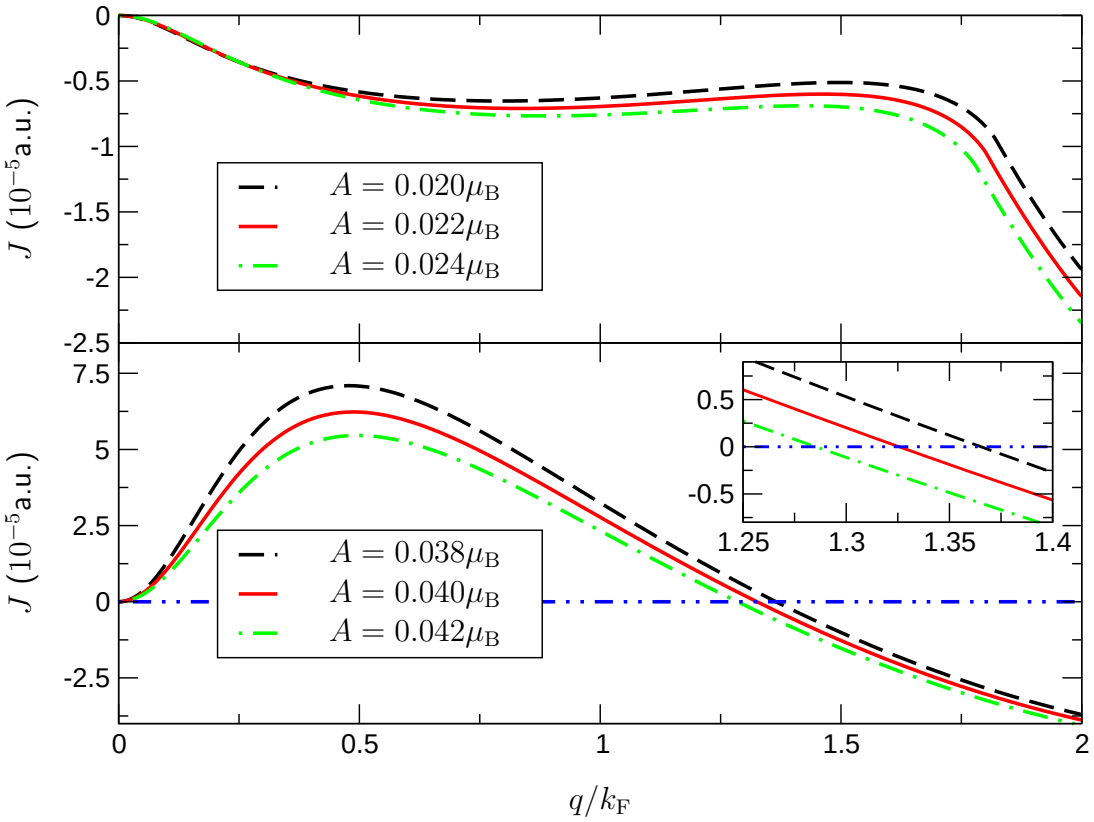

Figure 7.5:

Upper panel: $J(r_s, A, q)$ of Eq. (7.33) for $r_s = 5.4$ as function of q/k_F and different values of A for the case with occupations in two bands. The parameter values are the same as in Fig. 7.1 for which a minimum in the total energy per particle was found. Since $J(r_s, A, q)$ never crosses zero, in this case the minimum of the total energy is not consistent with the solution of the OEP equation.

Lower panel: same as above but now for occupied single particle states only in the lower band. The parameter values are the same as in Fig. 7.2. In contrast to the two-band case, now $J(r_s, A, q)$ not only crosses zero but also does so at those values of q/k_F for which a local minimum was found in Fig. 7.2 (see inset for magnification around the intersections with the zero axiss). Therefore, the OEP equation in this case is consistent with the minimization of the total energy per particle.

Chapter 8

Non-collinear functional derived from the spin-spiral-wave state

So far we have used DFTs to investigate the instability of the uniform electron gas w.r.t. the formation of a spin-spiral wave. Motivated by Overhauser's proof that the instability is present at the level of a Hartree-Fock treatment of the uniform electron gas, we generalized Overhauser's explicit ansatz for the effective single-particle orbitals to RDMFT which allowed us to include correlation effects. Furthermore we compared the Hartree-Fock results (obtained via RDMFT) to the results stemming from the local version of the Hartree-Fock-energy functional, i.e. , the exact-exchange-energy functional within SDFT. In the present chapter we will pursue a different goal. We ask the question whether we can use the SSW state of the uniform electron gas to obtain a new functional for SDFT. We find that this is indeed possible, by constructing the functional in close analogy to the Local-Spin-Density Approximation (LSDA). This means that we assign a local xc-energy density determined from local characteristic parameters of the SSW state. Those are, in addition to the density n and the magnitude of the magnetization $m = n\chi$, which are already present in the LSDA, the sine of the azimuthal angle, i.e. , $s = \sin(\theta)$, and the magnitude of SSW wave vector q. A similar approach was proposed in [KA03] restricted, however, to the small-q limit. We will demonstrate that the definition of the additional two parameters involves gradients of the spin-magnetization $\boldsymbol{m}$. Therefore the proposed functional is an explicit density functional including gradients of the spin-magnetization, which is not obtained by generalizing a collinear functional by means of the so-called Kübler trick [KHSW88, PSF07].

8.1 Exact properties from symmetries

Before discussing the construction of the functional, we review briefly some exact conditions on xc-energy functionals derived from symmetry considerations. Assume two different coordinate systems R and X. A vector in coordinate system R is denoted by $\boldsymbol{r}$ and a vector in coordinate system X by $\boldsymbol{x}$. If the origins of the two coordinate systems differ by a translation $\boldsymbol{t} = t\boldsymbol{e}_t$ we have $\boldsymbol{x} = \boldsymbol{r} + \boldsymbol{t}$. We define the density n' which is the density n translated by $\boldsymbol{t}$, i.e. ,

$$n'(\boldsymbol{r}) = n(\boldsymbol{x}) = n(\boldsymbol{r} + \boldsymbol{t})\,. \tag{8.1}$$

For infinitesimal translations $\boldsymbol{t} = \varepsilon\boldsymbol{e}_t$ the difference δn of the two densities is

$$\delta n(\boldsymbol{r}) = n'(\boldsymbol{r}) - n(\boldsymbol{r}) = \varepsilon\boldsymbol{e}_t \cdot \nabla n(\boldsymbol{r})\,. \tag{8.2}$$

Since the kinetic energy and the interaction energy are translationally invariant the universal functionals $F[n]$ and $T_s[n]$ yield the same energy for both densities n and n'. Moreover, the Hartree energy functional $E_H[n]$ is translationally invariant as can be inferred directly from its definition (cf. Eq. (3.7)). Hence an approximation for the xc-energy functional also has to give the same energy for both densities,

$$\begin{aligned} 0 = E_{xc}[n'] - E_{xc}[n] &= \int \mathrm{d}^3r\ \frac{\delta E_{xc}[n]}{\delta n(\boldsymbol{r})}\delta n(\boldsymbol{r}) \\ &= \varepsilon\boldsymbol{e}_t \cdot \int \mathrm{d}^3r\ v_{xc}(\boldsymbol{r})\,(\nabla n(\boldsymbol{r})) = \varepsilon\boldsymbol{e}_t \cdot \int \mathrm{d}^3r\ (\nabla v_{xc}(\boldsymbol{r}))\,n(\boldsymbol{r})\,. \end{aligned} \tag{8.3}$$

For the partial integration in the second line of Eq. (8.3) we assumed that the boundary contributions vanish. As Eq. (8.3) has to be valid for arbitrary infinitesimal translations $\boldsymbol{t}$, we obtain the so-called zero-force theorem,

$$0 = \int \mathrm{d}^3r\ (\nabla v_{xc}(\boldsymbol{r}))\,n(\boldsymbol{r})\,. \tag{8.4}$$

It states that the xc-potential cannot exert a net force on the electrons.

Similarly we can investigate the situation when the coordinate system X has the same origin as the coordinate system R, but is rotated compared to R, i.e. , $\boldsymbol{x} = \mathcal{R}\boldsymbol{r}$ with $\mathcal{R}$ being a 3×3 rotation matrix. For infinitesimal rotations around an axis $\boldsymbol{e}_\omega$ we have $\boldsymbol{x} = \boldsymbol{r} + d\boldsymbol{\omega} \times \boldsymbol{r}$ with $d\boldsymbol{\omega} = \varepsilon\boldsymbol{e}_\omega$. This means that the difference of the densities is given by

$$\delta n(\boldsymbol{r}) = n'(\boldsymbol{r}) - n(\boldsymbol{r}) = n(\mathcal{R}\boldsymbol{r}) - n(\boldsymbol{r}) = \varepsilon\,(\boldsymbol{e}_\omega \times \boldsymbol{r}) \cdot \nabla n(\boldsymbol{r})\,. \tag{8.5}$$

Again, the kinetic, interaction and Hartree energy are rotationally invariant and hence we get

$$\begin{aligned} 0 = E_{xc}[n'] - E_{xc}[n] &= \int \mathrm{d}^3r\ \frac{\delta E_{xc}[n]}{\delta n(\boldsymbol{r})}\delta n(\boldsymbol{r}) \\ &= \varepsilon\boldsymbol{e}_\omega \cdot \int \mathrm{d}^3r\ v_{xc}(\boldsymbol{r})\,\boldsymbol{r} \times (\nabla n(\boldsymbol{r})) = \varepsilon\boldsymbol{e}_\omega \cdot \int \mathrm{d}^3r\ \boldsymbol{r} \times (\nabla v_{xc}(\boldsymbol{r}))\,n(\boldsymbol{r})\,. \end{aligned} \tag{8.6}$$

Since Eq. (8.6) has to hold for any $\boldsymbol{e}_\omega$ we obtain a zero-torque theorem

$$0 = \int \mathrm{d}^3 r \; \boldsymbol{r} \times (\nabla v_{xc}(\boldsymbol{r}))\, n(\boldsymbol{r})\,. \tag{8.7}$$

Turning to SDFT we also have to investigate how the spin magnetization transforms. For translations in analogy to Eq. (8.8) we define

$$\boldsymbol{m}'(\boldsymbol{r}) = \boldsymbol{m}(\boldsymbol{x}) = \boldsymbol{m}(\boldsymbol{r}+\boldsymbol{t})\,. \tag{8.8}$$

For infinitesimal translations we get

$$\delta\boldsymbol{m}(\boldsymbol{r}) = \boldsymbol{m}'(\boldsymbol{r}) - \boldsymbol{m}(\boldsymbol{r}) = \varepsilon \boldsymbol{e}_t \cdot \nabla \otimes \boldsymbol{m}(\boldsymbol{r})\,, \tag{8.9}$$

where it is implied that the components of ∇ are contracted with the unit vector $\boldsymbol{e}_t$. Similar to Eq. (8.3) we require

$$\begin{aligned} 0 = E_{xc}[n', \boldsymbol{m}'] - E_{xc}[n, \boldsymbol{m}] &= \int \mathrm{d}^3 r \; \left(\frac{\delta E_{xc}[n, \boldsymbol{m}]}{\delta n(\boldsymbol{r})} \delta n(\boldsymbol{r}) + \frac{\delta E_{xc}[n, \boldsymbol{m}]}{\delta \boldsymbol{m}(\boldsymbol{r})} \delta \boldsymbol{m}(\boldsymbol{r}) \right) \\ &= \varepsilon \boldsymbol{e}_t \cdot \int \mathrm{d}^3 r \; \left((\nabla v_s(\boldsymbol{r}))\, n(\boldsymbol{r}) + \mu_\mathrm{B} \left(\nabla \otimes \boldsymbol{B}_{xc}\right) \cdot \boldsymbol{m}(\boldsymbol{r}) \right). \end{aligned} \tag{8.10}$$

Since $\boldsymbol{e}_t$ is arbitrary we obtain the zero-force theorem for SDFT,

$$0 = \int \mathrm{d}^3 r \; \left((\partial_j v_s(\boldsymbol{r}))\, n(\boldsymbol{r}) + \mu_\mathrm{B} \left(\partial_j B^\kappa_{xc}\right) m_\kappa(\boldsymbol{r}) \right), \tag{8.11}$$

where we employed a notation in terms of the components of $\boldsymbol{B}_{xc}$, $\boldsymbol{m}$ and ∇, together with Einstein's summation convention, in order to show explicit which components are contracted. Considering spatial rotations in SDFT we compare the rotated spin magnetization

$$\boldsymbol{m}'(\boldsymbol{r}) = \left\langle \hat{\Phi}^\dagger(\mathcal{R}\boldsymbol{r})\, \boldsymbol{\sigma} \hat{\Phi}(\mathcal{R}\boldsymbol{r}) \right\rangle = \boldsymbol{m}(\mathcal{R}\boldsymbol{r})\,, \tag{8.12}$$

to the rotated paramagnetic current

$$\begin{aligned} \boldsymbol{\jmath}'(\boldsymbol{r}) &= \tfrac{1}{2i} \left\langle \hat{\Phi}^\dagger(\mathcal{R}\boldsymbol{r}) \left(\nabla \hat{\Phi}(\mathcal{R}\boldsymbol{r}) \right) - \left(\nabla \hat{\Phi}^\dagger(\mathcal{R}\boldsymbol{r}) \right) \hat{\Phi}(\mathcal{R}\boldsymbol{r}) \right\rangle \\ &= \mathcal{R} \tfrac{1}{2i} \left\langle \hat{\Phi}^\dagger(\mathcal{R}\boldsymbol{r}) \left(\nabla \hat{\Phi} \right)(\mathcal{R}\boldsymbol{r}) - \left(\nabla \hat{\Phi}^\dagger \right)(\mathcal{R}\boldsymbol{r})\, \hat{\Phi}(\mathcal{R}\boldsymbol{r}) \right\rangle \\ &= \mathcal{R} \boldsymbol{\jmath}(\mathcal{R}\boldsymbol{r})\,. \end{aligned} \tag{8.13}$$

We can see that while the paramagnetic current $\boldsymbol{\jmath}$ transforms as a vector under spatial rotation the spin magnetization $\boldsymbol{m}$ does not. This is due to the fact that the three components of the spin magnetization are a reflection of the internal degree of freedom, i.e. , the two-componentness of the fundamental Pauli field, whereas the three components of the current arise due to the definition of the current in terms of gradients of the fundamental Pauli field.

We can generalize the zero-torque theorem Eq. (8.7) for SDFT by calculating the change in the spin magnetization under infinitesimal spatial rotations

$$\delta \boldsymbol{m}(\boldsymbol{r}) = \boldsymbol{m}'(\boldsymbol{r}) - \boldsymbol{m}(\boldsymbol{r}) = \varepsilon \left(\boldsymbol{e}_\omega \times \boldsymbol{r}\right) \cdot \nabla \otimes \boldsymbol{m}(\boldsymbol{r}) \,, \tag{8.14}$$

and requiring

$$\begin{aligned} 0 = E_{xc}[n', \boldsymbol{m}'] - E_{xc}[n, \boldsymbol{m}] &= \int \mathrm{d}^3 r \, \left(\frac{\delta E_{xc}[n, \boldsymbol{m}]}{\delta n(\boldsymbol{r})} \delta n(\boldsymbol{r}) + \frac{\delta E_{xc}[n, \boldsymbol{m}]}{\delta \boldsymbol{m}(\boldsymbol{r})} \delta \boldsymbol{m}(\boldsymbol{r}) \right) \\ &= \varepsilon \boldsymbol{e}_\omega \cdot \int \mathrm{d}^3 r \, \left(\boldsymbol{r} \times \left(\nabla v_{xc}(\boldsymbol{r})\right) n(\boldsymbol{r}) + \mu_\mathrm{B} \boldsymbol{r} \times \left(\nabla \otimes \boldsymbol{B}_{xc}(\boldsymbol{r})\right) \boldsymbol{m}(\boldsymbol{r}) \right) . \end{aligned} \tag{8.15}$$

This leads to a zero-torque theorem for SDFT,

$$0 = \int \mathrm{d}^3 r \, \epsilon_{jkl} \, r_k \left(\left(\partial_l v_{xc}(\boldsymbol{r})\right) n(\boldsymbol{r}) + \mu_\mathrm{B} \left(\partial_l B^\kappa_{xc}(\boldsymbol{r})\right) m_\kappa(\boldsymbol{r}) \right) . \tag{8.16}$$

As discussed above SDFT employs with the spin magnetization an additional fundamental variable that reflects the internal degree of freedom of the fundamental Pauli field. Hence we can also derive conditions on the xc-energy functional by investigating a change of the internal coordinate system. A rotation of the internal coordinate system is achieved by

$$\hat{\Phi}'(\boldsymbol{r}) = \mathcal{U} \hat{\Phi}(\boldsymbol{r}) \,, \tag{8.17}$$

where $\mathcal{U}$ corresponds to a unitary 2×2-matrix with a trace equal to one, i.e. , an element of $\mathrm{SU}(2)$. A generic rotation around an axis specified by a unit vector $\boldsymbol{n}$ is given by

$$\mathcal{U} = e^{-\imath \boldsymbol{n} \cdot \boldsymbol{\sigma} \frac{\varphi}{2}} = \cos\left(\frac{\varphi}{2}\right) \sigma^0 - \imath \sin\left(\frac{\varphi}{2}\right) \boldsymbol{n} \cdot \boldsymbol{\sigma}, \tag{8.18}$$

From the fundamental commutation relation of the Pauli matrices we obtain

$$\begin{aligned} \mathcal{U}^\dagger \sigma^\kappa \mathcal{U} &= \left(\cos\left(\frac{\varphi}{2}\right) \sigma^0 + \imath \sin\left(\frac{\varphi}{2}\right) \right) \sigma^\kappa \left(\cos\left(\frac{\varphi}{2}\right) \sigma^0 - \imath \sin\left(\frac{\varphi}{2}\right) \right) \\ &= \cos(\varphi) \, \sigma^\kappa + \sin(\varphi) \, \epsilon_{\kappa\lambda\mu} n_\lambda \sigma^\mu + \left(1 - \cos(\varphi)\right) n_\kappa n_\lambda \sigma^\lambda, \end{aligned} \tag{8.19}$$

which can be rewritten in vectorial notation as

$$\begin{aligned} \mathcal{U}^\dagger \boldsymbol{\sigma} \mathcal{U} &= \left(\cos(\varphi) + \sin(\varphi) \, \boldsymbol{n} \times + \left(1 - \cos(\varphi)\right) \boldsymbol{n} \otimes \boldsymbol{n}\right) \boldsymbol{\sigma} \\ &= \mathcal{R} \boldsymbol{\sigma}, \end{aligned} \tag{8.20}$$

with $\mathcal{R}$ being the 3×3-rotation matrix corresponding to a spatial rotation by an angle φ around the axis $\boldsymbol{n}$. Therefore the transformed magnetization is given by

$$\boldsymbol{m}'(\boldsymbol{r}) = \left\langle \hat{\Phi}^\dagger(\boldsymbol{r}) \mathcal{U}^\dagger \boldsymbol{\sigma} \mathcal{U} \hat{\Phi}(\boldsymbol{r}) \right\rangle = \mathcal{R} \boldsymbol{m}(\boldsymbol{r}) \,. \tag{8.21}$$

It is straight forward to see that the density does not change under a rotation of the internal coordinate system,

$$n'(\boldsymbol{r}) = \left\langle \hat{\Phi}^\dagger(\boldsymbol{r}) \mathcal{U}^\dagger \mathcal{U} \hat{\Phi}(\boldsymbol{r}) \right\rangle = n(\boldsymbol{r}) \,. \tag{8.22}$$

The same is true for the paramagnetic current,

$$\boldsymbol{\jmath}'(\boldsymbol{r}) = \tfrac{1}{2i} \left\langle \hat{\Phi}^\dagger(\boldsymbol{r}) \mathcal{U}^\dagger \left(\nabla \mathcal{U} \hat{\Phi}(\boldsymbol{r}) \right) - \left(\nabla \hat{\Phi}^\dagger(\boldsymbol{r}) \mathcal{U}^\dagger \right) \mathcal{U} \hat{\Phi}(\boldsymbol{r}) \right\rangle = \boldsymbol{\jmath}(\boldsymbol{r}) \,, \tag{8.23}$$

since here we are only considering global rotations of the internal coordinate system, i.e. , $\mathcal{U}$ does not depend on $\boldsymbol{r}$. The spin magnetization transforms as a vector under rotations of the internal coordinate system, whereas the current remains unchanged, which is the opposite of the transformation properties of the spin magnetization and the paramagnetic current under spatial rotations. For infinitesimal internal rotations we get

$$\delta \boldsymbol{m}(\boldsymbol{r}) = \boldsymbol{m}'(\boldsymbol{r}) - \boldsymbol{m}(\boldsymbol{r}) = d\boldsymbol{\omega} \times \boldsymbol{m}(\boldsymbol{r}) \,. \tag{8.24}$$

Imposing

$$\begin{aligned} 0 = E_{xc}[n', \boldsymbol{m}'] - E_{xc}[n, \boldsymbol{m}] &= \int \mathrm{d}^3 r \; \frac{\delta E_{xc}[n, \boldsymbol{m}]}{\delta \boldsymbol{m}(\boldsymbol{r})} \delta \boldsymbol{m}(\boldsymbol{r}) \\ &= \varepsilon \int \mathrm{d}^3 r \; \mu_\mathrm{B} \boldsymbol{B}_{xc}(\boldsymbol{r}) \cdot (\boldsymbol{e}_\omega \times \boldsymbol{m}(\boldsymbol{r})) \\ &= \varepsilon \boldsymbol{e}_\omega \cdot \int \mathrm{d}^3 r \; \mu_\mathrm{B} \boldsymbol{m}(\boldsymbol{r}) \times \boldsymbol{B}_{xc}(\boldsymbol{r}) \,, \end{aligned} \tag{8.25}$$

we arrive at another zero-torque theorem for SDFT, since the rotation axis $\boldsymbol{e}_\omega$ is arbitrary,

$$0 = \int \mathrm{d}^3 r \; \mu_\mathrm{B} \boldsymbol{m}(\boldsymbol{r}) \times \boldsymbol{B}_{xc}(\boldsymbol{r}) \,. \tag{8.26}$$

This zero-torque theorem was first derived by Capelle, Vignale and Györffy [CVG01] from the equation of motion for the spin magnetization in time-dependent SDFT. It states that the xc-magnetic field must not exert a net torque on the system.

8.2 The definition of the Spin-Gradient Extension

From the discussion of the previous section we conclude that if we want to construct an explicit xc-energy functional it should depend only on scalars, i.e. , quantities that remain unchanged under a change of the coordinate system. Therefore a functional for SDFT cannot depend on single components of the spin magnetization, because their value depends on the orientation of the internal coordinate system. For the construction of a strictly local approximation this

implies that it can only depend on the density n and the magnitude of the spin magnetization $m = \boldsymbol{m} \cdot \boldsymbol{m}$. This leads to the well-known Local-Spin-Density Approximation (LSDA),

$$E_{xc}[n, \boldsymbol{m}] = \int \mathrm{d}^3 r \; n(\boldsymbol{r}) \, \varepsilon_{xc}^{\mathrm{unif}}(n(\boldsymbol{r}) \, , m(\boldsymbol{r})) \, . \tag{8.27}$$

For a strictly local approximation the local xc-energy density is determined by two scalar quantities. The SSW state however is characterized by 4 parameters so we cannot define a strictly local functional using the SSW state of the uniform electron gas reference system. Accordingly a functional based on the SSW state has to include gradients of the fundamental densities. We can immediately discard the divergence of the spin magnetization $\nabla \cdot \boldsymbol{m}$, because it contracts the spatial components of ∇ with the spin components of $\boldsymbol{m}$. For the same reason we exclude combinations like $\boldsymbol{m} \cdot (\nabla n)$. Moreover the density of the SSW state remains constant and hence we do not consider gradients of the density. We recall the magnetization of the SSW state,

$$\boldsymbol{m}(\boldsymbol{r}) = m \begin{pmatrix} s \cos(\boldsymbol{q} \cdot \boldsymbol{r}) \\ s \sin(\boldsymbol{q} \cdot \boldsymbol{r}) \\ \sqrt{1 - s^2} \end{pmatrix} , \tag{8.28}$$

and compute the first-order gradient,

$$\underline{\boldsymbol{D}}(\boldsymbol{r}) = \nabla \otimes \boldsymbol{m}(\boldsymbol{r}) = m \begin{pmatrix} -sq_x \sin(\boldsymbol{q} \cdot \boldsymbol{r}) & -sq_y \sin(\boldsymbol{q} \cdot \boldsymbol{r}) & -sq_z \sin(\boldsymbol{q} \cdot \boldsymbol{r}) \\ sq_x \cos(\boldsymbol{q} \cdot \boldsymbol{r}) & sq_y \cos(\boldsymbol{q} \cdot \boldsymbol{r}) & sq_z \cos(\boldsymbol{q} \cdot \boldsymbol{r}) \\ 0 & 0 & 0 \end{pmatrix} . \tag{8.29}$$

It is important to note that the the components $D_{j\kappa} = \partial_j m_\kappa$ of the tensor $\underline{\boldsymbol{D}}$ have a spatial index j and a spin index κ. Therefore the index j must be contracted with another spatial index and index κ with another spin index. One possibility is to contract the spin index of $\underline{\boldsymbol{D}}$ with the spin index of the magnetization and square the remaining spatial vector, i.e.

$$D_{\mathrm{L}} = m_\kappa \, (\partial_j m_\kappa) \, m_\lambda \, (\partial_j m_\lambda) \, . \tag{8.30}$$

This scalar measures the change of the magnetization along the direction specified by the magnetization. It is no surprise that this quantity vanishes for the SSW state, because the spin magnetization rotates in space, which means that the change of the magnetization is perpendicular to the direction of the magnetization. Another possibility to contract the indices of $D_{j\kappa}$ would be to square $\underline{\boldsymbol{D}}$ in both indices,

$$D(\boldsymbol{r}) = |\underline{\boldsymbol{D}}(\boldsymbol{r}) \, |^2 = (\partial_j m_\kappa(\boldsymbol{r})) \, (\partial_j m_\kappa(\boldsymbol{r})) \, . \tag{8.31}$$

Evaluating D for the SSW magnetization yields $m^2 s^2 q^2$ at any point in space, which means that the total change of the spin magnetization is homogeneous. One might be tempted to use a dependence on D for the definition of the functional constructed with the SSW state as reference system, because, much like the density and the magnitude of the magnetization, D has a global value for the SSW state. However we have seen that the longitudinal change of the magnetization vanishes for the SSW state and therefore also

$$D_{\mathrm{T}}(\boldsymbol{r}) = m^2(\boldsymbol{r})\, D(\boldsymbol{r}) - D_{\mathrm{L}}(\boldsymbol{r})\,, \tag{8.32}$$

would yield the same information as D for the SSW state. We weighted the total change D with the square of the magnetization, since we projected in the definition of the longitudinal change of the magnetization on $\boldsymbol{m}$ and not on the unit vector along $\boldsymbol{m}$. We can rewrite Eq. (8.32)

$$\begin{aligned} D_{\mathrm{T}} &= m_\kappa m_\kappa \left(\partial_j m_\lambda\right)\left(\partial_j m_\lambda\right) - m_\kappa \left(\partial_j m_\kappa\right) m_\lambda \left(\partial_j m_\lambda\right) \\ &= \left(\delta_{\kappa\mu}\delta_{\lambda\nu} - \delta_{\kappa\nu}\delta_{\lambda\mu}\right) m_\kappa m_\mu \left(\partial_j m_\lambda\right)\left(\partial_j m_\nu\right) \\ &= \epsilon_{\tau\kappa\lambda}\epsilon_{\tau\mu\nu} m_\kappa m_\mu \left(\partial_j m_\lambda\right)\left(\partial_j m_\nu\right), \end{aligned} \tag{8.33}$$

which explicitly shows that $D_{\mathrm{T}}(\boldsymbol{r})$ is the square of

$$\underline{\boldsymbol{D}}_{\mathrm{T}}(\boldsymbol{r}) = \boldsymbol{m}(\boldsymbol{r}) \times \left(\nabla \otimes \boldsymbol{m}\left(\boldsymbol{r}\right)\right), \tag{8.34}$$

which measures the change of the magnetization perpendicular to the magnetization. Since the magnetization of SSW state varies only transversally the physical choice is to include the transversal gradient $D_{\mathrm{T}}(\boldsymbol{r})$ in the definition of the functional. D_{T} only determines the combination $s^2 q^2$, which forces us to include second-order gradients. Evaluating the Laplacian of the magnetization for the SSW state,

$$\boldsymbol{d}(\boldsymbol{r}) = \Delta \boldsymbol{m}(\boldsymbol{r}) = m \begin{pmatrix} -sq^2 \cos(\boldsymbol{q}\cdot\boldsymbol{r}) \\ -sq^2 \sin(\boldsymbol{q}\cdot\boldsymbol{r}) \\ 0 \end{pmatrix} \tag{8.35}$$

we see that the contraction $\boldsymbol{m}(\boldsymbol{r}) \cdot \boldsymbol{d}(\boldsymbol{r})$ yields $-m^2 s^2 q^2$ for the SSW state which is competing with D_{T}, because it provides the same information $s^2 q^2$. Adopting the convention that the SSW parameters are obtained as local as possible we choose D_{T} to determine $s^2 q^2$. Squaring $\boldsymbol{d}$ we obtain $d(\boldsymbol{r}) = \boldsymbol{d}(\boldsymbol{r}) \cdot \boldsymbol{d}(\boldsymbol{r}) = m^2 s^2 q^4$ which seems to provide the missing information, because from the ratio of D_{T} and d we might define the local SSW parameters

$$s^2(\boldsymbol{r}) = \frac{D_{\mathrm{T}}^2(\boldsymbol{r})}{m^6(\boldsymbol{r})\, d(\boldsymbol{r})}, \tag{8.36}$$

$$q^2(\boldsymbol{r}) = \frac{m^2(\boldsymbol{r})\, d(\boldsymbol{r})}{D_{\mathrm{T}}(\boldsymbol{r})}. \tag{8.37}$$

However, for a generic system, Eq. (8.36) might yield an s^2 which is larger than one. This is inconsistent with the fact that s represents the sine of the azimuthal angle of the spin-spiral magnetization. Since $d_{\mathrm{L}}(\boldsymbol{r}) = (\boldsymbol{m}(\boldsymbol{r}) \cdot \boldsymbol{d}(\boldsymbol{r}))^2$ represent the longitudinal contribution of the Laplacian we can in analogy to Eq. (8.32) define

$$d_{\mathrm{T}}(\boldsymbol{r}) = m^2(\boldsymbol{r})\, d(\boldsymbol{r}) - d_{\mathrm{L}}(\boldsymbol{r})\,, \tag{8.38}$$

which can be recasted into

$$\begin{aligned} d_{\mathrm{T}} &= m_\kappa m_\kappa \left(\partial_j \partial_j m_\lambda\right) \left(\partial_k \partial_k m_\lambda\right) - m_\kappa \left(\partial_j \partial_j m_\kappa\right) m_\lambda \left(\partial_k \partial_k m_\lambda\right) \\ &= \epsilon_{\tau\kappa\lambda} \epsilon_{\tau\mu\nu} m_\kappa m_\mu \left(\partial_j \partial_j m_\lambda\right) \left(\partial_k \partial_k m_\nu\right). \end{aligned} \tag{8.39}$$

Again, this is the square of the contribution of the Laplacian which is perpendicular to the magnetization,

$$\boldsymbol{d}_{\mathrm{T}}(\boldsymbol{r}) = \boldsymbol{m}(\boldsymbol{r}) \times \left(\Delta \boldsymbol{m}(\boldsymbol{r})\right). \tag{8.40}$$

For the SSW state it is straight forward to verify that $d_{\mathrm{T}} = m^4 s^2 \left(1 - s^2\right) q^4$ and hence we arrive at the final definitions for the local parameters

$$s^2(\boldsymbol{r}) = \frac{D_{\mathrm{T}}^2(\boldsymbol{r})}{D_{\mathrm{T}}^2(\boldsymbol{r}) + m^4(\boldsymbol{r})\, d_{\mathrm{T}}(\boldsymbol{r})}, \tag{8.41}$$

$$q^2(\boldsymbol{r}) = \frac{D_{\mathrm{T}}^2(\boldsymbol{r}) + m^4(\boldsymbol{r})\, d_{\mathrm{T}}(\boldsymbol{r})}{m^4(\boldsymbol{r})\, D_{\mathrm{T}}(\boldsymbol{r})}, \tag{8.42}$$

where now, by construction, s^2 is between zero and one. In definitions Eqs. (8.41), (8.42) we have implicitly replaced the part of the second-order gradient, providing information already obtained by means of the first-order gradient, by the first-order gradient containing this information. Finally we define the SSW functional

$$E_{xc}^{\mathrm{SSW}}[n, \boldsymbol{m}] = \int \mathrm{d}^3 r\; n(\boldsymbol{r})\, \varepsilon_{xc}^{\mathrm{SSW}}(n(\boldsymbol{r})\,, m(\boldsymbol{r})\,, D_{\mathrm{T}}(\boldsymbol{r})\,, d_{\mathrm{T}}(\boldsymbol{r}))\,, \tag{8.43}$$

where the function $\varepsilon_{xc}^{\mathrm{SSW}}(n, m, D_{\mathrm{T}}, d_{\mathrm{T}})$ or equivalently $\varepsilon_{xc}^{\mathrm{SSW}}(r_s, \chi, s, q)$ is the exchange-correlation-energy density of the uniform gas in the spin-spiral-wave state. In analogy to the definition of a generic GGA (cf. (4.14)), we can rewrite the xc-energy functional as

$$E_{xc}^{\mathrm{SSW}}[n, \boldsymbol{m}] = \int \mathrm{d}^3 r\; n(\boldsymbol{r})\, \varepsilon_{xc}^{\mathrm{unif}}(n(\boldsymbol{r})\,, m(\boldsymbol{r}))\, (1 + S_{xc}(n(\boldsymbol{r})\,, m(\boldsymbol{r})\,, D_{\mathrm{T}}(\boldsymbol{r})\,, d_{\mathrm{T}}(\boldsymbol{r})))\,, \tag{8.44}$$

introducing the Spin-Gradient Extension (SGE) S_{xc} to the LSDA functional,

$$S_{xc}(n, m, D_{\mathrm{T}}, d_{\mathrm{T}}) = \frac{\varepsilon_{xc}^{\mathrm{SSW}}(n, m, D_{\mathrm{T}}, d_{\mathrm{T}}) - \varepsilon_{xc}^{\mathrm{unif}}(n, m)}{\varepsilon_{xc}^{\mathrm{unif}}(n, m)}. \tag{8.45}$$

Note that

$$\varepsilon_{xc}^{\mathrm{SSW}}(n, m, D_{\mathrm{T}} = 0, d_{\mathrm{T}}) = \varepsilon_{xc}^{\mathrm{SSW}}(n, m, D_{\mathrm{T}} = 0, d_{\mathrm{T}} = 0) = \varepsilon_{xc}^{\mathrm{unif}}(n, m)\,.$$

8.3 Kohn-Sham potentials from the Spin-Gradient Extension

Having defined the SSW functional we can investigate the corresponding xc-potential and xc-magnetic field. First we have a look at the usual LSDA potentials, i.e.

$$v_{xc}^{\mathrm{LSDA}}(\boldsymbol{r}) = \frac{\delta E_{xc}^{\mathrm{LSDA}}}{\delta n(\boldsymbol{r})} = \varepsilon_{xc}^{\mathrm{unif}}(n(\boldsymbol{r}), m(\boldsymbol{r})) + n(\boldsymbol{r}) \left(\partial_n \varepsilon_{xc}^{\mathrm{unif}}(n(\boldsymbol{r}), m(\boldsymbol{r}))\right), \tag{8.46}$$

$$\mu_{\mathrm{B}} \boldsymbol{B}_{xc}^{\mathrm{LSDA}}(\boldsymbol{r}) = \frac{\delta E_{xc}^{\mathrm{LSDA}}}{\delta \boldsymbol{m}(\boldsymbol{r})} = n(\boldsymbol{r}) \left(\partial_m \varepsilon_{xc}^{\mathrm{unif}}(n(\boldsymbol{r}), m(\boldsymbol{r}))\right) \frac{\boldsymbol{m}(\boldsymbol{r})}{m(\boldsymbol{r})}. \tag{8.47}$$

In order to streamline the derivation of the xc-potentials for the SSW functional we drop the super- and subscripts of $\varepsilon_{xc}^{\mathrm{SSW}}$ and we only indicate a spatial dependence of ε implied through its explicit dependence on the local values of n, m, D_{T} and d_{T}. Furthermore we drop the subscript T of the gradients D_{T}, d_{T} and introduce the abbreviations $\varepsilon_n = \partial_n \varepsilon$, $\varepsilon_m = \partial_m \varepsilon$, $\varepsilon_D = \partial_D \varepsilon$ and $\varepsilon_d = \partial_d \varepsilon$. The xc-potential has the same form as the LSDA potential, since ε does only depend on the density and not on gradients of the density,

$$v_{xc}^{\mathrm{SSW}}(\boldsymbol{r}) = \frac{\delta E_{xc}^{\mathrm{SSW}}}{\delta n(\boldsymbol{r})} = \varepsilon(\boldsymbol{r}) + n(\boldsymbol{r})\, \varepsilon_n(\boldsymbol{r})\,. \tag{8.48}$$

The xc-magnetic field has three contributions,

$$\boldsymbol{B}_{xc}^{\mathrm{SSW}}(\boldsymbol{r}) = \boldsymbol{B}_m(\boldsymbol{r}) + \boldsymbol{B}_D(\boldsymbol{r}) + \boldsymbol{B}_d(\boldsymbol{r})\,, \tag{8.49}$$

where $\boldsymbol{B}_m$, $\boldsymbol{B}_D$, $\boldsymbol{B}_d$ contain ε_m, ε_D, ε_d, respectively. The first contribution is formally equivalent to the LSDA xc-magnetic field,

$$\mu_{\mathrm{B}} \boldsymbol{B}_m(\boldsymbol{r}) = n(\boldsymbol{r})\, \varepsilon_m(\boldsymbol{r})\, \frac{\boldsymbol{m}(\boldsymbol{r})}{m(\boldsymbol{r})}. \tag{8.50}$$

For the determination of $\boldsymbol{B}_D$ we need to compute

$$\begin{aligned}
\frac{\delta D(\boldsymbol{r}')}{\delta m_\kappa(\boldsymbol{r})} &= \frac{\delta}{\delta m_\kappa(\boldsymbol{r})} \Big(m_\lambda m_\lambda \left(\partial_j m_\mu\right) \left(\partial_j m_\mu\right) - m_\lambda \left(\partial_j m_\lambda\right) m_\mu \left(\partial_j m_\mu\right) \Big)(\boldsymbol{r}') \\
&= 2 \Big(m_\kappa(\boldsymbol{r}') \left(\partial'_j m_\lambda(\boldsymbol{r}')\right) \left(\partial'_j m_\lambda(\boldsymbol{r}')\right) - \left(\partial'_j m_\kappa(\boldsymbol{r}')\right) m_\lambda(\boldsymbol{r}') \left(\partial'_j m_\lambda(\boldsymbol{r}')\right) \Big) \delta(\boldsymbol{r}' - \boldsymbol{r}) \\
&\quad + 2 \Big(\left(\partial'_j m_\kappa(\boldsymbol{r}')\right) m_\lambda(\boldsymbol{r}')\, m_\lambda(\boldsymbol{r}') - m_\kappa(\boldsymbol{r}')\, m_\lambda(\boldsymbol{r}') \left(\partial'_j m_\lambda(\boldsymbol{r}')\right) \Big) \partial'_j \delta(\boldsymbol{r}' - \boldsymbol{r})\,.
\end{aligned} \tag{8.51}$$

Using a partial integration we obtain

$$\begin{aligned}
\mu_{\mathrm{B}} \left(\boldsymbol{B}_D\right)_\kappa &= 4 n \varepsilon_D \Big(m_\kappa \left(\partial_j m_\lambda\right) \left(\partial_j m_\lambda\right) - \left(\partial_j m_\kappa\right) \left(\partial_j m_\lambda\right) m_\lambda \Big) \\
&\quad + 2 n \varepsilon_D \Big(m_\kappa m_\lambda \left(\partial_j \partial_j m_\lambda\right) - \left(\partial_j \partial_j m_\kappa\right) m_\lambda m_\lambda \Big) \\
&\quad + 2 \left(\partial_j n \varepsilon_D\right) \Big(m_\kappa m_\lambda \left(\partial_j m_\lambda\right) - \left(\partial_j m_\kappa\right) m_\lambda m_\lambda \Big),
\end{aligned} \tag{8.52}$$

where we dropped the spatial arguments for brevity. In vectorial notation $\boldsymbol{B}_D$ can be written as

$$\begin{aligned}\mu_{\mathrm{B}}\boldsymbol{B}_D = {} & 4\,(n\varepsilon_D)\,(\nabla\otimes\boldsymbol{m})\times\big(\boldsymbol{m}\times(\nabla\otimes\boldsymbol{m})\big) + 2\,(n\varepsilon_D)\,\boldsymbol{m}\times(\boldsymbol{m}\times\boldsymbol{d}) \\ & + 2\,(\nabla n\varepsilon_D)\,\boldsymbol{m}\times\big(\boldsymbol{m}\times(\nabla\otimes\boldsymbol{m})\big),\end{aligned} \tag{8.53}$$

where the cross-product $\times$ acts on the spin components, i.e. , the components of $\boldsymbol{m}$. Furthermore it is implied the components of the ∇ are contracted. The energy contribution due to $\boldsymbol{B}_D$ in the Kohn-Sham system can be computed without employing a partial integration by using $\partial'_j\delta(\boldsymbol{r}'-\boldsymbol{r}) = -\partial_j\delta(\boldsymbol{r}'-\boldsymbol{r})$,

$$\begin{aligned}E_{\boldsymbol{B}_D} &= \mu_{\mathrm{B}}\int \mathrm{d}^3r\; \boldsymbol{m}(\boldsymbol{r})\cdot\boldsymbol{B}_D(\boldsymbol{r}) \\ &= 4\int \mathrm{d}^3r\; n(\boldsymbol{r})\,\varepsilon_D(\boldsymbol{r})\,(\boldsymbol{m}(\boldsymbol{r})\times(\nabla\otimes\boldsymbol{m}(\boldsymbol{r})))\cdot(\boldsymbol{m}(\boldsymbol{r})\times(\nabla\otimes\boldsymbol{m}(\boldsymbol{r}))) \\ &= 4\int \mathrm{d}^3r\; n(\boldsymbol{r})\,\varepsilon_D(\boldsymbol{r})\,D(\boldsymbol{r})\,.\end{aligned} \tag{8.54}$$

A similar calculation can be used to verify that the net torque due to $\boldsymbol{B}_D$ vanishes. Now we compute

$$\begin{aligned}&\frac{\delta d(\boldsymbol{r}')}{\delta m_\kappa(\boldsymbol{r})} = \frac{\delta}{\delta m_\kappa(\boldsymbol{r})}\Big(m_\lambda m_\lambda\,(\partial_j\partial_j m_\mu)\,(\partial_k\partial_k m_\mu) - m_\lambda\,(\partial_j\partial_j m_\lambda)\,m_\mu\,(\partial_k\partial_k m_\mu)\Big)(\boldsymbol{r}') \\ &= 2\Big(m_\kappa(\boldsymbol{r}')\,\big(\partial'_j\partial'_j m_\lambda(\boldsymbol{r}')\big)\,(\partial'_k\partial'_k m_\lambda(\boldsymbol{r}')) - \big(\partial'_j\partial'_j m_\kappa(\boldsymbol{r}')\big)\,m_\lambda(\boldsymbol{r}')\,(\partial'_k\partial'_k m_\lambda(\boldsymbol{r}'))\Big)\delta(\boldsymbol{r}'-\boldsymbol{r}) \\ &+ 2\Big(\big(\partial'_j\partial'_j m_\kappa(\boldsymbol{r}')\big)\,m_\lambda(\boldsymbol{r}')\,m_\lambda(\boldsymbol{r}') - m_\kappa(\boldsymbol{r}')\,m_\lambda(\boldsymbol{r}')\,\big(\partial'_j\partial'_j m_\lambda(\boldsymbol{r}')\big)\Big)\partial'_k\partial'_k\delta(\boldsymbol{r}'-\boldsymbol{r})\,.\end{aligned} \tag{8.55}$$

Again, using two partial integrations, we get

$$\begin{aligned}\mu_{\mathrm{B}}\,(\boldsymbol{B}_d)_\kappa = {} & 2n\varepsilon_d\Big((\partial_j\partial_j\partial_k\partial_k m_\kappa)\,m_\lambda m_\lambda - m_\kappa m_\lambda\,(\partial_j\partial_j\partial_k\partial_k m_\lambda)\Big) \\ & + 4n\varepsilon_d\Big((\partial_j\partial_j m_\kappa)\,(\partial_k m_\lambda)\,(\partial_k m_\lambda) - (\partial_k m_\kappa)\,(\partial_k m_\lambda)\,(\partial_j\partial_j m_\lambda)\Big) \\ & + 4n\varepsilon_d\Big((\partial_k\partial_j\partial_j m_\kappa)\,(\partial_k m_\lambda)\,m_\lambda - m_\kappa\,(\partial_k m_\lambda)\,(\partial_k\partial_j\partial_j m_\lambda)\Big) \\ & + 4n\varepsilon_d\Big((\partial_k\partial_j\partial_j m_\kappa)\,m_\lambda\,(\partial_k m_\lambda) - (\partial_k m_\kappa)\,m_\lambda\,(\partial_k\partial_j\partial_j m_\lambda)\Big) \\ & + 4\,(\partial_k n\varepsilon_d)\,\Big((\partial_k\partial_j\partial_j m_\kappa)\,m_\lambda m_\lambda - m_\kappa m_\lambda\,(\partial_k\partial_j\partial_j m_\lambda)\Big) \\ & + 4\,(\partial_k n\varepsilon_d)\,\Big((\partial_j\partial_j m_\kappa)\,(\partial_k m_\lambda)\,m_\lambda - m_\kappa\,(\partial_k m_\lambda)\,(\partial_j\partial_j m_\lambda)\Big) \\ & + 4\,(\partial_k n\varepsilon_d)\,\Big((\partial_j\partial_j m_\kappa)\,m_\lambda\,(\partial_k m_\lambda) - (\partial_k m_\kappa)\,m_\lambda\,(\partial_j\partial_j m_\lambda)\Big) \\ & + 2\,(\partial_k\partial_k n\varepsilon_d)\,\Big((\partial_j\partial_j m_\kappa)\,m_\lambda m_\lambda - m_\kappa m_\lambda\,(\partial_j\partial_j m_\lambda)\Big).\end{aligned} \tag{8.56}$$

Introducing $\boldsymbol{\delta} = \Delta\boldsymbol{d}$ this reads in vectorial notation,

$$\begin{aligned}\mu_{\mathrm{B}}\boldsymbol{B}_d = {} & 4\,(\nabla n\varepsilon_d)\,\Big(\boldsymbol{m}\times\big((\nabla\otimes\boldsymbol{d})\times\boldsymbol{m}\big) + (\nabla\otimes\boldsymbol{m})\times\big(\boldsymbol{d}\times\boldsymbol{m}\big) + \boldsymbol{m}\times\big(\boldsymbol{d}\times(\nabla\otimes\boldsymbol{m})\big)\Big) \\ & + 4\,(n\varepsilon_d)\,\Big((\nabla\otimes\boldsymbol{m})\times\big(\boldsymbol{d}\times(\nabla\otimes\boldsymbol{m})\big) + (\nabla\otimes\boldsymbol{m})\times\big((\nabla\otimes\boldsymbol{d})\times\boldsymbol{m}\big) + \boldsymbol{m}\times\big((\nabla\otimes\boldsymbol{d})\times(\nabla\otimes\boldsymbol{m})\big)\Big) \\ & + 2\Big((n\varepsilon_d)\,\boldsymbol{m}\times\big(\boldsymbol{\delta}\times\boldsymbol{m}\big) + (\Delta n\varepsilon_d)\,\boldsymbol{m}\times\big(\boldsymbol{d}\times\boldsymbol{m}\big)\Big). \end{aligned} \tag{8.57}$$

The energy contribution for the Kohn-Sham system due to $\boldsymbol{B}_d$ is given by

$$\begin{aligned} E_{\boldsymbol{B}_d} &= \mu_{\mathrm{B}}\int \mathrm{d}^3r\; \boldsymbol{m}(\boldsymbol{r})\cdot\boldsymbol{B}_d(\boldsymbol{r}) \\ &= 4\int \mathrm{d}^3r\; n(\boldsymbol{r})\,\varepsilon_d(\boldsymbol{r})\,(\boldsymbol{m}(\boldsymbol{r})\times\boldsymbol{d}(\boldsymbol{r}))\cdot(\boldsymbol{m}(\boldsymbol{r})\times\boldsymbol{d}(\boldsymbol{r})) \\ &= 4\int \mathrm{d}^3r\; n(\boldsymbol{r})\,\varepsilon_d(\boldsymbol{r})\,d(\boldsymbol{r})\,, \end{aligned} \tag{8.58}$$

where we used $\partial'_k\partial'_k\delta(\boldsymbol{r}'-\boldsymbol{r}) = \partial_k\partial_k\delta(\boldsymbol{r}'-\boldsymbol{r})$. In the same way we can verify that also the net torque due to $\boldsymbol{B}_d$ vanishes and therefore the net torque of the full $\boldsymbol{B}_{xc}^{\mathrm{SSW}}$ vanishes as expected, since we defined the SSW functional using only properly contracted quantities. From the explicit form of $\boldsymbol{B}_D$, Eq. (8.53), and $\boldsymbol{B}_d$, Eq. (8.57), it is evident that for a generic magnetization $\boldsymbol{B}_{xc}^{\mathrm{SSW}}$ is not parallel to $\boldsymbol{m}$. This means that the xc-magnetic field exerts a local torque on the system. For a collinear magnetization, i.e. a magnetization that points in the same direction everywhere in space, only the first term $\boldsymbol{B}_m$ is non-vanishing. Therefore in collinear situations $\boldsymbol{B}_{xc}^{\mathrm{SSW}}$ is identical to $\boldsymbol{B}_{xc}^{\mathrm{LSDA}}$. If one is interested in finding the ground-state magnetic configuration of a specific system without external magnetic field, one has to start the self-consistent Kohn-Sham calculation from a initial magnetization that is non-collinear, i.e. that points in various directions in space, and investigate to which magnetic configuration the Kohn-Sham self-consistent loop converges.

8.4 Random-Phase Approximation for the spin-spiral-wave state

The definition of the SSW functional is completed by the determination of the xc-energy of the uniform electron gas in the spin-spiral configuration. As a first approximation one might consider to use only the exchange energy of the uniform electron gas either from a self-consistent Hartree-Fock calculation (cf. Chap. 6) or from first-order perturbation theory (cf. Chap. 7). As we have discussed extensively in Chapter 6, the uniform electron gas exhibits an instability w.r.t. the formation of a SSW when treated in the Hartree-Fock approximation, and in Chapter 7 we found that this instability is at least partially present if we consider

the OEP exact-exchange functional, which is equivalent to treating the energy in first-order perturbation theory for the uniform electron gas. However an analytical argument by Giuliani and Vignale [GV08] showed that this instability is not present if one considers the Random-Phase Approximation which corresponds to the inclusion of correlations. Also our investigation of the SSW within RDMFT in Sec. 6.6 indicates that an inclusion of correlation effects opposes the Overhauser instability. Since we do not want to encode an artificial instability in the functional, we decided to obtain the reference energies from the Random-Phase Approximation for the uniform electron gas in the SSW configuration. Optimally one would like to use exact Quantum Monte-Carlo methods to obtain the reference energies, but to our knowledge there are no studies of the uniform electron gas including non-collinear spin magnetizations employing Quantum Monte-Carlo methods. At this point it is important to stress that the reference energies are not obtained from a ground state calculation of the uniform electron gas, but from a minimization of the energy under the *constraint* that the uniform electron gas has a SSW spin magnetization. Note that the same is true for the reference energies used to construct the usual LSDA, i.e. , the energies are obtained from the uniform electron gas being constrained to have a specific value of the spin magnetization. This means that, in spite of the fact that the uniform electron gas is not spin polarized at a density corresponding to $r_s = 1$, the minimal energy corresponding to a spin polarized electron gas at this density enters the definition of the LSDA.

Employing the coupling constant technique or, equivalently, the adiabatic-connection fluctuation-dissipation theorem of many-body perturbation theory the correlation energy in the RPA of the uniform electron gas is given by

$$\varepsilon_{c,\mathrm{RPA}} = \frac{\imath}{2} \int_0^1 \mathrm{d}\lambda \, \frac{1}{\lambda} \iint \mathrm{d}^3 q \mathrm{d}\omega \, \frac{\left(\lambda W(\boldsymbol{q}) \, P_0(\boldsymbol{q};\omega)\right)^2}{1 - \lambda W(\boldsymbol{q}) \, P_0(\boldsymbol{q};\omega)}. \tag{8.59}$$

From a DFT point-of-view the RPA correlation energy also contains kinetic energy contributions by means of the coupling constant integration. One might argue that this is responsible for the suppression of the Overhauser instability, since the kinetic energy opposes the formation of a SSW. In Eq. (8.59) we have introduced the polarizability P_0 of the non-interacting uniform electron gas in the SSW state. In order to obtain the explicit form of P_0 we first write

down the non-interacting time-ordered Green's function for the SSW state

$$\begin{aligned}\mathcal{G}_0(\boldsymbol{r};\boldsymbol{r}';\tau) &= -\imath\sum_{b=\mp}\int\mathrm{d}^3k\; e^{-\imath\epsilon_b(\boldsymbol{k})\tau}\xi_{\boldsymbol{k}b}(\boldsymbol{r})\,\xi^\dagger_{\boldsymbol{k}b}(\boldsymbol{r}')\left(\left(1-n_b(\boldsymbol{k})\right)\Theta(\tau)-n_b(\boldsymbol{k})\,\Theta(-\tau)\right)\\ &= \frac{1}{2\pi}\int\mathrm{d}\omega\;\frac{1}{(2\pi)^3}\int\mathrm{d}^3k\; e^{\imath(\boldsymbol{k}\cdot(\boldsymbol{r}-\boldsymbol{r}')-\omega\tau)}\\ &\times\left(\mathcal{M}_{\boldsymbol{k}-}(\boldsymbol{r};\boldsymbol{r}')\left(\frac{1-n_-(\boldsymbol{k})}{\omega-\epsilon_-(\boldsymbol{k})+\imath\eta}+\frac{n_-(\boldsymbol{k})}{\omega-\epsilon_-(\boldsymbol{k})-\imath\eta}\right)\right.\\ &\left.+\mathcal{M}_{\boldsymbol{k}+}(\boldsymbol{r};\boldsymbol{r}')\left(\frac{1-n_+(\boldsymbol{k})}{\omega-\epsilon_+(\boldsymbol{k})+\imath\eta}+\frac{n_+(\boldsymbol{k})}{\omega-\epsilon_+(\boldsymbol{k})-\imath\eta}\right)\right),\end{aligned}\tag{8.60}$$

where we introduced the two 2×2-matrices

$$\mathcal{M}_{\boldsymbol{k}-}(\boldsymbol{r};\boldsymbol{r}') = \begin{pmatrix}\cos^2\left(\frac{1}{2}\theta(\boldsymbol{k})\right)e^{-\imath\frac{1}{2}\boldsymbol{q}\cdot(\boldsymbol{r}-\boldsymbol{r}')} & \sin\left(\frac{1}{2}\theta(\boldsymbol{k})\right)\cos\left(\frac{1}{2}\theta(\boldsymbol{k})\right)e^{-\imath\frac{1}{2}\boldsymbol{q}\cdot(\boldsymbol{r}+\boldsymbol{r}')}\\ \sin\left(\frac{1}{2}\theta(\boldsymbol{k})\right)\cos\left(\frac{1}{2}\theta(\boldsymbol{k})\right)e^{\imath\frac{1}{2}\boldsymbol{q}\cdot(\boldsymbol{r}+\boldsymbol{r}')} & \sin^2\left(\frac{1}{2}\theta(\boldsymbol{k})\right)e^{\imath\frac{1}{2}\boldsymbol{q}\cdot(\boldsymbol{r}-\boldsymbol{r}')}\end{pmatrix},\tag{8.61a}$$

$$\mathcal{M}_{\boldsymbol{k}+}(\boldsymbol{r};\boldsymbol{r}') = \begin{pmatrix}\sin^2\left(\frac{1}{2}\theta(\boldsymbol{k})\right)e^{-\imath\frac{1}{2}\boldsymbol{q}\cdot(\boldsymbol{r}-\boldsymbol{r}')} & -\sin\left(\frac{1}{2}\theta(\boldsymbol{k})\right)\cos\left(\frac{1}{2}\theta(\boldsymbol{k})\right)e^{-\imath\frac{1}{2}\boldsymbol{q}\cdot(\boldsymbol{r}+\boldsymbol{r}')}\\ -\sin\left(\frac{1}{2}\theta(\boldsymbol{k})\right)\cos\left(\frac{1}{2}\theta(\boldsymbol{k})\right)e^{\imath\frac{1}{2}\boldsymbol{q}\cdot(\boldsymbol{r}+\boldsymbol{r}')} & \cos^2\left(\frac{1}{2}\theta(\boldsymbol{k})\right)e^{\imath\frac{1}{2}\boldsymbol{q}\cdot(\boldsymbol{r}-\boldsymbol{r}')}\end{pmatrix}.\tag{8.61b}$$

The non-interacting dynamical density-density correlation function, also known as the polarization propagator, is related to the Green's function Eq. (8.60) by

$$\begin{aligned}P_0(\boldsymbol{r};\boldsymbol{r}';\tau) &= -\imath\,\mathrm{tr}\{\mathcal{G}_0(\boldsymbol{r};\boldsymbol{r}';\tau)\,\mathcal{G}_0(\boldsymbol{r}';\boldsymbol{r};\tau)\}\\ &= \frac{1}{2\pi}\int\mathrm{d}\omega\;\frac{1}{(2\pi)^3}\int\mathrm{d}^3k_1\;\frac{1}{(2\pi)^3}\int\mathrm{d}^3k_2\; e^{\imath((\boldsymbol{k}_1-\boldsymbol{k}_2)\cdot(\boldsymbol{r}-\boldsymbol{r}')-\omega\tau)}\\ &\times\left(A(\boldsymbol{k}_1,\boldsymbol{k}_2)\left(\frac{\left(1-n_-(\boldsymbol{k}_1)\right)n_-(\boldsymbol{k}_2)}{\omega-(\epsilon_-(\boldsymbol{k}_1)-\epsilon_-(\boldsymbol{k}_2))+\imath\eta}-\frac{n_-(\boldsymbol{k}_1)\left(1-n_-(\boldsymbol{k}_2)\right)}{\omega-(\epsilon_-(\boldsymbol{k}_1)-\epsilon_-(\boldsymbol{k}_2))-\imath\eta}\right.\right.\\ &\qquad\left.\frac{\left(1-n_+(\boldsymbol{k}_1)\right)n_+(\boldsymbol{k}_2)}{\omega-(\epsilon_+(\boldsymbol{k}_1)-\epsilon_+(\boldsymbol{k}_2))+\imath\eta}-\frac{n_+(\boldsymbol{k}_1)\left(1-n_+(\boldsymbol{k}_2)\right)}{\omega-(\epsilon_+(\boldsymbol{k}_1)-\epsilon_+(\boldsymbol{k}_2))-\imath\eta}\right)\\ &\quad+B(\boldsymbol{k}_1,\boldsymbol{k}_2)\left(\frac{\left(1-n_-(\boldsymbol{k}_1)\right)n_+(\boldsymbol{k}_2)}{\omega-(\epsilon_-(\boldsymbol{k}_1)-\epsilon_+(\boldsymbol{k}_2))+\imath\eta}-\frac{n_-(\boldsymbol{k}_1)\left(1-n_+(\boldsymbol{k}_2)\right)}{\omega-(\epsilon_-(\boldsymbol{k}_1)-\epsilon_+(\boldsymbol{k}_2))-\imath\eta}\right.\\ &\qquad\left.\left.\frac{\left(1-n_+(\boldsymbol{k}_1)\right)n_-(\boldsymbol{k}_2)}{\omega-(\epsilon_+(\boldsymbol{k}_1)-\epsilon_-(\boldsymbol{k}_2))+\imath\eta}-\frac{n_+(\boldsymbol{k}_1)\left(1-n_-(\boldsymbol{k}_2)\right)}{\omega-(\epsilon_+(\boldsymbol{k}_1)-\epsilon_-(\boldsymbol{k}_2))-\imath\eta}\right)\right),\end{aligned}\tag{8.62}$$

where we have executed one ω-integration by means of the residue theorem of complex analysis.

Moreover we introduced

$$\begin{aligned} A(\boldsymbol{k}_1,\boldsymbol{k}_2) &= \mathrm{tr}\{\mathcal{M}_{\boldsymbol{k}_1-}(\boldsymbol{r};\boldsymbol{r}')\,\mathcal{M}_{\boldsymbol{k}_2-}(\boldsymbol{r}';\boldsymbol{r})\} = \mathrm{tr}\{\mathcal{M}_{\boldsymbol{k}_1+}(\boldsymbol{r};\boldsymbol{r}')\,\mathcal{M}_{\boldsymbol{k}_2+}(\boldsymbol{r}';\boldsymbol{r})\} \\ &= \tfrac{1}{2}\left(1+C(\boldsymbol{k}_1;\boldsymbol{k}_2)\right) \qquad (8.63a) \\ B(\boldsymbol{k}_1,\boldsymbol{k}_2) &= \mathrm{tr}\{\mathcal{M}_{\boldsymbol{k}_1-}(\boldsymbol{r};\boldsymbol{r}')\,\mathcal{M}_{\boldsymbol{k}_2+}(\boldsymbol{r}';\boldsymbol{r})\} = \mathrm{tr}\{\mathcal{M}_{\boldsymbol{k}_1+}(\boldsymbol{r};\boldsymbol{r}')\,\mathcal{M}_{\boldsymbol{k}_2-}(\boldsymbol{r}';\boldsymbol{r})\} \\ &= \tfrac{1}{2}\left(1+C(\boldsymbol{k}_1;\boldsymbol{k}_2)\right) \qquad (8.63b) \\ C(\boldsymbol{k}_1;\boldsymbol{k}_2) &= \cos(\theta(\boldsymbol{k}_1))\cos(\theta(\boldsymbol{k}_2)) + \sin(\theta(\boldsymbol{k}_1))\sin(\theta(\boldsymbol{k}_2))\,. \qquad (8.63c) \end{aligned}$$

Relabeling $\boldsymbol{k}_1 \to \boldsymbol{k}$ and $\boldsymbol{k}_2 \to \boldsymbol{k}-\boldsymbol{q}$ in Eq. (8.62), we can read-off the Fourier transform of the polarization propagator,

$$\begin{aligned} P_0(\boldsymbol{q};\omega) = \sum_{b_1=\mp}\sum_{b_2=\mp}\frac{1}{(2\pi)^3}\int \mathrm{d}^3k\ \tfrac{1}{2}\left(1+b_1b_2C(\boldsymbol{k};\boldsymbol{k}-\boldsymbol{q})\right) \\ \times\left(\frac{(1-n_{b_1}(\boldsymbol{k}))\,n_{b_2}(\boldsymbol{k}-\boldsymbol{q})}{\omega-(\epsilon_{b_1}(\boldsymbol{k})-\epsilon_{b_2}(\boldsymbol{k}-\boldsymbol{q}))+\imath\eta} - \frac{n_{b_1}(\boldsymbol{k})\,(1-n_{b_2}(\boldsymbol{k}-\boldsymbol{q}))}{\omega-(\epsilon_{b_1}(\boldsymbol{k})-\epsilon_{b_2}(\boldsymbol{k}-\boldsymbol{q}))-\imath\eta}\right). \qquad (8.64) \end{aligned}$$

From the Lehmann representation we know that time-ordered correlation functions are analytic in the first and third quadrant of the complex ω-plane and hence we can deform the integration contour for the frequency integral in the expression for the correlation energy Eq. (8.59) to run along the imaginary axis, i.e. ,

$$\varepsilon_{c,\mathrm{RPA}} = -\frac{1}{2}\int_0^1 \mathrm{d}\lambda\,\frac{1}{\lambda}\iint \mathrm{d}^3q\mathrm{d}\omega\,\frac{\left(\lambda W(\boldsymbol{q})\,P_0(\boldsymbol{q};\omega)\right)^2}{1-\lambda W(\boldsymbol{q})\,P_0(\boldsymbol{q};\omega)}. \qquad (8.65)$$

Carrying out the coupling constant integration we get

$$\varepsilon_{c,\mathrm{RPA}} = \frac{1}{2}\iint \mathrm{d}^3q\mathrm{d}\omega\ \left(\ln(1-W(\boldsymbol{q})\,P_0(\boldsymbol{q};\imath\omega)) + W(\boldsymbol{q})\,P_0(\boldsymbol{q};\imath\omega)\right). \qquad (8.66)$$

Accordingly we only need the polarizability for purely imaginary frequencies, i.e.

$$P_0(\boldsymbol{q};\imath\omega) = \sum_{b_1=\mp}\sum_{b_2=\mp}\frac{1}{(2\pi)^3}\int \mathrm{d}^3k\ \tfrac{1}{2}\left(1+b_1b_2C(\boldsymbol{k};\boldsymbol{k}-\boldsymbol{q})\right)\frac{n_{b_1}(\boldsymbol{k})-n_{b_2}(\boldsymbol{k}-\boldsymbol{q})}{(\epsilon_{b_1}(\boldsymbol{k})-\epsilon_{b_2}(\boldsymbol{k}-\boldsymbol{q}))-\imath\omega}, \qquad (8.67)$$

where we dropped the $\pm\imath\eta$ prescription since the polarizability has no poles on the imaginary axis. It is straight forward to obtain the real and imaginary part of the polarizability along the imaginary ω-axis,

$$\begin{aligned} \mathrm{Re}[P_0(\boldsymbol{k};\imath\omega)] = \sum_{b_1=\mp}\sum_{b_2=\mp}\frac{1}{(2\pi)^3}\int \mathrm{d}^3k\ \tfrac{1}{2}\left(1+b_1b_2C(\boldsymbol{k};\boldsymbol{k}-\boldsymbol{q})\right) \\ \times\frac{\left(n_{b_1}(\boldsymbol{k})-n_{b_2}(\boldsymbol{k}-\boldsymbol{q})\right)\left(\epsilon_{b_1}(\boldsymbol{k})-\epsilon_{b_2}(\boldsymbol{k}-\boldsymbol{q})\right)}{\left(\epsilon_{b_1}(\boldsymbol{k})-\epsilon_{b_2}(\boldsymbol{k}-\boldsymbol{q})\right)^2+\omega^2}, \qquad (8.68) \\ \mathrm{Im}[P_0(\boldsymbol{k};\imath\omega)] = \sum_{b_1=\mp}\sum_{b_2=\mp}\frac{1}{(2\pi)^3}\int \mathrm{d}^3k\ \tfrac{1}{2}\left(1+b_1b_2C(\boldsymbol{k};\boldsymbol{k}-\boldsymbol{q})\right) \\ \times\frac{\left(n_{b_1}(\boldsymbol{k})-n_{b_2}(\boldsymbol{k}-\boldsymbol{q})\right)\omega}{\left(\epsilon_{b_1}(\boldsymbol{k})-\epsilon_{b_2}(\boldsymbol{k}-\boldsymbol{q})\right)^2+\omega^2}. \qquad (8.69) \end{aligned}$$

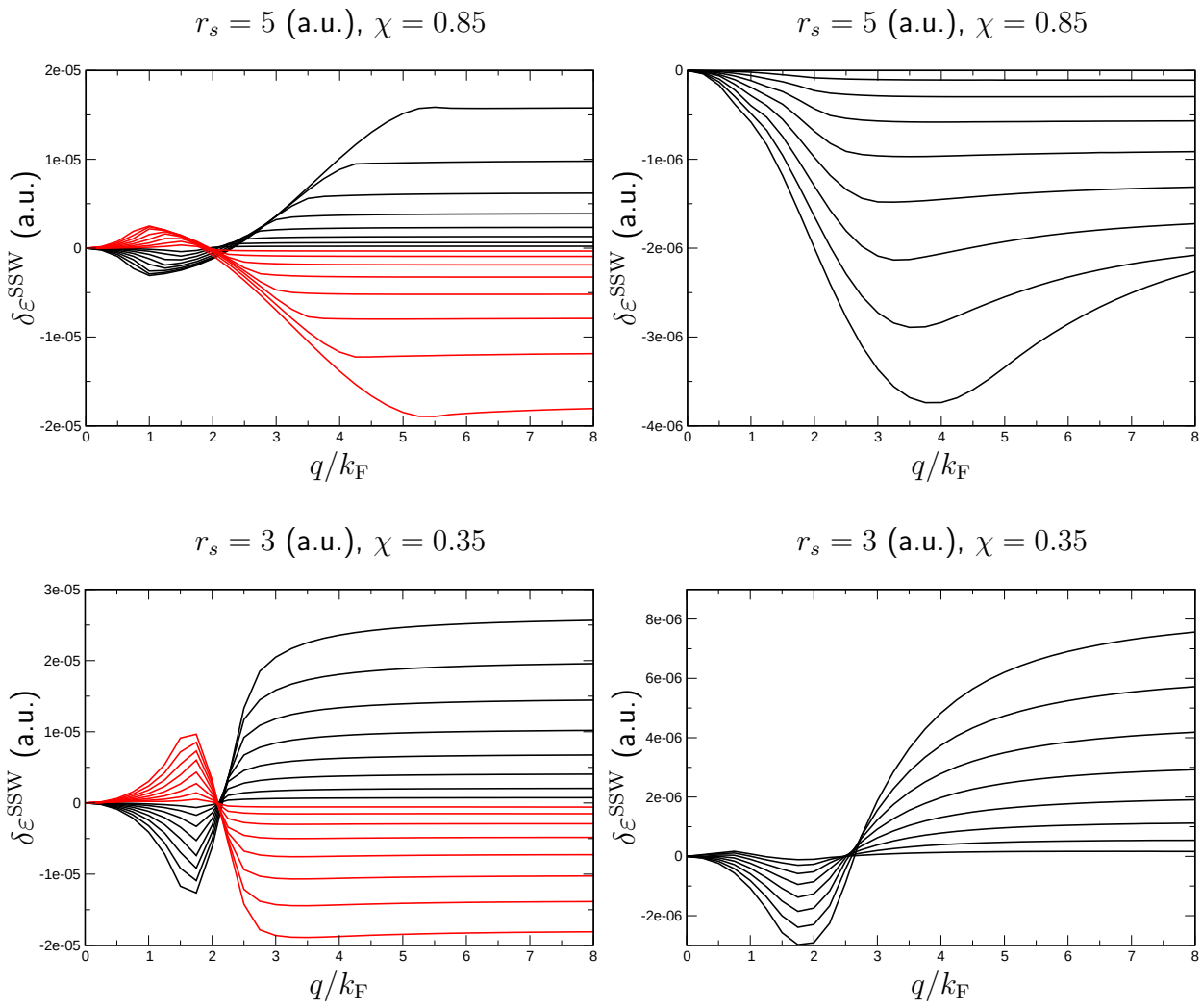

Figure 8.1:
Representative results for the change in energy $\delta\varepsilon^{\mathrm{SSW}} = \varepsilon^{\mathrm{SSW}} - \varepsilon^{\mathrm{unif}}$. $\delta\varepsilon$ is plotted as a function of the spin-spiral wave vector q. The various curves represent results for $s = 0.15, 0.25, 0.35, 0.45, 0.55, 0.65, 0.75, 0.85$, where the overall variation increases with s. In the left panels the changes in exchange energy (black curves) and the changes in correlation energy (red curves) are shown. The right panels show the combined change of the exchange-correlation energy of the uniform electron gas due to the formation of a spin-spiral wave. In agreement with our results from RDMFT (cf. Sec. 6.6) the correlation contribution cancels largely the exchange contribution.

We can see that the real and imaginary part of the polarizability are even and odd functions of ω, respectively. Using these definite parities we can restrict the frequency integration to positive ω,

$$\varepsilon_{c,\mathrm{RPA}} = \int \mathrm{d}^3q \int_0^\infty \mathrm{d}\omega \, \Big(\tfrac{1}{2} \ln\big((1 - W(\boldsymbol{q}) \, \mathrm{Re}[P_0(\boldsymbol{q}; \imath\omega)])^2 + (\mathrm{Im}[P_0(\boldsymbol{q}; \imath\omega)])^2 \big) + W(\boldsymbol{q}) \, \mathrm{Re}[P_0(\boldsymbol{q}; \imath\omega)] \Big). \tag{8.70}$$

The explicit calculation of the non-interacting polarizability for imaginary frequencies is done in App. B, here it shall just be mentioned that it can be reduced to a one-dimensional integration that has to be carried out numerically. The 4 integrals to be computed in order to obtain the correlation energy include a trivial angle integration, but the remaining three-dimensional integral has to be performed numerically. In Figure 8.1 we compare the RPA-correlation energy for the SSW state to the exchange energy for some representative characteristic parameters of the SSW state.

8.5 Parameterization of the Random-Phase Approximation results

Instead of using the RPA xc-energy as an approximation to $\varepsilon_{xc}^{\mathrm{SSW}}(r_s, \chi, s, q)$, we use the results from RPA to approximate the SGE enhancement factor $S_{xc}(r_s, \chi, s, q)$, Eq. (8.45). This has the advantage that for collinear systems the SSW functional reduces to the well-known LSDA, obtained by parameterizing the Quantum Monte Carlo results, e.g. the parameterization by Perdew and Wang [PW92], and not to the RPA-LSDA. For any practical application of the SSW functional it is necessary to have a numerically accessible representation of the SGE enhancement factor, since it is not possible to calculate the xc-energy of the uniform electron gas on-the-fly. S_{xc} is a function of 4 variables and hence it is not straight forward to guess an approximate form. We decided to construct a polynomial representation $\tilde{S}_{xc}$ of the enhancement factor that is optimized using the RPA results described in the previous section. We chose a polynomial representation of the form

$$\tilde{S}_{xc}^n = \sum_{2j+k+l+m \leq 2n} C_{jklm} R_j(r_s) \, X_k(\chi) \, S_l(s) \, Q_m(q/k_{\mathrm{F}}) \, . \tag{8.71}$$

The polynomials R, X, S and Q are defined in terms of the Chebychev polynomials $T_n(x)$, i.e. ,

$$R_j(r_s) = T_j\left(\frac{r_s}{r_s+2}\right), \tag{8.72a}$$

$$X_k(\chi) = \tfrac{1}{2}\left(T_{2k}(\chi) + T_{2k+2}(\chi)\right) = \chi T_{2k+1}(\chi)\,, \tag{8.72b}$$

$$S_l(s) = \tfrac{1}{2}\left(T_{2l}(s) + T_{2l+2}(s)\right) = s T_{2s+1}(s)\,, \tag{8.72c}$$

$$\begin{aligned} Q_m(q) &= \tfrac{1}{2}\left(T_{2m}\left(\frac{q/k_\mathrm{F}}{q/k_\mathrm{F}+2}\right) + T_{2m+2}\left(\frac{q/k_\mathrm{F}}{q/k_\mathrm{F}+2}\right)\right) \\ &= \left(\frac{q/k_\mathrm{F}}{q/k_\mathrm{F}+2}\right) T_{2m+1}\left(\frac{q/k_\mathrm{F}}{q/k_\mathrm{F}+2}\right). \end{aligned} \tag{8.72d}$$

With this choice the polynomial representation of S_{xc} fulfills by construction the important limit $S_{xc} \to 0$ for either $\chi \to 0$, $s \to 0$ or $q \to 0$. The parameter n of $\tilde{S}^n_{xc}$ determines the maximal degree (which is roughly $2n$) of the the polynomials. Note that $\tilde{S}_{xc}$ is a rational function in r_s and q since we mapped the intervals $r_s \in [0,\infty]$ and $q/k_\mathrm{F} \in [0,\infty]$ onto the unit interval via $\frac{r_s}{r_s+2}$ and $\frac{q/k_\mathrm{F}}{q/k_\mathrm{F}+2}$, respectively. In order to determine the optimal C_{jklm} we compute the RPA xc-energy on an equidistant mesh in the 4-dimensional parameter space, i.e. ,

$$\begin{aligned} (r_s, \chi, s, q/k_\mathrm{F}) \in &[1,2,\ldots,10] \times [0.05, 0.15, \ldots, 0.95] \\ &\times [0.05, 0.15, \ldots, 0.95] \times [0, 0.25, \ldots, 16.0]\,, \end{aligned} \tag{8.73}$$

which yields 65000 data points for the least-square fitting of the coefficients. The results of the fit for various n are summarized in table 8.1. We can see that by increasing the degree of

n	3	4	5	6	7
Number of coefficients	35	70	126	210	330
RMS deviation ($\times 10^{-2}$)	2.7	2.5	2.2	2.1	2.0

Table 8.1: Table summarizing the least-square fit of $S_{xc,\mathrm{RPA}}$.

the fitting polynomial we reduce the root-mean-square deviation. For 330 coefficients some of the coefficients are considerably larger than the average fitting coefficient, which gives a hint that we are starting to over-fit the reference data. This is not surprising since we are using polynomials for our fit and hence increasing the degree of the polynomial induces uncontrolled oscillations at some point (Runge's phenomenon). We find that $\tilde{S}^{n=6}_{xc}$ is a reasonable choice for the polynomial representation of $S_{xc,\mathrm{RPA}}$ and in Fig. 8.2 we compare this polynomial representation to the RPA results for some representative characteristic SSW parameters. The coefficients for $\tilde{S}^{n=6}_{xc}$ are tabulated in appendix C.

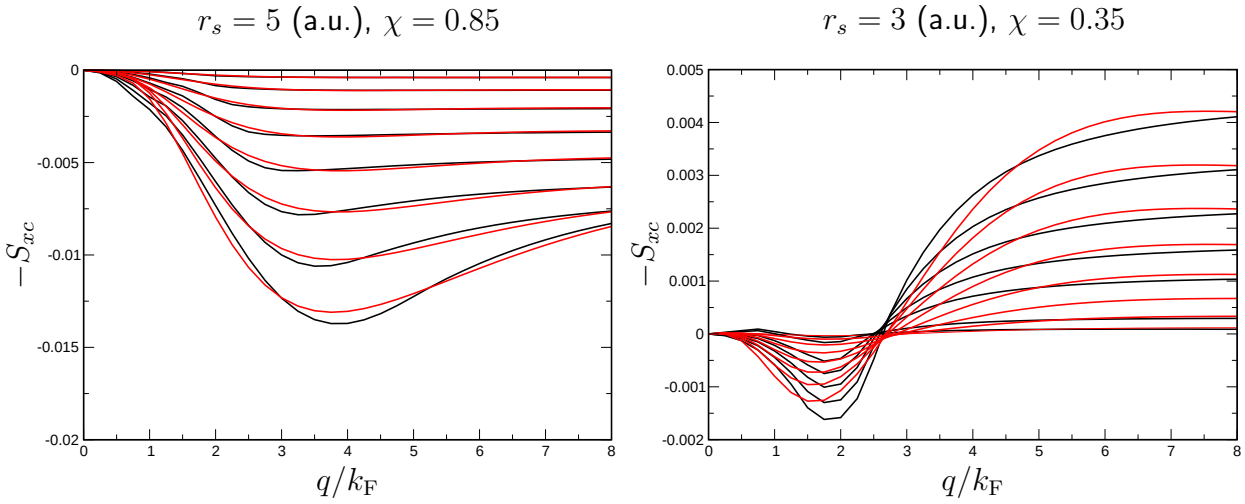

Figure 8.2: Representative results for the SGE enhancement S_{xc}. Here we plot $-S_{xc}$ as a function of the spin-spiral wave vector q, because then the curves may directly be compared to the energy differences shown in Fig. 8.1 ($\varepsilon_{xc}^{\mathrm{unif}}(r_s, \chi)$ is strictly negative, hence minima/maxima are interchange in S_{xc} compared to $\delta\varepsilon$). The various curves represent results for $s = 0.15, 0.25, 0.35, 0.45, 0.55, 0.65, 0.75, 0.85$, where, again (cf. Fig. 8.1), the overall variation increases with s. The results from the RPA calculation are shown in black and the results from the polynomial representation $\tilde{S}_{xc}^{n=6}$ are shown in red. We see that $\tilde{S}_{xc}^{n=6}$ is a qualitatively correct representation of $S_{xc,\mathrm{RPA}}$.

8.6 First results and discussion

In order to investigate the effects of the inclusion of transversal gradients of the spin magnetization we implemented the polynomial representation, constructed in the previous section, in the ELK code [ELK]. The ELK code is an all-electron full-potential linearized augmented-plane-wave (FP-LAPW) code, which allows a fully non-collinear treatment of periodic systems. Accordingly it allows for an investigation of intra-atomic, as well as inter-atomic non-collinear magnetism and therefore is perfectly suited for the application of the SSW functional. The interested reader may find an excellent overview and reference on the FP-LAPW method in the book by Singh and Nordström [SN05]. For the implementation of the xc-magnetic field there are two distinct strategies. The first is to compute the spatially dependent $\boldsymbol{B}_{xc}(\boldsymbol{r})$ from Eqs. (8.50), (8.53), (8.57), which involves 4th-order gradients of the spin magnetization and second order gradients of $n(\boldsymbol{r})\,\varepsilon(\boldsymbol{r})$, that have to be obtained numerically. This implementation will be referred to as the local implementation. The second strategy uses that the eigenstates, i.e. , the Kohn-Sham orbitals $\left\{\Phi_j^s\right\}$, of the effective Kohn-Sham Hamiltonian $\hat{\mathcal{H}}_s$,

including the xc-magnetic field, are obtained by diagonalizing a matrix-representation of $\hat{\mathcal{H}}_s$ on a Pauli spinor basis $\left\{\Phi_j(\boldsymbol{r})\right\}$. Since the determination of the matrix-representation of $\hat{\mathcal{H}}_s$ only requires the matrix elements of $\boldsymbol{B}_{xc}(\boldsymbol{r})$, i.e. ,

$$\begin{aligned}(\mathcal{B}_{xc})_{jk} &= \mu_{\mathrm{B}} \int \mathrm{d}^3 r \; \Phi_j^\dagger(\boldsymbol{r})\, \boldsymbol{B}_{xc}(\boldsymbol{r}) \cdot \boldsymbol{\sigma} \Phi_k(\boldsymbol{r}) \\ &= (\mathcal{B}_m)_{jk} + (\mathcal{B}_D)_{jk} + (\mathcal{B}_d)_{jk}\,, \end{aligned} \tag{8.74}$$

one can directly use Eqs. (8.51) and (8.55) in connection with $\partial'\delta(\boldsymbol{r}-\boldsymbol{r}') = -\partial\delta(\boldsymbol{r}-\boldsymbol{r}')$ and $\partial'\partial'\delta(\boldsymbol{r}-\boldsymbol{r}') = \partial\partial\delta(\boldsymbol{r}-\boldsymbol{r}')$, respectively, in order to obtain the matrix elements Eq. (8.74) in terms of second-order gradients, i.e. ,

$$(\mathcal{B}_m)_{jk} = \int \mathrm{d}^3 r \; \frac{n(\boldsymbol{r})\, \varepsilon_m(\boldsymbol{r})}{m(\boldsymbol{r})} \boldsymbol{m}_{jk}(\boldsymbol{r}) \cdot \boldsymbol{m}(\boldsymbol{r})\,, \tag{8.75}$$

for the contribution stemming from the dependence on the magnitude of the spin magnetization,

$$\begin{aligned}(\mathcal{B}_D)_{jk} = 2 \int \mathrm{d}^3 r \; n(\boldsymbol{r})\, \varepsilon_D(\boldsymbol{r}) \Big(& (\boldsymbol{m}_{jk}(\boldsymbol{r}) \times (\nabla \otimes \boldsymbol{m}(\boldsymbol{r}))) \cdot (\boldsymbol{m}(\boldsymbol{r}) \times (\nabla \otimes \boldsymbol{m}(\boldsymbol{r}))) \\ & + (\boldsymbol{m}(\boldsymbol{r}) \times (\nabla \otimes \boldsymbol{m}_{jk}(\boldsymbol{r}))) \cdot (\boldsymbol{m}(\boldsymbol{r}) \times (\nabla \otimes \boldsymbol{m}(\boldsymbol{r}))) \Big), \end{aligned} \tag{8.76}$$

for the contribution due to the dependence on the transversal first-order gradient, and finally

$$\begin{aligned}(\mathcal{B}_d)_{jk} = 2 \int \mathrm{d}^3 r \; n(\boldsymbol{r})\, \varepsilon_d(\boldsymbol{r}) \Big(& (\boldsymbol{m}_{jk}(\boldsymbol{r}) \times (\Delta \boldsymbol{m}(\boldsymbol{r}))) \cdot (\boldsymbol{m}(\boldsymbol{r}) \times (\Delta \boldsymbol{m}(\boldsymbol{r}))) \\ & + (\boldsymbol{m}(\boldsymbol{r}) \times (\Delta \boldsymbol{m}_{jk}(\boldsymbol{r}))) \cdot (\boldsymbol{m}(\boldsymbol{r}) \times (\Delta \boldsymbol{m}(\boldsymbol{r}))) \Big), \end{aligned} \tag{8.77}$$

for the contribution of the xc-magnetic field implied by the dependence on the second-order transversal gradient. One realizes that now second-order gradients for all spin-magnetization matrix elements

$$\boldsymbol{m}_{jk}(\boldsymbol{r}) = \Phi_j^\dagger(\boldsymbol{r})\, \boldsymbol{\sigma} \Phi_k(\boldsymbol{r})\,, \tag{8.78}$$

have to be computed. For electronic-structure codes using a fixed basis set, these gradients could be computed once, at the beginning of the self-consistent Kohn-Sham cycle. In the LAPW method, however, an optimized basis is determined in each self-consistent loop, which requires a re-calculation of the gradients of the spin-magnetization matrix elements in each iteration. This increases considerably the numerical effort of the second implementation strategy compared to the local implementation, which requires the computation of 4th-order gradients, but only of the total spin magnetization $\boldsymbol{m}(\boldsymbol{r})$.

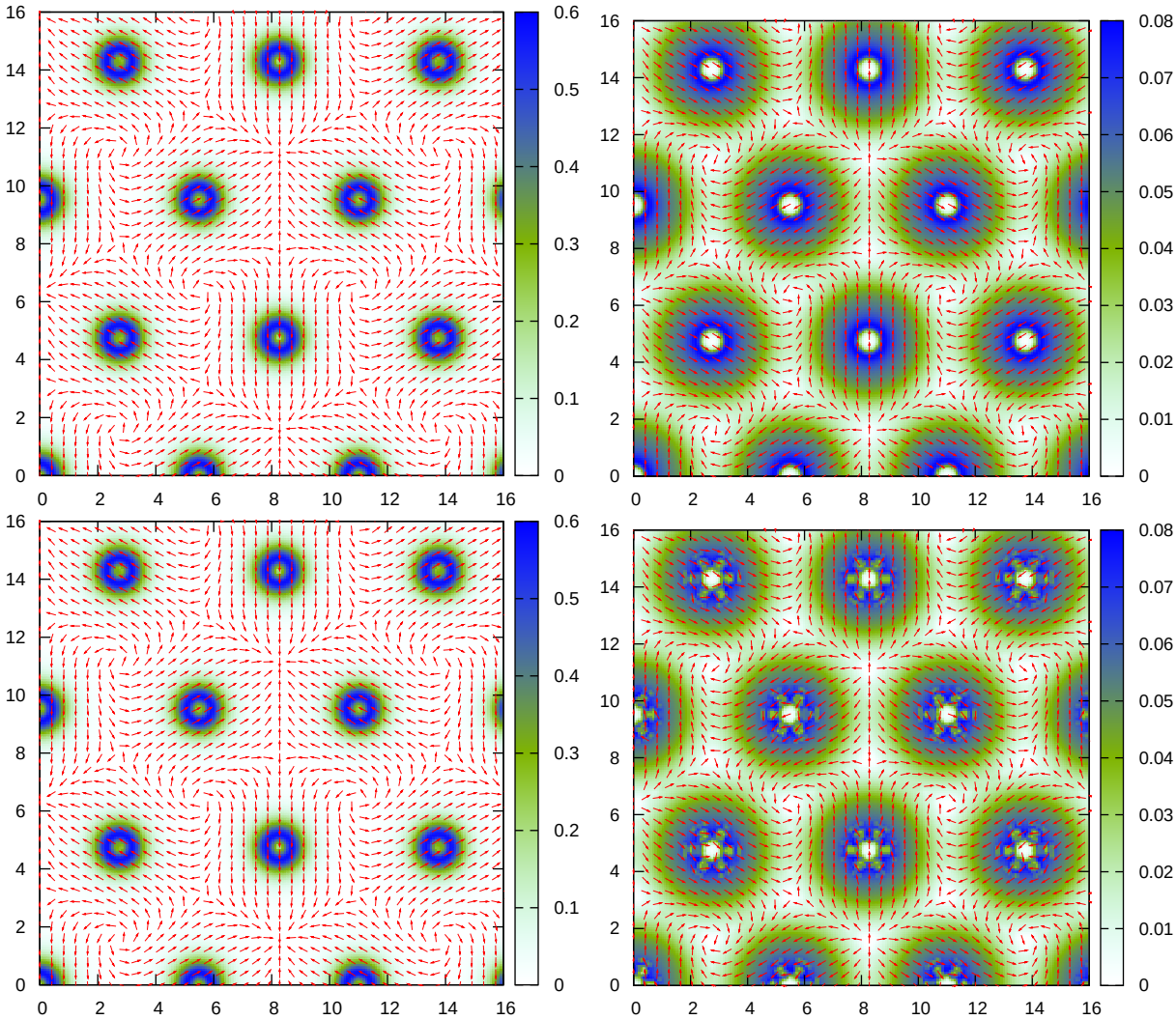

Figure 8.3:

The left panels show the spin magnetization of the Chromium mono-layer. The direction of the spin magnetization is indicated by the red arrows and the magnitude is shown by the color map. The upper left panel depicts the result from the LSDA calculation and the lower left panel from the local implementation of the SSW functional.

The right panels show the exchange-correlation-magnetic field of the Chromium mono-layer. Again, the direction of of $\boldsymbol{B}_{xc}$ is indicated by the red arrows and the magnitude is shown by the color map. Result from the LSDA calculation are given in the upper right panel and the result for the SSW functional in the lower right panel.

While the spin magnetization remains virtually unchanged, the xc-magnetic field employing the spin-gradient extension to the LSDA exhibits more structure. The xc-magnetic field of the LSDA is by construction proportional to the spin magnetization which is essentially spherically symmetric, the xc-magnetic field of the SSW functional shows the 3-fold symmetry of the hexagonal Chromium mono-layer (cf. Fig. 8.4).

As a first testing scenario we choose to investigate an unsupported Chromium mono-layer with the lattice constant ($a = 7.79$ a.u.) and geometry of a Ag(111) surface. We would like to emphasize that the presented results are not a systematic investigation of its magnetic ground state since we are not investigating different magnetic structures. Instead we are focusing on the 120° Néel state which is known to be a solution of the classical Heisenberg model for antiferromagnets with nearest-neighbor interactions. The main aim of this proof of principle calculation is to compare the LSDA functional which, by construction, yields xc-magnetic fields that are collinear w.r.t. the spin magnetization, to the SSW functional proposed in this work. All calculations were performed using a $23\times23\times1$ k-point grid with a plane-wave cutoff of $|\boldsymbol{G}+\boldsymbol{k}| \leq 2.5$ a.u. and touching muffin-tin radii of 2.73 a.u. . The symmetry is broken by applying a small magnetic field inside the muffin-tin spheres in order to induce the 120° Néel state. During the self-consistent iteration the external magnetic field is switched off successively. In Fig. 8.3 we compare the result from the LSDA calculation in the Perdew-Wang parameterization [PW92] and the SSW functional, i.e. the aforementioned LSDA including the polynomial representation $\tilde{S}_{xc}^{n=6}$ of the SGE, defined in Sec. 8.5. The spin magnetization for both functionals yield similar results and we find atomic moments of $3.9732\mu_\mathrm{B}$ for the LSDA and $3.9724\mu_\mathrm{B}$ for the SSW functional. The xc-magnetic field from the SSW functional exhibits more structure and reflects the 3-fold rotation symmetry of the 120° Néel state.

The main difference of the SSW functional compared to the LSDA is the non-collinearity of the xc-magnetic field w.r.t. the spin magnetization, which is shown in Fig. 8.4. Introducing the spin-current-density operator

$$\hat{\underline{\boldsymbol{J}}}(\boldsymbol{r}) = -\tfrac{\imath}{2}\left(\hat{\Phi}^\dagger(\boldsymbol{r})\,\boldsymbol{\sigma}\otimes\left(\nabla\hat{\Phi}(\boldsymbol{r})\right) - \left(\nabla\hat{\Phi}^\dagger(\boldsymbol{r})\right)\otimes\boldsymbol{\sigma}\hat{\Phi}(\boldsymbol{r})\right), \tag{8.79}$$

we can write the Kohn-Sham equation of motion for the spin magnetization, i.e.,

$$\partial_t \boldsymbol{m}(\boldsymbol{r}) + \nabla\cdot\underline{\boldsymbol{J}}_s(\boldsymbol{r}) = -2\mu_\mathrm{B}\boldsymbol{m}(\boldsymbol{r})\times\boldsymbol{B}_s(\boldsymbol{r})\,. \tag{8.80}$$

For static SDFT with a vanishing external magnetic field this implies

$$\nabla\cdot\underline{\boldsymbol{J}}_s(\boldsymbol{r}) = 2\mu_\mathrm{B}\boldsymbol{m}(\boldsymbol{r})\times\boldsymbol{B}_{xc}(\boldsymbol{r})\,, \tag{8.81}$$

i.e. the local torque due the exchange-correlation magnetic field is identical to the divergence of the Kohn-Sham spin-current density for vanishing external fields. For the example of the chromium mono-layer in the 120° Néel state we therefore see that the transversal component of the Kohn-Sham ground-state spin-current does not vanish (cf. Fig. 8.4).

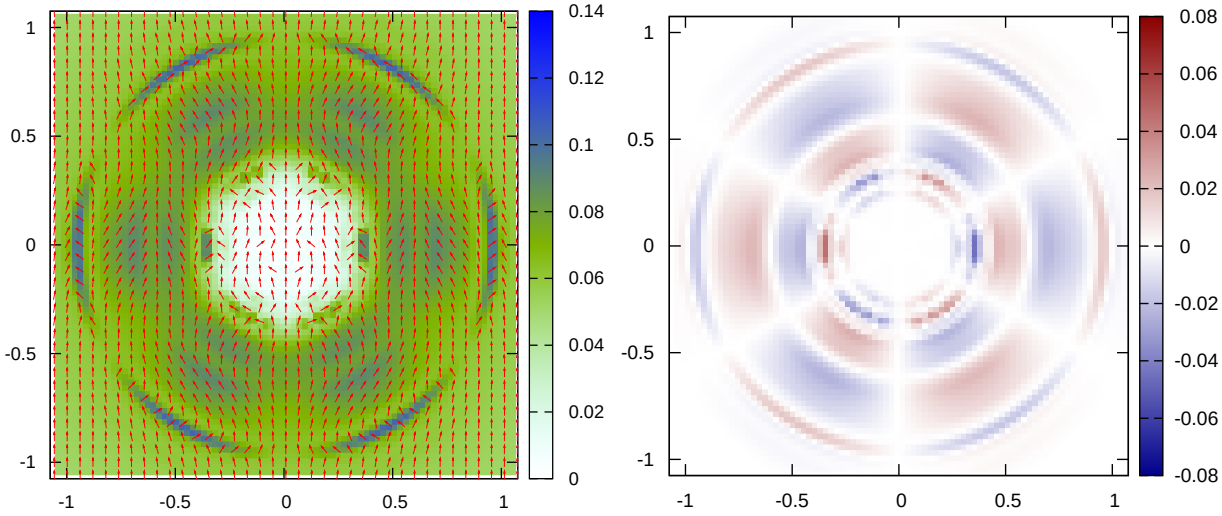

Figure 8.4:
Right panel: Zoom on a single Chromium atom. The xc-magnetic field, calculated using the SSW functional in the local implementation (cf. lower right panel of Fig. 8.3). Here, in contrast to Fig. 8.3, the full range of the magnitude of $\boldsymbol{B}_{xc}$ is shown.
Left panel: The z-component of the local torque $\boldsymbol{m} \times \boldsymbol{B}_{xc}$. Since the spin magnetization and the xc-magnetic field vary in the x-y plane, the other components of the local torque vanish. A non-vanishing local torque indicates that the SSW functional accounts for the difference between the Kohn-Sham spin-current density $\underline{\boldsymbol{J}}_s(\boldsymbol{r})$ and the physical spin-current $\underline{\boldsymbol{J}}(\boldsymbol{r})$.

Considering the time-dependent version of Density-Functional Theory, introduced first by Runge and Gross in 1984 [RG84], we compare the equation of motion for the spin magnetization in the physical system

$$\partial_t \boldsymbol{m}(\boldsymbol{r},t) + \nabla \cdot \underline{\boldsymbol{J}}(\boldsymbol{r},t) = -2\mu_{\mathrm{B}} \boldsymbol{m}(\boldsymbol{r},t) \times \boldsymbol{B}(\boldsymbol{r},t)\,. \tag{8.82}$$

to the equation of motion for the Kohn-Sham system (cf. (8.80)). TD-SDFT reproduces the physical time-dependent spin magnetization but not the spin-current density and hence we can introduce the so-called exchange-correlation spin-current density

$$\underline{\boldsymbol{J}}_{xc}(\boldsymbol{r},t) = \underline{\boldsymbol{J}}(\boldsymbol{r},t) - \underline{\boldsymbol{J}}_s(\boldsymbol{r},t)\,. \tag{8.83}$$

Subtracting Eq. (8.82) from Eq. (8.80) we see that the longitudinal part of the xc-spin-current density is equal to the local torque due to the time-dependent $\boldsymbol{B}_{xc}$ [CVG01]. Hence an adiabatic application of the proposed SSW functional is able to take the difference of Kohn-Sham and physical spin-current density into account. In fact it can easily be verified that the

local torque due to the SSW functional can be written as

$$
\begin{aligned}
2\mu_{\mathrm{B}}\boldsymbol{m}(\boldsymbol{r})\times\boldsymbol{B}_{xc}^{\mathrm{SSW}}(\boldsymbol{r}) = 2\nabla\cdot\Big(&-2n(\boldsymbol{r})\,\varepsilon_D(\boldsymbol{r})\,\boldsymbol{m}(\boldsymbol{r})\times(\nabla\otimes\boldsymbol{m}(\boldsymbol{r}))\,m^2(\boldsymbol{r}) \\
&-4n(\boldsymbol{r})\,\varepsilon_d(\boldsymbol{r})\,(\nabla\otimes\boldsymbol{m}(\boldsymbol{r}))\times(\Delta\boldsymbol{m}(\boldsymbol{r}))\,m^2(\boldsymbol{r}) \\
&-4n(\boldsymbol{r})\,\varepsilon_d(\boldsymbol{r})\,\boldsymbol{m}(\boldsymbol{r})\times(\nabla\otimes\boldsymbol{m}(\boldsymbol{r}))\,m(\boldsymbol{r})\cdot(\Delta\boldsymbol{m}(\boldsymbol{r})) \\
&+\nabla\otimes\big(2n(\boldsymbol{r})\,\varepsilon_d(\boldsymbol{r})\,\boldsymbol{m}(\boldsymbol{r})\times(\Delta\boldsymbol{m}(\boldsymbol{r}))\,m^2(\boldsymbol{r})\big)\Big) \qquad (8.84)\\
= \nabla\cdot\underline{\boldsymbol{J}}_{xc}(\boldsymbol{r})\,. \qquad (8.85)
\end{aligned}
$$

This suggests the notion that the part of $\boldsymbol{B}_{xc}^{\mathrm{SSW}}$ that is perpendicular to the spin magnetization actually implies an explicit functional for the longitudinal part of the exchange-correlation spin-current density, whereas the parallel part determines the energetics of the Kohn-Sham system.

In conclusion we believe that the SSW functional not only advances the equilibrium description of non-collinear systems, but also the ab-initio description of non-collinear spin dynamics. An interesting question will be if the exchange-correlation spin-current functional proves to be useful when spin-orbit coupling is included.

Outlook

The main motif of the presented thesis was the spin-spiral-wave state. We investigated its properties starting with a quantitative analysis of Overhauser's instability theorem. The main outcome of this work is an incorporation of the spin-spiral-wave state into Spin-Density-Functional Theory. To this end we showed that the idea of a local-density approximation can be generalized to use the spin-spiral-wave state of the uniform electron gas as reference system. The aim was to make the density-functional treatment of real materials sensitive to directional changes of the spin-magnetic moment.

Recently non-collinear magnetic structures in the form of skyrmions have attracted attention due to their experimental observation [MBJ+09]. The Spin-Gradient Extension to the Local-Spin-Density Approximation may proves useful in the theoretical confirmation and prediction of these structures. Whether a quantitative agreement with experiments can be achieved remains to be seen. Employing large super cells, necessary to allow for the description of magnetic structures that involve multiple unit cells, seems feasible since the proposed functional retains the numerical simplicity of a local approximation. As a side remark we mention that the generalized Bloch theorem for spin-spiral structures, which are related but not identical to the spin-spiral state described in this thesis, allows to simulate a spin magnetization with a periodicity incommensurate with the chemical unit cell using only the chemical unit cell with modified boundary conditions for the spin-up and spin-down components of the orbitals. A notorious example to study would be the γ-phase of iron which was found to exhibit a spin spiral structure some time ago [Tsu89, TNN93].

The field of spintronics is believed to provide the next step in the everlasting aim of miniaturization of electronic devices. The development of new spintronic devices requires a microscopic understanding of how electron transport properties are affected by the spin degree of freedom. Therefore it would be desirable to expand the present work to include time dependence. A first possibility is to directly use the functional adiabatically in the framework time-dependent spin-density-functional theory. In the linear response regime this would require the evaluation of the exchange-correlation kernel, which is the functional derivative of the exchange-correlation potential and magnetic field of the spin-spiral-wave functional. An interesting question is

to what extend the charge and spin linear response are coupled. Furthermore within time-dependent Spin-Density-Functional Theory the non-linear regime is accessible using real time propagation of the Kohn-Sham equations. Leaving the adiabatic domain a challenge would be to investigate whether a frequency dependent exchange-correlation kernel can be derived using a spin-spiral-wave state that rotates also in time.

Appendix A

Exchange integrals for cylindrical volume elements

In this appendix we present the computation of the exchange-integral weights, defined in Chap. 6, Sec. 6.4, Eq. (6.34c). The integral to compute reads

$$\begin{aligned}\mathrm{DXI}_{ij} = \frac{1}{2n}\frac{1}{(2\pi)^3}\iiint_{\Omega_i}\mathrm{d}k_{\rho 1}\mathrm{d}k_{z1}\mathrm{d}\phi_1\ \frac{1}{(2\pi)^3}\iiint_{\Omega_j}\mathrm{d}k_{\rho 2}\mathrm{d}k_{z2}\mathrm{d}\phi_2 \\ \times\frac{4\pi k_{\rho 1}k_{\rho 2}}{k_{\rho 1}^2+k_{\rho 2}^2+\left(k_{z1}-k_{z2}\right)^2-2k_{\rho 1}k_{\rho 2}\cos(\phi_1-\phi_2)}\end{aligned} \tag{A.1}$$

After shifting $\phi_1 \to \phi_1+\phi_2$, which is possible without changing the limits in ϕ_1 because of the periodicity of the cosine, we have an integral of the type

$$\int_0^{2\pi}\mathrm{d}\phi\ \frac{1}{1+a\cos(\phi)} = \frac{2\pi}{\sqrt{1-a^2}}\ ,\ a^2<1\ , \tag{A.2}$$

where

$$a = \frac{-2k_{\rho 1}k_{\rho 2}}{k_{\rho 1}^2+k_{\rho 2}^2+\left(k_{z1}-k_{z2}\right)^2}. \tag{A.3}$$

From the second angular integration we get trivially a factor of 2π. Renaming the integration variables $k_i = k_{\rho i}$ and $z_i = k_{zi}$ we have,

$$\mathrm{DXI}_{ij} = \frac{1}{(2\pi)^3 n}\iint_{\Omega_i}\mathrm{d}k_1\mathrm{d}z_1\ \iint_{\Omega_j}\mathrm{d}k_2\mathrm{d}z_2\ \frac{k_1k_2}{\sqrt{\left(k_1^2-k_2^2\right)^2+\left(z_1-z_2\right)^4+2\left(k_1^2+k_2^2\right)\left(z_1-z_2\right)^2}}. \tag{A.4}$$

After introducing

$$\begin{aligned}\epsilon_1 = \frac{k_1^2}{2}\ ,\ a_1 = \frac{\left(k_\rho^i\right)^2}{2}\ ,\ b_1 = \frac{\left(k_\rho^i+\delta_\rho^i\right)^2}{2}\ ,\ c_1 = k_z^i\ ,\ d_1 = k_z^i+\delta_z^i, \\ \epsilon_2 = \frac{k_2^2}{2}\ ,\ a_2 = \frac{\left(k_\rho^j\right)^2}{2}\ ,\ b_2 = \frac{\left(k_\rho^j+\delta_\rho^j\right)^2}{2}\ ,\ c_2 = k_z^j\ ,\ d_2 = k_z^j+\delta_z^j,\end{aligned} \tag{A.5}$$

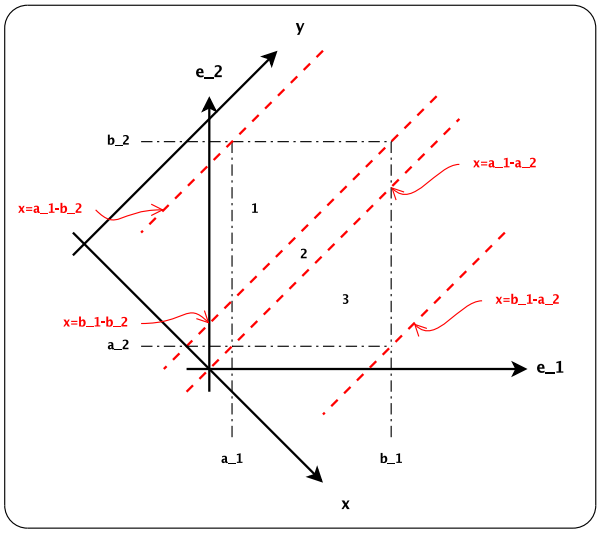

Figure A.1: case A: $(b_1 - a_1) < (b_2 - a_2)$

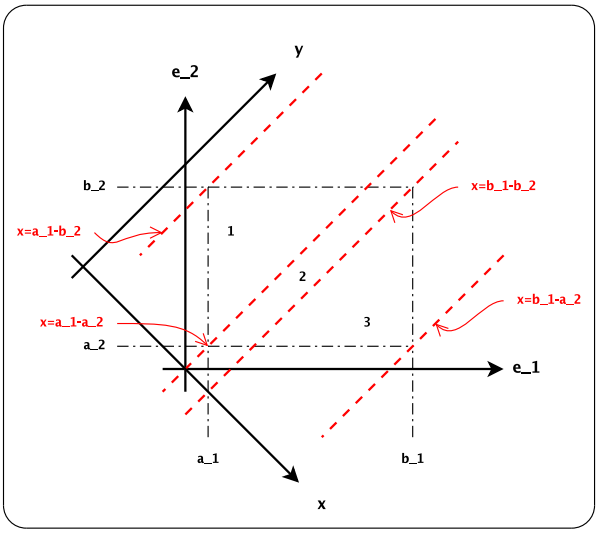

Figure A.2: case B: $(b_1 - a_1) > (b_2 - a_2)$

the integral reads

$$\mathrm{DXI}_{ij} = \frac{1}{(2\pi)^3 2n} \int_{a_1}^{b_1} \mathrm{d}\epsilon_1 \int_{c_1}^{d_1} \mathrm{d}z_1 \int_{a_2}^{b_2} \mathrm{d}\epsilon_2 \int_{c_2}^{d_2} \mathrm{d}z_2 \times \frac{1}{\sqrt{(\epsilon_1 - \epsilon_2)^2 + \frac{1}{4}(z_1 - z_2)^4 + (\epsilon_1 + \epsilon_2)(z_1 - z_2)^2}}. \tag{A.6}$$

Obviously the remaining integrand depends only on the three coordinates $(\epsilon_1 - \epsilon_2)$, $(\epsilon_1 + \epsilon_2)$ and $(z_1 - z_2)$, wich suggests the following transformation of variables:

$$x = \epsilon_1 - \epsilon_2 \ , \ y = \epsilon_1 + \epsilon_2 \ , \ s = z_1 - z_2 \ , \ t = z_1 + z_2, \tag{A.7}$$

which leads to the following expression for the integral in terms of the new integration variables,

$$\mathrm{DXI}_{ij} = \frac{1}{(2\pi)^3 8n} \int \mathrm{d}s \int \mathrm{d}t \underbrace{\int \mathrm{d}x \int \mathrm{d}y \frac{1}{\sqrt{x^2 + \frac{1}{4}s^4 + ys^2}}}_{=I(s)} \tag{A.8}$$

where we omitted the limits of integration, because they are not changing in a simple way. In fact they depend on the order in which the integrals are carried out. In Eq. (A.8) we already indicate in which order we would like to compute the integrals, this means that now we have to find the correct implementation of the limits.

In order to find the correct limits of integration after the variable transformation in Eq. (A.8) we have to distinguish the two cases that are depicted in Fig. A.1 and Fig. A.2, respectively. We can see that we have to split the integral over x for both cases in three regions. The lower and the upper limit for y depend on the boundaries of the rectangle, which are given by

different equations in each region. In case A the resulting integral is given by

$$I^A(s) = \int_{a_1-b_2}^{b_1-b_2} \mathrm{d}x \underbrace{\int_{2a_1-x}^{2b_2+x} \mathrm{d}y \ (\cdots)}_{=F_1^A(x,s)} + \int_{b_1-b_2}^{a_1-a_2} \mathrm{d}x \underbrace{\int_{2a_1-x}^{2b_1-x} \mathrm{d}y \ (\cdots)}_{=F_2^A(x,s)} + \int_{a_1-a_2}^{b_1-a_2} \mathrm{d}x \underbrace{\int_{2a_2+x}^{2b_1-x} \mathrm{d}y \ (\cdots)}_{=F_3^A(x,s)}, \tag{A.9}$$

and in case B by

$$I^B(s) = \int_{a_1-b_2}^{a_1-a_2} \mathrm{d}x \underbrace{\int_{2a_1-x}^{2b_2+x} \mathrm{d}y \ (\cdots)}_{=F_1^B(x,s)} + \int_{a_1-a_2}^{b_1-b_2} \mathrm{d}x \underbrace{\int_{2a_2+x}^{2b_2+x} \mathrm{d}y \ (\cdots)}_{=F_2^B(x,s)} + \int_{b_1-b_2}^{b_1-a_2} \mathrm{d}x \underbrace{\int_{2a_2+x}^{2b_1-x} \mathrm{d}y \ (\cdots)}_{=F_3^B(x,s)}. \tag{A.10}$$

It is an easy matter to compute the partial contributions

$$F_1^A(x,s) = \frac{2}{s^2}\left(\sqrt{\left(x+\tfrac{1}{2}s^2\right)^2 + 2b_2s^2} - \sqrt{\left(x-\tfrac{1}{2}s^2\right)^2 + 2a_1s^2}\right), \tag{A.11a}$$

$$F_2^A(x,s) = \frac{2}{s^2}\left(\sqrt{\left(x-\tfrac{1}{2}s^2\right)^2 + 2b_1s^2} - \sqrt{\left(x-\tfrac{1}{2}s^2\right)^2 + 2a_1s^2}\right), \tag{A.11b}$$

$$F_3^A(x,s) = \frac{2}{s^2}\left(\sqrt{\left(x-\tfrac{1}{2}s^2\right)^2 + 2b_1s^2} - \sqrt{\left(x+\tfrac{1}{2}s^2\right)^2 + 2a_2s^2}\right), \tag{A.11c}$$

$$F_1^B(x,s) = \frac{2}{s^2}\left(\sqrt{\left(x+\tfrac{1}{2}s^2\right)^2 + 2b_2s^2} - \sqrt{\left(x-\tfrac{1}{2}s^2\right)^2 + 2a_1s^2}\right), \tag{A.11d}$$

$$F_2^B(x,s) = \frac{2}{s^2}\left(\sqrt{\left(x+\tfrac{1}{2}s^2\right)^2 + 2b_2s^2} - \sqrt{\left(x+\tfrac{1}{2}s^2\right)^2 + 2a_2s^2}\right), \tag{A.11e}$$

$$F_3^B(x,s) = \frac{2}{s^2}\left(\sqrt{\left(x-\tfrac{1}{2}s^2\right)^2 + 2b_1s^2} - \sqrt{\left(x+\tfrac{1}{2}s^2\right)^2 + 2a_2s^2}\right). \tag{A.11f}$$

We realize that, by recombining the integrals over x with the same integrand, the two cases, A and B, give exactly the same contribution. Since we have four different integrands we can rewrite

$$I(s) = G_1(s) - G_2(s) + G_3(s) - G_4(s), \tag{A.12}$$

by introducing

$$G_1(s) = \frac{2}{s^2}\int_{a_1-b_2+\frac{1}{2}s^2}^{b_1-b_2+\frac{1}{2}s^2} dx\sqrt{x^2+\alpha_1}\ ,\ \alpha_1 = 2b_2s^2\ , \tag{A.13}$$

$$G_2(s) = \frac{2}{s^2}\int_{a_1-b_2-\frac{1}{2}s^2}^{a_1-a_2-\frac{1}{2}s^2} dx\sqrt{x^2+\alpha_2}\ ,\ \alpha_2 = 2a_1s^2\ , \tag{A.14}$$

$$G_3(s) = \frac{2}{s^2}\int_{b_1-b_2-\frac{1}{2}s^2}^{b_1-a_2-\frac{1}{2}s^2} dx\sqrt{x^2+\alpha_3}\ ,\ \alpha_3 = 2b_1s^2\ , \tag{A.15}$$

$$G_4(s) = \frac{2}{s^2}\int_{a_1-a_2+\frac{1}{2}s^2}^{b_1-a_2+\frac{1}{2}s^2} dx\sqrt{x^2+\alpha_4}\ ,\ \alpha_4 = 2a_2s^2\ , \tag{A.16}$$

where we shifted the integration variable $x \to x \pm \frac{1}{2}s^2$ and defined the α_i in order to emphasize the similarity of the four integrals. Using

$$\int \mathrm{d}x\, \sqrt{x^2+\alpha} = \frac{\alpha}{2}\ln\left(x+\sqrt{x^2+\alpha}\right) + \frac{x}{2}\sqrt{x^2+\alpha}, \tag{A.17}$$

we get after some elementary calculations

$$\begin{aligned}
I(s) &= 2b_2 \ln\left(b_1 - b_2 + \tfrac{1}{2}s^2 + \sqrt{(b_1-b_2)^2 + (b_1+b_2)\,s^2 + \tfrac{1}{4}s^4}\right) \\
&\quad - 2b_1 \ln\left(b_1 - b_2 - \tfrac{1}{2}s^2 + \sqrt{(b_1-b_2)^2 + (b_1+b_2)\,s^2 + \tfrac{1}{4}s^4}\right) \\
&\quad + \sqrt{(b_1-b_2)^2 + (b_1+b_2)\,s^2 + \tfrac{1}{4}s^4} \\
&\quad - 2b_2 \ln\left(a_1 - b_2 + \tfrac{1}{2}s^2 + \sqrt{(a_1-b_2)^2 + (a_1+b_2)\,s^2 + \tfrac{1}{4}s^4}\right) \\
&\quad + 2a_1 \ln\left(a_1 - b_2 - \tfrac{1}{2}s^2 + \sqrt{(a_1-b_2)^2 + (a_1+b_2)\,s^2 + \tfrac{1}{4}s^4}\right) \\
&\quad - \sqrt{(a_1-b_2)^2 + (a_1+b_2)\,s^2 + \tfrac{1}{4}s^4} \\
&\quad - 2a_2 \ln\left(b_1 - a_2 + \tfrac{1}{2}s^2 + \sqrt{(b_1-a_2)^2 + (b_1+a_2)\,s^2 + \tfrac{1}{4}s^4}\right) \\
&\quad + 2b_1 \ln\left(b_1 - a_2 - \tfrac{1}{2}s^2 + \sqrt{(b_1-a_2)^2 + (b_1+a_2)\,s^2 + \tfrac{1}{4}s^4}\right) \\
&\quad - \sqrt{(b_1-a_2)^2 + (b_1+a_2)\,s^2 + \tfrac{1}{4}s^4} \\
&\quad + 2a_2 \ln\left(a_1 - a_2 + \tfrac{1}{2}s^2 + \sqrt{(a_1-a_2)^2 + (a_1+a_2)\,s^2 + \tfrac{1}{4}s^4}\right) \\
&\quad - 2a_1 \ln\left(a_1 - a_2 - \tfrac{1}{2}s^2 + \sqrt{(a_1-a_2)^2 + (a_1+a_2)\,s^2 + \tfrac{1}{4}s^4}\right) \\
&\quad + \sqrt{(a_1-a_2)^2 + (a_1+a_2)\,s^2 + \tfrac{1}{4}s^4}, \\
&= I(s;b_2,b_1) - I(s;b_2,a_1) - I(s;a_2,b_1) + I(s;a_2,a_1)\,,
\end{aligned} \tag{A.18}$$

where we introduced,

$$\begin{aligned}
I(s;b,a) &= 2b \ln\left(a - b + \tfrac{1}{2}s^2 + \sqrt{(a-b)^2 + (a+b)\,s^2 + \tfrac{1}{4}s^4}\right) \\
&\quad - 2a \ln\left(a - b - \tfrac{1}{2}s^2 + \sqrt{(a-b)^2 + (a+b)\,s^2 + \tfrac{1}{4}s^4}\right) \\
&\quad + \sqrt{(a-b)^2 + (a+b)\,s^2 + \tfrac{1}{4}s^4}.
\end{aligned} \tag{A.19}$$

The integral of the absolute coordinate t is trivial, however we need to be careful with the integration regions. With the same considerations as in Figs. A.1, A.2 we arrive at the following two expressions:

case $(d_1 - c_1) < (d_2 - c_2)$:

$$\mathrm{DXI}_{ij} = \frac{1}{(2\pi)^3 4n}\left(\int_{c_1-d_2}^{d_1-d_2} \mathrm{d}s\ \left((d_2 - c_1)\, I(s) + sI(s)\right) + \int_{d_1-d_2}^{c_1-c_2} \mathrm{d}s\ \left((d_1 - c_1)\, I(s)\right) + \int_{c_1-c_2}^{d_1-c_2} \mathrm{d}s\ \left((d_1 - c_2)\, I(s) - sI(s)\right)\right). \tag{A.20}$$

case $(d_1 - c_1) < (d_2 - c_2)$:

$$\mathrm{DXI}_{ij} = \frac{1}{(2\pi)^3 4n}\left(\int_{c_1-d_2}^{c_1-c_2} \mathrm{d}s\ \left((d_2 - c_1)\, I(s) + sI(s)\right) + \int_{c_1-c_2}^{d_1-d_2} \mathrm{d}s\ \left((d_2 - c_2)\, I(s)\right) + \int_{d_1-d_2}^{d_1-c_2} \mathrm{d}s\ \left((d_1 - c_2)\, I(s) - sI(s)\right)\right). \tag{A.21}$$

This time the two cases do not yield the same result. The final result can be written in terms of the indefinite integrals

$$\mathcal{F}(a,b,s) = \int \mathrm{d}s\ I(s;a,b)\,, \tag{A.22}$$

$$\mathcal{G}(a,b,s) = \int \mathrm{d}s\ sI(s;a,b)\,. \tag{A.23}$$

With the help of *Mathematica* we get for the second integral,

$$\begin{aligned}\mathcal{G}(a,b,s) = \int \mathrm{d}s\ \Bigg(& sb^2 \ln\left(a^2 - b^2 + s^2 + \sqrt{\left(a^2-b^2\right)^2 + 2\left(a^2+b^2\right)s^2 + s^4}\right) \\ & - sa^2 \ln\left(a^2 - b^2 - s^2 + \sqrt{\left(a^2-b^2\right)^2 + 2\left(a^2+b^2\right)s^2 + s^4}\right) \\ & + \frac{s}{2}\sqrt{\left(a^2-b^2\right)^2 + 2\left(a^2+b^2\right)s^2 + s^4}\Bigg) \\ = \tfrac{1}{4}\Bigg(& \left(a^2-b^2\right)s^2 - \tfrac{1}{2}\left(a^2+b^2-s^2\right)\sqrt{a^4 - 2a^2\left(b^2-s^2\right) + \left(b^2+s^2\right)^2} \\ & - 2a^2s^2 \ln\left(a^2 - b^2 - s^2 + \sqrt{a^4 - 2a^2\left(b^2-s^2\right) + \left(b^2+s^2\right)^2}\right) \\ & + 2b^2s^2 \ln\left(a^2 - b^2 + s^2 + \sqrt{a^4 - 2a^2\left(b^2-s^2\right) + \left(b^2+s^2\right)^2}\right) \\ & - 2a^2b^2 \ln\left(a^2 + b^2 + s^2 + \sqrt{a^4 - 2a^2\left(b^2-s^2\right) + \left(b^2+s^2\right)^2}\right)\Bigg).\end{aligned} \tag{A.24}$$

Mathematica converts the integral $\mathcal{F}$ into an expression in terms of elliptical integrals of the first kind $F(\phi|k)$ and second kind $E(\phi|k)$ with complex arguments. Using properties of the elliptic integrals, c.f. [GR80], we can rewrite *Mathematica*'s result in terms of real quantities,

i.e. ,

$$\begin{aligned}
\mathcal{F}(a,b,s) = \int \mathrm{d}s \Bigg(& b^2 \ln\Big(a^2 - b^2 + s^2 + \sqrt{\left(a^2-b^2\right)^2 + 2\left(a^2+b^2\right)s^2 + s^4}\Big) \\
& - a^2 \ln\Big(a^2 - b^2 - s^2 + \sqrt{\left(a^2-b^2\right)^2 + 2\left(a^2+b^2\right)s^2 + s^4}\Big) \\
& + \tfrac{1}{2}\sqrt{\left(a^2-b^2\right)^2 + 2\left(a^2+b^2\right)s^2 + s^4}\Bigg) \\
= s\Bigg(& \frac{1}{6}\sqrt{a^4 - 2a^2\left(b^2-s^2\right) + \left(b^2+s^2\right)^2} + a^2 - b^2 \\
& - a^2 \ln\Big(a^2 - b^2 - s^2 + \sqrt{a^4 - 2a^2\left(b^2-s^2\right) + \left(b^2+s^2\right)^2}\Big) \\
& + b^2 \ln\Big(a^2 - b^2 + s^2 + \sqrt{a^4 - 2a^2\left(b^2-s^2\right) + \left(b^2+s^2\right)^2}\Big)\Bigg) \\
& - \frac{2}{3}\sqrt{\left(a^2-b^2\right)^2(a-b)^2}\,F\left(\arctan\left(\frac{s}{\sqrt{(a-b)^2}}\right)\Big|\sqrt{\frac{4ab}{(a+b)^2}}\right) \\
& + \frac{2}{3}\sqrt{\left(a^2+b^2\right)^2(a+b)^2}\,E\left(\arctan\left(\frac{s}{\sqrt{(a-b)^2}}\right)\Big|\sqrt{\frac{4ab}{(a+b)^2}}\right) \\
& - \frac{2}{3}s\left(a^2+b^2\right)\sqrt{\frac{(a+b)^2+s^2}{(a-b)^2+s^2}}.
\end{aligned} \tag{A.25}$$

Appendix B

Non-interacting polarizability for the spin-spiral-wave state

Here we perform the integration for the non-interacting polarizability of the SSW state defined in Chap. 8, Sec. 8.4, Eq. (8.67). The polarizability for the SSW state at imaginary frequencies is given by,

$$P_0(\boldsymbol{q}, \imath\omega) = \frac{1}{(2\pi)^3} \sum_{b_1=\mp} \sum_{b_2=\pm} \int \mathrm{d}^3k \; \tfrac{1}{2} n_{b_1}(\boldsymbol{k}) \times \left(\frac{1 + b_1 b_2 C(\boldsymbol{k}; \boldsymbol{k}-\boldsymbol{q})}{(\epsilon_{b_1}(\boldsymbol{k}) - \epsilon_{b_2}(\boldsymbol{k}-\boldsymbol{q})) - \imath\omega} + \frac{1 + b_1 b_2 C(\boldsymbol{k}; \boldsymbol{k}+\boldsymbol{q})}{(\epsilon_{b_1}(\boldsymbol{k}) - \epsilon_{b_2}(\boldsymbol{k}+\boldsymbol{q})) + \imath\omega} \right). \tag{B.1}$$

From now on we shall use $\boldsymbol{k} = (y\cos(\phi), y\sin(\phi), s)$ and w.l.o.g. $\boldsymbol{q} = (x, 0, z)$. The region of integration is specified by $n_b(\boldsymbol{k}) = n_b(y, s)$ and therefore we get

$$\begin{aligned} P_0(\boldsymbol{q}, \imath\omega) = {} & \frac{1}{(2\pi)^3} \int_{z_0-}^{z_1-} \mathrm{d}s \int_0^{x_0^-} \mathrm{d}y \; \tfrac{1}{2} y \int_0^{2\pi} \mathrm{d}\phi \sum_{b=\mp} \\ & \times \left(\frac{1 - bC(s; s-z)}{\left(\epsilon_-(y,s) - \epsilon_b\left(\sqrt{y^2 - 2xy\cos(\phi) + x^2}, s-z\right)\right) - \imath\omega} \right. \\ & \left. + \frac{1 - bC(s; s+z)}{\left(\epsilon_-(y,s) - \epsilon_b\left(\sqrt{y^2 + 2xy\cos(\phi) + x^2}, s+z\right)\right) + \imath\omega} \right) \\ & + \frac{1}{(2\pi)^3} \int_{z_0+}^{z_1+} \mathrm{d}s \int_0^{x_0+} \mathrm{d}y \; \tfrac{1}{2} y \int_0^{2\pi} \mathrm{d}\phi \sum_{b=\mp} \\ & \times \left(\frac{1 + bC(s; s-z)}{\left(\epsilon_+(y,s) - \epsilon_b\left(\sqrt{y^2 - 2xy\cos(\phi) + x^2}, s-z\right)\right) - \imath\omega} \right. \\ & \left. + \frac{1 + bC(s; s+z)}{\left(\epsilon_+(y,s) - \epsilon_b\left(\sqrt{y^2 + 2xy\cos(\phi) + x^2}, s+z\right)\right) + \imath\omega} \right). \end{aligned} \tag{B.2}$$

The $\mathrm{d}\phi$- and $\mathrm{d}y$-integrals can be solved analytically

$$\begin{aligned}
Q\left(\alpha, x_0; x\right) &= \frac{1}{4\pi^2}\int_0^{x_0}\mathrm{d}y\ \frac{y}{2}\int\mathrm{d}\phi\ 02\pi\frac{1}{\alpha \pm xy\cos(\phi)} = \frac{1}{4\pi^2}\int_0^{x_0}\mathrm{d}y\ y\int\mathrm{d}t\ \frac{1}{\alpha\left(1+t^2\right)\pm xy\left(1-t^2\right)} \\
&= \frac{1}{4\pi^2}\int_0^{x_0}\mathrm{d}y\ y\frac{1}{\alpha\mp xy}\int\mathrm{d}t\ \frac{1}{\left(t-\imath\sqrt{\frac{\alpha\pm xy}{\alpha\mp xy}}\right)\left(t+\imath\sqrt{\frac{\alpha\pm xy}{\alpha\mp xy}}\right)} \\
&= \frac{1}{4\pi^2}\int_0^{x_0}\mathrm{d}y\ \frac{y}{\sqrt{\alpha^2-x^2x^2}} \\
&= \frac{1}{4\pi x^2}\left(\sqrt{\alpha^2}-\sqrt{\alpha^2-x_0^2x^2}\right),
\end{aligned}$$

with

$$x_0^{\mp}\left(z\right) = \mathrm{Max}\left[0, 2\left(\mu \pm S\left(z\right)\right) - z^2\right], \tag{B.3}$$

$$S(z) = \tfrac{1}{2}\sqrt{\left(zq+B\right)^2+A^2}. \tag{B.4}$$

being the radial integration limits, given a fixed z, for the upper and lower band, respectively. Realizing that $\alpha = \beta \pm \imath\omega$ is the only complex quantity, we can separate real- and imaginary-parts

$$\begin{aligned}
\mathrm{Re}[Q\left(\beta, x_0; x, \pm\omega\right)] &= \frac{1}{4\pi x^2} \\
&\times\left(\left|\beta\right| - \sqrt{\left(\sqrt{\left(\beta^2-\omega^2-x_0^2x^2\right)^2+4\beta^2\omega^2}+\left(\beta^2-\omega^2-x_0^2x^2\right)\right)/2}\right), \\
\mathrm{Im}[Q\left(\beta, x_0; x, \pm\omega\right)] &= \frac{\mathrm{sgn}(\pm\beta\omega)}{4\pi x^2} \\
&\times\left(\left|\omega\right| - \sqrt{\left(\sqrt{\left(\beta^2-\omega^2-x_0^2x^2\right)^2+4\beta^2\omega^2}-\left(\beta^2-\omega^2-x_0^2x^2\right)\right)/2}\right).
\end{aligned}$$

Together we get

$$P_0\left(x, z, \imath\omega\right) = \frac{1}{2\pi}\int_{z_0-}^{z_1-}\mathrm{d}s\ Q_-\left(x, z, \omega; s\right) + \frac{1}{2\pi}\int_{z_0+}^{z_1+}\mathrm{d}s\ Q_+\left(x, z, \omega; s\right). \tag{B.5}$$

with

$$\begin{aligned} Q_{-}(x,z,\omega;s) \equiv \quad & \{1+C(s,s-z)\}\, Q\left(\beta_1(z;s), x_0^{-}(s); x, -\omega\right) \\ & + \{1+C(s,s+z)\}\, Q\left(\beta_2(z;s), x_0^{-}(s); x, \omega\right) \\ & + \{1-C(s,s-z)\}\, Q\left(\beta_3(z;s), x_0^{-}(s); x, -\omega\right) \\ & + \{1-C(s,s+z)\}\, Q\left(\beta_4\{z;s\}, x_0^{-}(s); x, \omega\right), \end{aligned} \tag{B.6}$$

$$\beta_1(z;s) \equiv +zs - \frac{z^2}{2} - S(s) + S(s-z), \tag{B.7}$$

$$\beta_2(z;s) \equiv -zs - \frac{z^2}{2} - S(s) + S(s+z), \tag{B.8}$$

$$\beta_3(z;s) \equiv +zs - \frac{z^2}{2} - S(s) - S(s-z), \tag{B.9}$$

$$\beta_4(z;s) \equiv -zs - \frac{z^2}{2} - S(s) - S(s+z). \tag{B.10}$$

and

$$\begin{aligned} Q_{+}(x,z,\omega;s) \equiv \quad & \{1+C(s,s-z)\}\, Q\left(\beta_5(z;s), x_0^{+}(s); x, -\omega\right) \\ & + \{1+C(s,s+z)\}\, Q\left(\beta_6(z;s), x_0^{+}(s); x, \omega\right) \\ & + \{1-C(s,s-z)\}\, Q\left(\beta_7(z;s), x_0^{+}(s); x, -\omega\right) \\ & + \{1-C(s,s+z)\}\, Q\left(\beta_8(z;s), x_0^{+}(s); x, \omega\right), \end{aligned} \tag{B.11}$$

$$\beta_5(z;s) \equiv +zs - \frac{z^2}{2} + S(s) - S(s-z), \tag{B.12}$$

$$\beta_6(z;s) \equiv -zs - \frac{z^2}{2} + S(s) - S(s+z), \tag{B.13}$$

$$\beta_7(z;s) \equiv +zs - \frac{z^2}{2} + S(s) + S(s-z), \tag{B.14}$$

$$\beta_8(z;s) \equiv -zs - \frac{z^2}{2} + S(s) + S(s+z). \tag{B.15}$$

The integral Eq. (B.5) has to be solved numerically.

Appendix C

Tabulated coefficients for the Spin-Gradient Extension

In the following we tabulated the coefficients for the polynomial representation $\tilde{S}_{xc}^{n=6}$. These coefficients may be used to implement the polynomial representation of $S_{xc,\mathrm{RPA}}$ defined in Chap. 8, Sec. 8.5, Eq. (8.71).

(j,k,l,m)	C_{jklm}
$(0,0,0,0)$	-2.74813
$(0,0,0,1)$	-1.81168
$(0,0,0,2)$	0.211674
$(0,0,0,3)$	0.0948286
$(0,0,0,4)$	0.0174232
$(0,0,0,5)$	0.0153099
$(0,0,0,6)$	0.00168742
$(0,0,1,0)$	-0.403313
$(0,0,1,1)$	0.0144716
$(0,0,1,2)$	0.00367438
$(0,0,1,3)$	0.035482
$(0,0,1,4)$	0.00349679
$(0,0,1,5)$	-0.000687232

(j,k,l,m)	C_{jklm}
$(0,0,2,0)$	-0.062503
$(0,0,2,1)$	-0.0336132
$(0,0,2,2)$	-0.00595854
$(0,0,2,3)$	0.00498222
$(0,0,2,4)$	0.000734493
$(0,0,3,0)$	-0.0148836
$(0,0,3,1)$	-0.0127118
$(0,0,3,2)$	-0.00685191
$(0,0,3,3)$	-0.000260289
$(0,0,4,0)$	-0.00336768
$(0,0,4,1)$	-0.0026275
$(0,0,4,2)$	-0.000670918
$(0,0,5,0)$	-0.000235186

(j,k,l,m)	C_{jklm}
$(0,0,5,1)$	-0.000143852
$(0,0,6,0)$	-2.84×10^{-6}
$(0,1,0,0)$	-0.992457
$(0,1,0,1)$	0.0241714
$(0,1,0,2)$	0.0170056
$(0,1,0,3)$	0.101777
$(0,1,0,4)$	0.0314557
$(0,1,0,5)$	-0.000659524
$(0,1,1,0)$	0.00853378
$(0,1,1,1)$	-0.0284641
$(0,1,1,2)$	-0.00812592
$(0,1,1,3)$	0.00561304
$(0,1,1,4)$	0.00148409

Table C.1: Coefficients for $\tilde{S}_{xc}^{n=6}$ (part 1).

(j,k,l,m)	C_{jklm}
$(0,1,2,0)$	-0.0270776
$(0,1,2,1)$	-0.0209393
$(0,1,2,2)$	-0.0100666
$(0,1,2,3)$	-0.00133606
$(0,1,3,0)$	-0.00598277
$(0,1,3,1)$	-0.00599263
$(0,1,3,2)$	-0.00092737
$(0,1,4,0)$	-0.000744697
$(0,1,4,1)$	-0.00037085
$(0,1,5,0)$	0.0000245588
$(0,2,0,0)$	0.0659134
$(0,2,0,1)$	-0.025517
$(0,2,0,2)$	-0.0308906
$(0,2,0,3)$	-0.00402752
$(0,2,0,4)$	0.00040717
$(0,2,1,0)$	-0.0175784
$(0,2,1,1)$	-0.023275
$(0,2,1,2)$	-0.0176265
$(0,2,1,3)$	-0.00426414
$(0,2,2,0)$	-0.00418172
$(0,2,2,1)$	-0.0050033
$(0,2,2,2)$	-0.000161088
$(0,2,3,0)$	-0.00113118
$(0,2,3,1)$	-0.000473242
$(0,2,4,0)$	-0.0000348719
$(0,3,0,0)$	-0.00389398
$(0,3,0,1)$	-0.0118013
$(0,3,0,2)$	-0.0100464
$(0,3,0,3)$	-0.00181306
$(0,3,1,0)$	0.00090383
$(0,3,1,1)$	-0.00115289
$(0,3,1,2)$	-0.0000464157
$(0,3,2,0)$	0.000169848
$(0,3,2,1)$	0.0000283274
$(0,3,3,0)$	-0.000124823
$(0,4,0,0)$	0.00165377
$(0,4,0,1)$	-0.000285921
$(0,4,0,2)$	-0.00019673
$(0,4,1,0)$	0.000889862
$(0,4,1,1)$	0.000260928
$(0,4,2,0)$	2.32×10^{-6}
$(0,5,0,0)$	0.000337346
$(0,5,0,1)$	0.0000815987
$(0,5,1,0)$	0.0000887041
$(0,6,0,0)$	0.0000540729
$(1,0,0,0)$	4.88182
$(1,0,0,1)$	3.15805
$(1,0,0,2)$	-0.33788
$(1,0,0,3)$	-0.147639
$(1,0,0,4)$	-0.020039
$(1,0,0,5)$	-0.0229298
$(1,0,1,0)$	0.677765
$(1,0,1,1)$	-0.0294751
$(1,0,1,2)$	-0.00358372
$(1,0,1,3)$	-0.0532579
$(1,0,1,4)$	-0.00206774
$(1,0,2,0)$	0.0895932
$(1,0,2,1)$	0.0448107
$(1,0,2,2)$	0.00671602
$(1,0,2,3)$	-0.00754708
$(1,0,3,0)$	0.0162721
$(1,0,3,1)$	0.0142432
$(1,0,3,2)$	0.00773634
$(1,0,4,0)$	0.00329261
$(1,0,4,1)$	0.00266186
$(1,0,5,0)$	0.000235576
$(1,1,0,0)$	1.81843
$(1,1,0,1)$	0.00621741
$(1,1,0,2)$	-0.0152351
$(1,1,0,3)$	-0.144333
$(1,1,0,4)$	-0.0329551
$(1,1,1,0)$	-0.0333261
$(1,1,1,1)$	0.0358591
$(1,1,1,2)$	0.00740061
$(1,1,1,3)$	-0.0127594
$(1,1,2,0)$	0.0315141
$(1,1,2,1)$	0.0237553
$(1,1,2,2)$	0.0121981
$(1,1,3,0)$	0.00585056
$(1,1,3,1)$	0.006568
$(1,1,4,0)$	0.000755296
$(1,2,0,0)$	-0.126782
$(1,2,0,1)$	0.0255648
$(1,2,0,2)$	0.0353875
$(1,2,0,3)$	-0.00315256
$(1,2,1,0)$	0.015461
$(1,2,1,1)$	0.0260865
$(1,2,1,2)$	0.0204812
$(1,2,2,0)$	0.00494602
$(1,2,2,1)$	0.00674589
$(1,2,3,0)$	0.00102883
$(1,3,0,0)$	0.00311403
$(1,3,0,1)$	0.0151853
$(1,3,0,2)$	0.01251
$(1,3,1,0)$	-0.000204817
$(1,3,1,1)$	0.0032024
$(1,3,2,0)$	-0.000354866
$(1,4,0,0)$	-0.00177483
$(1,4,0,1)$	0.00115815

Table C.2: Coefficients for $\tilde{S}_{xc}^{n=6}$ (part 2).

(j,k,l,m)	C_{jklm}
$(1,4,1,0)$	-0.00098733
$(1,5,0,0)$	-0.000303327
$(2,0,0,0)$	-3.25938
$(2,0,0,1)$	-2.11157
$(2,0,0,2)$	0.125372
$(2,0,0,3)$	0.0563263
$(2,0,0,4)$	0.00826714
$(2,0,1,0)$	-0.423334
$(2,0,1,1)$	0.0107458
$(2,0,1,2)$	-0.00960004
$(2,0,1,3)$	0.00425997
$(2,0,2,0)$	-0.0354086
$(2,0,2,1)$	-0.0119025
$(2,0,2,2)$	0.000545622
$(2,0,3,0)$	0.000124589
$(2,0,3,1)$	-0.0010616
$(2,0,4,0)$	-0.00066995
$(2,1,0,0)$	-1.29638
$(2,1,0,1)$	-0.0801677
$(2,1,0,2)$	-0.0218154
$(2,1,0,3)$	0.0188277
$(2,1,1,0)$	0.0390195
$(2,1,1,1)$	-0.00742304
$(2,1,1,2)$	0.00173533

(j,k,l,m)	C_{jklm}
$(2,1,2,0)$	-0.00182753
$(2,1,2,1)$	-0.0014003
$(2,1,3,0)$	-0.000477194
$(2,2,0,0)$	0.0887224
$(2,2,0,1)$	0.00271825
$(2,2,0,2)$	-0.00122261
$(2,2,1,0)$	0.00357829
$(2,2,1,1)$	-0.00339669
$(2,2,2,0)$	-0.000577064
$(2,3,0,0)$	0.00239283
$(2,3,0,1)$	-0.00217325
$(2,3,1,0)$	-0.0010054
$(2,4,0,0)$	-0.000295843
$(3,0,0,0)$	1.72836
$(3,0,0,1)$	1.04238
$(3,0,0,2)$	-0.0408074
$(3,0,0,3)$	-0.0211725
$(3,0,1,0)$	0.196539
$(3,0,1,1)$	-0.00237496
$(3,0,1,2)$	0.00550707
$(3,0,2,0)$	0.0122217
$(3,0,2,1)$	0.00286426
$(3,0,3,0)$	-0.000419612
$(3,1,0,0)$	0.613507

(j,k,l,m)	C_{jklm}
$(3,1,0,1)$	0.040842
$(3,1,0,2)$	0.0116186
$(3,1,1,0)$	-0.0163221
$(3,1,1,1)$	0.00141247
$(3,1,2,0)$	0.0000428224
$(3,2,0,0)$	-0.0355089
$(3,2,0,1)$	-0.00295355
$(3,2,1,0)$	-0.00164191
$(3,3,0,0)$	-0.000845625
$(4,0,0,0)$	-0.656854
$(4,0,0,1)$	-0.346214
$(4,0,0,2)$	0.00415935
$(4,0,1,0)$	-0.0565585
$(4,0,1,1)$	0.00200562
$(4,0,2,0)$	-0.00227527
$(4,1,0,0)$	-0.185283
$(4,1,0,1)$	-0.00794914
$(4,1,1,0)$	0.00368631
$(4,2,0,0)$	0.00663028
$(5,0,0,0)$	0.163641
$(5,0,0,1)$	0.0639688
$(5,0,1,0)$	0.00883955
$(5,1,0,0)$	0.0287817
$(6,0,0,0)$	-0.0189881

Table C.3: Coefficients for $\tilde{S}_{xc}^{n=6}$ (part 3).

Bibliography

[BB02] M.A. Buijse and E.J. Baerends, *An approximate exchange-correlation hole density as a functional of the natural orbitals*, Mol. Phys. **100** (2002), 401.

[Bec88] A.D. Becke, *Density-functional exchange-energy approximation with correct asymptotic behavior*, Phys. Rev. A **38** (1988), 3098.

[BLLS94] Volker Bach, Elliott H. Lieb, Michael Loss, and Jan Philip Solovej, *There are no unfilled shells in unrestricted hartree-fock theory*, Phys. Rev. Lett. **72** (1994), 2981.

[CA80] D.M. Ceperley and B.J. Alder, *Ground state of the electron gas by a stochastic method*, Phys. Rev. Lett. **45** (1980), 566.

[CCR85] J.T. Chayes, L. Chayes, and Mary Beth Ruskai, *Density functional approach to quantum lattice systems*, J. Stat. Phys. **38** (1985), 497.

[Cep04] D.M. Ceperley, *Introduction to quantum monte carlo methods applied to the electron gas*, The Electron Liquid Paradigm in Condensed Matter Physics (G.F. Giuliani and G. Vignale, eds.), Proceedings of the International School of Physics "Enrico Fermi", vol. 157, 2004, p. 3.

[CGA02] G. Csányi, S. Goedecker, and T.A. Arias, *Improved tensor-product expansions for the two-particle density matrix*, Phys. Rev. A **65** (2002), 032510.

[CO00a] K. Capelle and L.N. Oliveira, *Density-functional approach to spin-density waves*, Europhys. Lett. **49** (2000), 376.

[CO00b] ———, *Density-functional theory for spin-density waves and antiferromagnetic systems*, Phys. Rev. B **61** (2000), 15228.

[Col63] A.J. Coleman, *Structure of fermion density matrices*, Rev. Mod. Phys. **35** (1963), 668.

[CVG01] K. Capelle, G. Vignale, and B.L. Györffy, *Spin currents and spin dynamics in time-dependent density-functional theory*, Phys. Rev. Lett. **78** (2001), 206403.

[DG90] R.M. Dreizler and E.K.U. Gross, *Density functional theory*, Springer-Verlag, Berlin Heidelberg, 1990.

[Dir28] P.A.M. Dirac, *The quantum theory of the electron*, Proc. R. Soc. London. A **117** (1928), 610.

[EE84a] H. Englisch and R. Englisch, *Exact density functionals for ground-state energies i. general results*, Phys. Stat. Sol. (b) **123** (1984), 711.

[EE84b] ———, *Exact density functionals for ground-state energies ii. details and remarks*, Phys. Stat. Sol. (b) **124** (1984), 373.

[EKP+10] F. G. Eich, S. Kurth, C.R. Proetto, S. Sharma, and E.K.U. Gross, *Noncollinear spin-spiral phase for the uniform electron gas within reduced-density-matrix-functional theory*, Phys. Rev. B **81** (2010), 024430.

[ELK] *The elk fp-lapw code*, http://elk.sourceforge.net/.

[Foc30] V. Fock, *Näherungsmethode zur lösung des quantenmechanischen mehrkörperproblems*, Z. Physik **61** (1930), 126.

[FV71] Alexander L. Fetter and John Dirk Valecka, *Quantum theory of many-particle systems*, McGraw-Hill Book Company, New York, 1971.

[FW50] Leslie L. Foldy and Siegfried A. Wouthuysen, *On the dirac theory of spin 1/2 particles and its non-relativistic limit*, Phys. Rev. **78** (1950), 29.

[GG95] Tobias Grabo and E.K.U. Gross, *Density-functional theory using an optimized exchange-correlation potential*, Chem. Phys. Lett. **240** (1995), no. 1-3, 141–150.

[Gil75] T.L. Gilbert, *Hohenberg-kohn theorem for nonlocal external potentials*, Phys. Rev. B **12** (1975), 2111.

[GKKG00] T. Grabo, T. Kreibich, S. Kurth, and E.K.U. Gross, *Orbital functionals in density functional theory: the optimized effective potential method*, Strong Coulomb Correlations in Electronic Structure Calculations: Beyond the Local Density Approximation (V.I. Anisimov, ed.), Gordon and Breach, 2000, p. 203.

[GMB57] Murray Gell-Mann and Keith A. Brueckner, *Correlation energy of an electron gas at high density*, Phys. Rev. **106** (1957), 364.

[GPB05] O. Gritsenko, K. Pernal, and E.J. Baerends, *An improved density matrix functional by physically motivated repulsive corrections*, J. Chem. Phys. **122** (2005), 204102.

[GR80] I.S. Gradshteyn and I.M. Ryzhik, *Table of integrals, series, and products*, Academic Press, New York, 1980.

[GRH91] E.K.U. Gross, E. Runge, and O. Heinonen, *Many-particle theory*, Taylor & Francis, 1991.

[GS22] Walther Gerlach and Otto Stern, *Das magnetische moment des silberatoms*, Z. Phys. A **9** (1922), 353.

[GU98] S. Goedecker and C.J. Umrigar, *Natural orbital functional for the many-electron problem*, Phys. Rev. Lett. **81** (1998), 866.

[GV05] G.F. Giuliani and G. Vignale, *Quantum theory of the electron liquid*, Cambridge University Press, Cambridge, 2005.

[GV08] Gabriele F. Giuliani and Giovanni Vignale, *Absence of certain exchange driven instabilities of an electron gas at high densities*, Phys. Rev. B **78** (2008), 075110.

[Har28] D.R. Hartree, *The wave mechanics of an atom with a non-coulomb central field. i. theory and methods*, Proc. Cambridge Phil. Soc. **24** (1928), 98.

[HBP+11] Markus Holzmann, Bernard Bernu, Carlo Pierleoni, Jeremy McMinis, David M. Ceperley, Valerio Olevano, and Luigi Delle Site, *Momentum distribution of the homogeneous electron gas*, Phys. Rev. Lett. **107** (2011), 110402.

[HK64] P. Hohenberg and W. Kohn, *Inhomogeneous electron gas*, Phys. Rev. **136** (1964), B864.

[KA03] M.I. Katsnelson and V.P. Antropov, *Spin angular gradient approximation in the density functional theory*, Phys. Rev. B **67** (2003), 140406(R).

[KE09] S. Kurth and F. G. Eich, *Overhauser's spin-density wave in exact-exchange spin-density functional theory*, Phys. Rev. B **80** (2009), 125120.

[KHSW88] J. Kübler, K.-H. Hock, J. Sticht, and A.R. Williams, *Density functional theory of non-collinear magnetism*, J. Phys. F **18** (1988), 469.

[KS65] W. Kohn and L.J. Sham, *Self-consistent equations including exchange and correlation effects*, Phys. Rev. **140** (1965), A1133.

[Lam71] John Lam, *Momentum distribution and pair correlation of the electron gas at metallic densities*, Phys. Rev. B **3** (1971), 3243.

[Lam10] Paul E. Lammert, *Well-behaved coarse-grained model of density-functional theory*, J. Stat. Phys. **82** (2010), 012109.

[Lev82] Mel Levy, *Electron densities in search of hamiltonians*, Phys. Rev. A **26** (1982), 1200.

[LHG07] N.N. Lathiotakis, N. Helbig, and E.K.U. Gross, *Performance of one-body reduced density-matrix functionals for the homogeneous electron gas*, Phys. Rev. B **75** (2007), 195120.

[Lie83] Elliott H. Lieb, *Density functionals for coulomb systems*, Int. J. Quantum Chem. **24** (1983), no. 3, 243.

[LP80] David C. Langreth and John P. Perdew, *Theory of nonuniform electronic systems. i. analysis of the gradient approximation and a generalization that works*, Phys. Rev. B **21** (1980), 5469.

[LSD+09] N. N. Lathiotakis, S. Sharma, J. K. Dewhurst, F. G. Eich, M. A. L. Marques, and E. K. U. Gross, *Density-matrix-power functional: Performance for finite systems and the homogeneous electron gas*, Phys. Rev. A **79** (2009), 040501(R).

[LYP88] Chengteh Lee, Weitao Yang, and Robert G. Parr, *Development of the colle-salvetti correlation-energy formula into a functional of the electron density*, Phys. Rev. B **37** (1988), 785.

[Mac50] W. Macke, Z.Naturforschg. **5a** (1950), 192.

[MBJ+09] S. Mühlbauer, B. Binz, F. Jonietz, C. Pfleiderer, A. Rosch, A. Neubauer, R. Georgii, and P. Böni, *Skyrmion lattice in a chiral magnet*, Science **323** (2009), no. 5916, 915–919.

[ML08] Miguel A.L. Marques and N.N. Lathiotakis, *Empirical functionals for reduced-density-matrix-functional theory*, Phys. Rev. A **77** (2008), 032509.

[Mül84] A.M.K. Müller, *Explicit approximate relation between reduced two- and one-particle density matrices*, Phys. Lett. **105** (1984), 446.

[OHB99] G. Ortiz, M. Harris, and P. Ballone, *Zero temperature phases of the electron gas*, Phys. Rev. Lett. **82** (1999), 5317.

[Ove62] A.W. Overhauser, *Spin density waves in an electron gas*, Phys. Rev. **128** (1962), 1437.

[Ove71] ———, *Simplified theory of electron correlations in metals*, Phys. Rev. B **3** (1971), 1888.

[Pau27] Wolfgang Pauli, *Zur quantenmechanik des magnetischen elektrons*, Z. Phys. A **43** (1927), 601.

[PBE96] John P. Perdew, Kieron Burke, and Matthias Ernzerhof, *Generalized gradient approximation made simple*, Phys. Rev. Lett. **77** (1996), 3865.

[Pin53] D. Pines, *A collective description of electron interactions: Iv. electron interaction in metals*, Phys. Rev. **92** (1953), 626.

[Pir05] Mario Piris, *A new approach for the two-electron cumulant in natural orbital functional theory*, Int. J. Quantum Chem. **106** (2005), 1093.

[PPLB82] John P. Perdew, Robert G. Parr, Mel Levy, and Jose L. Balduz, Jr., *Density-functional theory for fractional particle number: Derivative discontinuities of the energy*, Phys. Rev. Lett. **49** (1982), 1691.

[PSF07] Juan E. Peralta, Gustavo E. Scuseria, and Michael J. Frisch, *Noncollinear magnetism in density functional calculations*, Phys. Rev. B **75** (2007), 125119.

[PW92] John P. Perdew and Yue Wang, *Accurate and simple analytic representation of the electron-gas correlation energy*, Phys. Rev. B **45** (1992), 13244.

[RG84] Erich Runge and E.K.U. Gross, *Density-functional theory for time-dependent systems*, Phys. Rev. Lett. **52** (1984), 997.

[Sch26] E. Schrödinger, *Quantisierung als eigenwertproblem*, Ann. Phys. (Leipzig) **384** (1926), 361.

[SDAD+07] S. Sharma, J.K. Dewhurst, C. Ambrosch-Draxl, S. Kurth, N. Helbig, S. Pittalis, S. Shallcross, L. Nordström, and E.K.U. Gross, *First-principles approach to noncollinear magnetism: Towards spin dynamics*, Phys. Rev. Lett. **98** (2007), 196405.

[SDLG08] S. Sharma, J.K. Dewhurst, N.N. Lathiotakis, and E.K.U. Gross, *Reduced density matrix functional for many-electron systems*, Phys. Rev. B **78** (2008), 201103(R).

[SN05] David J. Singh and Lars Nordström, *Planewaves, pseudopotentials, and the lapw method*, Springer, New York, 2005.

[TNN93] Y. Tsunoda, Y. Nishioka, and R.M. Nicklow, *Spin fluctuations in small γ-fe precipitates*, Journal of Magnetism and Magnetic Materials **128** (1993), no. 1-2, 133 – 137.

[TS76] James D. Talman and William F. Shadwick, *Optimized effective atomic central potential*, Phys. Rev. A **14** (1976), 36.

[Tsu89] Y. Tsunoda, *Spin-density wave in cubic γ-fe and γ-fe 100-x co x precipitates in cu*, Journal of Physics: Condensed Matter **1** (1989), no. 51, 10427.

[TY91] Yasutami Takada and H. Yasuhara, *Momentum distribution function of the electron gas at metallic densities*, Phys. Rev. B **44** (1991), 7879.

[vBH72] U. von Barth and L. Hedin, *A local exchange-correlation potential for the spin polarized case*, J. Phys. C **5** (1972), 1629.

[Wig34] E. Wigner, *On the interaction of electrons in metals*, Phys. Rev. **46** (1934), 1002.

[ZC08] Shiwei Zhang and D.M. Ceperley, *Hartree-fock ground state of the three-dimensional electron gas*, Phys. Rev. Lett. **100** (2008), 236404.

Deutsche Kurzfassung

Dichtefunktionaltheorie (DFT) ist eine der am weitesten verbreiteten Methoden zur Bestimmung der elektronischen Struktur von Atomen, Molekülen und Festkörpern. Die Anwendbarkeit von DFT hängt von der Verfügbarkeit von physikalisch sinnvollen und numerisch stabilen Näherungen des Austausch-Korrelations-Energiefunktionals ab. Obwohl das Hohenberg-Kohn Theorem vor mehr als 30 Jahren durch von Barth und Hedin um die explizite Miteinbeziehung des Spin-Freiheitsgrades erweitert wurde, basieren die meisten Anwendungen heutzutage auf Austausch-Korrelations-Energiefunktionalen, die für kollineare Spinmagnetisierungen entwickelt wurden. In der vorliegenden Arbeit präsentieren wir ein neues Funktional für Spindichtefunktionaltheorie (SDFT), welches explizit für die Beschreibung von nicht-kollinearem Spinmagnetismus konzipiert wurde. Das Funktional berücksichtig die Möglichkeit der Spinmagnetisierung, seine Richtung räumlich zu verändern. Die Konstruktion des Funktionals erfolgt in Analogie zur Herleitung der bekannten lokalen Spinmagnetisierungsnäherung (LSDA), welche das homogene Elektronengas (HEG) mit einer konstanten Spinmagnetisierung als Referenzsystem heranzieht. Wir definieren eine semi-lokale Näherung für das Austausch-Korrelations-Energiefunktional, indem wir das HEG mit einer spiralförmigen Spinmagnetisierung als Referenzsystem benutzen, welches in den 60er Jahren von Overhauser qualitativ beschrieben wurde. Als Vorbereitung zur Konstruktion des Funktionals untersuchen wir das HEG mit einer spiralförmigen Magnetisierung quantitativ unter Anwendung verschiedener Vielteilchen-Methoden. Wir zeigen, dass das Funktional die LSDA um die Abhängigkeit von Gradienten der Spinmagnetisierung erweitert. Die sogenannte Spingradientenerweiterung erzeugt Austausch-Korrelations-Magnetfelder, welche nicht parallel zur Spinmagnetisierung sind, was die Tatsache berücksichtigt, dass die Spinstromdichten des physikalischen Systems und des Kohn-Sham Systems nicht identisch sind. Dies ist wichtig für die dynamische Beschreibung von Spinsystemen im Rahmen der zeitabhängigen SDFT. Zeitabhängigen SDFT ist von enormer Bedeutung für die ab-initio Behandlung von Spintronik, welche sich in jüngster Zeit als wichtiges Forschungsgebiet etabliert, da die Manipulation und Kontrolle des Spin-Freiheitsgrades der Elektronen vielversprechende Anwendungen auf dem Gebiet der Datenspeicherung und Informationsverarbeitung bietet.

Publications

1. *Density-matrix-power functional:*
   Performance for finite systems and the homogeneous electron gas
   N.N. Lathiotakis, S. Sharma, J.K. Dewhurst, F.G. Eich,
   M.A.L. Marques and E.K.U. Gross
   Phys. Rev. A**79**, 040501(R) (2009)

2. *Overhauser's spin-density wave in exact-exchange spin-density functional theory*
   S. Kurth and F.G. Eich
   Phys. Rev. B**80**, 125120 (2009)

3. *Noncollinear spin-spiral phase for the uniform electron gas*
   within reduced-density-matrix-functional theory
   F.G. Eich, S. Kurth, C.R. Proetto, S. Sharma and E.K.U. Gross
   Phys. Rev. B**81**, 024430 (2010)

4. *Discontinuities of the chemical potential in Reduced Density Matrix Functional Theory*
   N.N. Lathiotakis, S. Sharma, N. Helbig, J.K. Dewhurst, M.A.L. Marques, F.G. Eich,
   T. Baldsiefen, A. Zacarias and E.K.U. Gross
   Z. Phys. Chem. **224**, 467 (2010)

5. *Reduced density matrix functional theory at finite temperature. II.*
   Application to the electrongas: Exchange only
   T. Baldsiefen, F.G. Eich, and E.K.U. Gross
   arXiv:1208.4705 (2012), submitted to Phys. Rev. A

6. *Transverse spin gradient functional for non-collinear spin density functional theory*
   F.G. Eich and E.K.U. Gross
   arXiv:1212.3658 (2012), submitted to Phys. Rev. Lett.

Acknowledgements

First and foremost I thank Hardy Gross for giving me the opportunity to write a thesis in his group. I am deeply impressed by his rare skill to find the right tone when explaining and discussing physics.
I am very grateful to Prof. J. Bosse not just for excepting the role as second referee but also for supporting me during my undergraduate studies at the Freie Universität Berlin.

During the initial period of my PhD in Berlin I received a great deal of explanation and mentoring from Stefan Kurth and César Proetto. From Stefan I learned a lot about DFT and I certainly will not forget that César checked line by line the derivation of the exchange integral for cylindrical volume elements in momentum space.
Ali and Danilo were my steady officemates during my doctorate and I enjoyed their company and vivid discussions about physics and everyday life.
Kudos to Kay and Sangeeta for writing an almost self-explaining electronic-structure code and taking the time to explain its inner workings when it was not self-explaining.
Thanks to Tim, with whom I had tons of enlightening discussion about reduced density matrices and football. I thank the whole group for providing a stimulating and collegial atmosphere.

Finally I thank my parents for always supporting me. Without them none of what I have achieved would have been possible. My brother Simon remains to date the only non-physicist who showed genuine interest in what I was doing. I appreciate that he forced me time and again to explain physics without the use of equations.

Special thanks go to Fede for bearing with me during writing this thesis.